DEPARTMENT OF CIVIL AND STRUCTURAL ENGINEERING
UNIVERSITY OF SHEFFIELD

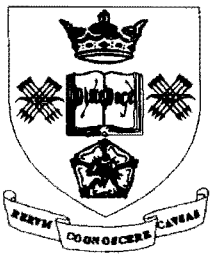

ASSESSMENT OF DETERIORATING POST-TENSIONED CONCRETE BRIDGES

by

Dominique Grace Cavell, B.Eng.

A thesis submitted to the University of Sheffield for the degree of Doctor of Philosophy in the Faculty of Engineering

November 1997

Dedicated to my parents,

and my husband

ABSTRACT

Assessment of Deteriorating Post-Tensioned Concrete Bridges
by
Dominique Grace Cavell

A non-linear analytical model was developed to assess the residual strength of deteriorating post-tensioned concrete bridges containing integral grouted tendons. The damage mechanisms addressed were those due to failure of the prestressing tendon as a result of corrosion, and the presence of grout voids within the ducts. The model was based principally on the method of strain compatibility, but modified to accommodate unbonded tendons in regions of incomplete grouting in the ducts. The phenomenon of tendon re-anchoring was also incorporated to estimate the distribution of residual prestress after tendon failure. This considered the distribution of grout voids along the beam and the quality of the grout surrounding the tendon.

Once validated, the model was used to study the effect of tendon failure and regions of ungrouted tendons on the residual structural capacity of typical bridge beams incorporating a variety of defects. It was found that the presence of voids within the re-anchoring length of failed tendons will affect the ability of the tendon to re-anchor fully and may affect the residual strength of the beam. The distribution of grout voids along the beam is thus an important factor when considering loss of strength. It was also demonstrated that significant levels of deterioration do not always compromise ultimate strength to a significant degree, hence avoiding the need for costly replacement.

In addition to the global analysis of beam strength due to failed tendons, the local effect of partial loss of tendon area was investigated with ANSYS finite element software. This enabled the level of stress enhancement in the corroded tendon and the amount of loss of prestressing force to be determined. Valid bond models were established based on results from available field observations. It was found that only a relatively small amount of prestressing force is lost as a result of partial loss of area in a tendon in part due to the re-distribution of force to adjacent tendons.

ACKNOWLEDGEMENTS

The author is very grateful to Professor Peter Waldron for his supervision, support and encouragement during the course of this research. He showed interest and enthusiasm and provided useful suggestions and advice throughout the research.

The financial support of the Engineering and Physical Sciences Research Council in funding this research project is also acknowledged. The author also wishes to thank Mr. John Darby for his advice and in providing some of the photos and figures used in this thesis.

The author's gratitude extends to her friends and colleagues who have provided assistance, moral support and friendship throughout this time. Thanks are also due to Dr. Kypros Pilakoutas for his advice and encouragement during this research. The author is also grateful to her parents, sister and brothers for their love and understanding.

Finally, to my husband for his continuous patience, support and encouragement throughout this work, my indebtedness is great.

TABLE OF CONTENTS

LIST OF FIGURES

CHAPTER 3

CHAPTER 4

CHAPTER 5

CHAPTER 6

LIST OF TABLES

LIST OF PLATES

NOTATIONS

A_b	area of bar
A_c	cross-sectional area of concrete
A_{ps}	cross-sectional area of prestressing tendon
A_{sw}	area of link reinforcement
b_w	width of beam
C	compressive force
d	depth of centroid of total steel area
d_b	nominal diameter of the bar/tendon
d_p	depth of centre of prestressing steel
d_s	depth of centre of ordinary reinforcement
dF_{ps}	change in tendon force
dF_T	loss of total tendon force
D	displacement
e_{yt}	eccentricity of the centroid of tendon group
E_c	elastic modulus of concrete
E_{ci}	elastic modulus of concrete at time of transfer
E_{ps}	elastic modulus of prestressing steel
E_s	elastic modulus of ordinary steel
f_b	bond stress
f_{bu}	bond strength
f_c	concrete stress
f_{ci}	concrete compressive strength at transfer
f_{cu}	characteristic strength of concrete
f_{pe}	effective prestress
f_{ps}	stress in the prestressing steel
f_{pu}	characteristic strength of the prestressing steel
f_{py}	yield strength of the prestressing steel
f_s	stress in the non-prestressed reinforcement
f_{se}	effective stress in tendon
f_{si}	initial prestress
f_t	tensile strength of concrete
f_y	yield strength of non-prestressed steel
f_{yv}	characteristic strength of link reinforcement
F_b	bond force
h	depth of section

I	second moment of area
j_e	end position of void region
j_s	start position of void region
l_d	unbonded length of tendon
l_u	void length
L_t	transfer length
M	applied bending moment
M_g	bending moment due to dead load
M_r	moment of resistance
M_u	bending moment due to ultimate load
N	number of beam segments
Pe	effective force in tendon
P_J	prestressing force in the tendon at the jacking end
$P(x)$	prestressing force at a distance x from jacking end
r	radius of wire
rlt	re-anchoring length (bonded)
rltu	re-anchoring length (unbonded)
r_{ps}	radius of curvature
s_1,s_2,s_3	slip values on bond stress-slip curve
S	span of beam
T	total tendon force
T_o	original tendon force
T_r	residual tendon force
V_c	shear force carried by concrete
V_p	shear force carried by prestressing tendon
V_u	shear strength
V_w	shear force carried by truss action in the web
x	neutral axis depth at ultimate
xcorros	distance of tendon failure from left hand end of beam
xvoid	distance of left end of void from left hand end of beam
z	section modulus
α_1	factor accounting for bond characteristics of reinforcement
α_2	factor accounting for sustained or repeated loading
β	ratio of corroded to total length of tendon
$\Delta\varepsilon$	fictitious concrete strain increase above decompression at level of tendon
$\Delta\varepsilon_c$	change in strain in the concrete

$\Delta\varepsilon_{ps}$	increase in strain in the prestressing steel
Δl_{ps}	total tendon elongation between the ends of the void
ε_c	concrete strain
ε_{cen}	strain in the concrete at the centroid of the section
ε_{cf}	average concrete strain
ε_{co}	precompressive strain in concrete at the level of prestressing steel
ε_{cu}	ultimate concrete strain in the top compression fibre
ε_o	strain corresponding to maximum stress reached in the concrete
ε_{pa}	actual strain increase in prestressing steel at decompression of concrete
ε_{pe}	effective prestrain in the prestressing steel
ε_{ps}	strain in the prestressing steel
ε_s	strain in non-prestressed reinforcement
ϕ	coefficient of friction between steel and concrete
γ_m	partial safety factor
η	stress concentration factor
μ	coefficient of friction between tendon and duct
μ_c, ν_c	Poisson's ratio of concrete
μ_s	Poisson's ratio of steel
ρ_p	prestressing steel ratio
σ_b	bond stress
σ_{cb}	concrete stress at extreme bottom fibre of the section
σ_{ct}	concrete stress at extreme top fibre of the section
σ_x	longitudinal stress
τ_f	residual bond stress
τ_{max}	maximum bond stress
$\%dA_{ps}$	percentage loss of area in corroded tendon
$\%dF_{ps}$	percentage loss of force in corroded tendon
$\%dF_T$	percentage loss of total tendon force

CHAPTER 1

Problems with Grouted Post-tensioned Concrete Bridges

1.1 INTRODUCTION

The discovery of tendon corrosion in post-tensioned concrete bridges containing integral grouted ducts has caused concern over the durability of such bridges and, in the UK, has resulted in a temporary ban on their construction (Department of Transport, 1992). Although this ban has recently been lifted, there still remains a lack of satisfactory methods to provide a quantitative assessment of the strength of such deteriorating bridges whilst accounting for the level of damage that has been discovered during inspection.

The problem of tendon corrosion in grouted post-tensioned concrete bridges is a relatively new problem in the UK. There are about 600 post-tensioned concrete bridges of this type owned by the Department of Transport. Some of these bridges would undoubtedly have suffered some degree of deterioration but, currently, satisfactory methods to assess the level of deterioration, and the residual structural capacity of these bridges are still lacking. This chapter presents an overview of the problems of deterioration in post-tensioned concrete bridges, and also identifies the areas where research is required.

1.2 DETERIORATION OF POST-TENSIONED CONCRETE BRIDGES

1.2.1 The Tendon Corrosion Problem

Bonded post-tensioned concrete construction normally involves casting ducts within the concrete section into which the steel tendons are fed after the concrete has achieved sufficient strength. The tendons are then stressed and the duct subsequently filled with

cementatious grout to protect the tendons against corrosion and also to provide structural bond between the steel tendons and the concrete. If the grouting operation is not carried out in accordance with specifications, it is possible for air and water voids to remain within the duct. In addition, if the ducts are not properly sealed, then chlorides, carbon dioxide, water vapour and oxygen may seep into the duct and cause corrosion of the tendons. Likely points of access are through the end anchorages, joints in segmental construction or permeable, poorly compacted concrete.

The post-tensioned tendons, normally concentrated into several large cables, are more vulnerable to localized corrosion than pre-tensioned cables due to their relatively low ratio of surface area to cross-sectional area. Localized corrosion resulting in a loss of up to 90% of tendon cross-sectional area has been reported (Woodward and Williams, 1988). Such extensive localized corrosion was shown to have seriously affected the service life of the prestressing tendons, and consequently the bridge member.

The problem is compounded by the fact that it is difficult to determine the condition of the tendons or the grout using currently available inspection techniques. Specialized non-destructive techniques may prove inconclusive as the presence of the steel duct distorts the results. Visual evidence like spalling, discoloration or local cracking of concrete which could indicate signs of distress, are lacking due to the position of the prestressing tendons embedded within the concrete, and the ability of any voids in the grout to accommodate the expansive products of corrosion. Consequently, visual methods of inspection are not sensitive to localized loss of prestressing tendon area although longitudinal cracking which follows the tendon profile may be detected (Woodward, 1981). Cracks of this type are believed to be attributed to the failure of the severely corroded tendons, which may occur suddenly after a significant loss of prestressing tendon area.

1.2.2 Loss of Bond

The lack of bond between the prestressing tendons and the concrete may arise from two sources. Firstly, the presence of voids, if any, reduces the degree of bond between the tendon and the grout, but also increases the risk of corrosion. Failure of bonded tendons due to corrosion has been shown to be related to the absence of grout or incomplete grouting within the duct (Woodward and Williams, 1988). Voids alone however, will not

cause corrosion unless the conditions to initiate corrosion are present as well. The second source of loss of bond is the consequence of corrosion, i.e. the partial loss of prestressing tendon area and, in more serious cases, failure of the prestressing wires or tendons.

Woolley and Clark (1993) described the design details and inspection methods of the grouting of tendons. The current requirements for grouting relies on good supervision on site to ensure properly filled ducts but, in practice, void-free grouting is often not achieved as the grouting operation is rarely up to specification. Improperly sealed joints in the ducts may allow concrete to seep into the duct, causing blockages and hindering proper grout flow. Fluidity and bleed tests are not frequent enough to provide effective control over the quality of the grout.

Field observations have shown that voids can remain within the ducts, especially near anchorages and at high points of the duct profile. The distribution of grout voids throughout the beam will determine whether the tendons act as totally ungrouted or partially grouted. If a void is continuous along the length of a tendon, the tendon can be considered to be 'unbonded' and the behaviour of unbonded post-tensioned tendons may dominate.

1.2.3 Durability of Post-tensioned Concrete Bridges

The performance in service of post-tensioned concrete bridges is generally regarded as good (Clark, 1992). Surveys of bridge durability undertaken world-wide revealed that the number of cases of serious corrosion is generally low although this could be distorted by the fact that the tendons are difficult to inspect. The problem of durability of post-tensioned concrete bridges seems more serious in the UK (Raiss, 1993) where two segmental post-tensioned bridges, Ynys-y-Gwas and Bickerton Meadows, have collapsed suddenly under their own self-weight. In both cases, the collapses were due to tendon corrosion as a result of insufficient grouting. There is a third bridge collapse in which a post-tensioned bridge across the River Schelde in Belgium collapsed suddenly due to corrosion of the post-tensioning wires.

The results of an investigation by the Transport Research Laboratory on the condition of the grout and prestressing tendons in ten bridges in situ and two demolished bridges, all

built between 1958 and 1977, were reported by Woodward (1981). The study concluded that although none of the bridges displayed any external signs of problems, voids were found in over half of the ducts examined, and in eleven of the bridges. The voids were not evenly distributed and, in some cases, were large enough to partially expose the tendons although there was no evidence of serious corrosion nor ingress of chlorides. In some of the bridges, the grout was dry and soft, but generally appeared to provide satisfactory protection against corrosion. The extent of the voids varied considerably, from being continuous over the length of the duct, to the duct being solidly grouted.

An increasing number of problems in post-tensioned bridges were subsequently found in the 1980's; this included leakage through joints, discovery of loose rusted wires near anchorages, spalled concrete, and tendon corrosion ranging from slight surface corrosion to extensive localized corrosion and fractures. In 1980, the Angel Road bridge in London was found to have broken wires due to corrosion near the anchorages, and in 1982, an inspection of the Taf Fawr bridge in Wales revealed severe corrosion of the tendons.

The most serious event which started the tendon scare occurred on 4 December 1985 when the Ynys-y-Gwas, a single-span segmental post-tensioned bridge collapsed without warning under its own self-weight (New Civil Engineer, 1985). The collapse of the 32-year-old bridge was believed to be the first collapse of a post-tensioned concrete bridge in the UK due to tendon corrosion. The bridge had been recently inspected but there was no advance warning of distress. A post-mortem revealed that the collapse was due to severe localized corrosion of the prestressing tendons at the joints, caused by chlorides from de-icing salts (Woodward and Williams, 1988). The emergence of increasing problems with grouted post-tensioned bridges was reported by Woodward (1993a). It is worrying to note that most of the problems were discovered by accident, either during minor contracts like re-waterproofing or resurfacing the bridge deck, or during demolition of redundant bridges.

Bridge deck deterioration resulting from corrosion of the prestressing steel caused by de-icing salts has also been a problem in the United States. Dickson et al (1993) reported on the condition of a post-tensioned concrete girder which had been removed from a bridge in

North Dakota after 34 years of service. The girder was generally found to be in good condition with only localized surface corrosion.

A field survey of the condition of prestressed concrete bridge elements located in adverse, potentially corrosive environments in the US was made by Whiting and Stejskal (1994). Localized corrosion of prestressing strands was observed particularly at the anchorage ends of the beams, where de-icing salts could seep through leaking joints. Corrosion affected various components of the anchorage, including end plates, bearing plates, conical wedges and stirrup steel. The results concluded that corrosion of the prestressing structures in most cases was due to poor construction practices, inattention to detail and improperly maintained joints and drainage systems. The post-tensioned bridges included in the survey revealed that, despite the severity of the exposure, the post-tensioned tendons performed extremely well, with the exception of the anchorages.

In Japan, a 20-year-old post-tensioned bridge in Osaka was reported to have suffered serious pitting corrosion to the extent that some of the post-tensioned bars had fractured and protruded through the concrete (Kobayashi et al, 1995). The bridge was subsequently repaired after regions of incomplete grouting were detected by non-destructive techniques.

The response in the UK however, has been different. Concerns over potential corrosion problems with grouted tendons and the difficulty of detecting them has forced the Department of Transport to issue a temporary ban on the commissioning of new post-tensioned concrete bridges containing grouted ducts. Instead, they have opted for the once-rejected unbonded tendon design, and insisted that tendons be inspectable and replaceable. This has been condemned by Schupack (1993), who has vast experience with corrosion of post-tensioned structures in the US, and has viewed this ban as an over-reaction.

Nonetheless, efforts have since been made to restore confidence in the construction of this type of bridge. A working party was set up by the Concrete Society and the Concrete Bridge Development Group to include the Department of Transport and the County Surveyors Society (Raiss, 1994). The aim was to find solutions to overcome some of the problems associated with grouted post-tensioned structures, with a view to getting the ban lifted. The results of the working party included a revised specification for grouting, and

recommendations for tendon protection. The progress of the working party was reported by Raiss (1995). In September 1996, the four year ban on grouted post-tensioned concrete bridges was lifted (New Civil Engineer, 1996).

Regarding the problem with existing post-tensioned bridges, Darby (1993, 1996) investigated the feasibility of strain monitoring techniques in detecting the loss of prestress as a result of tendon corrosion. The study, which was a contract to the Transport Research Laboratory, involved the monitoring of two post-tensioned bridges of similar construction in Oxfordshire, one of which has now been replaced after tendon corrosion problems were discovered.

It is feared that as a result of the emergence of problems with grouted post-tensioned bridges, some of the bridges will be prematurely condemned as soon as some deterioration is found. Demolition and replacement of all such bridges cannot be economically justified and analytical tools are urgently required in order to assist in the development of strategies for extending the life of deteriorating structures through strengthening and repair.

1.3 OBJECTIVES OF THE RESEARCH

It is evident that further research into the consequence of local loss of prestress due to corrosion, and its effect on the residual strength of grouted post-tensioned concrete bridges should be undertaken. An understanding of the general characteristics of the dynamic debonding and re-anchoring phenomenon of failed tendons is also required, so that this behaviour can be incorporated into an analytical model. This re-anchoring capability will depend on the bond conditions between the tendon and surrounding grout. The distribution of grout voids within a beam and the quality of the grout therefore needs consideration.

The effects of tendon failure in post-tensioned beams containing integral grouted tendons have been observed to vary from one structure to another, depending on the bridge deck configuration, prestressing system, and integrity of grout within the duct. This makes a prediction using probabilistic models, of the residual strength of the deteriorating bridge almost impossible. Therefore, development of analytical models which aim to provide a

basic and quantitative assessment of the problem whilst accounting for the level of deterioration discovered, is seen as the best approach.

The principal aim of this research is therefore to investigate the effect of tendon corrosion and the presence of incomplete grouting on the residual strength of deteriorating post-tensioned concrete bridges. The specific research objectives are:

- to investigate the re-anchoring phenomenon of broken wires and tendons, utilising available field data
- to study the effect of partial loss of prestressing tendon area due to corrosion
- to develop analytical models to assess the residual strength of post-tensioned concrete bridges with a number of failed wires and tendons
- to investigate repair and strengthening strategies for extending the life of deteriorating post-tensioned bridges.

The work presented in this thesis can basically be categorised into three main parts. The first part provides a background review of previous research of the tendon corrosion problem in deteriorating post-tensioned concrete bridges, and general topics related to the subject. The second part describes the development of appropriate analytical models. The final part involves validating the developed models with available experimental data of full-scale tests and then utilising them in a parametric study.

CHAPTER 2

Review of Related Literature

2.1 INTRODUCTION

This chapter presents a background review of the topics related to the problem of deteriorating post-tensioned concrete bridges suffering from tendon corrosion and incompletely grouted ducts. The aim is to provide an insight into the current knowledge in this field, which helps to identify the areas where additional work is required. The items of the review are presented only as far as they are relevant to the scope of the present study.

The need for reliable inspection methods to determine the extent of deterioration in grouted post-tensioned concrete bridges is highlighted which will enable the residual strength of deteriorating bridges to be evaluated and recommendations made for remedial work where necessary. The failure of bonded post-tensioned wires due to corrosion is not well covered in the literature but previous work into the mechanisms of the debonding process of post-tensioned tendons during demolition has provided the basis of an understanding into the debonding of tendons fractured due to corrosion. Bond between the tendon and surrounding grout, which provides frictional resistance and restraint to tendon movement thereby enabling the re-anchoring of failed tendons, is crucially important and is discussed in detail.

2.2 LIMITATION OF CURRENT INSPECTION TECHNIQUES

The methods of carrying out Special Inspections of post-tensioned concrete bridges is laid out in BA50/93 (Department of Transport, 1993). However, this is not exhaustive and it still remains difficult to assess the condition of the post-tensioned tendons or the grout using currently available inspection techniques. Specialised non-destructive methods of

inspection are often expensive yet may prove to be inconclusive as the presence of the steel duct often distorts the results. However, with careful choice of methods to complement each other, it is possible for the presence of corrosion and voids in the grout to be detected. Methods using impulse radar or radiography, coupled with the less sophisticated hole drilling/endoscopy method, have been found to be most effective (Stain and Dixon, 1993; Leeming et al, 1995). An overview of the currently available techniques to inspect post-tensioned concrete structures is presented here, and is summarised in Table 2.1. These techniques can basically be categorised into:

i. Visual inspection methods (semi-destructive)
ii. Non-destructive testing methods (NDT)
iii. Structural monitoring
iv. In-situ stress determination methods

2.2.1 Visual Inspection

Although deteriorating post-tensioned concrete structures do not demonstrate obvious signs of deterioration like spalling, discolouration or local cracking, some information can nevertheless be obtained by detecting signs of deck water leakage (Ricketts, 1993a) of vulnerable areas such as anchorage positions or joints. Limited cracking along the line of a tendon may indicate failure of strands in a partially grouted duct.

Ideally, non-destructive methods should be used for further inspection but since there are limitations to the techniques available, semi-destructive visual inspection methods are often necessary. These methods refer to the hole drilling/endoscopy technique (Woodward, 1981) which involves carefully drilling 25mm diameter holes into the duct to inspect inside it at suspect locations (e.g. low points where water may collect, high points where grouting may be incomplete) with the use of an endoscope (Figure 2.1). Although this technique is time-consuming and limited to local inspection, it is currently the single most effective way to inspect inside a duct and locate voids. However, the randomness of this technique cannot be regarded as a rigorous condition survey nor appropriate for routine inspection. Since only a limited number of holes can be drilled into each duct, there may be undiscovered voids. It is also often not possible to drill into ducts near the anchorages due to either geometric constraints, or the congestion of steel reinforcement.

Moreover, precautions must be taken to avoid damage to the tendon or bar during the drilling process. Usually, the drill is fitted with an alarm or automatic cut off to warn the operator when the duct is reached. A flat ended drill bit should be used for the final breakout to avoid damage to the tendons and to give the largest possible view of the tendons. Only a very small part of the tendon can be examined in this way and even if potential problem areas are targeted, the chances of locating them are low. Care must also be taken to select areas of the structure which would not be critically weakened by drilling, and to consider means of reinstatement where appropriate.

A vacuum or pressure test can be done at this stage to estimate the size of the void and to determine the continuity of voids within the ducts. A series of holes are drilled into the top of each duct and a vacuum is applied to each hole in turn. The pressure drop at the others gives an indication of the continuity of any voids present. The void volume can then be estimated by measuring the volume of air required to refill the void when the vacuum is released. By applying a small pressure to the duct and measuring the rate of leakage, an indication of the ease with which moisture and other contaminants can enter the duct is obtained.

2.2.2 Non-destructive Testing Methods

In employing NDT methods to determine the integrity of the tendon or grout, the steel duct encasing the tendons often acts as a barrier, severely limiting the value of most NDT methods. Only a small part of the structure can be examined and the results are often difficult to interpret.

Although the application of electro-potential measurements and resistivity measurements are successful in assessing levels of corrosion in reinforced concrete, their application to post-tensioned concrete is limited due to the presence of the metal duct (commonly used in post-tensioned construction) which inhibits proper electrical contact with the prestressing tendon (Bungey, 1993). In the former method, the tendon may not be embedded in an electrolyte where grout voids are present, which is precisely where more information is required to indicate any increased risk of corrosion.

A magnetic technique is claimed to be able to detect flaws in post-tensioned tendons (Ghorbanpoor and Shew, 1989). A steady magnetic field is applied to the concrete and any presence of defects in the tendons will cause disturbances in the magnetic field, which can be detected by Hall effect sensors. However, the results can be complicated by layers of signals from individual tendons and sometimes masked by secondary reinforcement (e.g. stirrups).

The NDT techniques which have been found to be most suitable for post-tensioned concrete are the electromagnetic radiation methods of radiography and impulse radar (Leeming et al, 1995; Williams and Hulse, 1995). In radiography, gamma rays or X-rays are used to produce radiographs through the structure (Figure 2.2) where an image of the interior of the concrete is produced, illustrating high-density material (prestressing steel) or low-density areas (voids). Areas of variable compaction in the concrete or voids within the grout can hence be detected. This method has been found to be the most successful NDT method for locating ducts and detection of voids. The disadvantage is that this method is very expensive and impractical; it requires long exposure times and the radiation presents a potentially dangerous health hazard at the time of operation. In addition, both sides of the member must be accessible.

In impulse radar, a high frequency electromagnetic pulse is transmitted across the concrete surface adjacent to where a tendon is expected to be. The pulse, upon reaching boundaries between electrically contrasting layers (e.g. concrete/steel, concrete/void) is partially reflected back to the source and partially transmitted through the interface. A 2D image of the structure is thus produced upon repeated transmission and recording of pulses (Williams, 1993). Large areas can be scanned quickly, but the fuzzy nature of the resulting radar profiles requires interpretation by an expert. Although the transducers do not require direct contact with the structure, this technique cannot be used to detect voids or corrosion in metallic ducts because the sheathing will either reflect or absorb energy in the radar wave (Forde and McCavitt, 1993). However, radar can be used to locate the position and depth of tendon ducts to a high level of accuracy for further intrusive surveys, and to detect damp areas in a structure, an indicator which may well reveal corrosion (Woodward, 1993b).

The pulse transmission methods (Impact-echo, Ultrasonic pulse velocity) work on the principle of the measurement of force and velocity signals upon transmission of a short duration pulse within the concrete. The Impact-echo method appears promising as, when used with more sophisticated equipment to analyse the frequency response due to a mechanical impact (by an instrumented hammer), it is able to detect voids in metallic tendon ducts (Carino and Sansalone, 1992). However, this method was reported to be unable to transmit signals further than 0.5m from the source (Williams, 1993). Moreover, although it can locate a void, it cannot determine the size of the void.

Additional research has since been undertaken to fully understand the impact echo response of grouted tendon ducts and to develop a reliable method to inspect grouted post-tensioned structures. The basic principles of the impact-echo method are described in detail by Jaeger et al (1996). The results from a finite element study, laboratory study and a supporting field study were also reported. Three-dimensional dynamic finite element analyses were performed to study the response of fully grouted, partially grouted and ungrouted tendon ducts to transient stress waves. The analytical and laboratory work showed that the impact-echo method can be successfully used to detect both complete and partial voids in grouted ducts. Typical impact-echo response from both grouted and ungrouted tendon ducts were presented (Figure 2.3). It is the difference between the frequency of displacements due to reflection from a concrete/steel interface vs. the reflection from a concrete/air interface that enables the voids in the ducts to be detected.

In the field investigation of an existing post-tensioned bridge, the test was performed as a blind study in which the extent of grouting in the ducts was unknown before testing. After the tests were completed, the results were confirmed by opening the ducts to visually inspect it. It was found that the impact-echo method correctly located the fully grouted, partially grouted and ungrouted ducts, which demonstrates that it can be used to detect voids in grouted ducts of existing post-tensioned members. In the case of the partial void, the results showed the presence of an air void but it was not known that it was a partial void until the duct was opened. A portable system comprising a hand-held unit with an impact source and transducer, and a portable computer for data acquisition and signal processing was used for performing the field work. This system is now commercially available (Jaeger et al, 1997).

Martin et al (1995) reported on a finite element investigation to indicate the size and depth of voids that should be detectable with the impulse-echo method. It was found that the size of the void can be estimated by comparing the frequency of the reflection from the base of the beam with that from a solid concrete beam. The larger the void, the lower the frequency of the reflection from the base of the beam. It was also shown that the shorter the contact time of impact, the smaller the defect that can be detected. In addition, the thin steel ducting was found not to affect the detectability of voids but care must be taken when deciding on the contact time of the impulse when used to detect circular defects.

In the measurement of ultrasonic pulse velocity, results can be masked by the presence of reinforcement and multiple reflections within the concrete at the interface with the aggregate particles (Woodward, 1993b). However, recent work has shown that it is now possible to obtain information from voided regions of a duct by using frequency domain digital signal processing techniques. A track mounted ultrasonic scanning system CANDI (Cable Analysis by Non-destructive Inspection) has been developed (Duncan et al, 1995). The system is used with a laptop equipped with a software which enables the operator to monitor the signals, position the transducers, carry out automatic scanning and process the data. The received signal (which is analysed in the frequency domain) is dominated by grain noise from the aggregate, and in the absence of voids the level of each spectral component varies randomly. However in the area of a void, the concrete/void interface is a reflecting surface and behaves as a secondary source of ultrasound. When a test beam with three 50mm diameter steel ducts containing combinations of tendon fractures and voids was scanned by this system, the study showed that it was possible to identify the location and length of the voids within the steel ducts.

2.2.3 Structural Monitoring

As shown in Table 2.1, the methods available for the structural monitoring of post-tensioned concrete bridges are (i) vibration measurement, (ii) deformation monitoring, (iii) acoustic emission, and (iv) strain measurement.

Measurement of the dynamic characteristics of a structure is based on the principle that each bridge has a unique natural frequency depending on its mass and stiffness, which will change if some deterioration occurs. However, this method of vibration measurement is

unsatisfactory since it is stiffness and not strength that is measured. Any loss of prestressing force due to corrosion or tendon failure which may result in some reduction in strength but insignificant loss of stiffness, will be difficult to detect by measuring the frequency response of a structure.

Even under the full service loading, a post-tensioned concrete section is still mainly in compression and a significant tendon area loss is required before the initial prestressing force is reduced to levels such that decompression or cracking of the concrete occurs. As a result, any increase in deflection and surface strains due to general corrosion will not be as easily detected as for reinforced concrete. Deformation monitoring may not be useful since any increased deflection resulting from corrosion or tendon fractures is extremely small and may be masked by changes due to temperature or concrete creep and shrinkage. Even a significant loss of tendon area due to corrosion may not reveal much evidence of cracking or increased deflection.

Load testing to determine the residual strength of post-tensioned bridges is potentially dangerous since it will not reveal any significant increase in deflection nor indicate any inherent problems unless a large proportion of the tendons have corroded or failed (Waldron, 1993). By then, the strength of the bridge suffering such a substantial loss of steel area would be seriously reduced and testing in this condition may well precipitate collapse of the bridge. Deflection monitoring to detect local tendon failures is thus inappropriate as there will be no significant reduction in overall beam stiffness prior to collapse. This also means that deformation monitoring to detect local loss of prestress due to corrosion which has not resulted in tendon fractures yet, is unlikely to be conclusive.

The third method of monitoring involves acoustic emissions (AE) which are produced as materials deform and part of the stored strain energy is released as mechanical or stress waves. Acoustic energy can be released as a result of cracking, corrosion or wire fractures. AE waves propagate through concrete and can be detected on the surface by an AE sensor which converts the vibrations into electrical signals. However, monitoring of a structure for pulses generated within it is unlikely to be useful as experience shows that it is difficult to detect single wire fractures, and distinguish them from other sources of noises.

Long-term monitoring of post-tensioned bridges by strain measurements to identify any future loss of prestress due to corrosion has been undertaken for structures with suspect durability. Since any local loss of prestress normally only results in a relatively small redistribution of the concrete compressive stresses locally around the defect, conventional methods of strain monitoring are unlikely to reveal any gradual deterioration due to loss of tendon area as the resulting extreme fibre strain changes are likely to be small (less than 100μm/m). However, measurements of strains to detect loss of prestress still appears to be the most promising structural monitoring method available. The ability to monitor large areas is desirable when assessing the condition of large structures such as bridges. Conventional vibrating wire strain gauges have been used for strain monitoring but this is limited to point-by-point measurement, which is not ideal when critical positions are not exactly known.

The use of optical fibre sensors for strain monitoring of post-tensioned concrete bridges was introduced in the UK through a German company called Sicom (Dill and Curtis, 1993). The method works on the basis that light transmission through an optical fibre is reduced when microbending occurs (Figure 2.4). By comparing the intensity of light emerging from the sensor as it is strained to the amount of light supplied, the increase in length of the sensor is determined. In view of the difficulties in locating corrosion, this technique appears more superior to conventional strain gauges as it enables strain measurements over long gauge lengths whilst enabling continuous and long-term monitoring. To monitor existing bridges, the sensors are usually externally attached to the structure at nodal points typically 1m or 2m apart. These sensors measure total concrete strains between their fixed end points, which means that any strain changes will be averaged over the whole gauge length. Vibrating wire gauges will therefore be more sensitive if a sufficient number is used. In both types of sensors, however, there is still the possibility that any change in strains due to loss of prestress will be disguised by other events such as the passage of heavy vehicles, diurnal temperature changes, or drift in the instrumentation system itself.

The feasibility of monitoring with optical fibres was investigated by Oxfordshire County Council on beams removed from the A34 Botley Flyover, where various methods of inspection and strain monitoring techniques were used (Darby, 1996). This study is

described in Chapter 3. The aim of the investigation was to assess the suitability of strain measurement as a means of identifying deterioration in post-tensioned bridges. Optical fibres were also used in the long-term monitoring of a nearby bridge of similar construction (Darby, 1993) where some of the results were found to correlate with those produced by vibrating wire strain gauges. The first study, which involved measuring strain changes as a result of total tendon failure being simulated, demonstrated that it is possible to detect tendon failures by strain monitoring, at least in the short-term. Concrete extreme fibre strain increase of about 80μm/m was recorded by the fibre optic sensor due to cutting one out of five of the tendons at quarter span. However, the main problem was distinguishing these strains from the effects of diurnal temperature changes. The vibrating wire strain gauges recorded temperature drifts of up to 50-100μm/m, and a similar magnitude was experienced by the fibre optic sensors. Although the optical fibre sensors have a low coefficient of thermal expansion, thermal effects induced in the concrete still had to be compensated for.

It remains doubtful if strain monitoring is able to pick up events such as general corrosion which has not caused tendon fractures yet. The extreme fibre strain changes which result may be extremely small (of the order of 10μm/m) as well as difficult to distinguish from other effects. For example, due to the passage of a 30-tonne vehicle over the Botley Flyover, an average strain of 8μm/m was recorded by a 6m length of optical fibre sensor. Although this correlated with vibrating wire strain gauge readings, it demonstrates the difficulty of discriminating this type of strains from those produced by loss of prestress due to corrosion. In order that these latter events can be detected, the accuracy and sensitivity of these fibre optic sensors still needs improvement, particularly its long-term drift characteristics and its sensitivity to temperature changes.

Merzbacher et al (1996) addressed the practical and logistical challenges of the implementation of fibre optic sensors to civil engineering structures. Localized sensors can only detect strains locally around the sensor and as with conventional strain gauges, require a large number of sensors to monitor a large area. In the fibre optic sensors marketed by Sicom, the sensing system is distributed along the length of the fibre, enabling a relatively large area to be monitored thus requiring fewer sensors. However, the location of any strain changes cannot be determined unless an additional probing method

like optical time domain reflectometry (OTDR) is used. Thus, although it responds to strain applied anywhere along the length of the sensor, it cannot locate the position where the strain is actually occurring. This distribution of strain can be obtained by using a high-resolution OTDR unit to locate reflective points along the fibre, but this is unsatisfactory since the reflections allows the positions of attenuation to be located only within ±0.75m. Since the strains are measured over gauge lengths of several metres, it is the integrated strain over several metres that is measured. Improvements are hence required before this long gauge length fibre optic sensing system can be useful.

The Sicom sensors are also intensiometric sensors, which depend on the amount of light detected through the fibre. These intensity-based microbend sensors have very limited sensitivity, accuracy, precision and range of detection (Merzbacher et al, 1996). In addition, many other phenomena that are unrelated to strain can also cause attenuation. Often, a single break in the optical fibre renders most of its sensing ability as ineffective. It is suggested that interferometric sensors are more suitable for measuring strains over long gauge lengths, although there has been report of its long-term drift due to temperature variation and creep. A third and most attractive type of fibre optic sensor is the fibre Bragg grating where strain is detected as a shift in the wavelength of the reflected light. This type of sensor has the distinct advantage that the sensed information is encoded directly into wavelength, which is an absolute parameter and is not susceptible to instrumental drift. The output does not depend on the total light levels, losses in the fibres or recalibration of the system.

The success of a practical fibre Bragg grating sensor system lies in the development of instrumentation capable of determining the relatively small shifts in wavelength induced by strain or temperature changes in these sensor elements. Due to their ease of multiplexing (quasi-distributed), this type of sensors was used in the multi-point strain monitoring of a full-scale bridge with artificial defects (Kodindouma et al, 1996). The main disadvantage of this type of sensor is its undesirable temperature sensitivity, which may negate its use as a strain gauge. From a single measurement of the wavelength shift, it is difficult if not impossible to differentiate between the effects of changes in strain and temperature. Xu et al (1994) suggested that these effects can be distinguished by

simultaneous measurement of strain and temperature using two superimposed fibre gratings with different Bragg wavelengths.

Optical fibre strain sensors have also been incorporated into new bridges, producing a 'smart' monitoring system with built-in intelligence for continuous bridge surveillance. The system can be connected remotely to the office and set up to give automatic warning signals and remote observations of the deformation of a bridge. Moser and Roner (1994) reported the implementation of this system on the Noetsch bridge, the first bridge in Austria with glass-fibre composite prestressing tendons. The authors reported a small but continuous increase of the optical fibre strains. This was attributed to the effect of temperatures over the 4 minute monitoring period, hence re-iterating the point that temperatures can affect the results of any long-term strain measurements.

Nevertheless, the inherent advantages of optical fibre sensors over conventional sensors, and their potential in smart structure applications, warrant further research to develop the current systems to become more practical and useful for long-term strain monitoring of concrete structures. The characteristics desirable in a fibre optic sensor to serve such a purpose include the following:

- stable
- localized
- adequate sensitivity
- insensitive to thermal fluctuations
- capable of absolute measurement
- immune to power interruption
- easy to mass produce
- durable (as a permanent monitoring system)
- low cost

At present, there is no single fibre optic sensor which fulfills all the above requirements. Optical fibre sensor technology has yet to be developed to its full potential and further sensing parameters are under consideration, including improvements to the existing ones to give better resolution and stability. The Sicom sensors are representative of the earlier types of fibre optic sensors. These early applications utilize simple intensity-based sensors,

but attention has since focused on interferometric and fibre Bragg grating systems which may be more promising (Measures et al, 1995). However, the challenges of the implementation of a fibre optic network as a routine strain monitoring tool still remain. The main issues requiring attention include the development of more sensitive distributed fibre optic strain sensors, and improved signal and data processing software to detect events due to corrosion and distinguish them from those due to temperature effects or heavy vehicle movements. Since the unit is intended for field use, a method to filter temperature drifts is required. Due to the wealth of data collected, sophisticated data acquisition equipment is required for careful handling, analysis and interpretation of data, and transmission of data from site to the client's office. Research is needed to establish the most suitable type of optical fibre sensor system which can fulfill the requirements for precision measurements, reliability, long-term performance and durability under such harsh external environments.

2.2.4 In-situ Stress Determination Methods

In a different classification of inspection techniques, in-situ stress determination methods have been used to determine existing stresses in a structure. These methods are not intended as alternatives to tendon inspection but more for assessment and rehabilitation purposes (Ricketts, 1993b). They all work on the principle of strain distribution due to local strain relief achieved semi-destructively through incremental coring, thereby enabling the direct measurement of the residual stress in a structure.

The more commonly used methods are the incremental coring technique (Brookes et al, 1990) which uses a rosette of eight vibrating wire gauges attached to the concrete prior to coring; and the centre hole/stress relief technique (Owens, 1993) which can determine the in-situ stresses in the reinforcement and prestressing tendons, by drilling a small hole (about 1.6mm diameter) to relieve stresses. Drilling the small hole is semi-destructive but the reduction in cross-section is small (8% for a 5mm diameter wire, and 4% for a 7mm diameter wire) and the loss of strength in one or two wires of a seven-wire strand or a twelve-wire tendon is not critical. However, these isolated stress measurements are unsatisfactory as they do not provide a complete or conclusive survey of the structure. The method also requires that the tendon/reinforcement be exposed before measurements can be taken. There is still a significant risk to the integrity of the tendons tested and the

method only provides a snapshot of the local conditions prevailing in the structure during the test. The measurements also include the locked-in manufacturing stresses from the wire drawing process, which can be accounted for either by repeating the test on an unstressed wire or by estimating the manufacturing stresses.

The other disadvantage is that only a partial relaxation of the strains may occur when the hole is formed, resulting in less strain relaxation detected. Any small errors in the measurement of the strains or forming of the hole, which is partly dependent on the varying skills of the operators, can have significant effect on the accuracy of the results. In addition, temperature increase during the coring process, which can be attributed to worn out or damaged drill bits or poor control of the supply of cooling water or the applied pressure, can affect the strain measurements. The total strain release may also include a combination of other effects such as stresses due to time dependent effects, presence of already-existing microcracks in the concrete, and temperature changes due to the environment. Hence any (small) in-situ stresses released due to prestress losses, may not be detected altogether. For example, in the assessment of the residual prestress in a continuous multi-cell concrete bridge, consideration had to be given to secondary structural effects such as temperature gradient in the box sections, transverse stresses caused by connections between adjacent sections, and the original construction sequence which may affect the secondary stress conditions and redistribution of loads.

2.2.5 Conclusions on the Most Effective Inspection Techniques

Neither hole drilling nor any other method will detect broken wires unless the fractures occur within the field of investigation. The exploratory hole drilling technique is the most direct and practical method of visually inspecting post-tensioned ducts but the main problems are:

- identifying where to drill as finding a fully grouted duct in one area does not necessarily mean that it is grouted and corrosion-free elsewhere
- the impracticality of drilling into all the ducts
- the risk of damaging the tendons during the drilling process

Radiography may be useful to inspect a fairly small area to reveal the location of ducts and detect voids in the duct. However, the definition may be poor and the method is expensive

as well as requiring strict safety precautions. Radar can successfully locate ducts but the current equipment cannot be used for detecting voids in metallic ducts.

Recent developments and improvements in the Impact-echo and Ultrasonic pulse velocity methods have provided a reliable and effective way of detecting voids in grouted post-tensioned members. These methods are also becoming more commercially available.

Structural monitoring by strain measurements to detect deterioration in post-tensioned bridges appears promising, but further developments are required before the method can become a feasible long-term strain monitoring tool to detect future loss of prestress due to corrosion. The currently available distributed fibre optic strain sensors which are based on intensity variations due to microbending losses, are not sensitive enough since they are unable to locate the position of strain change over their relatively long gauge lengths. Thus they are only likely to detect events such as tendon failures, but not general corrosion. Furthermore, the development of more sophisticated data processing software is required to differentiate these strains from other effects and to filter out temperature drifts.

In-situ stress determination methods can determine the residual stresses in a structure but again, the method is limited as a large number of tests would be required to give a representative distribution of stress along the beam. Moreover, the results can be affected by many other factors like errors during strain measurement, the drilling/coring process, and external temperature effects.

2.3 EXISTING METHODS OF RESIDUAL STRENGTH EVALUATION

Only limited attempts have been made to determine the residual strength of deteriorating post-tensioned concrete bridges, and most of these have been empirical. Most of the methods proposed so far to provide a quantitative assessment of the residual strength are based on expert systems and probabilistic methods (Andrade et al, 1989; Vrouwenvelder, 1993; Gao, 1993; Nowak, 1993).

Re-analysis of existing structures against new codes can reveal major deficiencies as the reinforced and prestressed concrete design rules in the limit state codes have changed significantly. One solution to this is to adopt alternative methods of analysis or employ reliability methods (Pritchard and Chubb, 1987). However, although the tendon corrosion problem is of a random nature, and some level of risk assessment is undoubtedly required, structural collapse cannot be ascertained by risk analysis alone. The few reported investigations into an analytical assessment of the residual strength of deteriorating post-tensioned concrete bridges have either used the grillage method of analysis or finite element analysis.

Woodward and Williams (1988) described the re-analysis of the collapsed Ynys-y-Gwas bridge (Figure 2.5). The simply-supported 18.3m span segmental bridge was longitudinally and transversely post-tensioned. The tendons comprised twelve 5mm diameter wires. A grillage analysis was carried out under both contemporary and current code requirements in order to assess the effects of transverse distribution of dead load and live load (HA and/or 25 units of HB). It was estimated that the residual prestressing force was 35-52% of the ultimate tensile strength of the tendons. The analysis revealed that shear capacity was marginally insufficient, but the bending capacity was very much less than the current code requirements and also possibly below contemporary requirements. The effect of the loss of a whole tendon within the central I-beam was simulated by applying an equal and opposite force to that applied by the tendon. This increased the bending moment at midspan of each beam by only 10kNm. Similarly, the loss of a whole tendon within an outer I-beam increased the bending moment of that beam by 30kNm and finally, failure of all the tendons in an outer I-beam increased the bending moment in the adjacent beam by about 40%. This suggests that progressive collapse can be caused by the transfer of load from the failed beam to adjacent beams, thus overloading them.

This study was preceeded by a finite element analysis of the edge beams that were left standing after the failure of the bridge (Woodward and Wilson, 1991). It formed part of a study commissioned by the Transport and Road Research Laboratory to determine if tendon failures in segmental structures can be detected early by monitoring structural deformations as prestress is lost. It also aimed to quantify the following:- degree of cracking, joint opening, level of deflection during service, and possible reduction in

strength as a result of loss of prestress. Load tests to failure of the edge beams had earlier been carried out in a separate study (Woodward, 1989). The beams were 19.6m long and were made up of eight 2.4m long segments, post-tensioned longitudinally by ten tendons, each consisting of twelve 5mm diameter wires.

In the analytical work, the LUSAS finite element program was used to develop models of the edge beams and the results were calibrated against experimental observations. The modelling work attempted to reproduce the deformation of the beam at all stages of loading from dead load only to failure. The effects of loss of prestressing area due to corrosion was also studied. The limitation of the model was that a single bar was used to represent the total prestressing tendon area at each level in the beam (Figure 2.6). Average properties, prestressing force and extent of corrosion had to be assumed, which meant that the whole of each tendon (or all of the tendons within the same level) would fail at the same time. This was partly resolved by using 'softening' material properties, allowing for progressive failure of individual wires or tendons within a tendon group. In addition, because the modelling was carried out in 2D, it was not possible to model the complex 3D behaviour of bond between concrete/grout and the prestressing tendons. Non-linear joint elements with a high elastic stiffness and a specified yield value to set a limit on the bond stress (Figure 2.7) were used to reproduce the effects of bond failure.

The sensitivity analyses revealed that the bond strength between the tendon and concrete/grout affects the slope of the moment-deflection curve, and the amount of prestressing force in the tendons affects the load level at which the moment-deflection behaviour of the beam first becomes nonlinear.

In assessing the response of a beam with different corrosion levels, the authors suggest that a distinction should be made as to whether the tendon failed or not as a result of corrosion. If no failure occurred (partial loss of area in a tendon), redistribution of the prestressing force that was in the corroded section is possible and equilibrium is restored by slight expansion of the precompressed concrete. In this case, the significant effect is the amount of stress increase in the tendons, as this affects the additional load that the tendon can carry. If tendon failure occurred, then prestress is lost over a substantial length as

debonding occurs. Considerably more extension of the precompressed concrete is required to restore equilibrium.

The study concluded that the deformation of a beam with no tendon fractures is almost independent of corrosion until collapse is imminent, although its capacity may be significantly reduced. It is only for corrosion involving tendon failures that deformation monitoring may indicate signs of distress, especially if the bond strength is weak, which results in increased debonding of the failed wires and thus increased deflection. This study confirmed that deflection monitoring to detect local loss of prestressing tendon force in grouted ducts will not be preceded by readily measurable deflections as there will be no significant loss in overall stiffness prior to collapse.

Shenoy and Frantz (1991) reported on the structural tests of two precast, prestressed concrete beams removed from the Walnut Street Bridge which was replaced in 1987 after deterioration and corrosion of the prestressing strands were found. The 16.5m simply-supported bridge was made up of 13 prestressed concrete box beams which were post-tensioned laterally. The main object of the study was to assess the effect of 27 years of service on the strength of the beams. It was originally intended to correlate the observed amount of deterioration with the residual beam strength, but this was not possible as the badly deteriorated beams could not be removed safely intact. The two beams tested under third point loading represented a beam at the centre of the bridge, and one located beside the most badly deteriorated beam. Both beams displayed ductile behaviour and produced similar results although the latter beam was more deteriorated. The methods of strain compatibility and moment-curvature analysis adopted were found to accurately predict the beam behaviour. Despite some deterioration, the measured ultimate flexural strength still exceeded the required strength at factored loads.

The effect of loss of reinforcing steel area on the flexural behaviour of *reinforced concrete* beams was studied by Ting and Nowak (1991) who developed an analytical model based on conventional bending theory to predict the flexural capacity of such deteriorating beams. Although the algorithm was generally more simplified than that for prestressed concrete, the procedure was basically the same. Material stress-strain relationship was based on Hognestead's model for concrete and an elastoplastic model for the

reinforcement. A linear strain distribution across the section depth was assumed (plane sections remain plane after bending). The neutral axis position was calculated by an iterative procedure until force equilibrium was achieved within an acceptable tolerance. This involved the use of the finite difference method to evaluate the integrals for calculating total compressive force in the concrete. The moment-curvature relationship for a typical concrete bridge T-beam of span 30m was predicted for the effect of loss of reinforcing bar area. The study demonstrated a linear relationship between the amount of steel area loss and reduction in the beam flexural strength.

Tabatabai and Dickson (1993) reported on the structural evaluation of a 34-year-old precast post-tensioned concrete girder which had been removed from a bridge in North Dakota, USA. The girder, of AASHTO Type II cross section, with a span of 12.9m, was post-tensioned with two tendons each comprising 12 No. 0.25" diameter wires and one comprising 16 No. 0.25" diameter wires. The beam was tested under two point loads within a constant moment region. The RESPONSE computer program developed by Collins and Mitchell (1991), which is based on strain compatibility methods of analysis, was used to predict the moment-curvature diagrams, with and without tension stiffening effects. When tension stiffening was considered, the average tensile stress in the concrete f_c, was estimated by

$$f_c = \frac{\alpha_1 \alpha_2 f_{cr}}{1 + \sqrt{500 \varepsilon_{cf}}} \qquad \text{.....(2.1)}$$

where α_1 = factor accounting for bond characteristics of reinforcement

α_2 = factor accounting for sustained or repeated loading

f_{cr} = tensile strength of concrete

ε_{cf} = concrete strain

A parallel study of the corrosion assessment of the girder by non-destructive testing and dissection of the girder to determine the condition of the post-tensioned wires and duct was reported by Dickson et al (1993). The girder was found to be in good overall condition with only localized surface corrosion of the tendons, interior of the duct and anchorages.

The analytical predictions by the RESPONSE program showed very good agreement with the measured results. The calculated moment-curvature response with tension stiffening

predicted the actual behaviour quite well in the cracking moment region, while the response without tension stiffening represented the behaviour better when the section was near failure. This is expected, due to the reduced contribution of the tension stiffening effect near failure as more cracks develop in the tension zone. The measured failure load was comparable to the predicted values, suggesting that the beam had not deteriorated significantly such that its ultimate strength was compromised.

2.4 FAILURE OF WIRES IN POST-TENSIONED CONCRETE

2.4.1 Controlled Demolition of Full-Scale Structures

Previous work into the mechanisms of the debonding process of post-tensioned tendons during demolition has provided the basis of an understanding into the debonding of tendons fractured due to corrosion. Research in this field materialised through concern over the possibility that large amounts of strain energy which is stored in the stressed tendon may be suddenly released upon cutting of the tendons during demolition of prestressed concrete structures.

Past investigators have highlighted the inherent dangers of demolishing grouted post-tensioned structures, particularly when the grout is defective (Lindsell, 1985; Belhadj et al, 1991; Belhadj and Waldron, 1992). Due to the concentration of the total prestressing force into a small number of large diameter tendons, the demolition of grouted post-tensioned beams is difficult and potentially dangerous as the relatively small effective bond area may not be sufficient to resist the bond stresses set up during movement of the tendons. If the grout is defective, insufficient bond between the tendon and the concrete may encourage a more violent release of tendon energy and increase the risk of tendon ejection from the beam. In contrast, large movement of tendons during demolition of pre-tensioned concrete is improbable because of the high ratio of surface area to cross-sectional area provided by the larger number of small diameter tendons.

Very little research has been carried out in the demolition of bonded post-tensioned concrete structures. The research work reported by Lindsell and Buchner (1975-1988) was limited to in-situ monitoring of a small number of post-tensioned beams, but this has

provided valuable information on the magnitude of tendon movement and the parameters affecting the behaviour of the structure when the tendons are cut. The early work by Lindsell (1975) emphasized the need for a well-defined demolition procedure before post-tensioned structures can be safely demolished. This was demonstrated in the demolition of a three-span segmental I-beam bridge with a composite prestressed deck slab which was suspected to have insufficient grout in the ducts. As each tendon was being burnt through, the last few wires snapped so that a sudden release of energy created shock waves which were felt and heard. The cable ends moved apart as the bond with the grout failed and longitudinal cracking appeared along the line of the duct. However, some force still remained in the end segments as there was no movement of end anchorages. Although the effect of cutting the tendons was undoubtedly transmitted through the adjacent deck in the form of an impact force, there was no obvious signs of damage or worsening of cracks in the other beams.

Felstead and Lindsell (1981) reported on the controlled demolition of a 10-year-old bonded post-tensioned beam. The beam contained ten CCL tendons, each comprising 12 No. 7mm straight wires, arranged in two groups of five on each side of the beam. As prestress was released, there was progressive increase in the strain energy in the remaining tendons as they took over the role of the severed tendons. No shock loading was experienced as the wires were severed, since the surrounding grout was sound and provided good restraint against tendon movement. Prestress losses as high as 50% were estimated, which is more than twice the original design value. Although the tendons were cut in a symmetrical sequence, it was observed that eccentric forces existed, indicating that possible sideways failure can occur as a result of the lateral bending effects.

Lindsell (1985) stressed that prior knowledge of the original design principles and construction sequence is essential in planning the demolition procedure. This knowledge would also help dictate the choice of demolition tool to be used. It was concluded that the prestress force can be safely released by burning and cutting the tendons. This was confirmed by Lindsell and Buchner (1987) in a technical note in which they addressed the long-term prestress losses, and the performance of different methods of cutting or breaking up prestressed sections. The thermic lance proved to be both safe and economical, and the technique of water-jetting was found suitable for precise cutting.

2.4.1.1 Evidence of Tendon Re-anchoring

Buchner and Lindsell (1987) described the monitoring during controlled demolition of three post-tensioned and one pre-tensioned structures. Surface measurements were made of the concrete strains released along the line of the tendons. These results yielded important information on the debonding characteristics of the prestressing systems and were also useful in indicating the damage that might be caused to a structure suffering from partly or wholly corroded tendons.

The authors reported evidence of failed tendons re-anchoring back into the surrounding grout, the extent of which was found to depend on the size of the prestress force released, the integrity of the surrounding grout, and the presence of shear reinforcement. Figure 2.8 illustrates the initial high tensile strains associated with release of tendons in two post-tensioned beams, which rapidly decreased and became compressive strains as the tendons re-anchored back into the grout. Debonding confirmed by cracking along the line of the duct, occurred over lengths of 1-3m in the case of relatively good grouting. The difference in debonding length was attributed to increased quantities of shear reinforcement provided by BS 5400 in the Abercynon beam as compared to the provisions of CP115 in the Basingstoke beam. The increased quantity of steel contained the large bursting forces in the Abercynon beam and prevented severe cracking near the cut point. Figure 2.9 illustrates the debonding pattern on cutting one tendon in the Orpington beam. The tensile strains did not become compressive, indicating incomplete re-anchoring of the cable within the section monitored. Records showed that the original grouting operation had been difficult (limited space within square ducts) and hence inadequate grout was the main cause for the extensive debonding. This demonstrates that where grouting is inadequate, friction between wires or strands alone may not be sufficient to prevent rapid release of the energy in a severed tendon.

More recently, Darby (1996) investigated the extent of tendon re-anchoring in full-scale post-tensioned beams removed from the demolished Botley Flyover in Oxford, where a wide range of tendon corrosion and grouting conditions was identified during inspection after demolition. The object of the study was to determine if local tendon failures can be detected by strain monitoring, and to investigate the re-anchoring of failed tendons under different grout conditions. The beams contained five post-tensioned tendons, each

comprising twelve 7mm individual wires. Tendon fracture was simulated by cutting or coring through individual tendon groups at the quarter point position whilst monitoring the resulting concrete and tendon strains. Details of this investigation will be discussed in Chapter 3. The study revealed the ability of failed tendons to re-anchor even in the presence of some voids.

2.4.1.2 Factors Affecting the Extent of Debonding

The literature demonstrates that the main forms of structural damage as a result of rapid release of the stored tendon energy are: (i) significant debonding of the tendon on either side of the cut point, (ii) longitudinal splitting of the concrete member, (iii) bursting of the end anchorages and (iv) possible unsymmetrical lateral bending of the member leading to uncontrolled collapse.

It was believed that although a severed tendon may not debond completely, it may release the prestress force for a distance of up to 5 to 10 metres, depending on the size of the force and restraint provided by the surrounding grout and tendons (Lindsell, 1985). The debonding measurements obtained in the full-scale tests by Buchner and Lindsell (1987) also demonstrated that provided the grouting in a tendon duct is sound, the most important parameter controlling damage and debonding length is the quantity of shear reinforcement around the cut point. Therefore, the degree of bond provided by the local condition of the grout, internal friction between individual wires or strands within a tendon, and the level of confinement provided by shear reinforcement are the main factors controlling the debonding of a fractured tendon.

2.4.2 Investigation into the Cutting of Grouted Post-tensioned Tendons

Further understanding of the dynamic debonding mechanisms associated with failure of bonded post-tensioned tendons was provided by Belhadj (1995) who performed an analytical and experimental investigation into the cutting of grouted post-tensioned tendons. An analytical model was developed with the DYNA3D finite element package to compare the predicted response of the post-tensioned beams with results from laboratory tests carried out on instrumented beam models.

Guidelines from the results of a series of preliminary tests were used to design the main testing programme (Belhadj et al, 1991). Generation of a measurable stress wave along the bar, a significant level of cracking in the test specimen and a safe testing environment were the main factors dictating the design of the main series of experiments.

Belhadj and Waldron (1992) reported on laboratory tests which were carried out on six beam models to simulate the cutting of grouted prestressing tendons during demolition. Tests were performed on a series of 20mm diameter Macalloy bars (2m long) having different surface finishes and cast in different grout types and strengths. The bars were stressed to 200kN and were either smooth, knurled or completely threaded, in either a weak cement grout or a relatively strong cement and sand mortar. The whole cutting mechanism and loaded specimen were placed within an enclosed rigid frame to ensure a safe cutting procedure. The authors observed that on cutting the loaded tendon at one end of the specimen, an elastic stress wave was generated. This supported an earlier study by Williams and Waldron (1989a, 1989b) on the cutting of *unbonded* post-tensioned tendons within a greased sheath. The sudden release of energy results in the formation of an axial stress wave which propagates along the tendon from the point of release. A large amount of this energy is dissipated in the debonding process. Belhadj and Waldron (1992) concluded that the two main energy dissipating mechanisms limiting longitudinal tendon movement are:

i. friction between the tendon and the grout
ii. cracking of the mortar surrounding the bar, the degree of which depends on the grout and bar type used.

The experimental results showed that appreciable slip occurred in the case of the smooth bar cast in a weak cement grout, but slip was more limited in the bar cast in stronger mortar. In the case of knurled and threaded bars, response was characterised by crushing of the beam specimens at the remote end, with more severe crushing experienced in the cement grout. This behaviour was due to the high friction provided by the rough surface of the knurled bar, and the mechanical wedging effect of the threaded bars. The study showed that although weakened by cracking of the grout around the smooth bar, resistance by friction between the grout and steel still appeared effective in restraining the tendon movement after bond failure.

This study highlights the importance of bond between the tendon and surrounding grout in providing frictional resistance and restraint to tendon movement (slip) in the event of tendon failure due to corrosion. If the grout is defective, the resultant bond stresses may be sufficiently high as to permit tendon slippage and excessive debonding.

A subsequent paper by Belhadj and Waldron (1993) reported on tendon re-anchoring behaviour after debonding, which was evidenced by presence of the residual tensile strains. The axial strain distributions illustrated the progression of debonding as the stress wave travelled along the tendon length. Compared to the smooth bars, both the knurled and threaded bars demonstrated limited debonding lengths and a greater degree of cracking and crushing of the grout specimen. This was due to higher friction provided by the roughness of the knurled bar and the threads of the deformed bar. The study concluded that demolition of grouted post-tensioned concrete structures is unlikely to result in excessive tendon movement, provided the grout is sound along the duct, and there is sufficient length of grout around the tendon to resist motion.

2.5 BOND BETWEEN STEEL AND CONCRETE

2.5.1 General Characteristics of Bond

One of the most important prerequisites of reinforced and prestressed concrete is the achievement of efficient bond between steel and concrete so that the two materials act compositely. It is only through bond that load can be transferred from the surrounding concrete to the steel. Bond of steel in concrete is based on interlocking of the uneven, rough or deformed surface of the bar with the concrete. Its quality therefore depends mainly on the interlocking area, the deformation behaviour and the shear strength of the concrete at the interface layer of the bar.

Bond forces are measured by the rate of change of force in the steel bars. Bond stress, u, normally defined as a shear force per unit area of bar surface, will not exist unless the steel stresses change between any two sections (Park and Paulay, 1975):

$$u = \frac{q}{\sum o} = \frac{\Delta f_s A_b}{\sum o} = \frac{d_b}{4} \Delta f_s \qquad \text{.....(2.2)}$$

where q = change of bar force over unit length

Σo = nominal surface area of a bar of unit length

d_b = nominal diameter of the bar

Δf_s = change of steel stress over unit length

A_b = area of bar.

The bond resistance of plain bars is mainly provided by chemical adhesion between the concrete and the bar surface, which is easily overcome even under low stresses. Once slip occurs, further bond can be developed only by friction and the wedging action at the bar surface irregularities. The frictional resistance depends on the surface conditions of the steel. Bond forces in this case act in the direction parallel to the interface between the bar and the concrete, and bond failure is usually caused by exceeding the ultimate interface shear strength.

Deformed bars have greater bond capacity mainly due to the interlocking of the ribs with the surrounding concrete. The bond strength developed between two ribs of a bar (Figure 2.10) consists of the following stresses:

i. shear stresses v_a developed through adhesion along the bar surface, which is easily destroyed
ii. bearing stresses f_b against the face of the rib
iii. shear stresses v_c acting on the cylindrical concrete surface between adjacent ribs, which is small compared to (ii)

The bond forces in this case radiate out into the surrounding concrete at some inclination α from the bar surface. Bond failure occurs either by pull-out failure if the ribs are high and closely spaced together, or by splitting of the surrounding concrete caused by partly crushed concrete forming a wedge in front of the rib (Figure 2.11). In the latter case, the wedging action of the concrete deformations at the ribs causes the concrete to 'separate' from the bar, thus circumferential tensile stresses are generated which may bring about the splitting failure.

The most common method of determining bond strength is by the pull-out test which consists of a short length of test specimen embedded in concrete, being pulled from the

surrounding concrete. The bond strength is usually expressed in terms of average bond stress developed by the pullout force around the embedded surface. In practice, the *peak* bond stress has been known to be well in excess of the average stress. During the test, the relationship between the local bond stress and relative displacement (slip) of the bar with respect to the concrete is determined.

These bond stress-slip relationships are used in analytical modelling of bond in reinforced and prestressed concrete. A general shape of a bond-slip model is shown in Figure 2.12. This curve can be considered as a statistical mean curve as it was formulated for a wide range of cases (CEB-FIP, 1993). The first part of the curve refers to the stage when local crushing and micro-cracking of the concrete occurs. The horizontal level occurs only for confined concrete, referring to advanced crushing and shearing off of the concrete between the ribs. The decreasing branch represents the reduction of bond resistance due to the occurrence of splitting cracks along the bars. The final horizontal part represents a residual bond capacity. This is maintained by minimum transverse reinforcement, which helps to keep a certain degree of integrity intact.

The bond-slip relation is unique, depending on the bar profiles and surface condition, concrete quality, loading rate, concrete cover, casting orientation, and the confinement provide by either radial pressure or transverse reinforcement. Each of these influences are briefly reviewed below:

Bar profiles and surface condition

As long as the angle α between the face of the rib and the axis of the bar (Figure 2.10) is greater than 40^{o}, friction between the rib face and the concrete is considered sufficient to restrict slip along this interface (Park and Paulay, 1975). The slip of the bar is then mainly due to the crushing of the concrete in front of the bar ribs (Figure 2.11b). However, if the angle α is small and the surface is smooth, slip can occur along the face of the rib, thus failure is by longitudinal splitting along the bar caused by the wedging action of the rib pushing the concrete away from the bar. In terms of surface condition, the bond characteristics of deformed bars are not adversely affected by varying degrees of surface rust but in the case of plain bars, the presence of pitting and some rusting can improve the bond performance.

Orientation of bars during casting

Bars which are placed parallel to the direction of casting of concrete have better bond performance than bars which are perpendicular to the casting direction. This is due to the settlement of fresh concrete under the bar in the latter case, resulting in poorer bond quality.

Confinement

The widening of splitting cracks can be restricted if the concrete surrounding a bar can be confined. Lateral confinement can be achieved by application of a radial compressive pressure on the concrete, use of transverse reinforcement and/or stirrups, or by increased concrete cover. This has the effect of increasing the frictional force on the steel-concrete or concrete-concrete failure surface and hence delaying splitting failure of the concrete. As a result, bond strength can be considerably increased.

Bond under high rates of loading

The discussion so far has been on static bond, of which much research has already been carried out. Very little consideration has been given to the behaviour of bond under impact loading conditions (dynamic bond). It is well-known that the loading rate influences the behaviour of concrete and mortar both in tension and compression. It is therefore expected that the loading rate will affect the bond stress-slip relationship.

Hansen and Liepins (1962) were one of the pioneers to study the influence of loading rate on the behaviour of bond between concrete and steel. Deformed bars were subjected to static and dynamic loading conditions using the pull-out test. They used 12.5mm diameter bars with an embedment length of 50mm. The tests concluded that the *local* ultimate bond strength may be as high as 75% of the compressive strength of concrete f_c' under static loading conditions, and increases to f_c' under dynamic loading. This means that the local ultimate bond strength under dynamic loading was about a third higher than that under static loading.

Vos and Reinhardt (1982) reported the results of an experimental investigation on the influence of loading rate on bond behaviour. Pull-out tests based on the Split Hopkinson Bar technique were undertaken on three types of specimen (10mm diameter plain bar, 3/8"

prestressing strand and 10mm deformed bar) in different concrete mixes. The study concluded that the loading rate had negligible effect on the bond stress-displacement relationship of plain bars and prestressing strands. It appears therefore that adhesion, friction and 'lack of fit' (in prestressing strand) are insensitive to the loading rate. This means in practice that bond resistance values and bond stress-displacement relationships for such bars can be taken from static tests and be used in cases of dynamic loading. The bond behaviour of deformed bars was however, found to be strongly influenced by loading rates. The higher the loading rate, the greater was the bond resistance and bond stiffness. This was believed to be due to both the tensile and compressive strength of concrete.

The influence of loading rate on bond behaviour was also found to be more pronounced for lower quality concrete. This can be attributed to the propagation of microcracks, which is governed by the brittleness of the concrete matrix and by crack arresters such as aggregates and pores. This means that high quality concrete which is more brittle and homogenous, will be less influenced by high loading rates.

2.5.2 Transfer Bond in Pre-tensioned Concrete

In pre-tensioned concrete, the prestressing force is transferred to the concrete solely by bonding of the prestressing strand to the surrounding concrete. This is achieved over a length of transfer L_t at each end of the tendon which performs the function of end anchorages when mechanical ones are not provided (Figure 2.13). Along this length, the stress in the tendon builds up from zero stress at end A to its full prestress at point B. As the tension is released and the wire starts to slip, the diameter of the bar increases in proportion to the reduction in tension due to the Poisson's ratio effect. This swelling of the tendon diameter along the length of transfer produces a radial pressure against the surrounding concrete, resulting in frictional forces which transmit the stress between the steel and concrete. Thus the prestressing force is transferred to the concrete by friction and the wedging action as the tendon attempts to return to its original unstressed diameter.

Much of the understanding of the behaviour of bond between pre-tensioned steel and concrete is attributed to Janney (1954), who suggested that the three main contributors of bond anchorage are adhesion, friction and mechanical resistance. Adhesion between concrete and steel is usually weak and is destroyed at very small relative displacements.

Mechanical resistance is provided by the interlocking of the spiral twisting of the outer wires forming a strand, or by the rough deformed surface of a prestressing tendon. In the case of smooth bars or wires, mechanical resistance is negligible. Janney concluded that friction between concrete and steel is mainly responsible for the transfer of stress to the concrete. This was supported by Base (1958) who investigated the various parameters affecting transfer length.

The frictional bond is assumed to be proportional to the radial pressure and to the coefficient of friction between the steel and the surrounding concrete. Based on the elastic theory of a thick-walled cylinder, considering only frictional bond forces and neglecting adhesion and mechanical interlock, the following expression was derived by Hoyer for the length of transfer (Lin and Burns, 1981):

$$L_t = \frac{d}{2\phi}(1+\mu_c)\left(\frac{n}{\mu_s}-\frac{f_{si}}{E_c}\right)\frac{f_{se}}{2f_{si}-f_{se}} \qquad \text{.....(2.3)}$$

where d= diameter of wire or tendon

μ_c = Poisson's ratio of concrete

μ_s = Poisson's ratio of steel

E_c = Elastic modulus of concrete

E_s = Elastic modulus of steel

f_{si} = initial prestress in steel

f_{se} = effective prestress in steel

ϕ = coefficient of friction between steel and concrete

$n = E_s/E_c$.

Janney then performed a similar elastic analysis based on the frictional bonding phenomena, and an exponential relationship between wire tension and length from free end of a pre-tensioned member resulted (Figure 2.14):

$$\log_e\left[\frac{f_{se}-f_s}{f_{se}}\right] = \frac{-2\phi\mu_s l}{r\left[1+(1+\mu_c)n\right]} \qquad \text{.....(2.4)}$$

where f_s = stress in wire at any point

r = radius of wire

l = distance from free end of pre-tensioned member.

The general shape of this theoretical curve was verified experimentally by Janney. The analysis however provided only a qualitative guide as the frictional bonding phenomena was based on an elastic analysis, but the resulting high stresses indicated plastic behaviour in the surrounding concrete. Since then, several equations have been developed to simplify the above equations for use in design.

BS 8110 (Part 1, Cl. 4.10.3)

The following formula is valid for initial prestress levels in the tendons of up to $0.75f_{pu}$, where f_{pu} is the characteristic strength of the prestressing steel:

$$L_t = K_t \frac{d}{\sqrt{f_{ci}}} \qquad \text{.....(2.5)}$$

where f_{ci} = concrete compressive strength at transfer (N/mm^2)

d = nominal diameter of tendon (mm)

K_t = coefficient for the type of tendon used. Values of K_t are shown below.

Type of tendon	K_t $\left(N^{\frac{1}{2}}/mm\right)$
Plain or indented wire	600
Crimped wire with wave height≥0.15d	400
7- wire standard or super strand	240
7- wire drawn strand	360

ACI 318-89 (Cl. 12.9.1)

The transfer length L_t, based on tests by Hanson and Kaar (1959), is expressed as a function of the effective prestress and the nominal strand diameter.

$$L_t = \frac{f_{se}}{3} d_b \qquad \text{.....(2.6)}$$

where f_{se} = effective stress in the prestressing reinforcement after all losses (ksi)

d_b = nominal strand diameter (inches).

The test specimens (¼", ⅜", ½" diameter seven-wire strands) used by Hanson and Kaar were released slowly as opposed to flame or saw cutting. The embedment length and the diameter of the strand were the principal variables investigated with respect to their influence on the bond performance of pre-tensioned prestressed beams. Later tests by Kaar

et al (1963) performed on members with varying strand diameters (¼", ⅜", ½") and concrete strengths indicated that although higher strength concrete can develop 75-80% of the transfer bond in a shorter distance than for lower strength concrete, the total distance required to develop 100% of the transfer bond was approximately the same irrespective of concrete strength.

Zia and Mostafa (1977) indicated that the denominator '3' in the expression for transfer length in the ACI Code represents a conservative average concrete strength. Tests carried out to investigate the nature of bond concluded that the transfer length is affected by many parameters, the most important of them are:

- type of steel (e.g. wire, strand)
- steel size (diameter)
- steel stress level
- surface condition of steel - clean, oiled, rusted
- concrete strength
- type of loading (e.g. static, repeated, impact)
- type of release (e.g. gradual, sudden - flame cutting, sawing)
- confining reinforcement around steel (e.g. helix or stirrups)
- time-dependent effect (time elapsed after transfer)
- consolidation and consistency of concrete around steel
- amount of concrete cover around steel

They proposed the following linear equation for the length of transfer

$$L_t = 1.5\frac{f_{si}}{f_{ci}}d_b - 4.6 \qquad \text{.....(2.7)}$$

where d_b = strand diameter (inches)

f_{si} = initial stress in the prestressing steel before losses (ksi)

f_{ci} = compressive strength of concrete at time of initial prestress (ksi).

2.5.3 Numerical Models to Represent Bond

The finite element method has been used since the late sixties to study the influence of bond in transferring forces between concrete and steel. Much effort has been given into

incorporating bond models to simulate the complex problem of cracking and bond slip associated with the steel-concrete bond.

The most commonly used finite element for modelling bond between steel and concrete is the linkage element as originally used by Ngo and Scordelis (1967). It consists of two orthogonal springs, having linear stiffnesses k_h and k_v but no physical dimensions, which connect and transmit shear and normal forces between nodes i and j (Figure 2.15). This linkage element is used to connect the steel and concrete elements at nodal points and at the same time, permits a certain amount of bond slip to take place during the transfer of force from steel to concrete.

The determination of the two spring stiffnesses in the linkage element is difficult in practice. For the vertical spring, a large value of k_v is usually assigned (i.e. steel and concrete are almost rigidly connected in the vertical direction). For the horizontal spring, the force-displacement relationship must be based on characteristics of bond in the actual member.

Most of the bond stress-slip relationships available in the literature have been obtained empirically by tests on a limited range of bar sizes, bar surface finish and concrete strength. There is hence no single bond-slip relation that is generally applicable to all situations. In addition, the different tests by different researchers have shown a wide variation of results. Various formulations have been proposed to represent some of these experimentally-derived bond stress-slip relationships. Nilson (1968) proposed a third-order polynomial relating local bond stress u to local bond slip d:

$$u = 3606(10^3 d) - 5356(10^3 d)^2 + 1986(10^3 d)^3 \quad \text{.....(2.8)}$$

From the equation, the spring nonlinear stiffness is obtained by differentiating the bond stress with respect to the displacement. The equation however, becomes invalid for large slips exceeding about 0.025mm.

Keuser et al (1983) developed a contact element which was added to the ADINA finite element program. The element adopted a nonlinear bond-slip relation in order to simulate the bond stress-slip behaviour of prestressing steel in concrete. Bond was modelled by a four node contact element with a linear displacement formulation. Two nodes of a concrete element were connected to the reinforcement element by a bond element which had no physical dimension in the transverse direction.

A disadvantage of the link element is that it is an artificially discrete element that 'lumps' at nodal points along the steel-concrete interface, the behaviour of bond that occurs all along this interface. An element that avoids this artificial discreteness of the bond link element is the interface element shown in Figure 2.16. These elements, which can be arrayed along the entire steel-concrete interface, have a constitutive relationship formulated in terms of relative displacements of its top and bottom surfaces, and the interface shear and normal stiffnesses.

2.6 GENERAL THEORY FOR UNBONDED POST-TENSIONED BEAMS

There are two types of unbonded prestressed concrete. Internal unbonded prestressing has the tendons (usually in a greased sleeve) embedded within the concrete, while external unbonded prestressing has the tendons outside the concrete. The former is usually employed in unbonded post-tensioned slabs while the latter is used principally in externally post-tensioned box girder bridges. The main difference between these two forms of prestressing is that the deflected shape of internal tendons follows the deflected shape of the beam along the whole span, whereas external tendons only follows the deflection of the beam at the deviator positions, but is different from the deflection of the beam everywhere else (Alkhairi and Naaman, 1993). Only internal unbonded prestressing is of interest here, and all further discussion will refer to this type of prestressing.

When a bonded prestressed concrete beam is loaded, the change in strain in the tendon at a particular section is equal to the change in strain in the adjacent concrete. Therefore, the increase in stress in a bonded tendon depends on the local deformation of the beam at that section. The perfect bond assumption between the prestressing steel and surrounding

concrete leads to a relatively simple sectional analysis at the section of maximum moment. The principles are laid out in the technical literature (Collins and Mitchell, 1991; Lin and Burns, 1981). However, in an unbonded prestressed concrete beam, the change in strain in the tendon is equal to the *average* change in strain in the concrete at the level of the tendon over the whole length of the unbonded tendon. In this case, the perfect bond assumption between the prestressing steel and the surrounding concrete is no longer valid, and strain compatibility at critical sections cannot be maintained. Instead, the stress in the prestressing steel at any load level depends on the total change in length of the concrete at the level of the tendon between end anchorages. This makes the stress in the tendon, member dependent rather than section dependent, and proper modelling of the overall deformations becomes necessary.

A comparative study of the behaviour of prestressed beams, with and without bond was presented by Mattock et al (1971). A series of simply supported and two-span continuous beams (T-beams or rectangular) were tested to failure under four equal point loads in each span. Both bonded and unbonded beams with different amounts of bonded unprestressed reinforcement were studied. The beams were either designed to ACI 318-63 or to a proposed equation to have the same ultimate strength. It was already established at this stage that unbonded beams with the tendons as the only flexural reinforcement, will behave as tied arches after cracking, i.e. a single wide crack develops at the critical section which increases rapidly in width and depth with increased loading. However, by including a small amount of bonded unprestressed reinforcement, the ductility and distribution of cracks can be controlled to levels comparable to those in bonded beams. It was confirmed by the test results that the provision of additional bonded reinforcement will ensure that an unbonded post-tensioned member behaves as a flexural member rather than as a tied arch.

The study also revealed that the actual ultimate strength of the unbonded beams was nearly 30% more than that calculated by the ACI Code. This highlights the conservativeness of the Code in predicting the stress in unbonded tendons at the ultimate load. This has led to a whole field of research into the ultimate behaviour of unbonded prestressed concrete members. Tam and Pannell (1976) reported that the span to depth ratio is a parameter which may influence the behaviour of unbonded beams at the ultimate condition. They proposed a revision to the conventional bending theory to include this span/depth ratio and

from this, simple design equations for the ultimate analysis of unbonded partially prestressed concrete beams were derived.

The influence of the span/depth ratio on the ultimate stress in the prestressing steel f_{ps} at the nominal flexural strength of unbonded prestressed beams was acknowledged by the ACI Building Code (1983) such that the following equations were proposed:
For span/depth ≤ 35,

$$f_{ps} = f_{pe} + 10000 + \frac{f_c'}{100\rho_p} \leq f_{py} \text{ or } f_{pe} + 60000 \text{ (psi)} \quad \text{.....(2.9a)}$$

For span/depth >35,

$$f_{ps} = f_{pe} + 10000 + \frac{f_c'}{300\rho_p} \leq f_{py} \text{ or } f_{pe} + 30000 \text{ (psi)} \quad \text{.....(2.9b)}$$

where f_{pe} = effective prestress

f_c' = compressive strength of concrete

f_{py} = yield strength of the prestressing steel

ρ_p = prestressing steel ratio.

However, the equations are not satisfactory as there is a discontinuity in the stress level at the span/depth ratio of 35. Moreover, they were based on limited experimental results. Harajli (1990) presented a theoretical model to provide a better understanding of the influence of the span/depth ratio on the value of f_{ps} at ultimate, and to include this parameter in the ACI Code in a more satisfactory way. An elegant model based on the strain compatibility method resulted, with the following simplifying assumptions:

i. Although the strain in the unbonded tendon is not compatible with the concrete strain because of slip, a linear strain distribution between the concrete and ordinary reinforcing steel across the depth of the beam sections is assumed. This means that the total tendon elongation between anchorages can be determined from the curvature distribution along the beam

ii. Friction which may develop between the unbonded prestressing steel and surrounding duct is neglected (i.e. the stress along the unbonded tendon is constant).

Figure 2.17 illustrates a typical strain distribution across the beam depth at ultimate condition, where

c = neutral axis depth at ultimate

d_p, d_s = depth of centre of prestressing steel and ordinary tension steel respectively

ε_{pe} = effective prestrain in the prestressing steel

$\Delta\varepsilon$ = 'fictitious' strain increase above decompression at level of pretressing steel

ε_{ce} = precompressive strain in concrete at the level of prestressing steel

ε_{pa} = actual increase in strain in the prestressing steel above decompression

ε_s = strain in ordinary steel

ε_{cu} = ultimate concrete strain in the top compression fibre.

From the figure,

$$\Delta\varepsilon = \frac{d_p - c}{c}\varepsilon_{cu} \qquad \text{.....(2.10)}$$

The total increase in tendon elongation between anchorages is assumed to occur within a plastic region length L_o (Figure 2.18),

$$\Delta l_{ps} = (\Delta\varepsilon + \varepsilon_{ce})L_o \qquad \text{.....(2.11)}$$

The increase in strain in the prestressing steel above the effective prestrain is

$$\Delta\varepsilon_{ps} = \frac{\Delta l_{ps}}{S} \qquad \text{.....(2.12)}$$

where S is the span of the member. Therefore, the strain ε_{ps} in the tendon at the ultimate condition is given by

$$\varepsilon_{ps} = \varepsilon_{pe} + \Delta\varepsilon_{ps}$$

$$= \varepsilon_{pe} + \varepsilon_{ce}(L_o / S) + \varepsilon_{cu}\frac{d_p - c}{c}(L_o / S) \qquad \text{.....(2.13)}$$

Solving for the depth of the neutral axis and considering equilibrium of forces at the beam section, an equation for f_{ps}, given as a function of L_o/S, is derived. The L_o/S parameter is dependent on loading type and the span/depth ratio; i.e. f_{ps} has been expressed as a function of the span/depth ratio and load-geometry. The predictions of the developed analytical model were found to be in agreement with experimental results obtained by

other researchers. It was found that increasing the span/depth ratio reduces the stress increase at ultimate Δf_{ps} in the prestressing steel.

The discussion so far has focussed on the behaviour of unbonded prestressed concrete beams at the ultimate condition. Harajli and Kanj (1992) realized that research into the service load behaviour of such beams was still lacking. They undertook an experimental and analytical investigation into the serviceability limit state characteristics of unbonded prestressed members. Twenty-six unbonded prestressed and partially prestressed rectangular beams were tested under different reinforcement index, partial prestressing ratio, span/depth ratio (ranging from 8 to 20) and loading type (single point load or one third loading). The results showed improved crack control and ductility in the beams with some unprestressed reinforcement as compared to the fully prestressed beams. Due to slip in the unbonded tendons, the stress increase in the tendons with increasing load was small before the cracking stage. This stress increased significantly after cracking. A general method of section analysis was developed to reduce the problem of section analysis of unbonded prestressed beams to that of bonded ones. This was done by introducing a strain reduction coefficient Ω to account for slip of the prestressing steel. This coefficient is defined as the ratio of increase in strain in the prestressing tendon above effective in the unbonded members to the same in bonded tendons for a given load level at the critical section,

$$\Omega = \frac{(\Delta \varepsilon_{ps})_{unbonded}}{(\Delta \varepsilon_{ps})_{bonded}} \qquad \text{.....(2.14)}$$

The analysis, which was solved iteratively, correlated with experimental observations.

A comprehensive study involving the development of a nonlinear analytical model to predict the complete moment-deformation response of concrete beams prestressed with unbonded internal or external tendons, was presented by Alkhairi and Naaman (1993). The authors addressed the effects of span/depth ratio and amount of shear force on the flexural deformation of the beam; and tendon eccentricity variations with increasing loads on the stress increase in unbonded *external* tendons. However, this second order effects due to eccentricity variations in external tendons is not relevant here. The model adopted the basic assumptions of strain compatibility and the force and moment equilibrium methods

to obtain the *average* tendon elongation for prediction of f_{ps} in unbonded tendons. This required a multi-level iterative nonlinear analysis at several locations throughout the beam. It was found that there was excellent correlation (within 10%) between predicted results and experimental observations obtained from 15 different investigations undertaken by others. The model accounted for the influence of shear deformations by using a truss mechanism. The study concluded that shear deformations may significantly affect the stress increase Δf_{ps} at ultimate in the unbonded tendons for beams with span/depth ratios less than 24, but neglecting this effect for higher span/depth ratios does not significantly change Δf_{ps}. This is irrespective if the tendons are internal or external.

2.7 REPAIR AND STRENGTHENING METHODS

The practice of using externally bonded steel plates to strengthen and rehabilitate deteriorating reinforced and prestressed concrete flexural members is now a proven and widely accepted method. The study in this field was prompted by the general deterioration of concrete structures, in particular the widespread deterioration of bridges, such that extensive repair work or replacement is required. The steel plates, normally bonded by epoxy resins to the tension face of flexural members, are relatively quick and simple to apply, resulting in negligible loss of overhead clearance. The result is a fully composite section with considerably improved strength and stiffness. More recently, attention has focused on the use of high strength fibre reinforced composite material as an alternative to using steel plates which have the disadvantage of greater weight and susceptibility to corrosion. Other types of strengthening applicable to post-tensioned concrete (e.g. additional prestressing) will be discussed in proceeding sections.

2.7.1 Strengthening by Bonded Steel Plates

A comprehensive survey on the strengthening of reinforced concrete flexural members with bonded steel plates and fibre composite sheets was provided by McKenna and Erki (1994). They reported that externally bonded steel plates were first used in 1964 in South Africa to strengthen beams in an apartment building. This method of strengthening was subsequently adopted in Switzerland, France, Russia and Japan as it was quickly realized that the cost of strengthening was more economical than replacement. As early as the

1970's, external steel plates had been used to strengthen existing highway bridges. Klaiber et al (1987) reported that steel plates were used in France to alleviate excessive deflections in a reinforced concrete bridge; and in Karastan (former USSR), epoxy bonded steel plates were used to repair a continuous reinforced concrete bridge which had lost a quarter of its reinforcing steel due to corrosion. In Belgium, two 15-year-old continuous prestressed concrete bridges were repaired by external post-tensioning and epoxy-bonded steel plates.

Research into the behaviour of plated concrete flexural members showed that the addition of bonded steel plates significantly improve the structural performance under both service and ultimate load conditions. Swamy et al (1987) evaluated the effect of the following parameters on the structural behaviour of plated beams: plate thickness, glue thickness, layered plates and lapped plates. Twenty-four simply-supported beams of span 2.3m were tested under third point loads. Glue and plate thicknesses of 1.5, 3.0, and 6.0mm were studied. It was found that the load to cause the first crack for the plated beams was about 50% higher than that of the unplated beam. Replacing thicker plates with equivalent thinner plates, lapping of plates, tapered glue thickness and plating of precracked beams did not significantly increase the first crack load. The stiffening effect of the plated beams was found to be superior over unplated beams in reducing deflections and providing better crack control. Composite action between the beam and the steel plate was preserved right up to failure, and the flexural stiffness of the plated beams near failure was up to three times more than that of the unplated ones. At ultimate load, the beams with 1.5 and 3.0mm plates had increased capacities of up to 16%.

The plate thickness was found to influence the failure mode of the beams. The beams with 1.5mm plates failed in flexure by yielding of the bar and/or plate before crushing of the concrete, but all the beams with 6mm plates failed prematurely in a sudden and brittle manner by shearing of the concrete along the internal bottom reinforcement, causing the concrete cover to 'peel' off. There was no sign of plate debonding, cracking in the glue, nor yielding of the steel bars or plate. There appears to be a limit to the plate thickness beyond which the predicted ultimate load may not be achieved. A plate width to thickness ratio of not less than 50 was recommended to ensure a ductile and flexural failure.

Several investigators have attempted to overcome the problem of premature peeling of the bonded plate. Jones et al (1988) explored a number of techniques such as using tapered plates, multiplates with curtailment, anchor bolts and glued anchor plates (Figure 2.19). A theoretical analysis revealed that plate separation, which starts at the ends of the plate, is due to high local interface bond stresses and peeling forces at the plate ends. This cannot be overcome by using tapered plates or multiplates. It was found that the anchorage detail significantly affects the ultimate strength and failure mode of the beams. The use of anchor bolts, although did not prevent debonding, was effective in restricting complete plate separation and increased the strength by 8% over the unplated beam. Glued anchor plates were found to be the most effective anchorage system; failure was by yielding of the plate in tension and the full theoretical flexural strength was achieved (36% over the unplated beam). Beams with either bolted or anchored plates exhibited ductile failure, compared to beams with unanchored plates which failed suddenly in a brittle manner.

Roberts and Haji-Kazemi (1989) described the strengthening of under-reinforced concrete beams by bolting the steel plates to prevent the premature peeling failure. The steel plates (2mm or 4mm) were attached to the tension face of the beam by 8mm diameter cast-in expanding bolts, or bolts which were drilled and fixed after curing. This technique achieved significant improvement in both the stiffness and ultimate strength; all the beams exhibited ductile flexural failure (plates yielded in tension). The method of bolting the plates to the concrete, the length of the bolts, and the occurrence of slip at the ends of the steel plates all had little influence on the ultimate moment of resistance. In 1992, Oehlers experimentally determined the shear forces which induce the plate separation. He studied the interaction between shear peeling and flexural peeling, and proposed design rules to ensure that plates glued to the soffits of existing beams do not debond before the design load is reached.

2.7.2 Strengthening by Bonded High Strength Fibre Sheets

These high strength fibre reinforced composite material (FRCM) sheets, composed of carbon, glass or aramid fibres bound by a resin or epoxy matrix, are high in strength (up to 5 times greater than the tensile strength of high yield steel) and stiffness (comparable to elastic modulus of steel), lightweight and resistant to corrosion. Although they are more expensive, some cost savings can be made because of easier application and handling. The

polymer matrix of the FRCM sheets is very susceptible to fire, and temperature fluctuations may cause a weakening of the material. However, additives can be added to improve their performance.

Meier et al (1992) reported on the use of FRCM sheet bonding on a continuous multi-span box beam bridge in Switzerland which had insufficient load capacity as a result of accidental damage to a prestressing tendon. Only 6.2kg of carbon fibre reinforced plastic (CFRP) sheets were used, compared to 175kg of steel plates which would have been required for the same strengthening work. The bridge was repaired with 3 CFRP sheets with a tensile strength of 1900 MPa and an elastic modulus of 129 GPa; 2 of the sheets were 150x5000x1.75mm thick and the other was 150x5000x2.0mm thick.

In Germany, the Kattenbusch bridge, which is a multi-span post-tensioned concrete bridge with double box girders, was strengthened with bonded glass fibre reinforced plastic (GFRP) plates after wide cracks were found at the joints caused by temperature restraint (Rostasy et al, 1992). The joints were strengthened with either 10x100x3000mm steel plates or 30x150x3200mm GFRP plates. Load testing of the bridge before and after strengthening revealed that the working stress levels in the prestressing steel was drastically reduced, and that both materials provided the same strengthening effect.

Saadatmanesh and Ehsani (1991) undertook an experimental study of the static strength of reinforced concrete beams strengthened with GFRP plates. Five rectangular beams and one T-beam, all strengthened with 6mm thick GFRP plates, were tested under two symmetric point loads. The results indicated that the GFRP plates significantly increased the flexural strength of the beams and provided better crack control by delaying the first crack load and reducing the crack widths. Comparison of the experimental results with analytical models developed by An et al (1991) which was based on the strain compatibility method, showed that the behaviour of beams strengthened with FRCM sheets can be predicted by the classical flexural theory. The testing programme also included cambering two of the beams before bonding the GFRP plates, in order to induce *external prestressing* effects. The bending tests showed that cambering the beams resulted in improved cracking behaviour and increased failure load.

In 1992, Triantafillou et al investigated the strengthening of beams using *prestressed* FRP sheets. A unidirectional FRP sheet was first pre-tensioned before being bonded to the tension face of the beam (Figure 2.20). The opposite ends were then cut after the adhesive has hardened, and the sheet was transformed into a prestressing element. Five 1.2m long rectangular beams, all reinforced with either 4mm or 6mm diameter bars and strengthened with prestressed CFRP sheets were tested in three point bending. The results showed that the strengthened beams exhibited increased strength (up to 4 times that of the control beam), stiffness and ductility characteristics as well as controlled cracking efficiently.

2.7.3 Repair by Additional Prestress

In recent years, post-tensioning has been used to strengthen prestressed concrete bridges and has proved to be a viable strengthening method. Besides requiring only minimal site preparation and traffic interruption, post-tensioning can add substantial live load capacity to an existing bridge (Klaiber et al, 1987). The Highways Agency (1994) regards additional prestressing as the most versatile and popular means of strengthening existing post-tensioned concrete bridges to increase the ultimate strength and improve the serviceability behaviour in both flexure and shear. The main disadvantage of this method is the need for anchorages for the additional tendons, and corrosion protection to the tendons and anchorages as they are often placed external to the concrete. The effects of additional prestressing on the whole structure, and the high local stresses at the anchorages of the additional tendons also require consideration. It is sometimes not possible to accommodate the additional prestress within the existing structure. One solution is to place the additional cable within new concrete attached to the structure. This was adopted in the repair of post-tensioned I-beams which were found to be defective during the construction of ten overbridges on the M3 Motorway (Highways Agency, 1994).

During an inspection of a continuous post-tensioned single cell box bridge in France, significant cracks were discovered in the web and bottom flange of the main span. Concerns over the shear and fatigue capacity of the bridge led to monitoring of strains in the tendons. The low stress range indicated tendon slip within a poorly grouted duct. The original design was also found to be fundamentally flawed. Strengthening was achieved by addition of twelve 15mm diameter strand cables anchored into new transverse reinforced

concrete beams. The external tendons were protected by ducts and grouted in the normal way. The cracks were then sealed by resin injection.

In the Pont De Fives post-tensioned multi-cell box bridge, cracks were found in the vertical joints in the beams after eleven years in service. Gamma radiography revealed that more than half the ducts were improperly grouted, and samples of the steel revealed corrosion and embrittlement. The bridge was monitored with acoustic detectors, and six years later in 1972, some wire failures were detected. Short-term strengthening work involved installing 4 No. 15mm diameter longitudinally prestressed strands, anchored to transverse diaphragms. To ensure long-term service, additional post-tensioning comprising 12 No. 15mm diameter strands were anchored into new concrete at each end of the bridge.

2.7.4 Choice of Strengthening

The choice of strengthening method for grouted post-tensioned concrete bridges depends on the extent of deterioration, availability of space, and access into the structure. In either case, a full appraisal of the existing condition of the deteriorating bridge is essential before any strengthening work can be undertaken. The choice also depends on the type of bridge deck, as addressed by The Highways Agency (1994). In beam and slab decks, additional prestressing is provided by incorporating external tendons between the beams, thus requiring additional concrete or transverse members to act as anchorages. Use of existing diaphragms, if suitably strengthened, can serve this purpose. Additional beams can also be included between existing widely spaced members to share the load. Where additional prestress is not feasible, elastic supports (propping) can be used to support the deck directly from the ground or the existing structure, as reported by Lindsell and Buchner (1993). This method is restricted by available space on which to build them. The use of bonded plates to strengthen this type of deck has proved simple and quick, requiring only minimum space and headroom.

The most widely used method for strengthening box girders is by additional prestressing. Most of the work has been undertaken to remedy service problems (deflection, cracking). Plate bonding is not considered suitable due to the large amount of dead load already present in the structure. For in-situ voided slabs, the main problem is that access into the

bridge is limited, thus additional prestresssing is difficult to achieve. Usually, additional tendons are installed below the soffit, but the overhead clearance may be compromised.

2.8 DISCUSSION

The aim of this chapter was to review the relevant topics related to the present study, and to highlight the important aspects of these topics. The following conclusions can be drawn from the review:

- Currently, satisfactory methods to assess the level of deterioration in post-tensioned concrete bridges using currently available inspection techniques, are lacking.

- Only limited attempts have been made to determine the residual strength of such deteriorating bridges, and most of these have been empirical. As each bridge configuration is unique, the extent of deterioration presents different areas of potential weakness. The lack of visual evidence suggests that considerable loss of prestress due to tendon fractures can occur before visible signs of distress appear. Therefore, conventional load testing commonly used to assess the structural capacity of reinforced concrete bridges may precipitate failure of deteriorating post-tensioned bridges.

- As yet, there are only limited analytical models to quantitatively assess the residual strength of deteriorating post-tensioned concrete bridges whilst accounting for the level of damage that has been discovered during inspection. The deterioration mechanisms which need to be addressed are those due to loss of tendon area as a result of corrosion, and the presence of voids within the grouted ducts.

- Although some of the tendons cut during controlled demolition have demonstrated re-anchoring behaviour back into the grout, this ability has not been considered in the presently available analytical models. Understanding of the influence of the bond conditions in affecting the re-anchoring length and the residual prestress levels of the failed tendons is therefore required to incorporate this behaviour into a developed analytical model.

- The effect of regions of ungrouted tendons (pockets of voids) on the residual strength of the beam has also not been previously accounted for. If a void is continuous along the length of a tendon, the behaviour of unbonded post-tensioned tendons may dominate. This will require an understanding of the behaviour of unbonded post-tensioned beams.

Kind of Examination	Method	Information obtained	Advantages	Limitations
Visual inspection	Visual examination of structure	Cracking of concrete, tendon fractures	Cheap, simple	Unable to inspect tendon/grout condition within duct
	Holes drilled into ducts: - endoscopy - volume measurement - sampling	Condition inside duct size of voids chloride content	Effective, reliable results	Low-tech, time-consuming, risk of damaging tendon. Limited to local inspection
Non-destructive testing	Electrode potential measurements	Electrode potential of tendons indicate risk of corrosion	Quick, cheap, simple to use. Can detect corrosive conditions near tendons	Metal duct inhibits electrical contact with tendon
	Electrical resistance	Change in electrical resistance due to fracture of tendons	Simple to use, cheap. Can detect fractures in tendons	Tendons are in electrical contact between tendons, ducts, anchorages and secondary reinforcement
	Time domain reflectometry	Lack of grouting, tendon corrosion	Quick, simple to use	Requires access to anchorages. Results from trials disappointing
	Magnetic flux exclusion	Defects in tendons (which produces a disturbance of the magnetic field)	Has potential to detect loss of tendon area due to corrosion	Difficult to distinguish between defects and other causes of disturbances. Limited to non-metallic ducts
	Radiography	Voids, tendon corrosion/ fractures	Able to detect voids in duct. Possible to scan whole structure using the French 'Scorpion'	Expensive, difficult to interpret results, requires long exposure times, safety precautions
	Radar	Location of ducts, Voids in non-metallic ducts, Damp areas in structure	Large areas can be scanned. Can locate position and depth of tendon ducts	Cannot be used to detect voids in metallic ducts, secondary reinforcement causes interference
	Thermography	Flaws (cause local variations in temperature)	Portable, provides permanent record	Not proven, risk of high thermal stresses induced
	Sonic/Impact echo	Delaminations, voids	Cheap, relatively simple to use. Able to detect voids in metallic ducts. Portable system available	May not distinguish between large void and shrinkage crack
	Ultrasonic pulse velocity	Location and length of voids in duct	Commercial equipment available. Automatic scanning	Results can be masked by presence of reinforcement
Structural monitoring	Vibration measurement	Corrosion, wire fractures (which changes frequency response of structure)	Examine condition of whole structure	Changes in stiffness are small, masked by other effects
	Deformation	Tendon corrosion or fracture (which may cause changes in deformation)	Can monitor whole structure	Changes small, masked by other effects. Potentially dangerous
	Acoustic emission	Tendon fractures (which release acoustic energy in the form of noise)	Can monitor whole structure, gives early warning of distress	Results difficult to interpret and differentiate from other sources of noise
	Strain measurement (Optical Fibres)	Change of strain which changes optical characteristics of a fibre	Automatic continuous monitoring. Can monitor along whole length of a beam	Not yet sensitive enough to distinguish between strains from temperature drifts or passage of vehicles. Unproven to have sufficient sensitivity to detect small strain changes due to general corrosion
Measurement of Stress	Incremental coring	Existing stresses. Young's modulus of concrete	Commercially available. Accurate to within 1 N/mm^2	Semi-destructive due to coring. Results can be affected by errors during measurement, drilling, and temperature effects
	Centre Hole/Stress Relief	In-situ stresses in reinforcement, prestressing tendons and concrete	Commercially available	Less accurate (22 N/mm^2). Tendon partly damaged by drilling.
	Flat Jacking	Existing stresses	Quick and easy to use. Accurate to within 2.5 N/mm^2	Affected by concrete creep and temperature during cutting

Table 2.1 - Summary of Inspection Methods

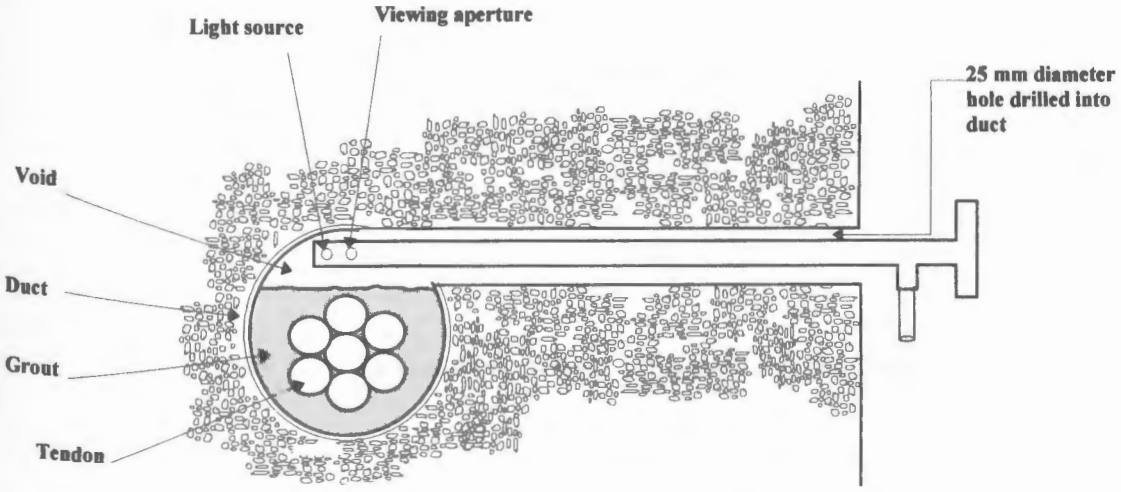

Figure 2.1 Endoscope inspection

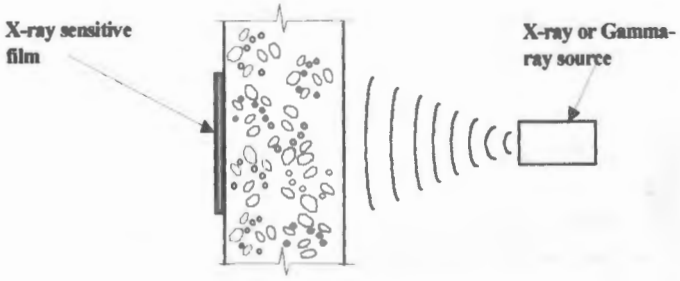

Figure 2.2 Radiography scan

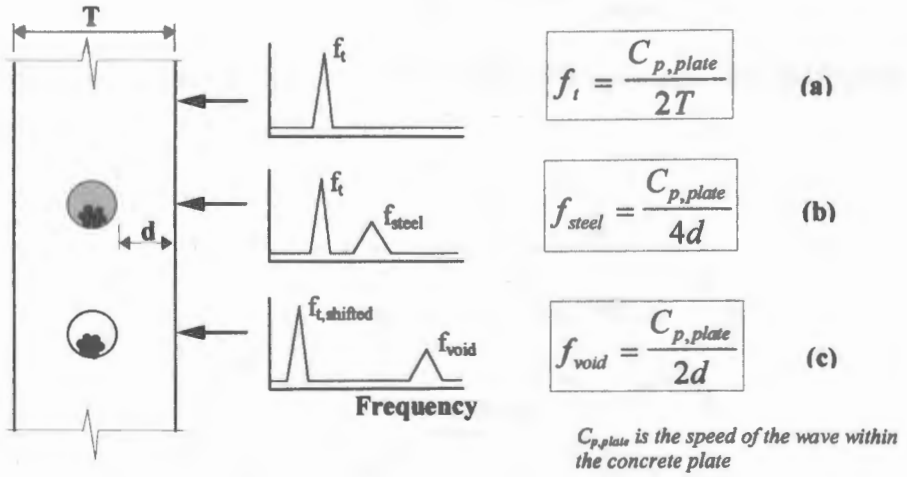

Figure 2.3 Schematic illustrations of the impact-echo responses obtained from (a) a solid plate, (b) a plate containing a grouted duct, and (c) a plate containing an ungrouted duct

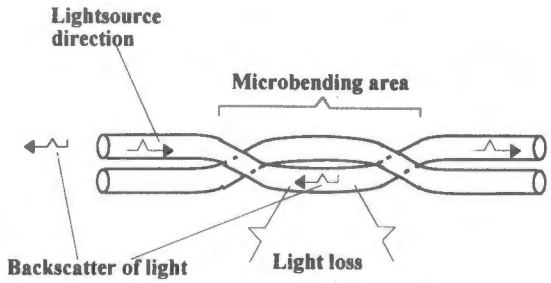

Figure 2.4 Optical fibre sensor (Dill and Curtis, 1993)

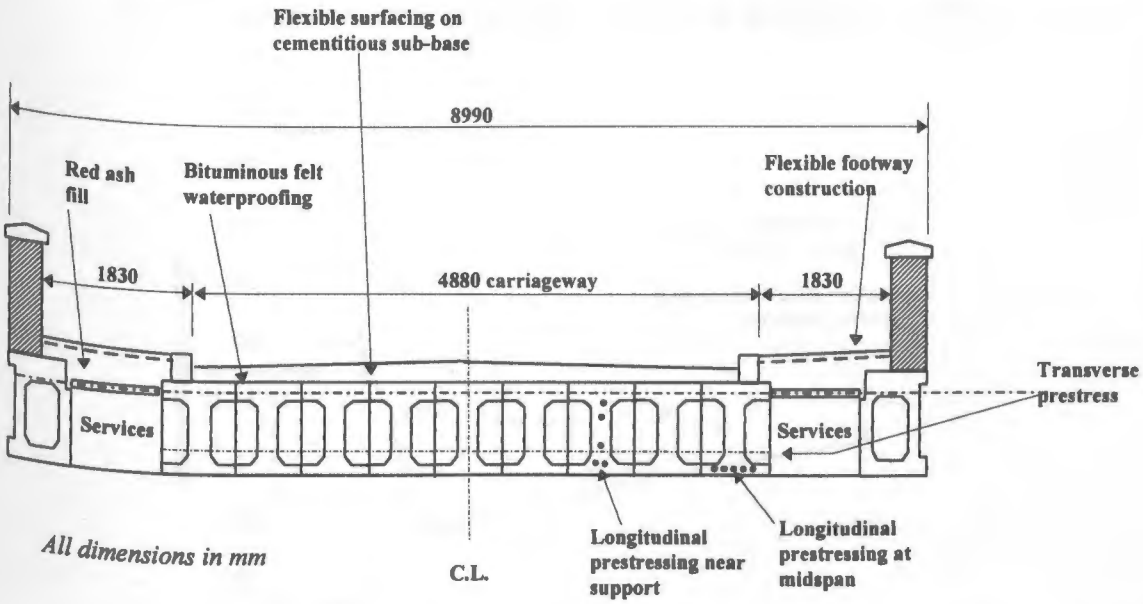

Figure 2.5 Cross-section of Ynys-y-Gwas bridge (Woodward and Williams, 1988)

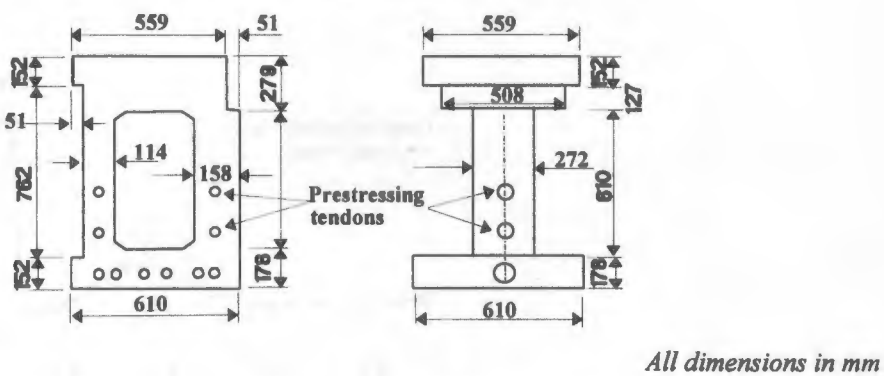

Figure 2.6 Cross-section of Ynys-y-Gwas edge beams (Woodward and Wilson, 1991)

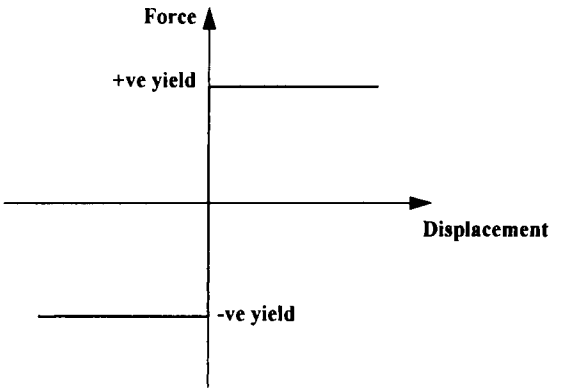

Figure 2.7 Simulation of bond between prestressing tendon and concrete in the finite element model (Woodward and Wilson, 1991)

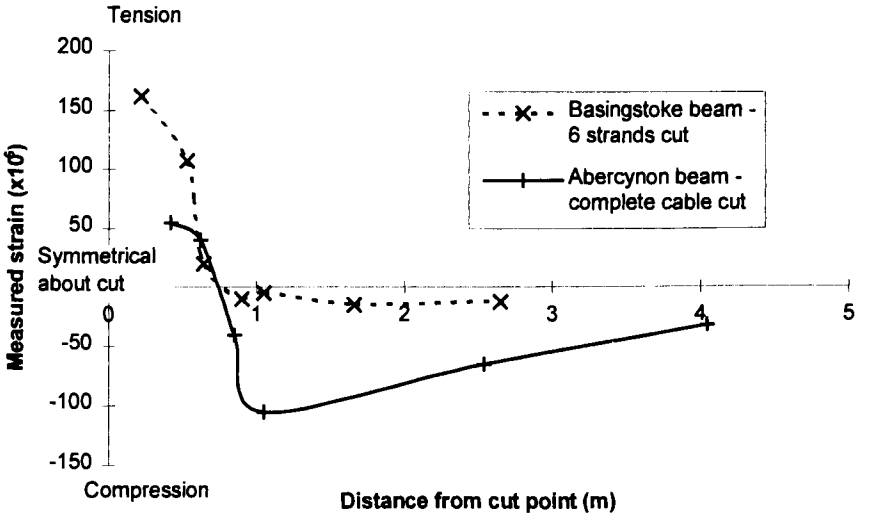

Figure 2.8 Concrete strains induced by cutting of cables (Buchner and Lindsell, 1987)

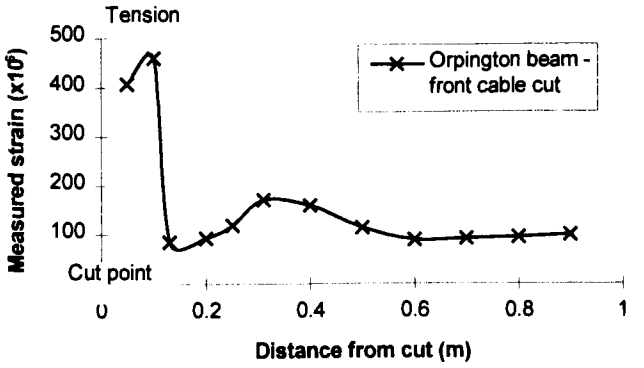

Figure 2.9 Concrete strains induced due to cutting plain wires (Buchner and Lindsell, 1987)

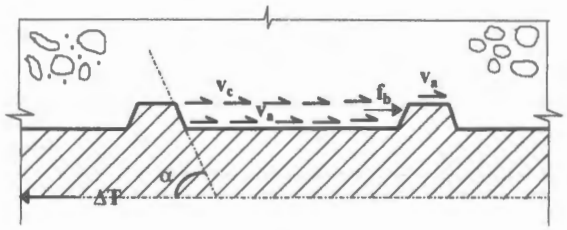

Figure 2.10 The stresses between two ribs of a deformed bar (Park and Paulay, 1975)

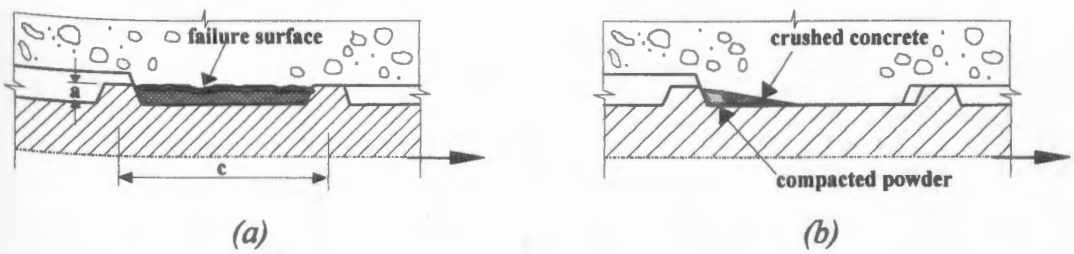

Figure 2.11 Failure mechanisms at the ribs of deformed bars - (a) a/c > 0.15 (b) a/c < 0.10 (Park and Paulay, 1975)

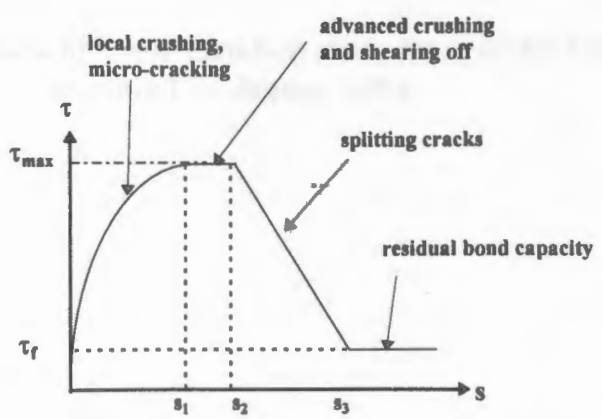

Figure 2.12 Analytical bond stress-slip relationship (CEB-FIP, 1993)

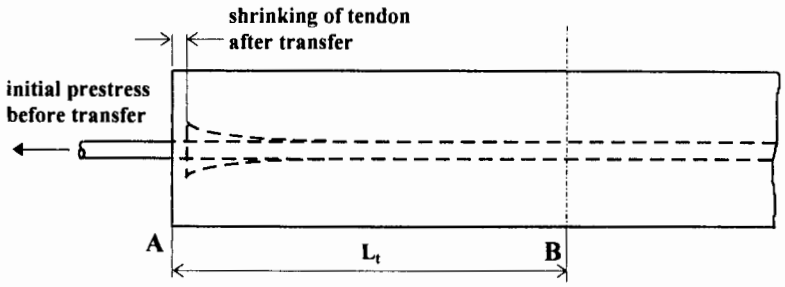

Figure 2.13 Prestress transfer at the end of a pre-tensioned beam (Lin and Burns, 1981)

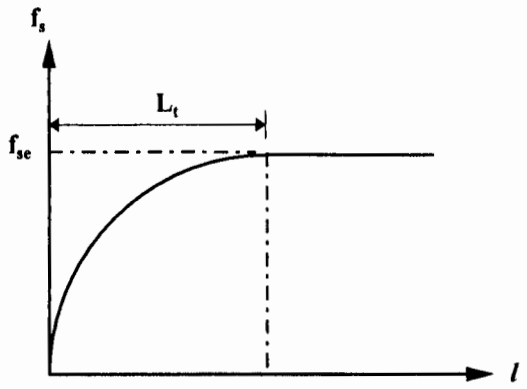

Figure 2.14 Form of stress variation along the transfer length produced by Janney, 1954

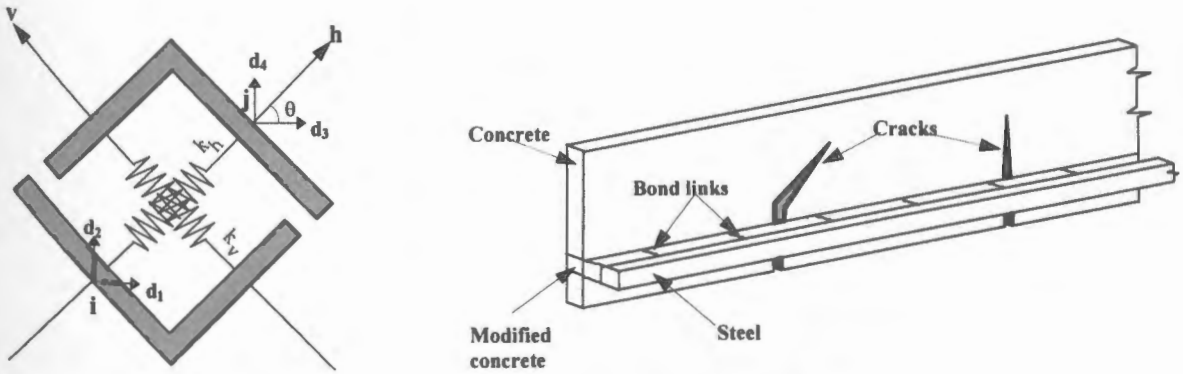

Linkage element *Analytical model*

Figure 2.15 Bond Model with Spring Elements (Ngo and Scordelis, 1967)

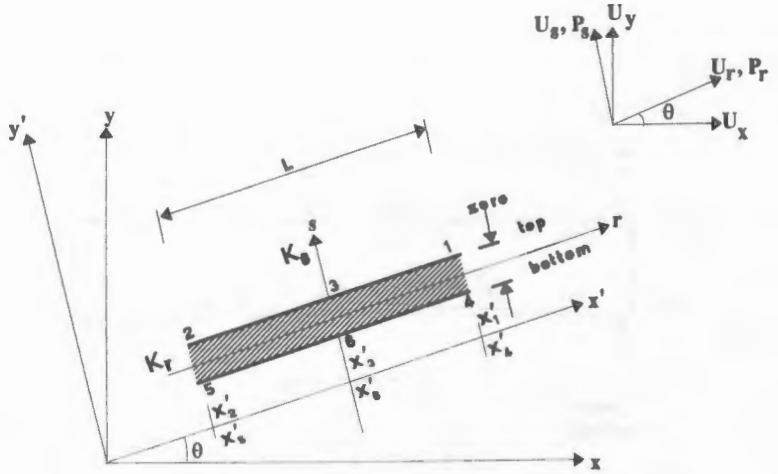

Figure 2.16 Bond Model with Interface Elements (ASCE, 1982)

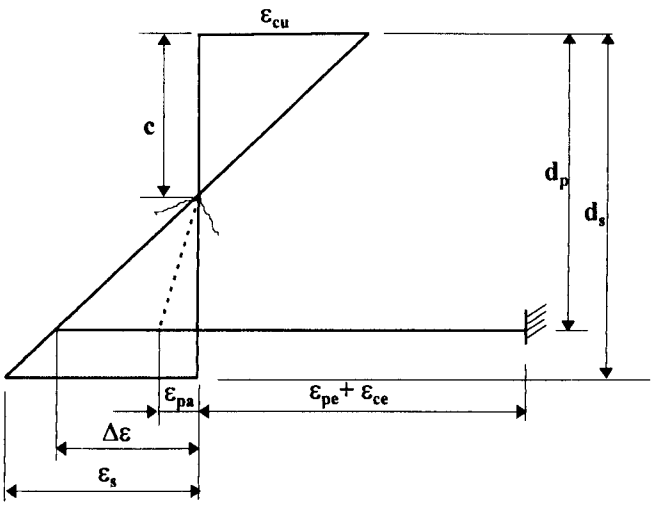

Figure 2.17 Strain distribution across the depth of an unbonded beam section (Harajli, 1990)

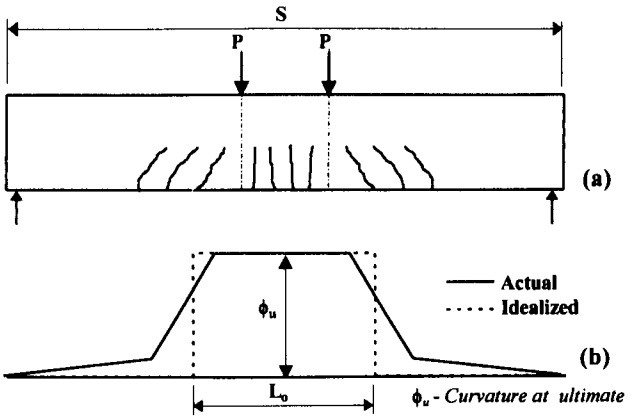

Figure 2.18 - (a) Simply-supported beam loaded by two concentrated loads, and (b) curvature distribution along the beam length (Harajli, 1990)

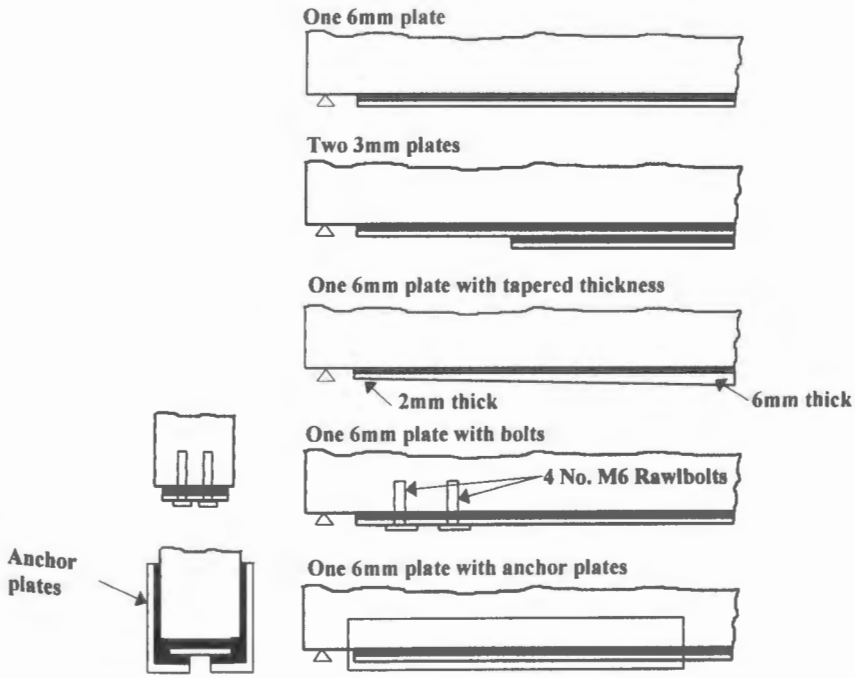

Glue thickness - 1.5mm in all cases

Dimensions in mm

Figure 2.19 Plating details for beams strengthened with steel plates (Jones et al, 1988)

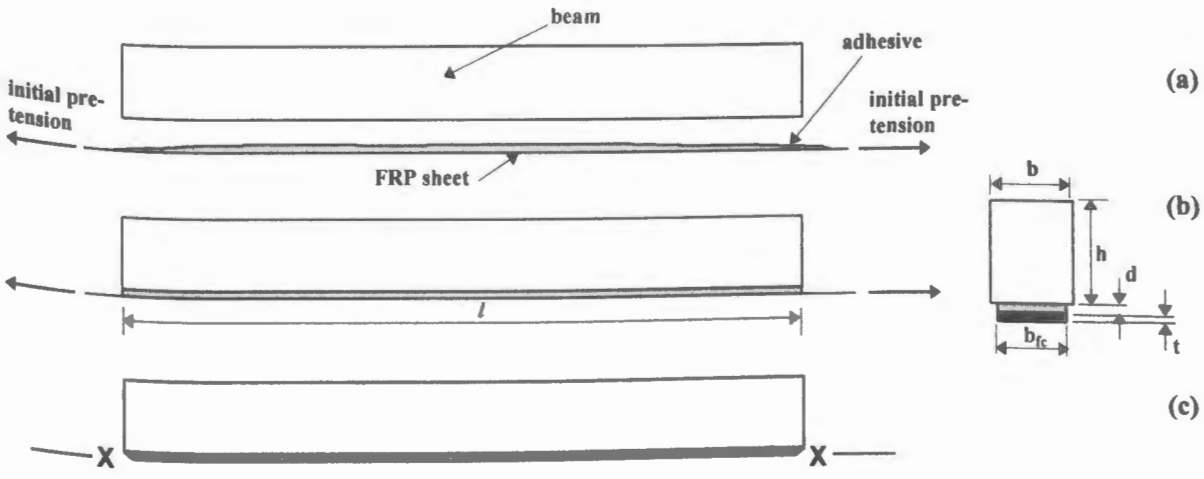

Figure 2.20 Reinforcing with pretensioned FRP sheets - (a) FRP prestressing (b) curing of the adhesive (c) FRP ends released (Triantafillou et al, 1992)

CHAPTER 3

Analysis of Results from Field Tests

3.1 INTRODUCTION

This chapter describes the field investigations carried out in association with Oxfordshire County Council on post-tensioned beams removed from the demolished Botley Flyover, where a wide range of corrosion and grouting conditions had been identified during inspection. A description of the original bridge deck before dismantling is first presented. This is followed by an overview of the field investigations of the full scale bridge beams utilising vibrating wire gauges and optical fibre sensors. The beams were damaged in a controlled manner by cutting or coring through individual tendon groups whilst monitoring the distribution of concrete and tendon strain. Some of the results are presented and discussed in the context of their relevance to this thesis.

The aim of the investigation was two-fold: (i) to determine the feasibility of strain monitoring in detecting local tendon fractures due to corrosion; and (ii) to investigate the extent of re-anchoring of failed tendons in a variety of grout conditions. The results of the investigation provided unique field data which were used to validate the analytical models developed in this research.

3.2 DESCRIPTION OF THE BRIDGE DECK

Botley Flyover was constructed in 1961, and carried the A34 dual carriageway over Botley Road (Plate 3.1). The 16m centre span comprised fifty-one beams of trapezoidal section, which were longitudinally and transversely post-tensioned. The beams of the shorter side spans were pre-tensioned. The section through the deck of the original centre span, which has now been replaced, is shown in Figure 3.1.

The detailing of the anchorage was such that it was vulnerable to entry of surface water. The steel anchorage plates to the longitudinal tendons were not recessed into the ends of the beam. In addition, the gaps between the three simply-supported spans were filled with poorly compacted concrete. Water leaking through the asphaltic plug joints could thus gain access to some of the anchorage plates and consequently into the ducts if the anchorage plates were not properly sealed.

The twelve 7mm wires within each of the five ducts in each longitudinal beam were anchored by individual collets and wedges. The construction record drawings showed that each wire was stressed to an initial tension of 36 kN. This corresponded to 60% of the ultimate strength of the prestressing wire. The bridge had originally been designed to CP114 and CP115, the codes of practice for reinforced and prestressed concrete, which have now been superseded by BS 8110. In the original design, the centre span had been designed as simply-supported and a lump sum overall loss of 15% to the prestressing system had been assumed.

During a re-surfacing contract in 1991, serious defects in the grouting of the longitudinal ducts were discovered. Eight ducts which were inspected all had extensive voids near the anchorage, and three of them contained water. Some wires had suffered pitting corrosion and two wires had failed. In some cases, the end collets were also severely corroded. As a short-term measure, the inspection holes within the ducts were grouted with epoxy resin, and the deck was temporarily propped. It was considered difficult to guarantee the condition of the bridge in the long-term, as the discovery of ungrouted ducts at the critical anchorage zones caused doubts over the durability of the bridge. As a result, the centre span of the bridge was replaced in 1992, and the beams were carefully dismantled from the deck for further tests.

3.3 BOTLEY BEAM TESTS

3.3.1 Tests Before Dismantling Deck

In-situ concrete stress measurement

The in-situ stresses on the soffit of two beams were measured prior to dismantling of the deck. Three instrumented cores using the incremental coring technique were taken near the

end anchorages and the stresses were found to be within 5% to 50% of those calculated for a beam with no corrosion.

Cutting of tendons before dismantling deck

Figure 3.2 shows the layout of the beams in the original deck. Tendons within one duct out of five were severed by coring holes in six beams, which were spaced alternately in the North-east corner of the centre span (see Figure 3.3). The resulting strains were measured by vibrating wire gauges and optical fibre sensors, and temperatures were measured by thermocouples.

3.3.2 Tests on Beams Removed From the Deck

The beams removed from the Botley Flyover following replacement of the deck, were transported to a site where a programme of tests were carried out by Oxfordshire County Council with the participation of the author. The main aim of the investigation, which formed a contract to the Transport Research Laboratory, was to assess the viability of strain monitoring as a means of indicating future loss of prestress. The extent of re-anchoring of tendons following cutting was also investigated by monitoring surface strains due to loss of prestress. A series of tests, divided into six groups, was carried out. Each test group had a particular purpose, as described in Table 3.1. The full range of tests carried out and the results obtained is reported by Darby (1996). This field investigation was considered to have provided evidence relevant to both the inspection and assessment of post-tensioned concrete structures. A brief description of each test is given below.

3.3.2.1 Inspection of Beams

The tendons which were selected for subsequent cutting and strain monitoring were chosen following a series of tests involving visual inspection, hole drilling into the ducts and pressure testing. This included external examination of the condition of the end plates and collets, which may indicate corrosion or the presence of chlorides in the anchorage area. Standard descriptions were used to report on the external condition of all fifty-one beams which were inspected in this way, and also the condition observed inside the drilled ducts.

One 25mm diameter hole was drilled at both ends of the five ducts in each of 27 beams (i.e. 270 holes in total). These holes were visually inspected and pressure tested by the Belmec method for void volume measurements, leakage rate of air and continuity of voids. However, there were problems in drawing conclusions from very localised visual inspection, as the duct was not penetrated at the level of an existing void in some cases. The work was also hampered by access problems. Additional pressure testing was carried out in a further seven selected ducts where intermediate holes at the centre and quarter points were drilled.

A system was introduced whereby the indicators of corrosion were each given a factor, called the Corrosion Risk Factor (CRF), according to the degree of risk they were assumed to impose. It was a matter of subjective judgement what value was to be assigned to each risk factor; a value within the range of 1-5 or 1-10 was given, with higher values indicating greater risk. These factors enabled the inspection results to be interpreted in a systematic way and helped determine the beams to be selected for further testing. The CRFs used were:

1) End plate condition risk factor - a measure of chloride contamination (CRF 1-5)
2) End collet condition risk factor - indicates chlorides close to tendons at anchorages, where grouting is most likely to be incomplete (CRF 1-10)
3) Leakage rate risk factor - likelihood of ingress paths for contaminants (CRF 1-10)
4) Void volume risk factor - measure of tendon exposure and an indicator of a route for the passage of contaminants. As the volumes cannot be considered in isolation (tendons within a perfectly sealed and alkaline condition are not at risk), this risk factor was combined with the leakage rate risk factor (CRF 1-10)
5) Visual evidence risk factor - depends on dry/damp conditions, distribution of grout, and extension of local conditions at drilled holes to overall conditions in the duct (CRF 1-10)

These individual risk factors were combined to give an overall risk of tendon corrosion within a duct. In this investigation, these were simply summed for each duct and then summed for each beam. It was concluded that this concept of CRF still needed refinement before being used on a bridge in service.

3.3.2.2 De-stressing Techniques

The beams that were selected for further tests to determine the effectiveness of tendon re-anchoring following de-stressing, covered a wide range of grout conditions. The de-stressing techniques employed were:

Removal of collets

By cutting off the exposed collets with an angle grinder, the stress within individual prestressing wires at the anchorage was released. This was undertaken on ducts already cored during the insitu tests. This test was intended to indicate if tendons had remained stressed at the anchorage even a few months after removal from the deck. Tendon movement (pull-in) was measured and the end plate was removed to inspect the duct to determine if tendons had failed due to corrosion.

Coring of tendons

A core drill penetrated the duct, and strain readings were taken as the wires were severed. These cores also enabled a thorough inspection of the local condition of the tendon and the grout. Some of the cores had up to 50% voids, exposing more than half of the wires within the tendon. A typical core illustrating an incompletely grouted duct, is shown in Plate 3.2.

Cutting of tendons

The tendons were exposed at the base of a 150mm core. Selected tendons were marked before cutting with either an angle grinder or by burning.

At all times during the tests, a timber and steel barrier was secured against all collets vulnerable to ejection as a result of release of stress.

3.3.2.3 Strain and Temperature Monitoring Techniques

Strain and temperature measurements were recorded during the tendon cutting operation and for two weeks after the release of prestress.

Tendon strain by pull-in at anchorage plates

The retraction from the face of the end plates of fully or partially unbonded tendons as a result of removal of collets was measured. This was measurable if the pull-in was less than the thickness of the plate (20mm). When the plates were removed, the pull-in of all wires could be measured.

Tendon strain at intermediate locations

Demec gauges and studs glued directly to the prestressing wire were used to measure strains in the tendons remote from a cut point. These tendons were first exposed at the base of 150mm diameter cores. By marking the wires adjacent to the cut point, instantaneous slip was determined.

Concrete strains by Optical Fibre Sensors

Optical fibre sensors (SOF) were retro-fitted to the beam soffit underneath the tendons to be cut. These sensors, of various lengths up to 5m, measured *total* concrete displacements between their fixed end points, and recorded them on data loggers. They were used to assess the effectiveness of strain monitoring, and to demonstrate the extent of tendon re-anchoring in ducts closer to the bottom surface of the beam.

Concrete strains by Vibrating wire gauges and Demec gauges

Concrete strains were also measured by vibrating wire gauges (VWG) and Demec gauges to compare with other forms of gauging. The VWGs were not meant for long-term use as they were not insulated or protected, but measurements were taken for up to two weeks following cutting of the tendons. Demec gauges with gauge lengths of up to 600mm were used and were more effective for short-term use. Concrete temperatures were recorded by thermocouples which were embedded in the beams at typical locations, and recorded on data loggers throughout the tests. These were used to assist in interpretation of data.

The sensors and gauges were placed to determine the short and medium term strain changes due to tendon failure; in particular strain changes along the length of the beam to determine the ability of tendons to re-anchor. It was aimed to correlate the measured re-anchoring length with the observed quality of grout. Where more than two types of monitoring were used in the same area, the gauges were offset by about 50mm on each side of the centre line of the duct, or by the smallest distance necessary.

3.4 SUMMARY OF RESULTS OF FIELD TESTS

3.4.1 Visual Inspection

There was widespread corrosion of collets and anchorage plates, but this was more evident on the edge beams and south west quarter of the deck which was the lowest area, where water may have collected. Plates 3.3 and 3.4 respectively illustrate an example of the condition of the collets at the anchorage plate, and ungrouted wires near the anchorage area.

The Belmec pressure tests demonstrated variable and generally poor grouting. Out of 135 ducts tested, 19% had voids below 0.2 litres, 11% had voids between 0.2 and 1.0 litres, 34% had voids between 1.0 and 5.0 litres, 16% had voids above 5 litres and a further 20% could not be tested because of gross leaks. One duct was completely empty (34 litres of voids).

The leakage rates measured were generally high, but most of the gross leaks (exceeding 10.0 litres/min) were attributed to water jetting and other demolition methods employed earlier during dismantling of the deck, which increased the likelihood of leakage compared to when the bridge was in service. Leakage was also evident around the anchorage and end plates; this was due to the poor condition of the concrete which filled the narrow gap between adjacent bridge decks. The rest of the ducts not damaged during demolition were considered to be well sealed, which explains the lower incidence of corrosion in these ducts. It was concluded that voids alone will not cause corrosion unless the leakage rate is sufficiently high to allow the ingress of chlorides, and thus cause corrosion of the tendons.

3.4.2 Methods of Strain Measurements

The relative merits of strain measurement by Demec gauges, Vibrating wire gauges and Optical fibre sensors in this application for monitoring prestressed concrete structures were compared. However, the main problem was separating the temperature effects from the effects of prestress loss due to tendon failure. As each gauge is generally influenced by temperature in a different manner, the relevant readings had to be suitably corrected for temperature.

The VWG sensors which were used for longer-term strain monitoring tended to exhibit general drift down of readings (Figure 3.4) for a few days after installation. This was thought to have been due to creep in the fixings or adhesive layer. The figure also shows that the recorded strains are clearly affected by the daily temperature cycles. Even after the strains had been corrected for the effect of diurnal temperature changes, the corrected results did not exhibit much improvement. In fact, they suggest that the original readings may have been over-compensated. The recorded strains should perhaps have been corrected by only 2 or 3μm/m/°C (i.e. difference between the coefficients of thermal expansion of steel and that of concrete) instead of the whole coefficient of expansion of concrete (assumed to be 11μm/m/°C in figure 3.4) as was applied.

This study shows that long-term monitoring by strain measurements cannot be regarded as providing a qualitative result, and that further developments are still required before the method can become a feasible long-term monitoring tool to detect future loss of prestress due to corrosion. To enable the results to be correctly interpreted, a system needs to be developed to differentiate between strains due to temperature and prestress loss. As was highlighted in Chapter 2, it remains doubtful if long-term monitoring by strain measurements is able to detect local loss of prestress due to corrosion as well as distinguish the resulting strains from other events such as the passage of heavy vehicles, diurnal temperature changes, or general drift of the instrumentation.

3.4.3 In-situ Tests (before dismantling deck)

The instrumented cores taken from the soffit of the deck before it was dismantled indicated an average compressive stress at the bottom fibre of 2.13N/mm^2. This corresponded to only one third of the expected calculated stress with no corrosion even after allowing for 30% losses. The difference may be either due to the fact that total losses to the system were more than the 30% assumed, or the original stressing did not reach its required level, or an error occurred in the instrumented core measurements.

The cutting of tendons before dismantling the deck provided valuable and unique results with regard to the magnitude and spread of strains, the viability of strain monitoring for prestress loss detection, and the relative efficiency of the VWGs and SOFs. The results

demonstrated considerable lateral spread of the effect of prestress loss over a distance of up to six beams (Figure 3.5), the effect reducing the further the sensor was from the cored position. The failure of tendons upon cutting produced clearly detectable strains on the deck soffit which was measurable by both the VWGs and SOFs. The latter have the advantage that they measure strain over a relatively longer gauge length and are therefore more likely to cross the point of tendon failure. However, as a result of the longer gauge length, the peak strains are averaged out and the values are hence less than those measured by VWGs. Surface strain changes due to loss of longitudinal prestress thus seem detectable by SOFs, but the difficulty is that the exact time and location of the prestress loss are not known.

Although spreading a long distance, the magnitude of the strain change remote from the cut point was small. This demonstrates the difficulty of identifying prestress loss due to tendon corrosion during the long-term monitoring of strains, bearing in mind that the strains may be masked by temperature effects and transient loading. This lateral spread of strains as a tendon is cut, demonstrated the load-sharing between beams within the deck, which may provide additional reserves of strength to the bridge. Figure 3.6 illustrates the spread of strains exhibited by the VWGs following cutting of Tendon D in Beam 5, and shows the effect on adjacent beams. The greatest strain effect was on Beam 5 where the tendon was cut, with progressively smaller strains on adjacent Beams 4, 3 and 2. The maximum strain was only about 15μm/m, demonstrating the high level of sensitivity required in the instrumentation system. The strains measured by the VWGs installed on Beam 5, positioned at 0.5m and 1.0m from the cored position respectively, showed that within just a very short distance, the strains had reduced to relatively small levels. This suggests that tendon re-anchoring had occurred over this short distance.

In all cases, the cutting of the prestressing tendons produced an expansion of the concrete around the tendon failure location, as the prestress in the tendon was released. However, this expansion always recovered to some extent as the stresses released by the failed tendon, redistributed. As shown in Figure 3.4, there seems to be an immediate recovery following an increase in the concrete strain of about 100μm/m when Tendon D was cut in Beam 14. The magnitude of this recovery decreased with time, possibly due to creep and

relaxation of the prestressing steel after re-anchoring. This trend was demonstrated by all the beams in test Group B.

3.4.4 Tests on Isolated Beams (removed from deck)

The cutting of collets indicated that the beams at the south end were more poorly grouted and contained more voids, which accommodated the pull-in of wires when they were cut. In some cases, the wires which did not initially pull in when they were severed, did so after some time. This is probably due to the presence of poor grout in the duct near the south end which enabled the bond to be progressively broken and allowed subsequent slippage as the tendon attempted to return to its unstressed state. Most of the wires severed at the north end did not retract, and this was the case when they were inspected again 15 months later.

Inspection of the cored holes suggests that very effective rebonding occurs in a well grouted duct, and this has held with time. There was also very little evidence of cracking of the hard dry grout which implies that the expansive bursting forces during tendon failure were not predominant.

When the effect of cutting the central tendon C in two beams of different grout conditions was considered, Beam 32 in which duct C was known to be completely ungrouted, exhibited a strain increase of about 70μm/m. This reading which was recorded by a 2m length SOF at the north quarter point, reduced to half its value after about 20 hours. Since the failed tendon could not re-anchor because there was initially no grout in the duct, this relief of strain was believed to be either due to the other four tendons taking up some of the force deficit, or elastic creep recovery of the concrete. As expected in this case, the VWG readings confirmed that the tendon did not re-anchor; a strain increase of about 50μm/m was recorded at the south and north ends of the beam. This strain increase was comparable with that obtained by the author, simply by hand calculation during an early investigation before the analytical model was developed (Cavell and Waldron, 1994). The calculated value was 71μm/m at the beam ends if 15% losses to the system was assumed (as in the original design), and 60μm/m for 30% assumed losses (as estimated by BS 5400, 1990).

Figure 3.7 shows the location of the instrumentation used to monitor the strains on Beam 31 and Beam 1. In Beam 31 where duct C was moderately well grouted, a strain increase of 74μm/m was recorded by VWG3 when Tendon C was cored at the north quarter point. The calculated value was 120μm/m and 100μm/m respectively for 15% and 30% assumed losses. Figure 3.8 illustrates the *total* strain increase after all the wires were cut (half the wires were cut the previous day). Tendon re-anchoring is demonstrated by smaller strains recorded by VWG4 and VWG5 which were 1m and 3m away from the cut point respectively. These strain values which were measured over a short time interval (where temperature effects are minimised), were used to validate the analytical models developed in this research.

When Tendon D was cored in Beam 1, a strain increase of about 100μm/m was recorded by the SOF. It is reported that duct D had a uniform void of about 7.4 litres. VWG3 at the cored position recorded about 162μm/m which reduced to 98μm/m after 15 minutes (Figure 3.9). The latter VWG value was chosen (that which has 'stabilised' after coring) to compare with the analytical models. On VWG2 and VWG4, which are 1m on either side of the cored position, the readings reduced to 45μm/m and 32μm/m respectively, indicating that some re-anchoring has occurred within 1m from the cored position. VWG5 and VWG22 at the south end did not seem affected by coring of Tendon D at the north quarter point, indicating that the strain increase at the cored position was relatively localised, and that the tendon had re-anchored. Although the void volume was not negligible (1/5 of duct volume), it did not seem to affect the re-anchoring ability of the failed tendon. The strains also did not seem to change much after 10 months, suggesting that the re-achoring effects were not lost over time.

3.5 CONCLUSIONS

In this chapter, the field investigation undertaken in association with Oxfordshire County Council on post-tensioned concrete beams removed from the demolished Botley Flyover, has been described. The following conclusion can be made from the field study of the full scale bridge beams:

- The Botley beams have demonstrated some typical problems being faced by similar beams of this age. In particular, they exhibit widespread voids near the anchorage ends where chlorides are most likely to gain access.

- The investigation aimed to provide a solution to the durability problem by monitoring post-tensioned bridges. It was believed that such bridges may be of suspect durability but still possess adequate residual strength. Hence by monitoring such structures, costly replacement could be avoided or delayed.

- The field study has demonstrated the difficulty of distinguishing the resulting strains due to tendon failure from the effects of diurnal temperature changes, and this questions the feasibility of long-term monitoring by strain measurements as a means of detecting future loss of prestress.

- The lateral spread of strains across the beams within the deck was also detected, indicating the load sharing between beams within the deck. This characteristic may provide the additional reserves of strength to the bridge.

- The study has shown that very effective rebonding occurs in a well-grouted duct, and this has held with time. The study also revealed the ability of failed tendons to re-anchor even in the presence of some voids in the grout.

GROUP	DESCRIPTION	PURPOSE OF TEST	TEST NO.	BEAM and END
A	Insitu concrete stress before dismantling deck	To check existing level of prestress	A1 A2 A3	2 2 11
B	Soffit cores before dismantling deck	To assess the longitudinal and transverse distribution of strain in the deck when tendons fail, and also to provide information on the effectiveness of sensors and their required spacing	B1 B2 B3 B4 B5 B6 B7	14D 11D 9D 7D 5D 2D Temperature & Transverse
C	Cutting of collets on beams already cored	To measure strain effects of destressing by cutting off collets on ducts already cored. To determine if wires have remained stressed over time, and vibration during demolition	C1 C2 C3 C4	2D* North 2D South 5D North 5D South 7D North 7D South 9D North 9D South
D	Cutting of tendons in central duct	To assess the effectiveness of monitoring. To compare the effect of de-stressing the central duct C in Beam 32 which is empty, with duct C in Beam 31 which is moderately well-grouted	D1 D2	32C 31C
E	Cutting of tendons in lower duct	To measure the external effects of cutting the lower tendon (most detectable position) on two beams of different grout quality. To compare the length tendons take to re-anchor in a variety of grout condition.	E1 E2	1D 4D
F	Cutting of tendons with tendon strain measurement	To measure the internal strains on prestressing wires as a result of cutting lower tendons	F1 F2 F3 F4	28E 29D 30D 6D

Note: (i) 2D denotes Duct D of Beam 2.

(ii) Key to duct lettering system (from North):

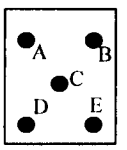

Table 3.1 Summary of Tests carried out on the Botley Beams

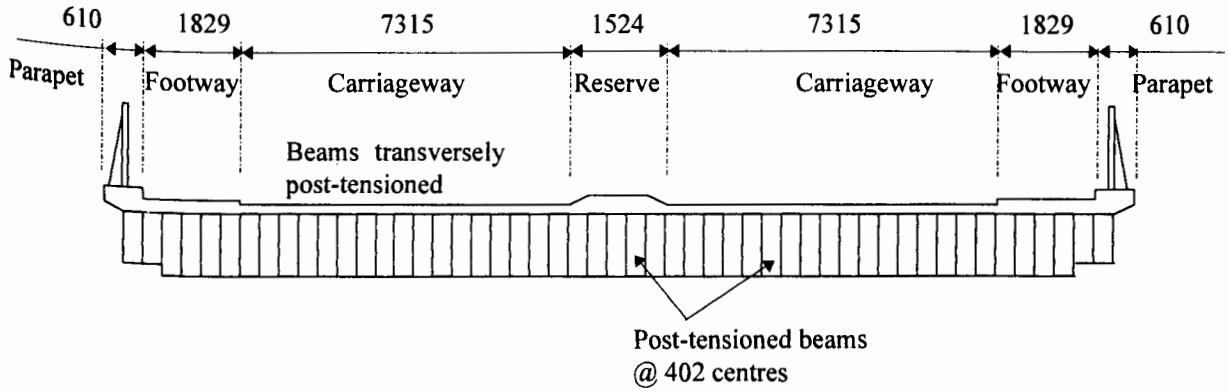

Figure 3.1 Section through the original deck centre span of the Botley Flyover

(All dimensions in mm; vertical scale distorted)

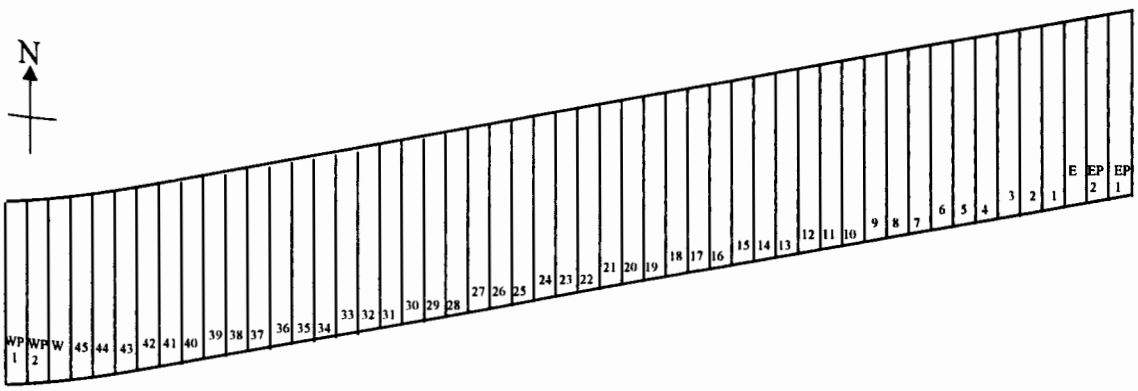

Figure 3.2 Layout of Botley Flyover centre span beams before demolition

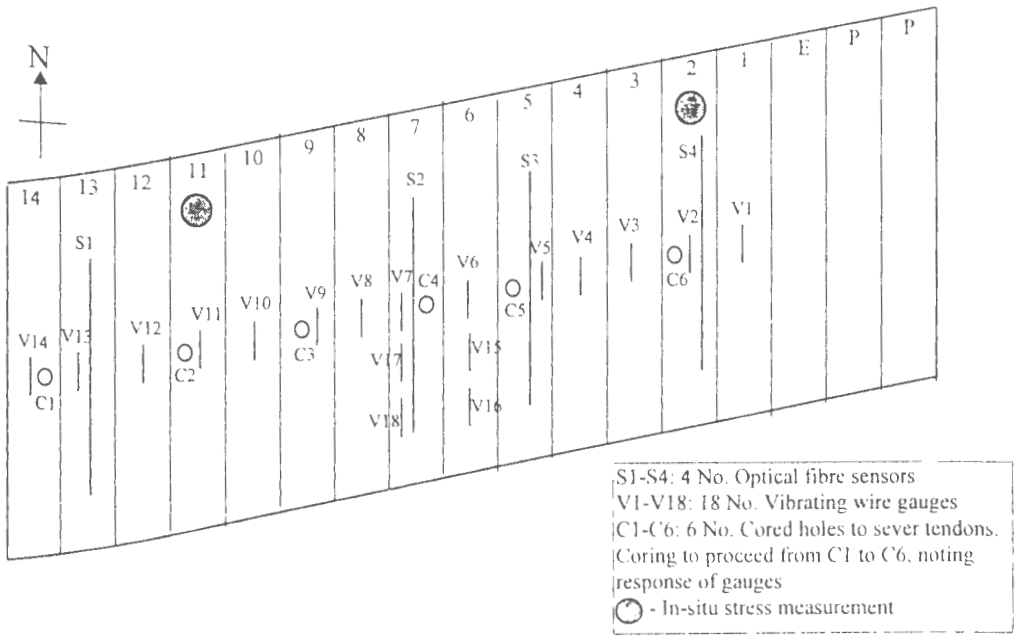

Figure 3.3 Layout of instrumentation on original deck before dismantling

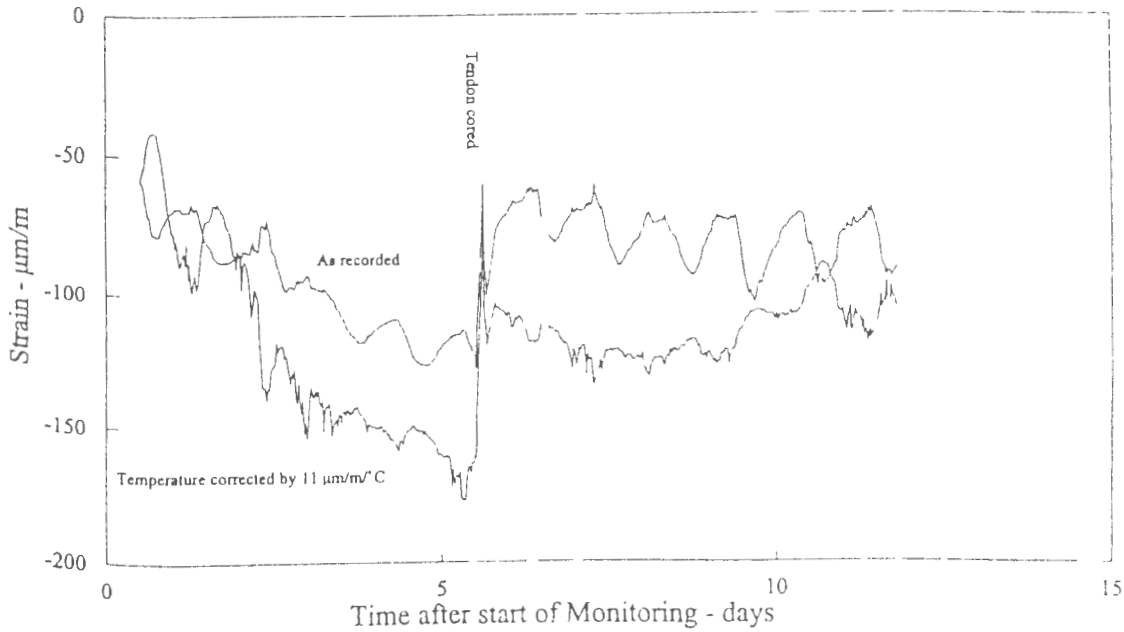

Figure 3.4 Strains recorded by VWG as a result of coring Tendon D on Beam 14 (Darby, 1996)

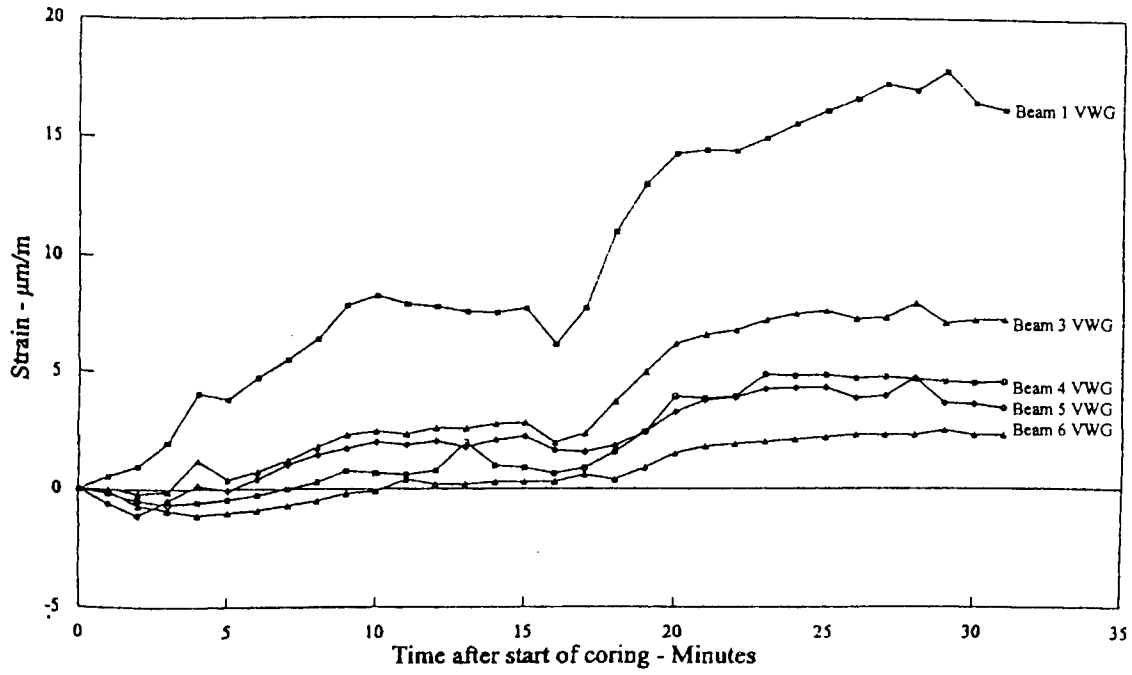

Figure 3.5 Strains recorded by VWG on adjacent beams as a result of coring Tendon D on Beam 2 (Darby, 1996)

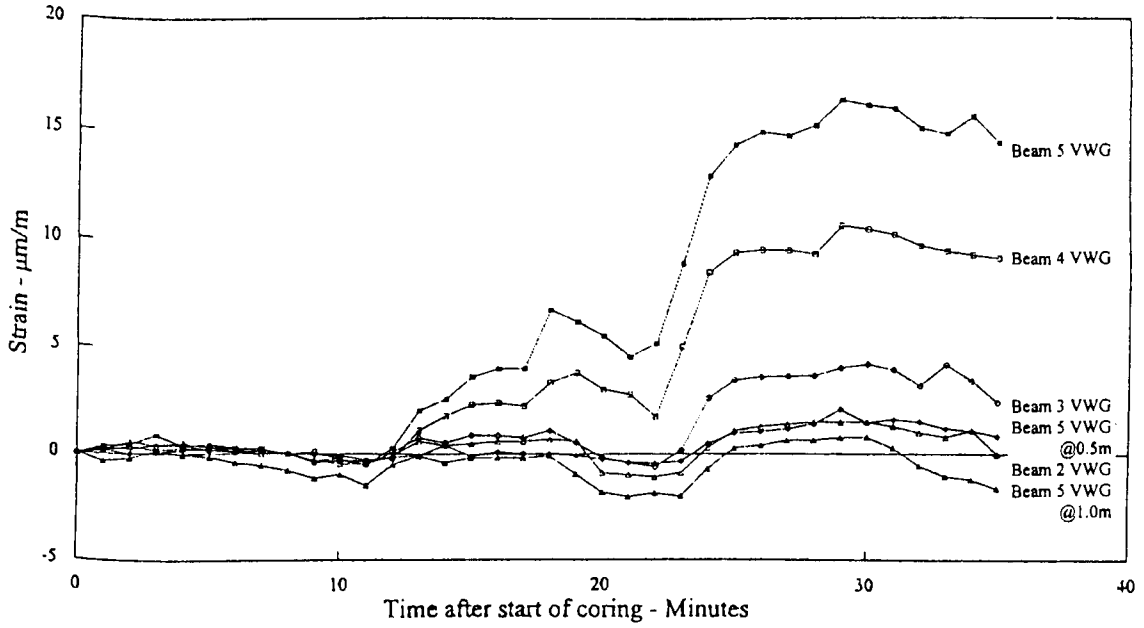

Figure 3.6 Strains recorded by VWGs as a result of coring Tendon D on Beam 5 (Darby, 1996)

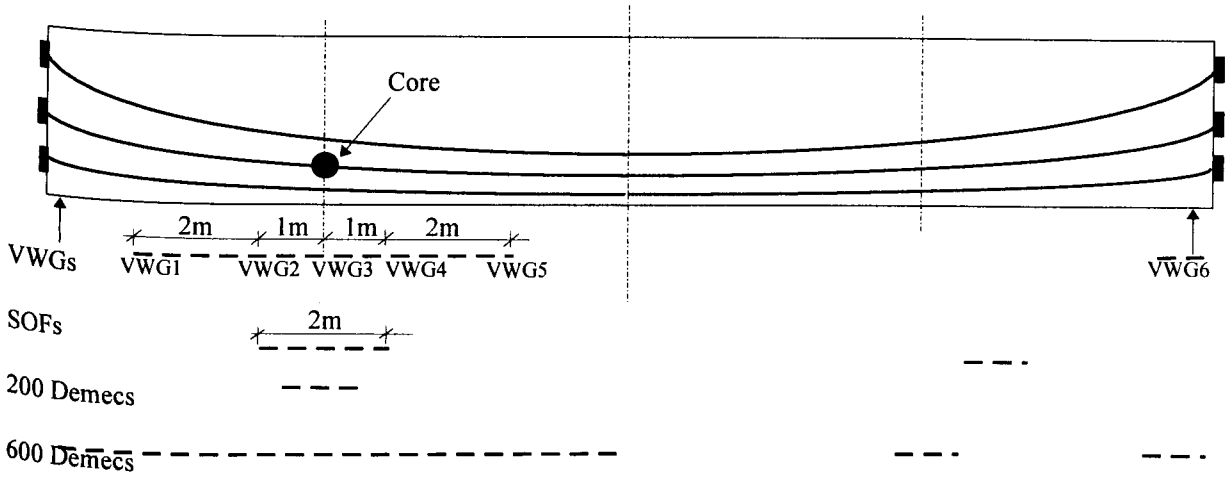

(One demec and one VWG also placed on top of beam at north quarter point)

(a) Beam 31

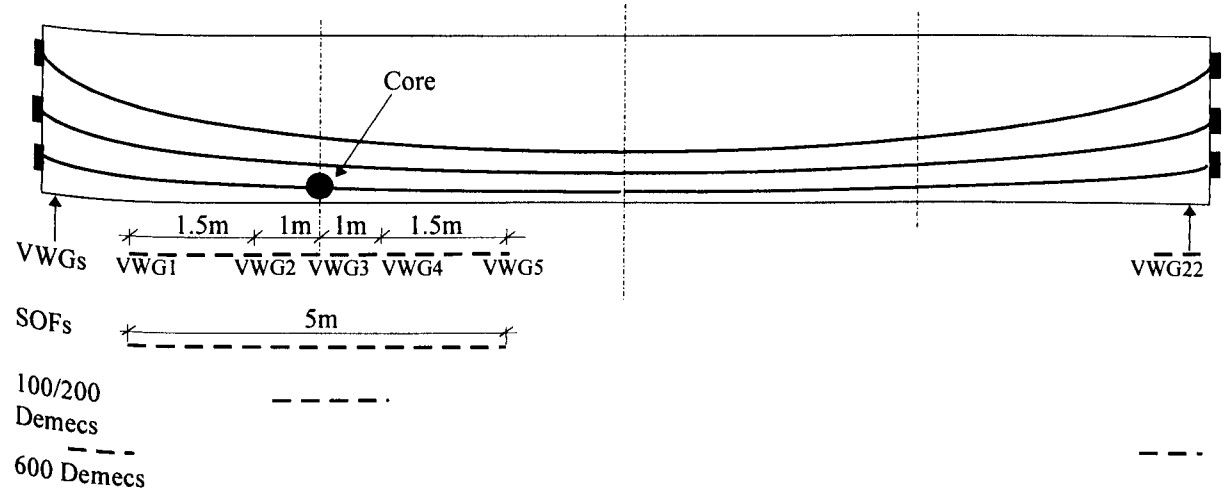

(600 demec gauges also placed at midspan on each side of beam)

(b) Beam 1

Figure 3.7 Monitoring locations for Beam 31 and Beam 1

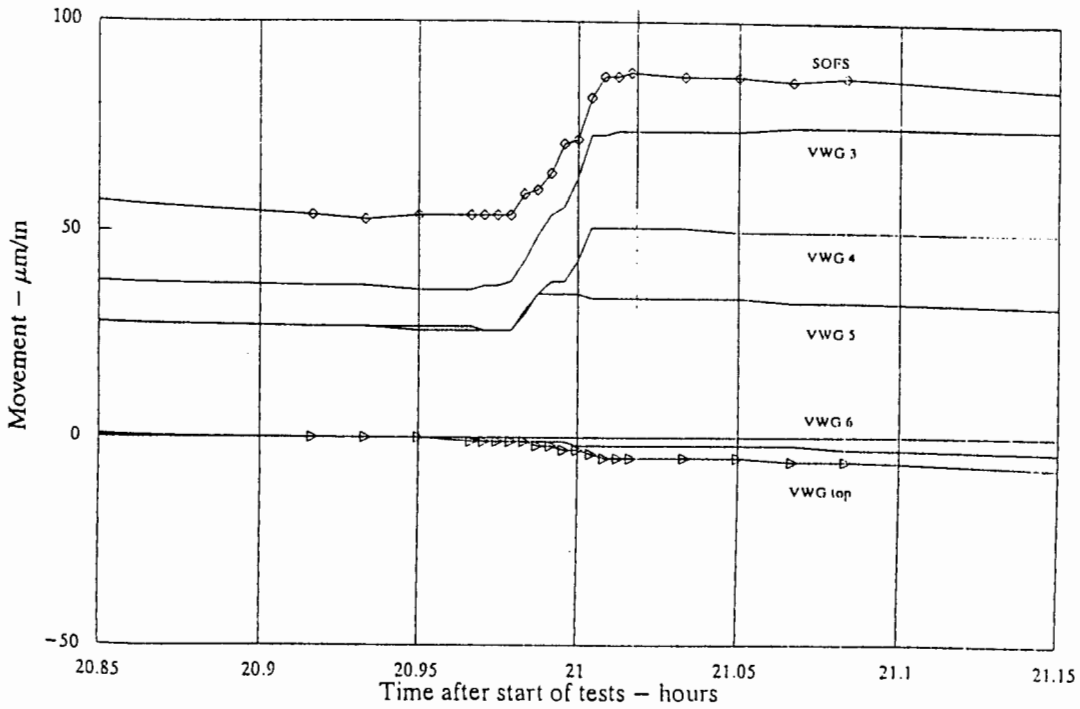

Figure 3.8 Strain changes along Beam 31 as a result of Tendon C cored at north quarter point (Darby, 1996)

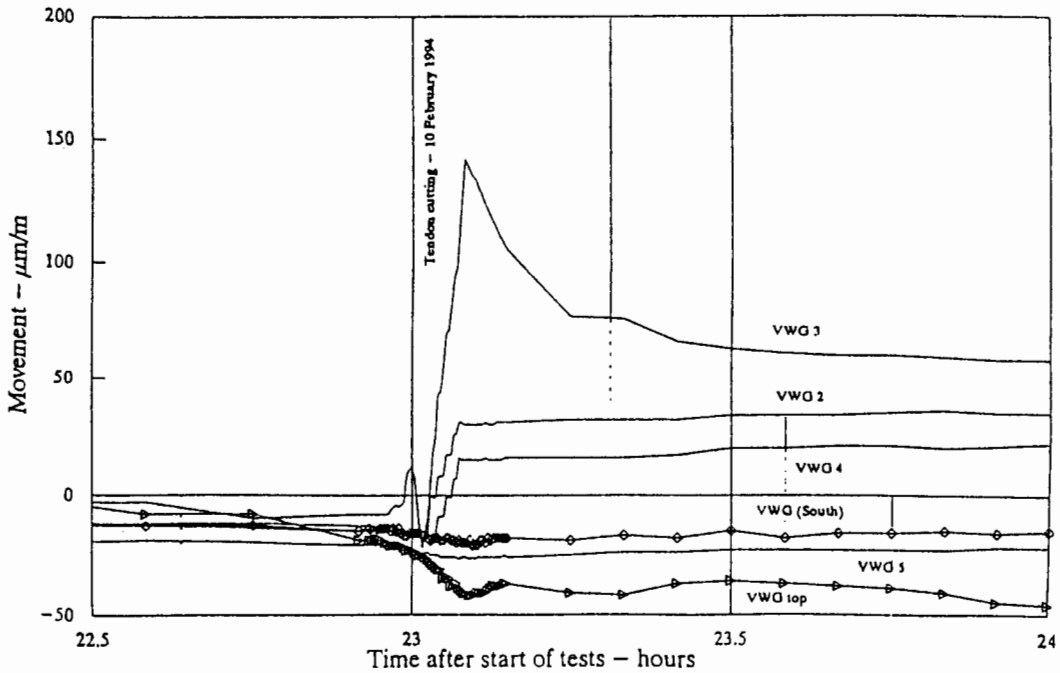

Figure 3.9 Strain changes along Beam 1 as a result of Tendon D cored at north quarter point (Darby, 1996)

Plate 3.1 Aerial view of the Botley Flyover (Darby, 1996)

Plate 3.2 Concrete core exhibiting an incompletely grouted tendon duct (Darby, 1996)

Plate 3.3 Severely corroded collets at the anchorage plate

Plate 3.4 Condition at anchorage of one of the Botley beams, showing ungrouted wires

CHAPTER 4

Localised Loss of Prestressing Tendon Area

4.1 INTRODUCTION

This chapter describes the methodology adopted in investigating the effect of localised loss of prestressing tendon area due to corrosion, on the stresses in the tendons. This can initially be studied by consideration of a simple analytical model comprising a single post-tensioned tendon, or a number of tendons. By applying the compatibility and equilibrium conditions, the stress enhancement in the corroded part of the tendon and the other supporting tendons can be determined.

However, the analysis is limited to simple models and a number of simplifying assumptions have to be made. Moreover, it is difficult to consider the respective contribution of both the concrete and the tendon towards restoring equilibrium upon the loss of tendon area. A knowledge of the bond characteristics between the tendon and the concrete is required. With the availability of more versatile numerical methods of analysis such as the finite element method, it is possible to study the effects of these two actions. This latter approach was judged most appropriate for the present study and was adopted.

After a short review of the subject of finite element modelling and available finite element packages suitable for the analytical work, the ANSYS program is briefly introduced. The rest of the chapter then describes the modelling work with this chosen finite element program. The discretization of the mesh and modelling of prestressing are first described. A description of the material models adopted in the analysis is also given, and finally, an account on the modelling of the interface between the concrete and the prestressing tendon is described. This is then followed by a discussion of the results of the analyses.

4.2 SIMPLE ANALYTICAL MODEL

The general effect of localised corrosion on the stress in a post-tensioned tendon was investigated with a simple analytical model comprising a single post-tensioned tendon of length L (Figure 4.1). Assuming that corrosion of the prestressing tendon is followed by an overall extension of length ΔL in the tendon, then considering compatibility of strains at the level of the corroded tendon,

$$\Delta L = \Delta l_1 + \Delta l_0$$

$$L\varepsilon_T = l_1\varepsilon_1 + l_0\varepsilon_0$$

$$L\frac{\sigma_T}{E_{ps}} = l_1\varepsilon_1 + (L - l_1)\varepsilon_0 \qquad \text{.....(4.1)}$$

where $l_0 = L\text{-}l_1$ is the uncorroded length of the tendon, Δl is the extension of the tendon within the respective region (corroded or uncorroded) of the tendon, E_{ps} is the modulus of elasticity of the prestressing steel, and ε_T and σ_T are respectively the original strain and stress in the tendon before corrosion.

By force equilibrium of the tendon alone (i.e. ignoring any contribution from the surrounding concrete), the force in the corroded part of the tendon and that in the uncorroded part is the same:

$$T_r = \sigma_1 a_1 = \sigma_0 a_0$$

thus

$$\sigma_0 = \phi\sigma_1 \qquad \text{.....(4.2)}$$

where $\phi = a_1/a_0$ is the ratio of corroded to original cross-sectional area of the tendon.

The residual stress σ_1 in the corroded part of the tendon can now be obtained from equations (4.1) and (4.2),

$$L\sigma_T = l_1\varepsilon_1 E_{ps} + (L - l_1)\varepsilon_0 E_{ps}$$

$$L\sigma_T = l_1\sigma_1 + (L - l_1)\sigma_1\phi$$

$$\frac{\sigma_T}{\sigma_1} = \frac{l_1}{L} + (1 - \frac{l_1}{L})\phi$$

Thus, the stress concentration factor by which the original tendon stress is approximately enhanced as a result of local loss of tendon area is given by

$$\eta = \frac{\sigma_1}{\sigma_T} = \frac{1}{\beta + (1-\beta)\phi} \qquad \text{.....(4.3)}$$

where $\beta = l_l/L$ is the ratio of corroded to total length of the tendon.

This equation was also given by Price and Aguilar (1988) when they considered the general effect of tendon corrosion with such a simple model. If the cross-sectional area of the tendon is reduced by the factor ϕ, over a length which is the proportion β of the total length of the tendon, the approximate amount by which the original stress is enhanced is shown in Figure 4.2. It can be seen that the more localised the corrosion, the greater is the stress enhancement. The stress concentration factor also increases with the degree of corrosion (ϕ factor). If the ratio of the residual tendon force to the original tendon force (T_r/T_0) is plotted against the length ratio β (Figure 4.3) the amount of force lost is seen to increase with the length over which the corrosion occurs. At $\beta = 1$ (i.e. full length corrosion), the ratio of force remaining is equal to ϕ, the ratio of tendon area remaining.

The significant effect of localised loss of tendon area is the amount of stress enhancement in the corroded tendon. This may result in tendon failure if the stress is excessively high. In practice, the total prestressing force will normally be provided by several tendons, either as a series of individual wires or groups of wires formed into strands. It is thus expected that the stress enhancement in a corroded tendon will be reduced through redistribution of stresses between the tendons. This was investigated by extension of the simple model to consider multiple number of tendons (of equal cross-sectional area) within an element of concrete. The analysis procedure was based on the same principle as presented above, but the equilibrium of forces among n number of tendons was also considered. It was also assumed that there was perfect bond between the tendons and concrete, and the tensile force contributed by the concrete was ignored. The derivation of the respective equations is given in Appendix A.

Figure 4.4 illustrates the case for a corroded tendon in a section which contains a number of tendons. It can be seen that the proportion of total tendon force carried by the corroded tendon decreases with the length and degree of corrosion, and the number of tendons to share the load. The force deficit of the corroded tendon was compensated for to a degree

by the uncorroded tendons which carried a greater proportion of the load than original. Figure 4.5 illustrates that the stress enhancement in the corroded tendon is reduced with the length over which the corrosion occurs and the number of tendons available, but it increases with the degree of corrosion. The stress increase in the other uncorroded tendons and its influence in reducing the stress enhancement in the corroded tendon, is shown in Figure 4.6 for the case of $\phi = 0.3$ (i.e. 70% loss of area in corroded tendon).

4.3 FINITE ELEMENT ANALYSIS

In order to obtain a better understanding of the contribution of the surrounding concrete in transferring forces from the corroded tendon to the other uncorroded tendons, and in providing additional restraint from the extension of the corroded tendon, a more rigorous analysis is required. The action of both the concrete and the prestressing tendons in restoring equilibrium upon the loss of some prestressing force due to corrosion, needs to be studied. The finite element method of analysis was considered suitable to provide further understanding of the effect of local loss of tendon area on the stresses in the tendons and the concrete. In addition, the finite element method allows for analysis of the overall behaviour of the whole structure, or any local part of it.

4.3.1 Basic Requirements of Analysis

There are now many finite element based software packages on the market, with some very specialized finite element codes to do a more specific job. In the current analytical study, the local loss of prestressing tendon area due to corrosion is to be considered. This will undoubtedly require that the prestressing tendons be discretely modelled (as opposed to smeared reinforcement), together with an appropriate level of prestressing (tensile) force. The interface between the prestressing tendon and concrete will also need to be modelled to allow for slip and the re-anchoring behaviour of failed tendons to be studied. In addition, appropriate non-linear material models are required to simulate the concrete and prestressing steel behaviour.

As a static analysis was to be undertaken, it was judged that any general finite element package would be suitable. ANSYS and ABAQUS are two user-friendly finite element

codes which were readily available in the department. They both have extensive documentation to guide the user through the analysis procedures. However, ABAQUS does not have its own in-built pre- and post-processors. Apart from very simple analyses, all other analyses which require more complicated mesh generation would need to be interfaced with an external pre- and post-processor such as FEMGEN/FEMVIEW. ANSYS however, has its own pre- and post-processors, together with a general code to solve a wide range of problems. Although it cannot easily model prestressing in a post-tensioned tendon, as some other software is able to do so, the effects of prestressing can be modelled indirectly.

4.3.2 Introduction to ANSYS

The ANSYS program was introduced in 1970. Since then, the program has grown to provide a complete family of finite element based products. It is a general purpose finite element analysis program which includes many general capabilities such as pre-processing, solution, post-processing, graphics, parametric modelling and design optimization. It can solve many types of problems such as structural, thermal, electric, magnetic, fluids; and includes both static and transient, linear and non-linear problems. It is one of the most widely recognized general-purpose program for engineering analysis available today, and is used extensively in the industry and universities.

The ANSYS element library consists of approximately 100 different element formulations or types, including spars, beams, 2D and 3D solids, shells, springs, masses and contact elements. ANSYS contains over 7 material models to characterize different types of material behaviour.

To run the ANSYS program revision 5.0a (Swanson Analysis Systems Inc., 1992), the minimum requirements are a 486 DX or DX2 microprocessor, 8 megabytes minimum total machine memory, and at least 120 megabytes of free disk space available on the hard disk. Some of the analyses of the present study were carried out on a PC, but for analyses taking longer run times (approximately five hours), these were run on the Silver platform which was available on the University network. This reduced the run time to just over thirty minutes.

4.4 FINITE ELEMENT MODELLING

4.4.1 Local Analysis Model

The initial analysis involved a local two-dimensional finite element model. The aim of this local analysis was to provide fundamental information on the tendon response upon local loss of its cross-sectional area. The ultimate aim was to develop this into a global analysis and correlate some of the analytical results with field observations of the post-tensioned beams from the Botley Flyover. Details of this field investigation were described in Chapter 3.

This local model was represented by a finite element mesh composed of 4-noded two-dimensional quadrilateral solid elements (PLANE42) to model the concrete, and 2-noded link elements (LINK1) to model the prestressing tendon (Figure 4.7). The model represents an element of concrete of length $L=1m$, which is stressed by a single post-tensioned tendon. An initial strain value $\varepsilon_{ps}=3.27x10^{-3}$ (corresponding to a stress of $654N/mm^2$) was applied to the tendon to model the effects of prestress in the tendon. Stiff end plates were also modelled to minimise end effects and reduce the very high (unrealistic) concrete stresses at the ends of the model as a result of the applied prestress. Table 4.1 shows the properties of the materials adopted for this local model. The interface between the concrete and prestressing tendon was not modelled, hence perfect bond was assumed.

This local model demonstrated that the effect of partial loss of area was very localised as the efficient bond enabled the concrete and steel to interact together to restore equilibrium quickly. The effect of 50% loss of area in the corroded tendon over a length of 100mm at midspan is shown in Figure 4.8, which indicates that this resulted in a relaxation of the compressive stress in the concrete around the corroded tendon. The resulting distribution of tendon stress along the corroded tendon is shown in Figure 4.9a, which illustrates the stress enhancement in the tendon at the corroded area, followed by slight stress decrease (shortening of tendon) on either side of it. The original stress in the tendon was enhanced by a factor of 1.1. This value is lower than the stress enhancement of $\eta=1.8$ which was estimated by the simple analytical model described in Section 4.2.

The longitudinal stresses σ_x obtained from the analysis were differentiated to give the bond stresses σ_b along the corroded tendon:

$$\sigma_b = \frac{d\sigma_x}{dx}\frac{\phi}{4} \qquad \text{.....(4.4)}$$

where ϕ is the diameter of the tendon. As shown in Figure 4.9b, the resultant bond stresses around the region of corrosion may be sufficiently high as to permit tendon slippage. This local analysis thus confirmed that a bond-slip model is required to allow for tendon slip to occur, as it is expected that this will smooth out and reduce the peaks of the localised bond stresses obtained here. The results from this preliminary study then led to the more rigorous global analysis. All further work described in this chapter will thus refer to the global model.

4.4.2 Mesh Discretization for Global Analysis

The global two-dimensional model was developed to represent the beams from the Botley Flyover. To take advantage of symmetry, only half the beam was modelled. The finite element mesh still consisted of 4-noded two-dimensional solid elements for the concrete, and 2-noded link elements to model the prestressing tendons. However, because the tendon profile was parabolic, the concrete mesh had to be discretized such that the concrete nodes coincided with the nodes of the prestressing tendons. The discretization adopted and the appropriate boundary conditions are shown in Figure 4.10. The maximum element aspect ratio of the mesh was kept roughly under 3, for good stress results. In this global model, the steel end plate ($E_{plate}=200kN/mm^2$, $\nu_{plate}=0.28$) to minimise end effects was only required at the left hand end of the model as symmetry (at midspan) at the right hand end of the model provided infinite stiffness.

The Botley beams actually had twelve individual wires within each of the five tendons, but in the analytical model, the wires within each tendon were represented as a single tendon of equivalent cross-sectional area. Since the analysis here is two-dimensional, the tendons at the same level were grouped together and located on the vertical symmetrical line of the beam cross-section as shown in Figure 4.11. This means that any biaxial bending effects which may arise due to eccentricity of forces as a result of failure or loss of area of a tendon, is ignored. The contribution of biaxial bending was judged not to influence significantly the overall behaviour of the beam in this case, as the beams within the bridge

deck are in practice not in isolation, but are instead flanked by other beams and surrounded by insitu concrete providing full lateral restraint. Hence, the finite element mesh was kept as two-dimensional.

The aim of this global model was to investigate both the effects of partial loss of prestressing tendon area, and the re-anchoring behaviour of failed tendons. Bond between concrete and the prestressing tendons was therefore required to be modelled to present a realistic simulation of the interplay of forces between concrete and the prestressing tendons. The development of the bond-slip model will be discussed later. It should be noted that although only half the Botley beam was modelled due to symmetry, the simulation of some local loss of tendon area meant that the model was no longer symmetrical. However, it was still considered acceptable to assume a symmetrical model, since the earlier local analysis had demonstrated that the effect of partial loss of tendon area is very localised.

4.4.3 Modelling of Post-tensioned Tendons

There are three main alternatives which can be used to model reinforcement in a reinforced concrete finite element model (ASCE, 1982). These are (i) distributed (ii) embedded and (iii) discrete representation. For a distributed representation (Figure 4.12a), the steel is assumed to be distributed over the concrete element, with a particular orientation θ. A composite concrete-reinforcement constitutive relation is used in this case. To derive such a relation, perfect bond must be assumed between the concrete and steel. An embedded representation (Figure 4.12b) may be used in connection with higher order isoparametric concrete elements. The reinforcing bar is considered to be an axial member built into the isoparametric element such that its displacements are consistent with those of the element. Again, perfect bond must be assumed. A discrete representation of the reinforcement, using one-dimensional elements (Figure 4.12c) has been most widely used. Axial force members, or bar links, may be used and assumed to be pin connected with two degrees of freedom at the nodal points. Alternatively, beam elements may be used, assumed to be capable of resisting axial force, shear and bending. In either case, the one-dimensional reinforcement elements are easily super-imposed on a two-dimensional finite element mesh such as might be used to represent the concrete.

In modelling the post-tensioned tendons in this study, the first two models are inappropriate since the tendons are not 'smeared' within the concrete (as can be considered with conventional reinforcement in reinforced concrete), but instead, are concentrated into several large tendon groups. Also, perfect bond cannot be assumed as it is known that the grouting conditions around the tendon can be defective. As a consequence, the discrete model was chosen to represent the prestressing tendons. A significant advantage of the discrete representation is that it can account for possible displacement of the tendons with respect to the surrounding concrete (slip).

The prestressing tendons were modelled with 2-noded link elements (LINK1) from the ANSYS library. As mentioned earlier, ANSYS cannot readily model prestress in a post-tensioned tendon. The effects of prestress in the post-tensioned tendons were, however, successfully modelled by imposing a pre-strain to the prestressing tendon. A constant strain value was applied to each tendon in the Botley beam, representing an overall effective prestress of 654N/mm^2. Although in practice, the prestress varies slightly along the length of the tendon due to frictional losses, a constant prestrain corresponding to an overall loss of 30% of the initial prestress at transfer was input. This amount of losses assumed is consistent with that estimated by the current code (BS 5400, 1990).

4.4.4 Description of Material Models

Steel Material:

The linear material properties of the prestressing steel were defined by the modulus of elasticity $E_{ps}=200\ kN/mm^2$. When non-linear material properties were required to describe the prestressing tendons, this was input in a non-linear material table available within ANSYS.

Since the actual stress-strain behaviour of the prestressing tendon was unknown, the non-linear behaviour of the tendon was based on the trilinear stress-strain curve for a prestressing wire proposed by BS 8110 (partial safety factor taken as 1.0), but modified to include a descending branch. Figure 4.13 illustrates the shape of the stress-strain curve defined for the LINK1 elements of the prestressing tendon. The Multi-linear Kinematic Hardening option was chosen from the non-linear material models available to define the stress-strain curve of the prestressing tendon. The descending branch of the curve was

required to enable the tendon to fail once it reaches its failure strain. If a trilinear curve had been used with no descending branch, the last (flat) slope of the model will be maintained, and the tendon will not fail even at exceedingly high strain values.

Concrete Material:

Both linear and non-linear concrete models were considered. The linear material properties were defined by the modulus of elasticity of concrete $E_c=32\ kN/mm^2$, and Poisson's ratio $\nu_c=0.2$.

ANSYS has a sophisticated three-dimensional non-linear concrete material model which predicts the failure of brittle materials. Both cracking and crushing failure modes are accounted for. However, this material model is only available with the 3D reinforced concrete solid element (SOLID65). Although the Botley beam could have been modelled with the 3D solid elements, it was judged that this would not have been justified by the considerably greater time and expense required in running this more complex model. The non-linearity of the concrete was not considered to be as important in this analysis as compared to other parameters. It was thus decided to maintain the 2D model, to enable the dominant behaviour of the beam to be captured rather than the complex mechanics of 3D behaviour.

The Drucker-Prager option was chosen to model the 2D non-linear concrete material model. This option is applicable to granular (frictional) materials such as soils, rock and concrete (Swanson Analysis Systems Inc., 1993). A more comprehensive description of the yield criterion is given by Chen (1982). The yield surface does not change with progressive yielding, hence there is no hardening rule and the material is elastic-perfectly plastic (Figure 4.14). The equivalent stress for Drucker-Prager is

$$\sigma_e = \alpha I_1 + \sqrt{J_2} = k \qquad \text{.....(4.5)}$$

where $I_1=3\sigma_m$; σ_m is the mean or hydrostatic stress = $1/3(\sigma_1+\sigma_2+\sigma_3)$, J_2 is the second invariant of the deviatoric stress tensor, α is the material constant, and k is the yield parameter.

This is a modification of the von Mises yield criterion that accounts for the influence of the hydrostatic stress component. α and k are respectively given by:

$$\alpha = \frac{2\sin\phi}{\sqrt{3}(3-\sin\phi)} \qquad \text{.....(4.6)}$$

$$k = \frac{6c.\cos\phi}{\sqrt{3}(3-\sin\phi)} \qquad \text{.....(4.7)}$$

where ϕ is the angle of internal friction and c is the cohesion value.

This yield surface is a circular cone (Figure 4.15) with the material parameters (equations (4.6) and (4.7)) chosen such that it corresponds to the outer aspices of the hexagonal Mohr-Coulomb yield surface. Additionally, volumetric expansion of the material resulting from yielding is accounted for. If the dilatancy angle $\phi_f = 0$, then no volumetric expansion will occur. If $\phi_f = \phi$, the flow rule is associative and plastic straining occurs normal to the yield surface and there will be volumetric expansion of the material.

The input required by ANSYS are the cohesion value (c), the angle (in degrees) of internal friction (ϕ), and the dilatancy angle (ϕ_f). These were obtained from α and k which are related to the compressive yield stress f_c and the tensile yield stress f_t by:

$$\alpha = \frac{f_c - f_t}{\sqrt{3}(f_c + f_t)} \qquad \text{.....(4.8)}$$

$$k = \frac{2f_c f_t}{\sqrt{3}(f_c + f_t)} \qquad \text{.....(4.9)}$$

4.4.5 Modelling of Bond-slip Layer

In the global finite element model, the interface between the prestressing tendon and the concrete was modelled to allow for tendon slip and the re-anchoring behaviour of failed tendons to be studied. Since the modelling was carried out in two dimensions, it was not possible to model the complex three-dimensional interplay of forces that constitutes bond. It was thus aimed to include a parameter that would, in terms of global deformation, reproduce reasonably accurately the effects of bond failure. This bond-slip behaviour was represented by the COMBIN39 element. This is a unidirectional spring with a non-linear force-deflection capability. The element has one degree of freedom at each node (either a

translation in a nodal coordinate direction or a rotation about a nodal coordinate axis) and has no mass or material properties.

The element is defined by two nodal points and a generalized force-deflection curve (Figure 4.16). The points on this curve (D1, F1, etc.) represent force versus relative translation in the context of this study. If the force-deflection curve is exceeded, the last defined slope is maintained, and the status remains equal to the last segment number. Both compressive and tensile regions of the force-deflection curve were defined, with the compressive region of the curve reflected from the tensile curve. Displacement along the nodal X axis was specified, and both nodes I and J of the spring element were made coincident (i.e. element of zero length).

The interface behaviour between steel and concrete was therefore 'lumped' into these spring elements which connect the steel and the concrete nodes together. Initially, each linkage contained two springs, one acting parallel to the tendon axis (longitudinal spring), and one acting perpendicular to it (transverse spring). Each node of the prestressing tendon was directly connected to an adjacent concrete node by the springs. The longitudinal spring stiffness was defined by an appropriate force-displacement curve to represent the bond conditions in the Botley beam. In the perpendicular direction, it was assumed that the steel and the concrete were rigidly connected, and this was accounted for by assigning a very high stiffness to the spring (i.e. a very steep slope in the force-displacement curve). However, in later analyses, the steel and adjacent concrete nodes were 'coupled' together in the y-direction by defining a set of coupled degrees of freedom with the ANSYS command. The coincident nodes of the steel and concrete then took the same displacement in the y-coordinate direction. This eliminated the need for very stiff transverse springs, thus reducing the number of elements and degrees of freedom (hence wavefront) in the model. Comparison of the results obtained showed that there was no difference whether the coincident nodes were coupled in the y-direction, or if stiff transverse spring elements were used. All further modelling was then carried out by coupling the coincident nodes of the steel and concrete in the direction perpendicular to the axis of the prestressing tendon.

Although the model had three layers of prestressing tendons, the interface bond-slip layer was only modelled along the tendon where corrosion was simulated. The other layers were

assumed to have full bond, and the concrete and tendon nodes were merged together. Where the bond layer was modelled, the longitudinal spring elements were used to link the tendon nodes and the coincident concrete nodes together, at all nodal positions along the tendon except at the ends of the tendon. The coincident nodes were rigidly fixed together at the left hand end of the tendon (anchorage position) and at the right hand end, where no slip will occur because of symmetry at midspan. These then form the boundary conditions for the bond layer.

As already mentioned, the bond conditions in each beam are unique and there is no general bond-slip model that can be applied with significant accuracy. In the absence of data on the bond conditions within the Botley beams, a sensitivity analysis was carried out to select the ranges of appropriate bond strength and shape of the force-displacement curve to be used. The basic force-displacement curve was based on the bond stress-slip relationship of the CEB-FIP (1993) model, but the shape of the curve was modified as described here.

A typical bond stress-slip curve by CEB-FIP (which represents a statistical mean curve for general application) is shown in Figure 4.17. τ_{max} and τ_f are the maximum bond stress and residual bond stress respectively. The values of the parameters $s_1, s_2, s_3, \alpha, \tau_{max}, \tau_f$ defining the curve for a ribbed reinforcing steel in unconfined concrete (s_1=s_2) are given in Table 4.2. For smooth prestressing steels, CEB-FIP (1993) recommends that a reduction factor of 0.2 be applied to the bond stress values. Therefore, for a concrete strength of f_{cu}=$42N/mm^2$ for the Botley beam,

for good bond conditions, $\tau_{max}= 0.2 \times 2.0\sqrt{42} = 2.59 N / mm^2$

$$\tau_f= 0.15\tau_{max} = 0.39 N / mm^2$$

for other bond conditions, $\tau_{max}= 0.2 \times 1.0\sqrt{42} = 1.29 N / mm^2$

$$\tau_f = 0.15\tau_{max} = 0.19 N / mm^2$$

From these data of maximum bond stresses, three bond strength values were chosen: f_{bu}=$2.0\ N/mm^2$, f_{bu}=$1.0\ N/mm^2$ and f_{bu}=$0.5\ N/mm^2$. These values formed the peak of the respective bond stress-slip curves considered. Since ANSYS required the input of a force-displacement curve, this was derived from the bond stress-slip curve by the following:

$$F_b = f_b \pi \phi l \qquad \text{.....(4.10)}$$

where F_b is the bond force, f_b is the bond stress, ϕ is the diameter of the tendon (or equivalent diameter of tendon group) and l is the bond length. It was assumed that the bond stress remained constant within one element length (Figure 4.18) and that this was acting on the tendon-concrete interface (i.e. the dimension of the spring was reduced to zero). Hence, although the bond stress was mesh-independent, the bond force was dependent on the element length (l=*50mm* in this case).

The analyses were carried out with two main types of force-displacement curves. In the first type of curves, as shown in Figure 4.19, no residual bond stress was considered. For the three bond strengths considered and an equivalent diameter ϕ=*24.25mm* for the tendon in the Botley beam, the corresponding bond force values were:

Bond 3a: $F_{b,2.0N/mm^2} = 2.0 \times \pi \times 24.25 \times 50 = 7.6kN$

Bond 3a1: $F_{b,1.0N/mm^2} = 1.0 \times \pi \times 24.25 \times 50 = 3.8kN$

Bond 3a2: $F_{b,0.5N/mm^2} = 0.5 \times \pi \times 24.25 \times 50 = 1.9kN$

The second type of force-displacement curve considered the residual bond stress levels. Although the bond can maintain its peak values locally, it was not expected that the maximum bond stress can be sustained over a long length. To investigate the extent by which the residual bond stresses influenced the bond behaviour, residual stress levels corresponding to 10%, 30% and 50% of the maximum bond stress values were considered for f_{bu}=*2.0 N/mm*^{2}. The corresponding bond force-slip curves, representing bond models *3aa,3ac* and *3ae* are shown in Figure 4.20. Note that a bond strength of 2.0 N/mm^2 with a residual value of half the maximum bond stress is similar to an overall bond strength of 1.0 N/mm^2.

4.5 INVESTIGATION OF FAILURE OF TENDONS DUE TO CORROSION

The results of the experimental investigation coordinated by Oxfordshire County Council on the extent of tendon re-anchoring in beams removed from the Botley Flyover were used to validate the bond models developed here. The two analytical simulations undertaken were:

(i) Failure of the middle tendon (Tendon C cut, Figure 4.11) at the quarter point position

ii) Failure of one of the bottom tendons (Tendon D cut) at the quarter point position.

The six bond models (Bond models 3a, 3a1, 3a2, 3aa, 3ac and 3ae) developed earlier were respectively adopted in the analyses, which were carried out under the action of dead load alone. This was done to represent the field conditions of the Botley beams which were only under their own self-weight when tendons were cut. The early results showed that the concrete stresses remained within the elastic limit even when total loss of area in a tendon was simulated. Since only dead load was considered, the loss of prestress in one whole tendon could still be accommodated within the relatively high level of pre-compression initially present in the concrete. In other words, the compressive concrete stresses had not been reduced to the decompression level, or beyond into the tensile range.

However, it is expected that once the concrete cracks, it will distribute the load which it was able to sustain before cracking, to the other uncorroded tendons. To study this, a large service loading (ten times the dead load) was applied to the beam to decompress the concrete and thus enable the concrete to crack when failure of a tendon is simulated. The non-linear concrete model was defined by $f_{cu}=42N/mm^2$ and $f_t=4N/mm^2$. To determine the role of the concrete in redistributing the load when a tendon fails, this analysis was compared to that with a linear concrete model. Failure of the middle tendon in the Botley beam was simulated at the quarter point position. It was found that for the analysis with the non-linear concrete model, the concrete cracked locally around the tendon failure location, and the stresses in the uncorroded tendons were found to increase more than that with a linear concrete model. This non-linear concrete model demonstrates the influential role of the surrounding concrete in the redistribution of tendon stresses after local loss of tendon area and will help to explain some of the results obtained later.

4.5.1 Re-anchoring of Failed Tendons

The rest of the analyses were undertaken with dead load alone, in order to be consistent with the field conditions of the Botley beams. As explained earlier, the concrete remained linear under these conditions, thus a linear concrete model was adopted for all further analytical work.

The results are illustrated for a half span of the beam. The convention used is that compressive strains are negative, and tensile strains are positive. A positive slip corresponds to a positive movement of the tendon relative to the grout/concrete, defined as being in the direction from the cut point to the midspan of the beam. Figure 4.21 illustrates the resulting concrete strain increase along the beam soffit, for the case of Tendon C cut at the quarter point position. The case for no loss of tendon area represents the control situation. It can be seen that the poorer the bond conditions, the required length for the failed tendon to re-anchor back into the grout/concrete is longer. The tendon is considered to have re-anchored when there is no longer any strain increase (compared to the control situation). The soffit strain readings obtained from the field tests is included in the figure. This represents measurements by the vibrating wire gauges installed at the cut point (x=*4500mm*) and at a distance 1.0m and 3.0m away from the cut point respectively. Some correlation is obtained with bond models *3a* and *3a1* (or *3ae*), but the other bond models appear to be too weak.

The corresponding concrete strain increase at the level of the failed tendon is shown in Figure 4.22. For comparison, the situation for total fixity between the coincident nodes of the tendon and concrete (i.e. perfect bond) is shown by the relatively much higher peak of strain obtained. In fact, the concrete strain has become tensile at the tendon failure location. It should be pointed out that the simulation with full bond did not actually allow the tendon to slip since a bond model was not incorporated (coincident concrete and tendon nodes were merged together). This 'ideal bond' was unrealistic, although it demonstrated the more efficient transfer of stresses to the concrete, thereby the higher strain increase (less compressive) in the concrete. Since no slip was allowed, the tendon re-anchored very quickly and the effect of the failed tendon was not apparent on the soffit strain profile (Figure 4.21). In all the bond models, the relaxation of the compressive strain in the concrete was followed by a small increase in the compressive strain in the concrete. This occurs at the end of the re-anchoring length of the failed tendon, and can be attributed to the rebonding effect of the failed wires. This small compression value, however, does not seem detectable at the level of the soffit, which is where strain sensors are normally installed.

Figure 4.23 shows the re-anchoring of the failed tendon to restore its stress to the original prestress level. As expected, bond model *3a* with the strongest bond (2.0N/mm^2), produced the shortest re-anchoring length. As a result of the failed tendon, the other uncorroded tendons (at levels 1 and 3) compensated for some of the loss of force in the failed tendon, by a slight enhancement in their respective tendon stresses. This relatively small stress enhancement is shown in Figures 4.24 and 4.25. As a result, it can be deduced that most of the force lost in the failed tendon is thus lost in the total prestressing system. In other words, a total loss of tendon area due to tendon failure, results in an almost proportionate loss of prestressing tendon force.

The bond force and corresponding bond stress in the bond spring elements along the failed tendon is shown in Figures 4.26 and 4.27. As demonstrated by Bond *3ae*, the maximum bond stress is achieved only when the amount of slip has decreased to within 0.5mm. Above this value of slip, the residual stress value of 1.0N/mm^2 was maintained. Figure 4.28 shows the declining amount of slip in the failed tendon as it re-anchors into the grout/concrete. It shows that Bond *3ae* (bond strength of 2.0N/mm^2, with a residual value of half the maximum bond stress) resulted in more tendon slippage and a longer re-anchoring length as compared to the elastic-plastic bond model of 2.0N/mm^2 (Bond *3a*). This bond model *3ae* is also almost equivalent to an overall bond strength of 1.0N/mm^2 (Bond *3a1*) which produced similar results.

The other field test which was simulated was the cut of one of the bottom tendons (Tendon D) at the quarter point position. In this case, the strain gauges were positioned at the cut point, at 1.0m on either side of it, and at 2.5m from the cut point. The concrete strain profile along the beam soffit (Figure 4.29) suggests that Bond *3a* was most representative of the bond conditions within this duct. The corresponding concrete strain increase at the level of the failed tendon is shown in Figure 4.30. Again, the trend of strain increase is as explained previously.

The distribution of stress in the failed tendon after re-anchoring is shown in Figure 4.31, Similarly, the distributions of stress in the other supporting tendons are shown in Figure 4.32 to Figure 4.34. Note that in Figure 4.32, the tendon is at the same level as the failed tendon, hence the very much higher tendon stress enhancement for the perfect bond

situation, as compared to stress enhancement in the tendons at the other levels. This is because the surrounding concrete has played a role in absorbing some of the stress increase around the corroded area (by expansion through decompression). Hence, by the time the stress is re-distributed to the other tendon layers, the stress enhancement is relatively low. The better the bond, the less is the stress enhancement in the other tendon layers as more load is transferred to the surrounding concrete first before reaching the other tendon layers.

A similar pattern of bond force, bond stress and corresponding tendon slip, as previously shown in Figures 4.26 to 4.28, was also obtained. From the above investigations, it can be deduced that a range of an overall bond strengths from 1.0 to 2.0 N/mm^2 was suitable to represent the bond conditions in the Botley beam. An overall bond strength of 0.5 N/mm^2 was found to be too low and this value was thus not considered further. The respective suitable bond models were then employed to study the case for localised loss of prestressing tendon area in the Botley beam, as is discussed next.

4.6 INVESTIGATION OF STRESS ENHANCEMENT IN PARTIALLY CORRODED TENDONS

4.6.1 Effect of Partial Loss of Area

The study so far has considered total loss of area in a tendon due to tendon fracture, which resulted in an almost proportionate loss of total tendon force. It still remained unclear what the effect of partial loss of prestressing tendon area is on the magnitude of stress enhancement in the corroded tendon, and the amount of loss of prestressing force.

The model of the Botley beam which was developed to study the re-anchoring behaviour of failed tendons, was used to investigate the effect of a local reduction of tendon area on the residual prestressing force in the system. With the use of a suitable bond model to represent the bond conditions in the Botley beam, the partial loss of tendon area (no fractures) as a result of corrosion in the middle tendon at the quarter point position, was simulated. This was achieved by reducing the cross-sectional area of the tendon at the corroded section over a simulated length of corrosion of 100mm. A typical input listing for ANSYS is given in Appendix B.

The amount of corrosion considered varied from 10% to 90% loss of area in the middle tendon. Bond model *3a* corresponding to an overall bond strength of 2.0N/mm^2 was adopted. The analysis was still carried out under the action of dead load alone. As such, the prestressing steel was idealised as an elastic material for most of the analyses. It was only for investigations of over 50% loss of tendon area, resulting in high stress concentrations in the corroded tendon, that non-linear material properties were required to define the prestressing tendon. For the concrete, a linear material model was adopted as it was found that the concrete remained elastic even up to 90% loss of area in the middle tendon.

Figure 4.35 shows that, as the percentage loss of area increases, the stress in the corroded tendon increases around the region of corrosion. In all corrosion cases, the stress increase was followed by a stress decrease (tendon 'relaxation') at either side of the corroded area. The other tendon layers, together with the surrounding concrete, contributed towards restraining the corroded tendon from extending freely due to the stress increase. It can also be seen from the figure that the case of 80% and 90% loss of area resulted in tendon failure due to the high stress which exceeded the strength of the tendon. When a tendon has failed, it will then start to re-anchor again if sufficient grout is available. This expected re-anchoring behaviour is shown by the gain of tendon stress along the re-anchoring length. As a comparison, the distributions of stress in the other tendons (at levels 1 and 3) are shown in Figures 4.36 and 4.37. The levels of stress in the other tendons increased as well, but at a much lower rate than for the corroded tendon. This is because as long as the concrete remains uncracked, it is able to accommodate some loss of prestress force due corrosion, thereby the stresses in the uncorroded tendons will not increase much.

As the level of corrosion increases, the amount of loss of total prestressing force (dF_T) increases (Figure 4.38). For 80% and 90% loss of area, which resulted in tendon failure, the loss of total tendon force was about 282 kN. The amount of force lost in the corroded tendon was 304 kN, which was the force originally in one whole tendon. Some of the force lost in the corroded tendon (tendon level 2) is compensated by the uncorroded tendons (tendon levels 1 and 3) which experience a small force increase, hence the total tendon force lost is slightly less than that corresponding to the corroded tendon. This is illustrated in Figure 4.39 for a typical case of 50% loss of area in the corroded tendon. Some amount

of the *total* force in the prestressing system is still lost, but this value is relatively small, which will be shown later. The force deficit is taken up by a relaxation of the compressive stress in the concrete, as described earlier in the study of re-anchoring of failed tendons. The concrete between these tendon layers therefore plays a role in restoring equilibrium and reducing the extent of free extension in the corroded tendon. The surrounding concrete can be seen to act as a 'coupler' between the corroded tendon and the other tendon layers.

Figure 4.40 shows the relationship between the percentage loss of area ($\%dA_{ps}$) in the corroded tendon, and the percentage loss of force ($\%dF_{ps}$) in the corroded tendon. The corresponding percentage loss of *total* tendon force ($\%dF_T$), is plotted on the secondary axis. For completeness, the case for 100% loss of area in the corroded tendon (20% overall loss of tendon area) is included in the figure. This was actually the study of total loss of area due to the tendon being cut which was previously investigated. It can be seen from Figure 4.40 that for up to 50% loss of area in the corroded tendon, the relationship is linear. Even for 70% loss of tendon area, only about 34% of the force in the corroded tendon was lost (6.3% loss of total tendon force). However, at this point, the stress in the tendon was 1450 N/mm^2, which is near its ultimate strength (Figure 4.41). At 80% and 90% loss of tendon area, the stress enhancement in the corroded tendon was so great that its failure strength was reached and the tendon fractured under this high stress. These latter two cases thus resulted in 100% loss of force in the corroded tendon as the tendon fails. This is demonstrated by the sharp peak in Figure 4.40. The significance of this is that when more than half of the tendon has corroded, it can be expected that failure of the tendon is imminent.

Figure 4.42 shows the resulting concrete strain increase which may be expected at the beam soffit as a result of localised loss of prestressing tendon area. It can be seen that for 80% and 90% loss of tendon area which resulted in tendon failure (and subsequent tendon re-anchoring), the strain increase is of the order of 80microstrain. However, when the tendon has not yet failed, the strain increase as a result of corrosion is relatively small. Even for 70% loss of tendon area in the corroded tendon (14% overall tendon area loss), the strain increase is only about 25microstrain. For lower percentages of corrosion, this value is even smaller and may be undetectable by the conventional strain gauges.

4.6.2 Effect of Different Bond Conditions

The investigation of partial loss of tendon area was so far undertaken with a bond strength of 2.0 N/mm^2 (Bond *3a*). In order to determine what the effect of poorer bond conditions would be on the stress in the tendons and the amount of loss of prestressing force, the analyses were repeated for an overall bond strength of 1.0N/mm^2 (Bond *3a1*), with everything else kept the same as in the analyses with Bond *3a*.

Figure 4.43 shows the similar trend demonstrated earlier, i.e. as the amount of corrosion increases, the residual stress in the corroded tendon increases around the region of corrosion. Again, the case of 80% and 90% loss of area resulted in tendon failure. The main difference was that in this case, a longer tendon re-anchoring length was required due to the weaker bond present. The stress in the other tendons (at levels 1 and 3) is shown in Figures 4.44 and 4.45. The increasing amount of loss of total prestressing force (dF_T) with corrosion is shown in Figure 4.46. This again illustrates the longer length required for the tendons to restore equilibrium within this weaker bond model. It can also be seen that the magnitude of change in tendon force is slightly less than that in the earlier stronger bond. This will be explained later.

Figure 4.47 illustrates the percentage loss of force ($\%dF_{ps}$) in the corroded tendon, corresponding to percentage loss of area ($\%dA_{ps}$) in the corroded tendon. Figure 4.48 shows the corresponding tendon stress enhancement, for the increasing amount of tendon area loss. The trend of results is similar to that with Bond *3a*.

The expected concrete strain increase at the beam soffit due to the various corrosion levels is shown in Figure 4.49. As can be seen, the strain increase as a result of localised loss of prestressing tendon area is relatively small, unless the tendon has failed as a result of corrosion. Figure 4.50 shows the concrete strain increase along the level of the corroded tendon. It shows that the concrete strains have not become tensile, i.e. the concrete has not decompressed yet as a result of this localised loss of area.

Comparing the effect of this poorer bond model *3a1* with that previously investigated (Bond *3a*), it can be seen in Figure 4.51 that, as a result of the poorer bond, the stress in the corroded tendon increased more than with Bond *3a* for the same level of corrosion.

This is because the poorer bond was less efficient in re-distributing the stress to the concrete. Hence less stress was transferred, resulting in the higher stresses in the tendon. In fact, at 70% loss of area, the stress in the corroded tendon was 1569N/mm^2 which is the strength of the wire, i.e. just before the failure strain was approached. This stress was about 8% higher for this level of corrosion, than that with the earlier bond model *3a*. This implies that a corroded tendon in a poorly grouted duct may be more in danger of failing as a result of high tendon stresses than that within a relatively well-grouted duct. In other words, failure of a corroded tendon could be reached earlier if it was within poor grout conditions.

By the same argument, it can be deduced that because of the poorer bond conditions and consequently higher stress in the corroded tendon, the force in the corroded tendon is thus higher than in the case for better bond. As a result, the amount of force lost in the corroded tendon is less than the case for the better bond model *3a*. This is illustrated in Figure 4.52. It should be stressed that although less force is lost in the corroded tendon in this case, tendon failure on the other hand, could still be sudden once more than half the tendon is lost since the tendon stress increases relatively quickly.

4.7 CONCLUSIONS

This chapter described the investigation of the consequence of localised loss of prestressing tendon area due to corrosion. A finite element model of a full scale bridge beam was developed with ANSYS finite element software. The following conclusions can be drawn from the work undertaken in this chapter:

- The study demonstrates that the effect of partial loss of area in a tendon due to corrosion, and the re-anchoring behaviour of a failed tendon can be investigated by the finite element method. In the analyses, the prestressing tendons were represented by non-linear link elements, within a 2D linear concrete model. The interface behaviour between the concrete and the tendon was simulated by non-linear spring elements, defined by a force-displacement curve to represent the bond conditions in the beam. Suitable bond models were established by reference to results of field investigations available.

- The study revealed that in cases of corrosion involving tendon fractures, the loss of prestressing force in the corroded tendon is almost proportional to the loss of tendon area. A small amount of this force which is lost in the broken tendon, is compensated by marginally higher stresses in the other uncorroded tendons.

- The bond conditions were found to affect the re-anchoring length of the failed tendon. The poorer the bond conditions within the beam, so the required length for the failed tendon to fully re-anchor increased. In some cases, the tendon experienced an appreciable amount of slip, and did not re-anchor.

- It was found that in cases of partial loss of area (no tendon fractures), equilibrium was restored by a slight relaxation of the compressive strain in the concrete and a higher level of residual tensile stress in the corroded tendon. The loss of force was found to be relatively low compared to the loss of tendon area (about 6% loss of total tendon force for 70% loss of area in a corroded tendon). However, when more than half the tendon has corroded, the tendon stress increased significantly. This was more pronounced in poorer bond conditions. Tendon failure was found to be dictated by levels of stress enhancement in the corroded tendon sufficiently large for the ultimate strength to be reached prematurely.

- The concrete strain increase due to localised loss of tendon area was relatively small, unless the tendon had failed as a result of the high level of corrosion. The strain effects may not be easily detectable by conventional strain gauges normally installed at the beam surface during monitoring. This is particularly so when the strain increase is masked by temperature effects.

	Parameter	Value
Concrete	E_c	32 kN/mm^2
	ν_c	0.2
Prestressing steel tendon	E_{ps}	200 kN/mm^2
End plate	E_{plate}	1000 kN/mm^2
	ν_{plate}	0.28

Table 4.1 Material data for local finite element model

	Good bond conditions	All other bond conditions
s_1	0.6 mm	0.6 mm
s_2	0.6 mm	0.6 mm
s_3	1.0 mm	2.5 mm
α	0.4	0.4
τ_{max}	$2.0\sqrt{f_{cu}}$	$1.0\sqrt{f_{cu}}$
τ_f	$0.15\tau_{max}$	$0.15\tau_{max}$

Table 4.2 Parameters for defining the mean bond stress-slip curve for a ribbed bar in unconfined concrete (CEB-FIP, 1993)

a_0 = original cross sectional area of tendon
a_1 = tendon cross-sectional area remaining after corrosion
l_1 = length over which the corrosion occurs
T_r = residual force in tendon after corrosion
σ = stress in the tendon
ε = strain in the tendon
subscript '0' refers to properties at the uncorroded parts of the tendon and subscript '1' refers to those at the corroded section

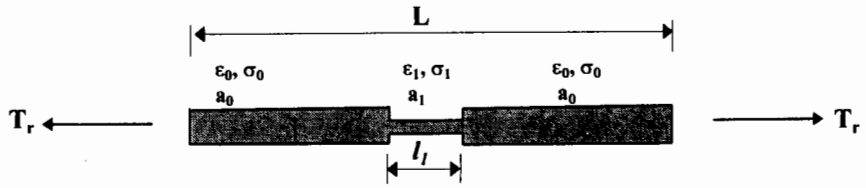

Figure 4.1 Localised corrosion in a single tendon

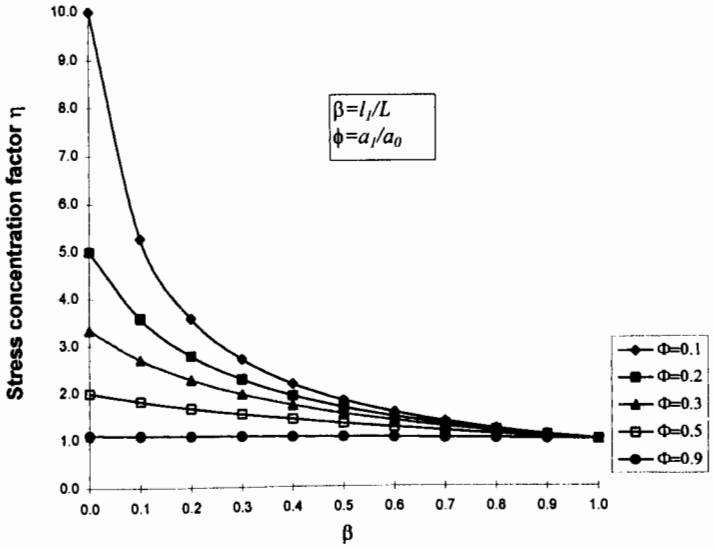

Figure 4.2 General effect of loss of prestressing area on tendon stress

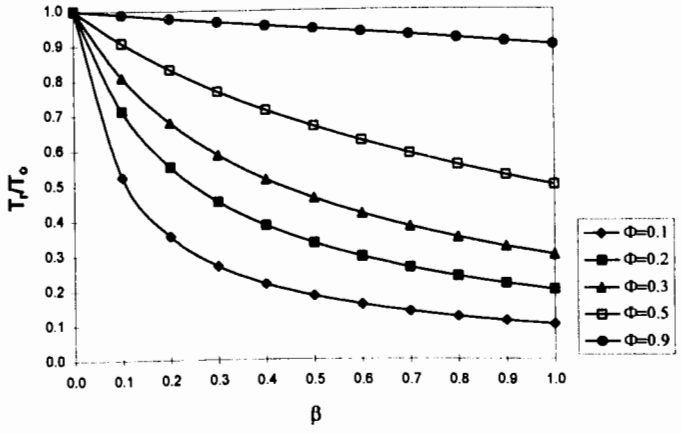

Figure 4.3 General effect of loss of prestressing area on tendon force

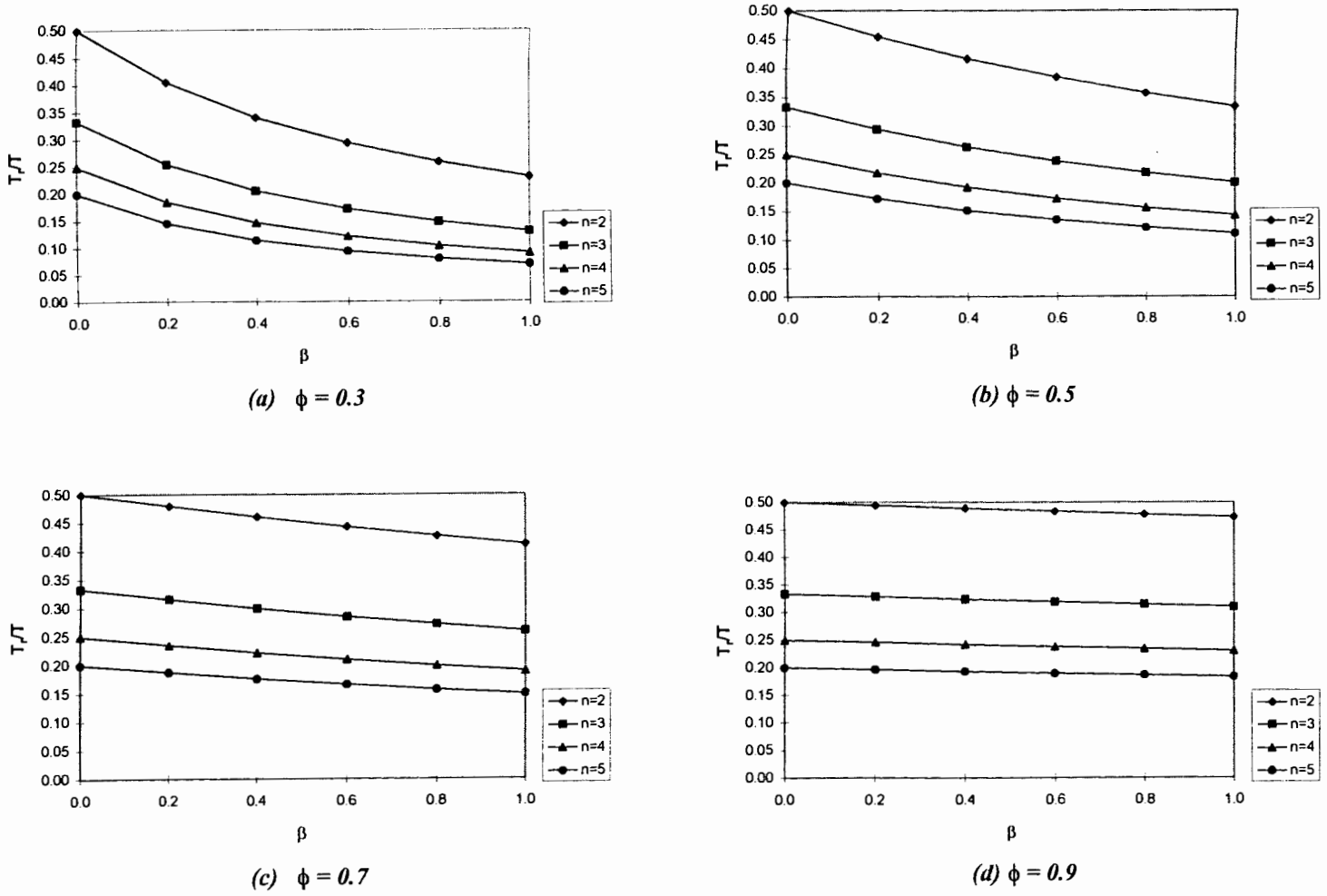

(a) $\phi = 0.3$ *(b)* $\phi = 0.5$

(c) $\phi = 0.7$ *(d)* $\phi = 0.9$

Figure 4.4 Effect of number of tendons on ratio of force in corroded tendon to total force in section

(ϕ = ratio of corroded to original cross-sectional area of corroded tendon)

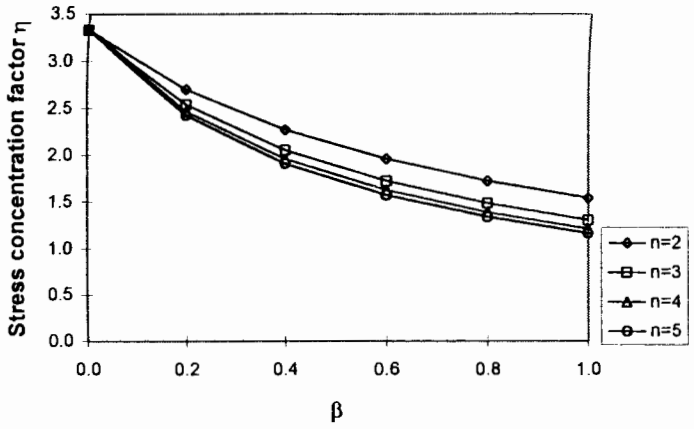

(a) $\phi = 0.3$

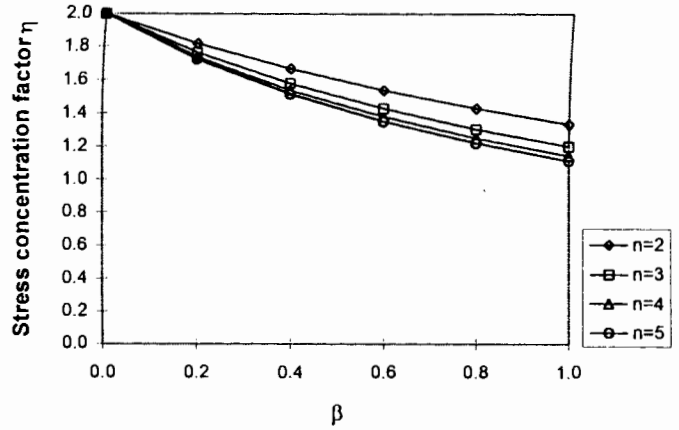

(b) $\phi = 0.5$

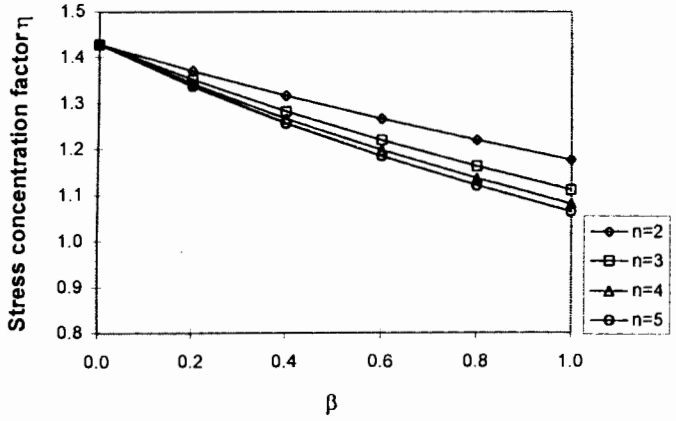

(c) $\phi = 0.7$

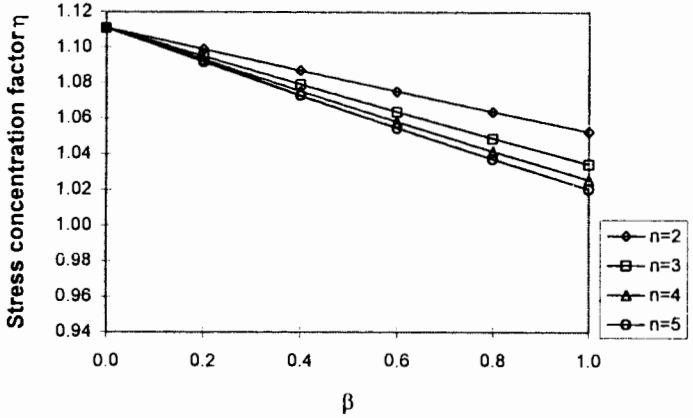

(d) $\phi = 0.9$

Figure 4.5 Effect of number of tendons on stress concentration in corroded tendon

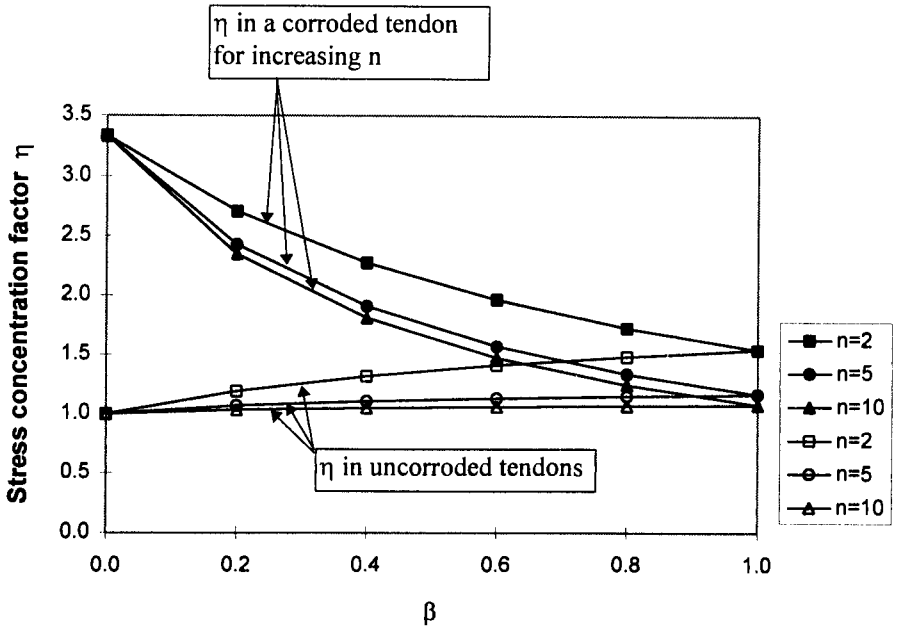

Figure 4.6 Stress concentration factor in a corroded tendon and in the uncorroded tendons for ϕ=0.3

(ϕ = ratio of corroded to original cross-sectional area of corroded tendon)

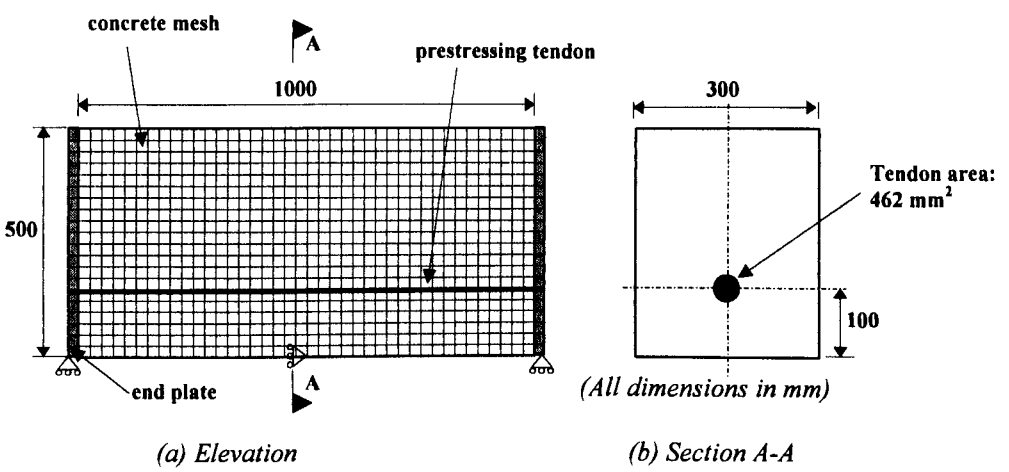

(a) Elevation *(b) Section A-A*

Figure 4.7 Finite element mesh of local model

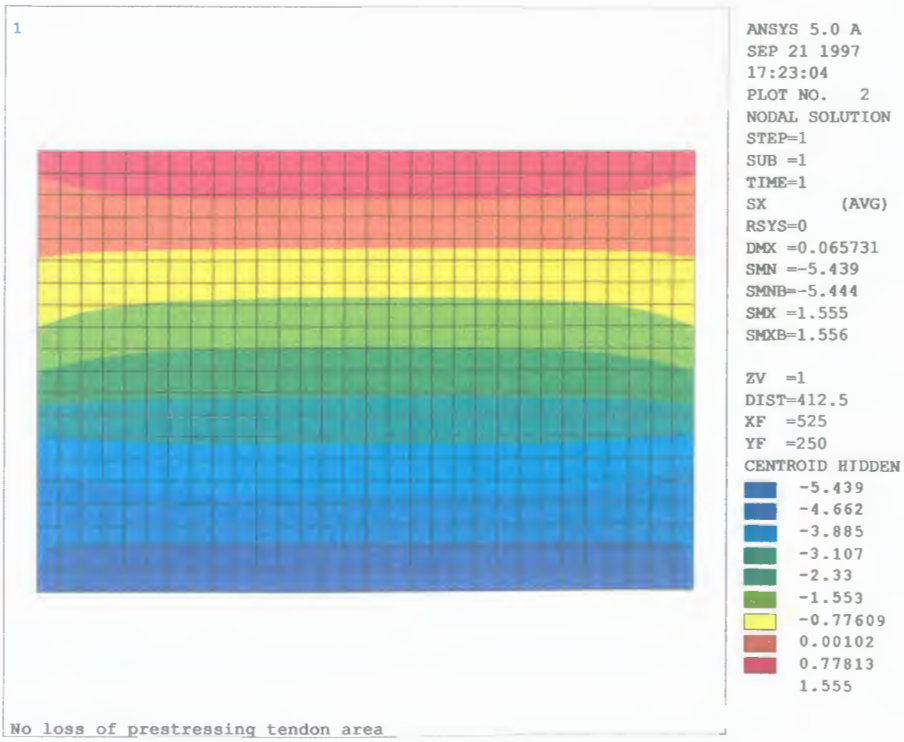

(a) No loss of tendon area

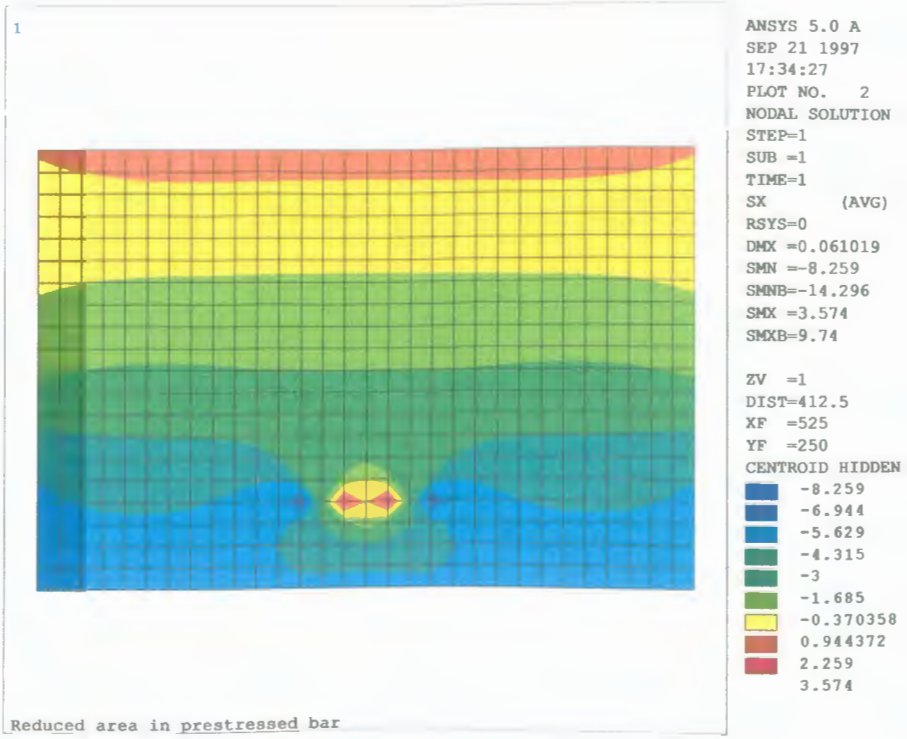

(b) 50% loss of area over a 100mm length in the corroded tendon at midspan

Figure 4.8 Axial stress contours in the concrete element

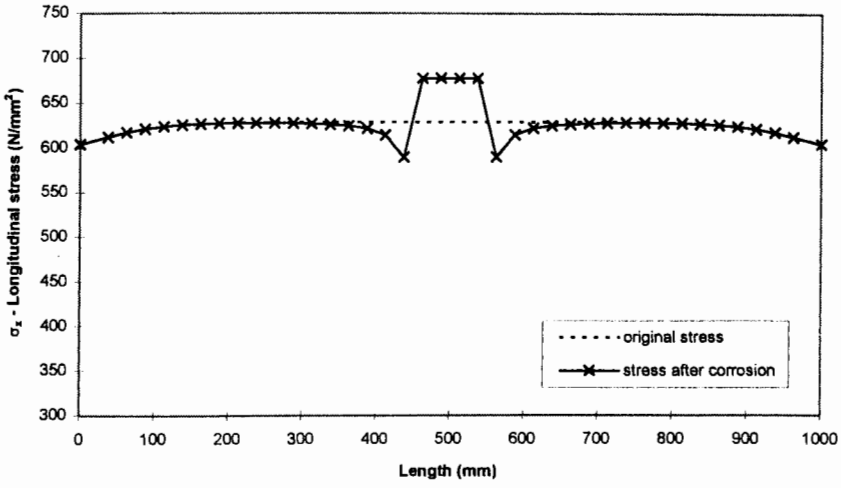

(a) Longitudinal stress along corroded tendon

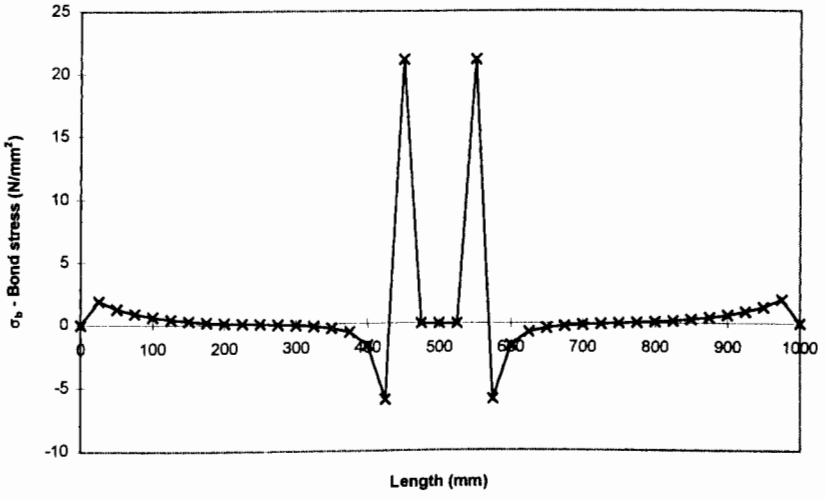

(b) Bond stress along corroded tendon

Figure 4.9 Longitudinal stress and resulting bond stress along the corroded tendon, due to 50% loss of area in the corroded tendon

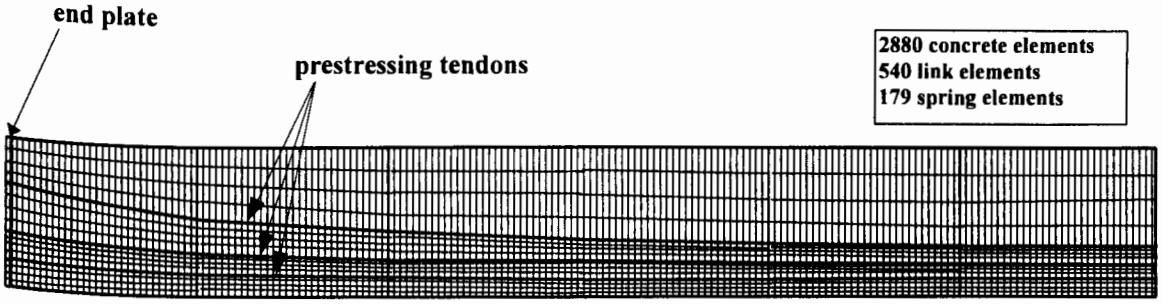

(a) mesh of global model

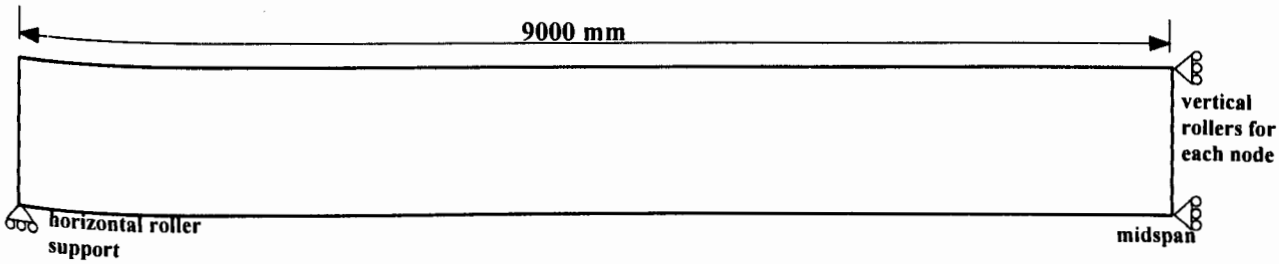

(b) boundary condition

Figure 4.10 Finite element idealization of Botley beam

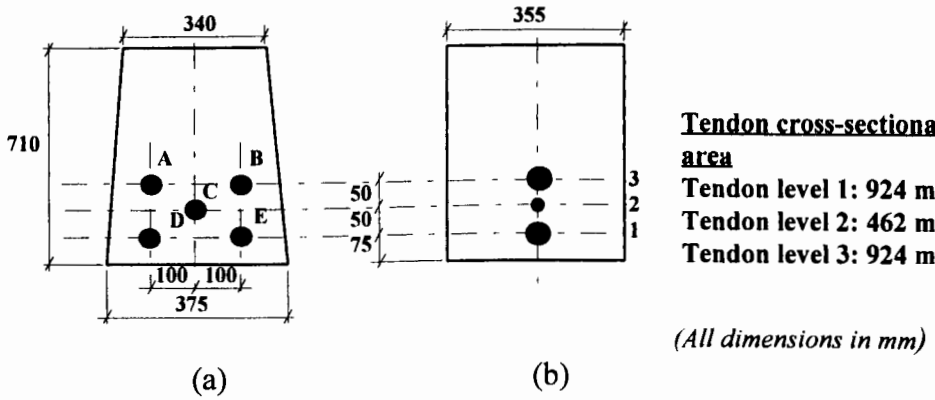

Figure 4.11 Cross-section at midspan of Botley beam - (a) actual cross-section, (b) modelled cross-section

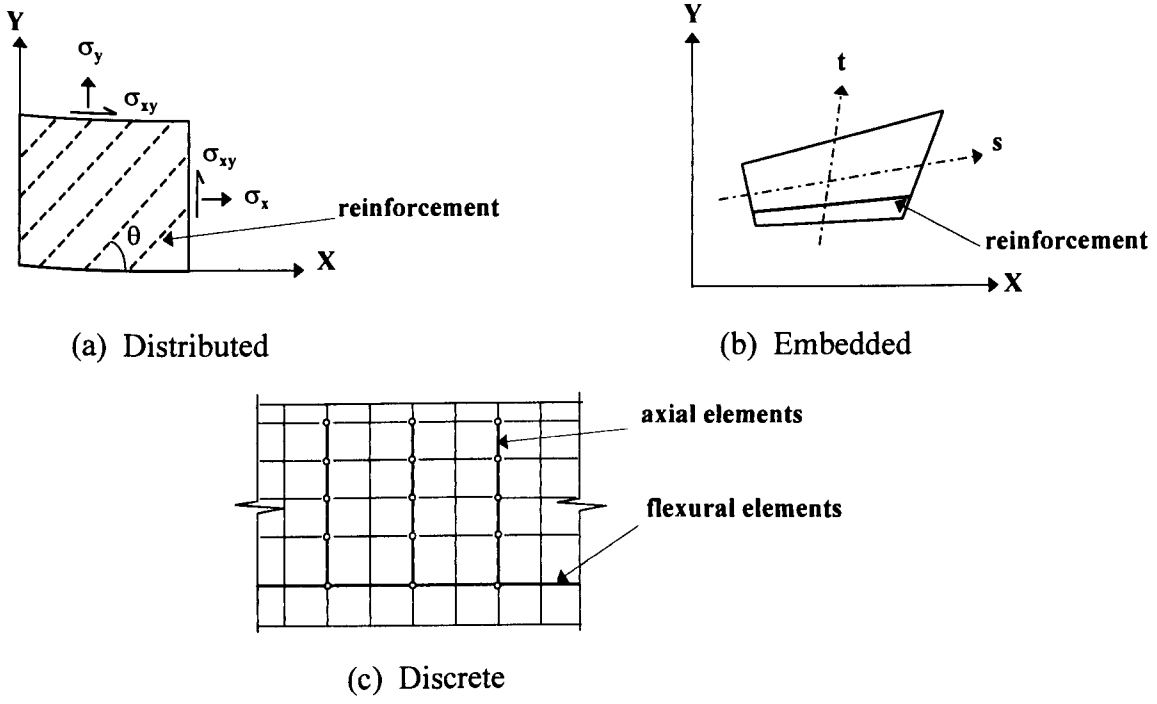

Figure 4.12 Alternate representations of steel reinforcement (ASCE, 1982)

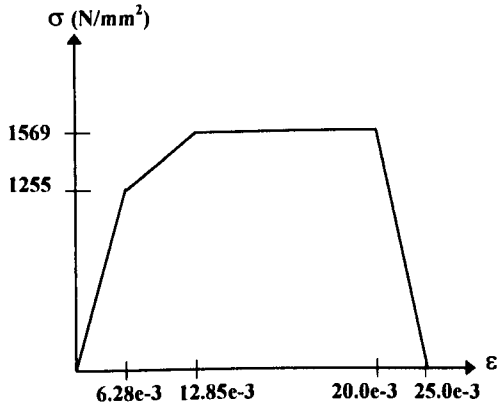

Figure 4.13 Stress-strain curve of the prestressing tendon which was adopted in the global finite element model

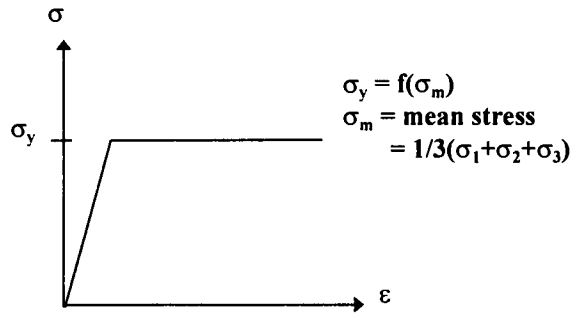

Figure 4.14 Stress-strain behaviour of the Drucker-Prager option

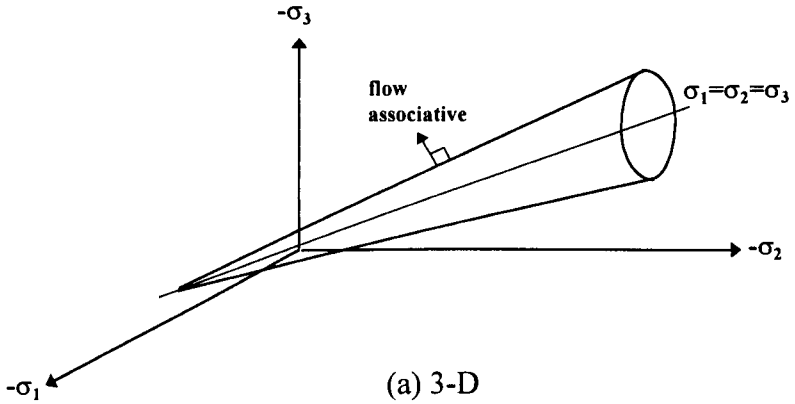

(a) 3-D

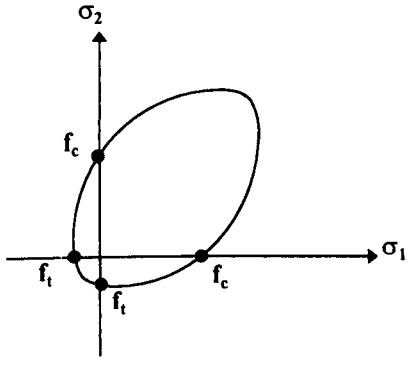

(b) 2-D

Figure 4.15 Yield surface for Drucker-Prager option

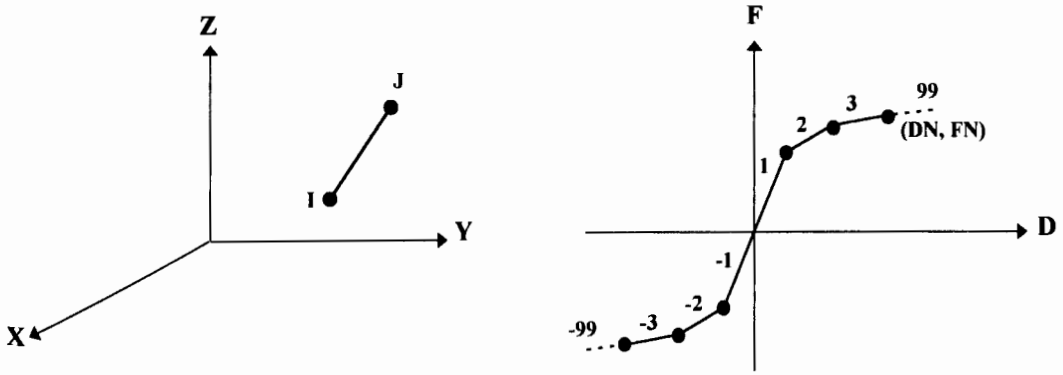

(a) Co-ordinate system (b) Force-displacement input curve

Figure 4.16 COMBIN39 Non-linear spring element

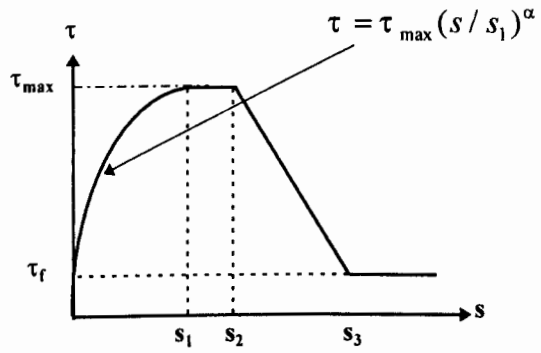

Figure 4.17 Analytical bond stress-slip relationship (CEB-FIP, 1993)

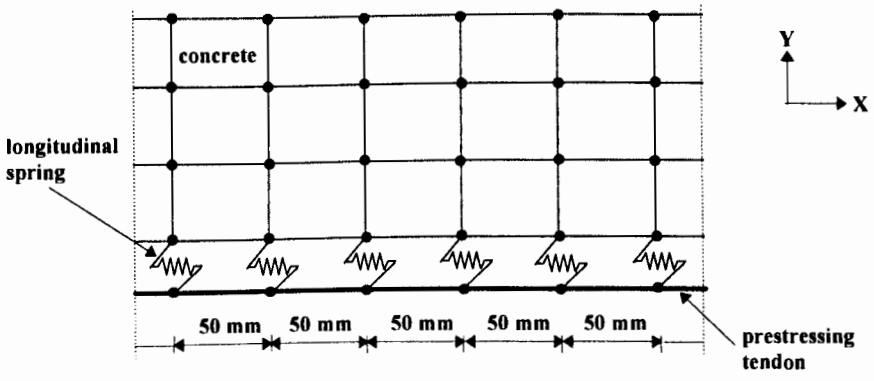

Figure 4.18 Concrete-tendon interface springs

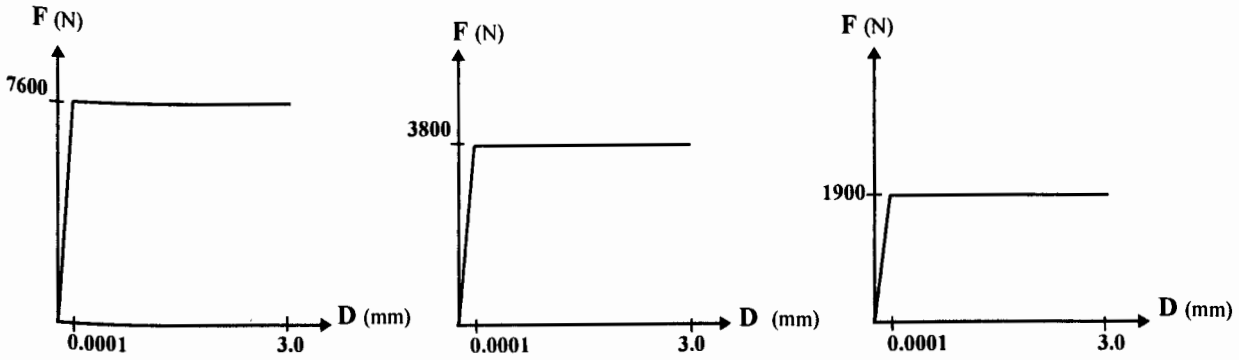

(a) $f_{bu} = 2.0$ N/mm^2 (Bond 3a)

(b) $f_{bu} = 1.0$ N/mm^2 (Bond 3a1)

(c) $f_{bu} = 0.5$ N/mm^2 (Bond 3a2)

Figure 4.19 Force-displacement curves for different bond strengths considered

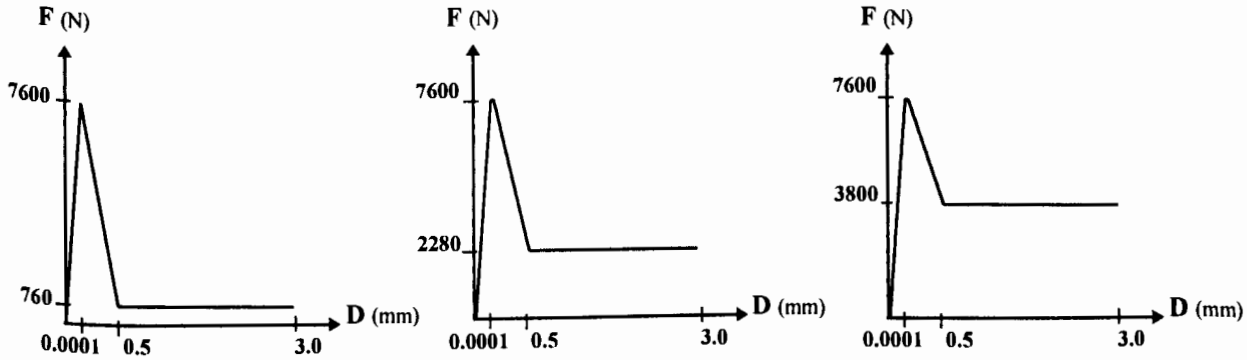

(a) $\tau_f = 0.1\tau_{max}$ (Bond 3aa)

(b) $\tau_f = 0.3\tau_{max}$ (Bond 3ac)

(c) $\tau_f = 0.5\tau_{max}$ (Bond 3ae)

Figure 4.20 Force-displacement curves with different residual stress levels for $f_{bu} = 2.0$ N/mm^2

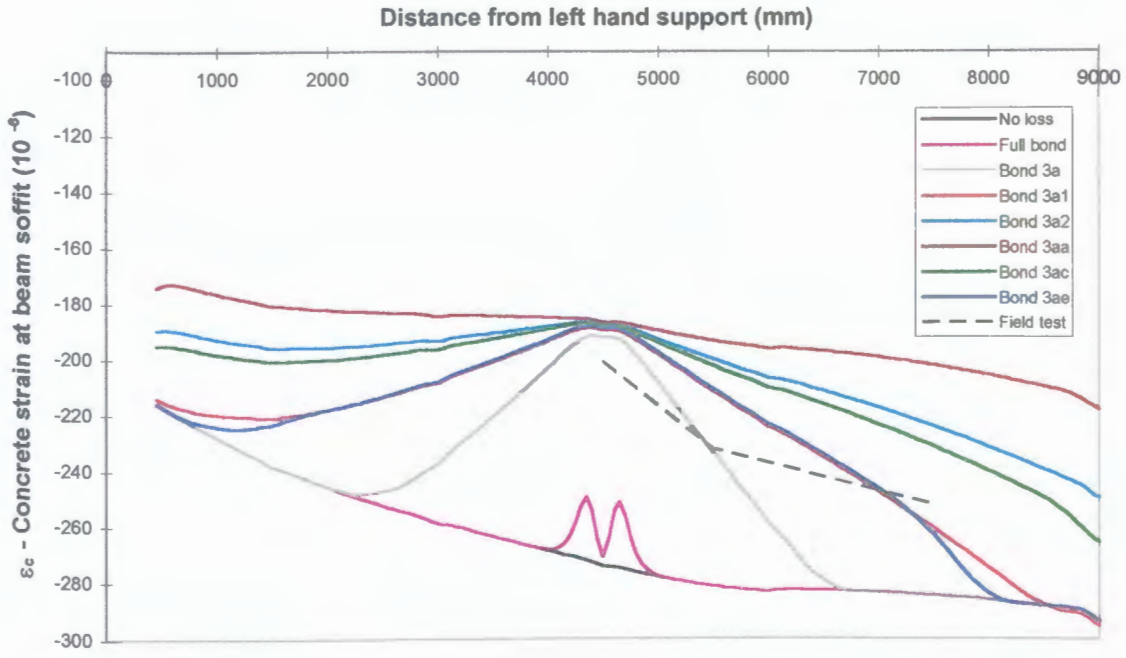

Figure 4.21 Concrete strain increase along beam soffit as a result of cutting Tendon C

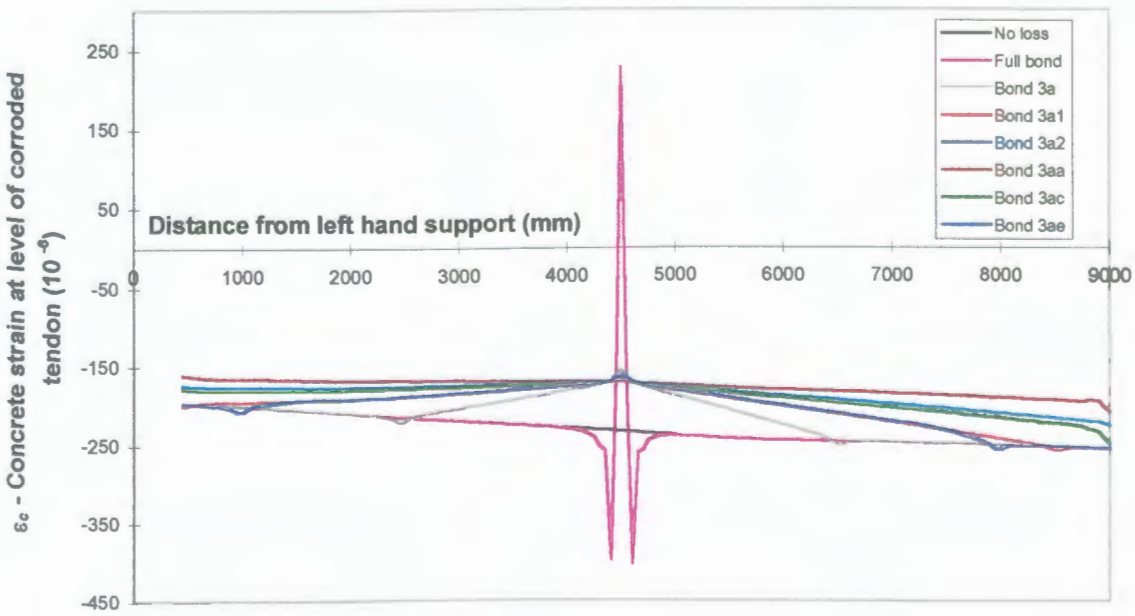

Figure 4.22 Concrete strain increase along level of corroded tendon as a result of cutting Tendon C

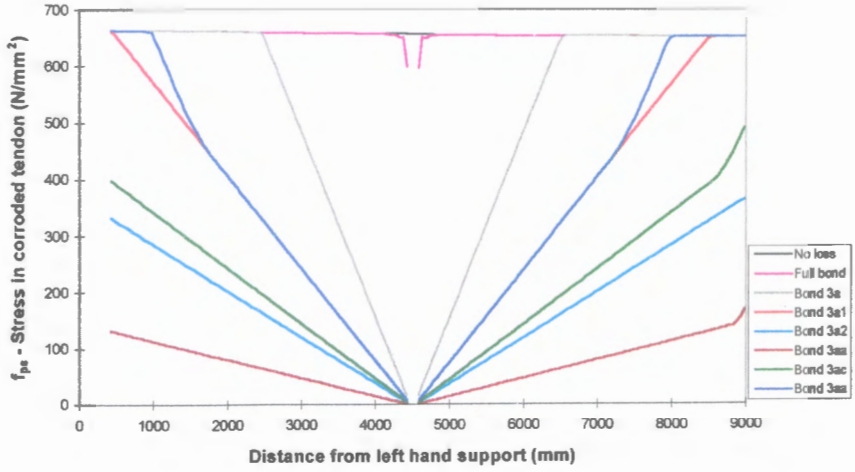

Figure 4.23 Tendon stress along the fractured Tendon C

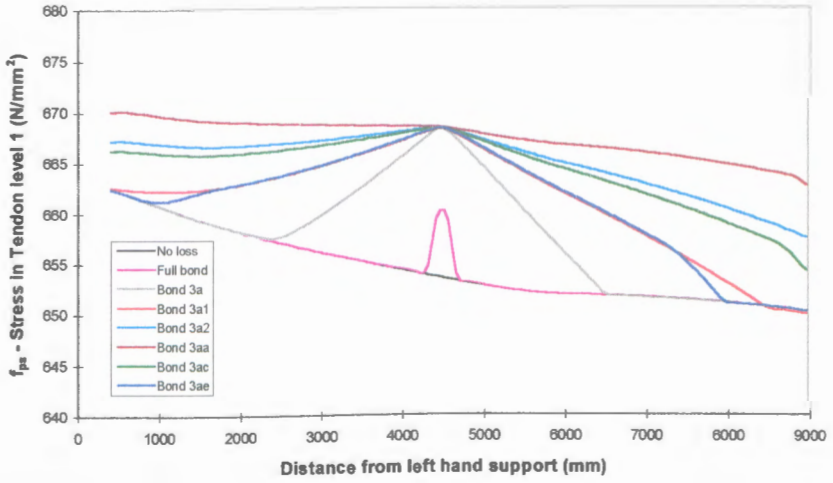

Figure 4.24 Stress in tendon level 1 as a result of cutting Tendon C

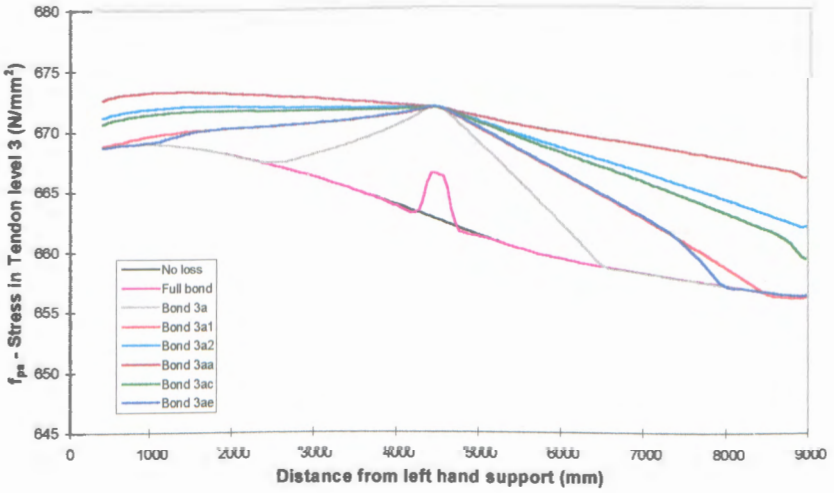

Figure 4.25 Stress in tendon level 3 as a result of cutting Tendon C

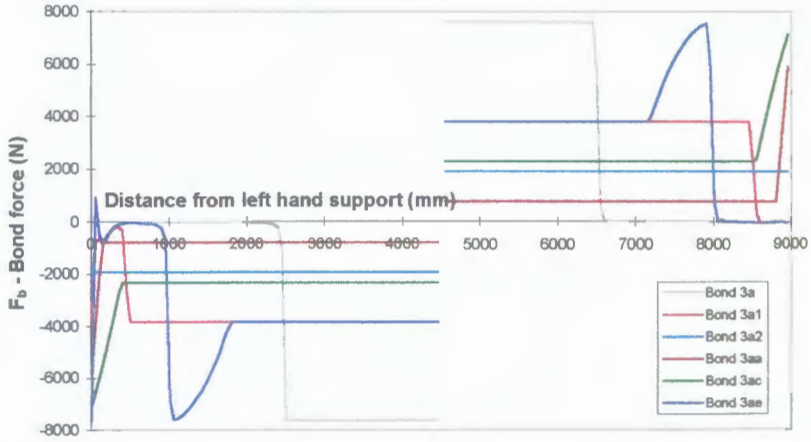

Figure 4.26 Bond force along the fractured Tendon C

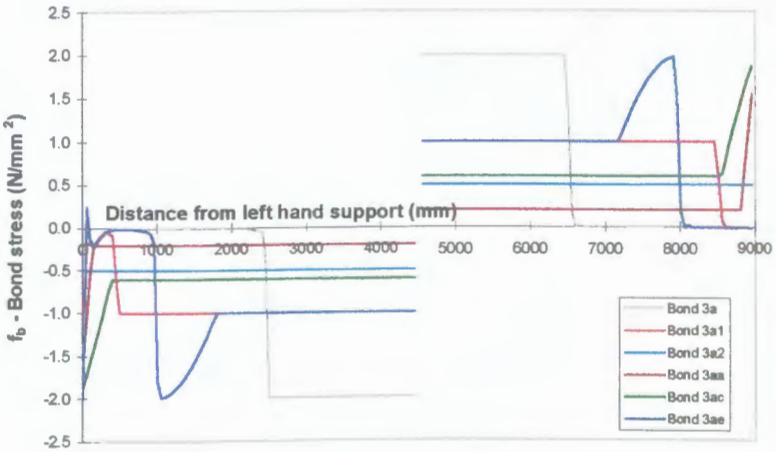

Figure 4.27 Bond stress along the fractured Tendon C

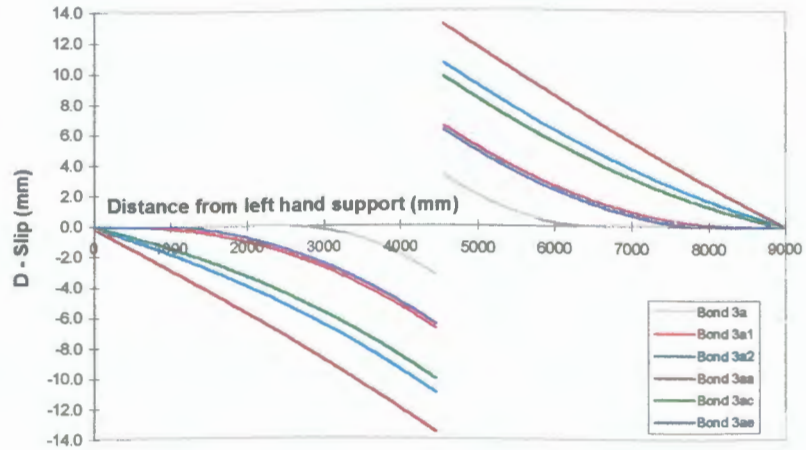

Figure 4.28 Relative slip of the fractured Tendon C

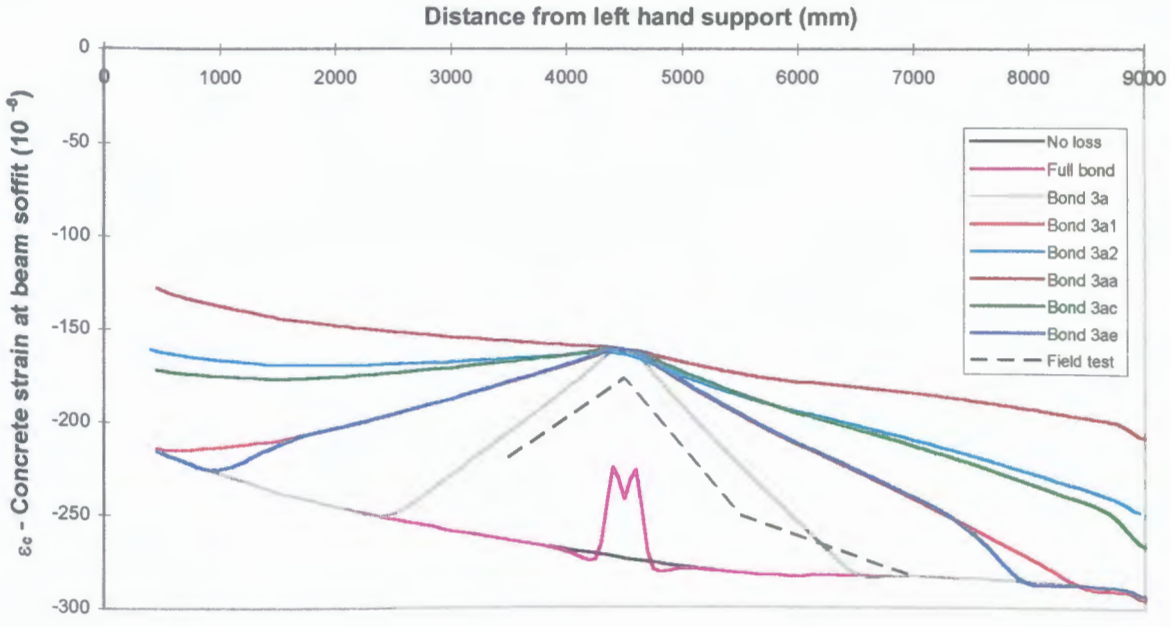

Figure 4.29 Concrete strain increase along beam soffit as a result of cutting Tendon D

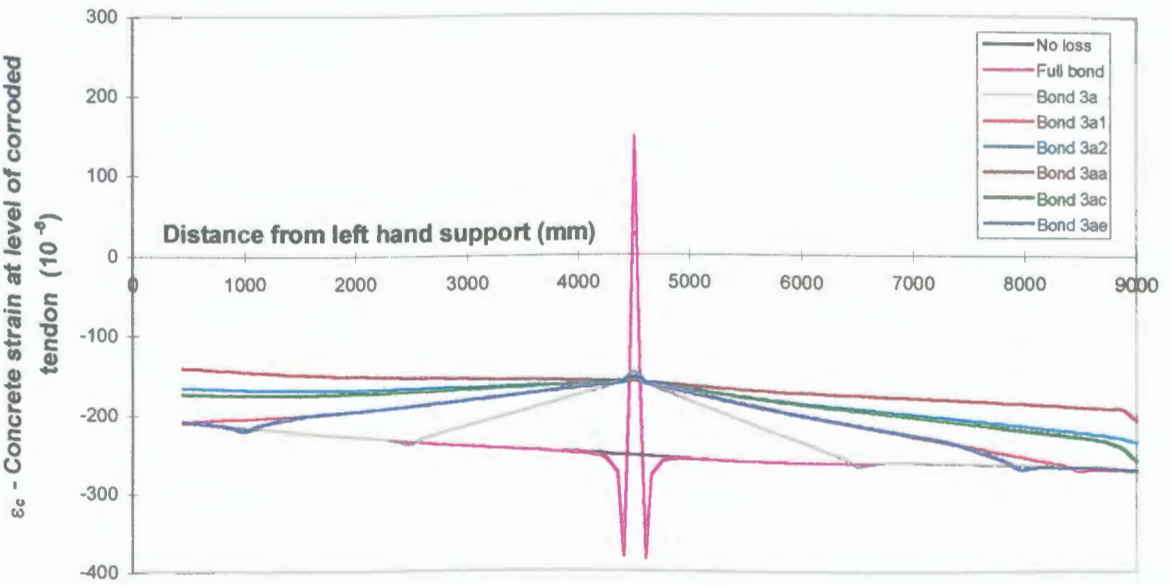

Figure 4.30 Concrete strain increase along level of corroded tendon as a result of cutting Tendon D

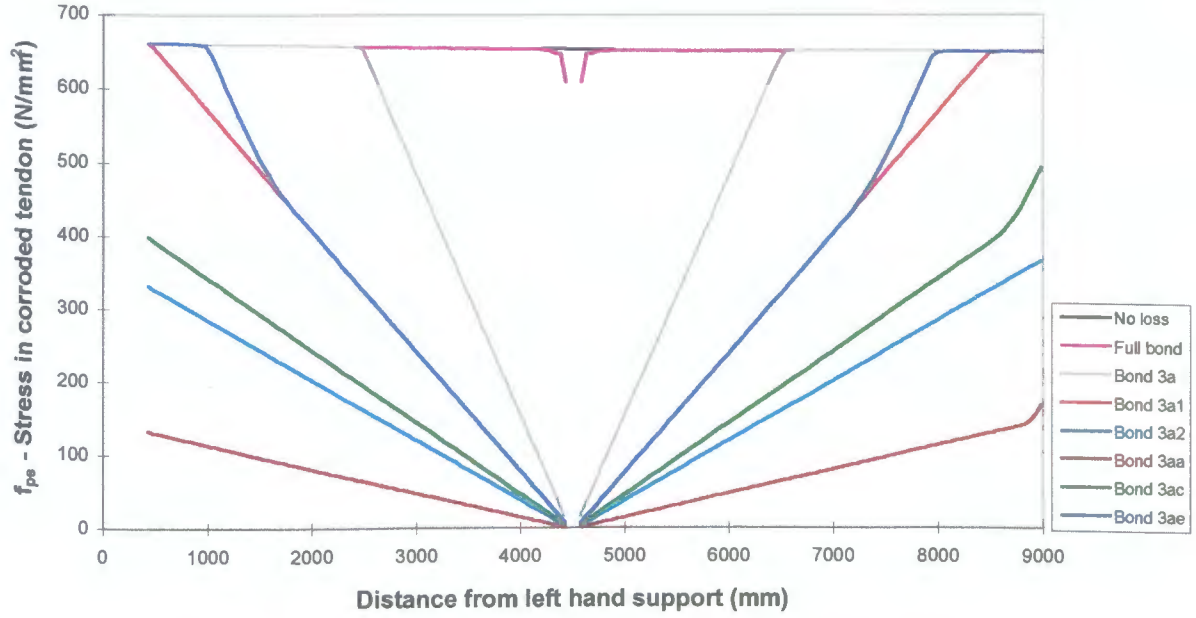

Figure 4.31 Tendon stress along the fractured Tendon D

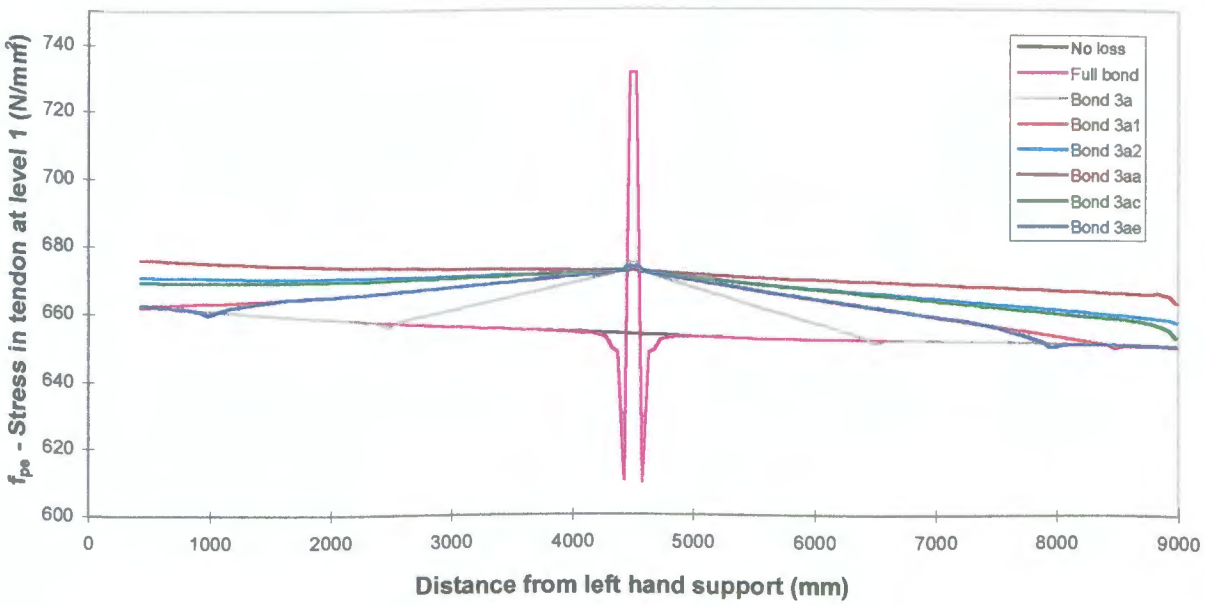

Figure 4.32 Stress in tendon at level 1 (same level as Tendon D) as a result of cutting Tendon D

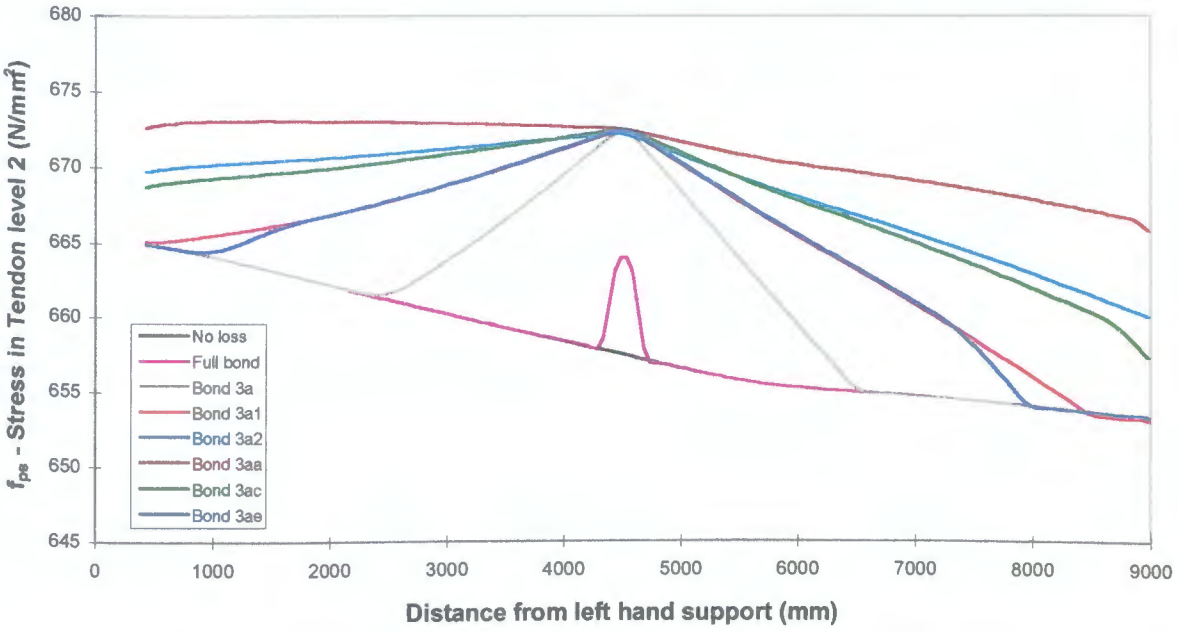

Figure 4.33 Stress in tendon level 2 as a result of cutting Tendon D

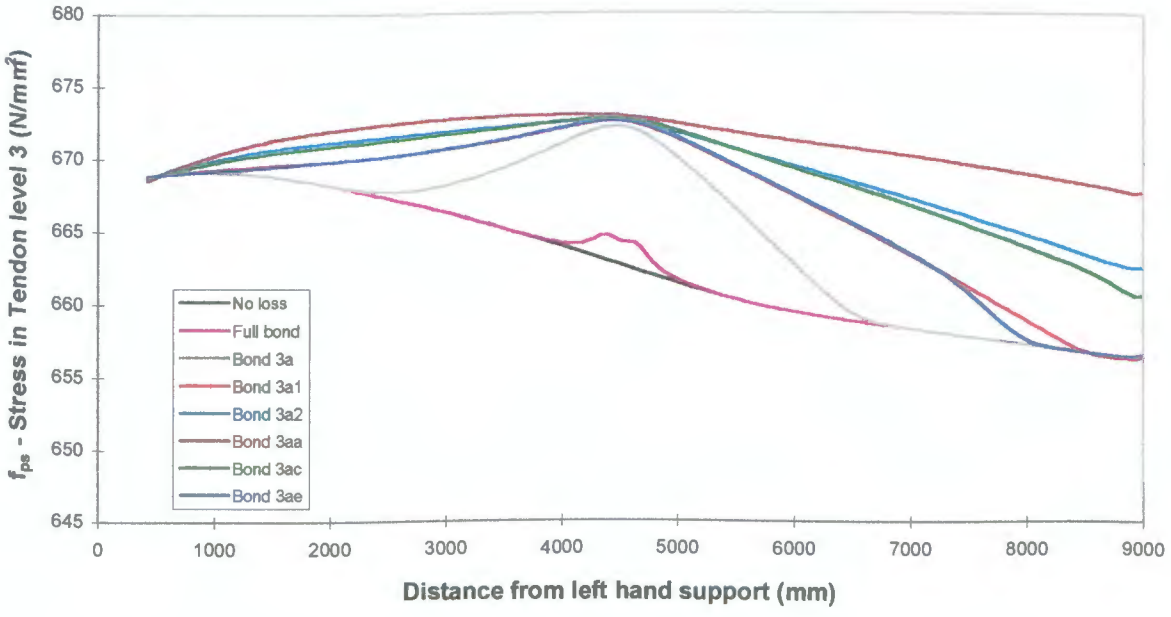

Figure 4.34 Stress in tendon level 3 as a result of cutting Tendon D

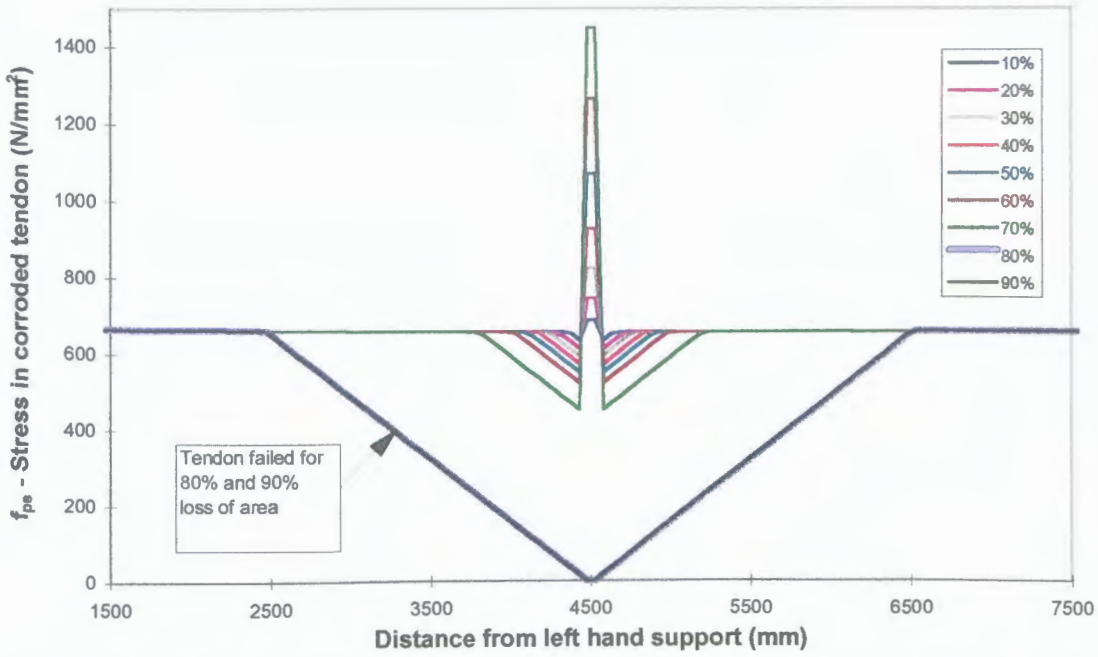

Figure 4.35 Stress in the corroded tendon due to increasing loss of tendon area (Bond strength 2.0 N/mm²)

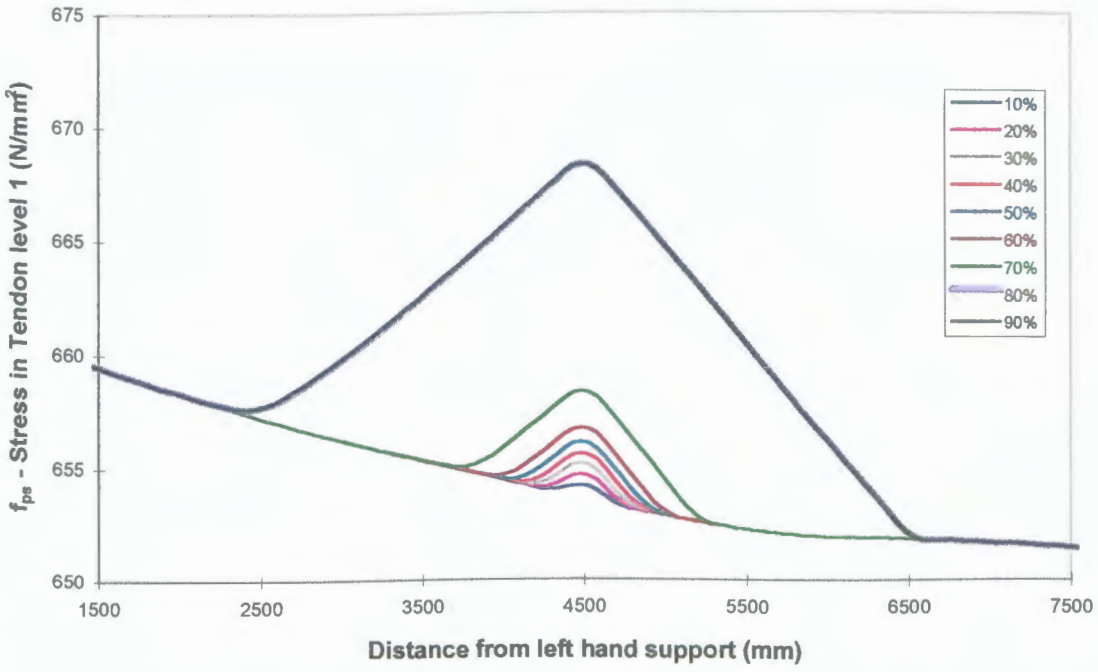

Figure 4.36 Stress in tendon level 1 due to increasing loss of area in the corroded tendon (Bond strength 2.0 N/mm²)

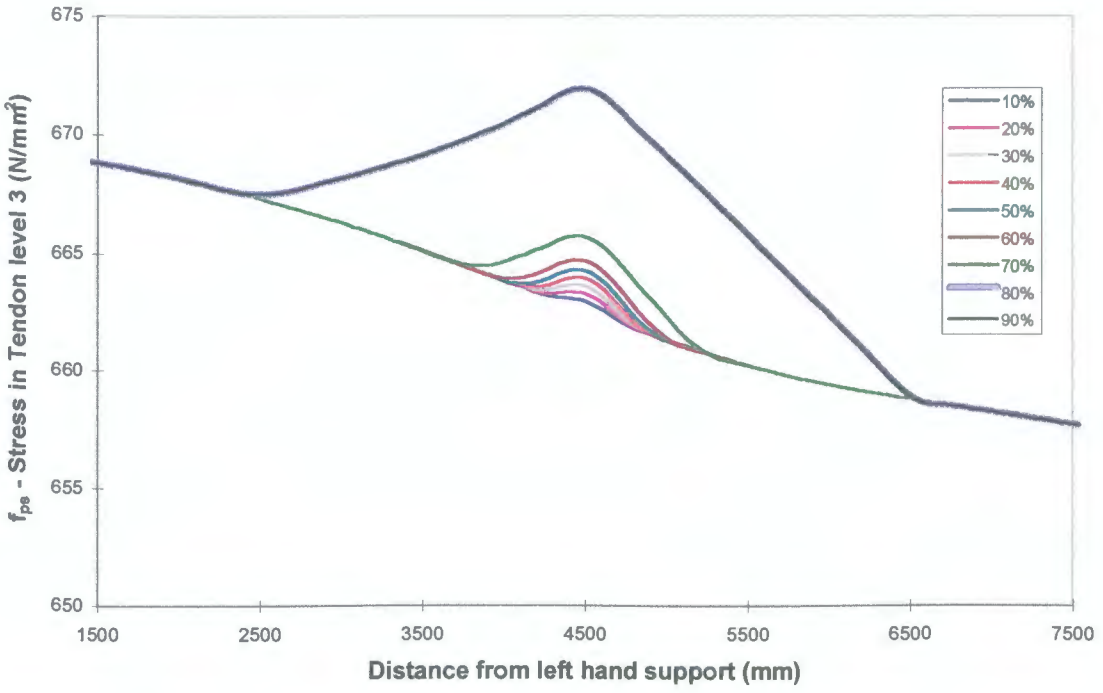

Figure 4.37 Stress in tendon level 3 due to increasing loss of area in the corroded tendon (Bond strength 2.0 N/mm^2)

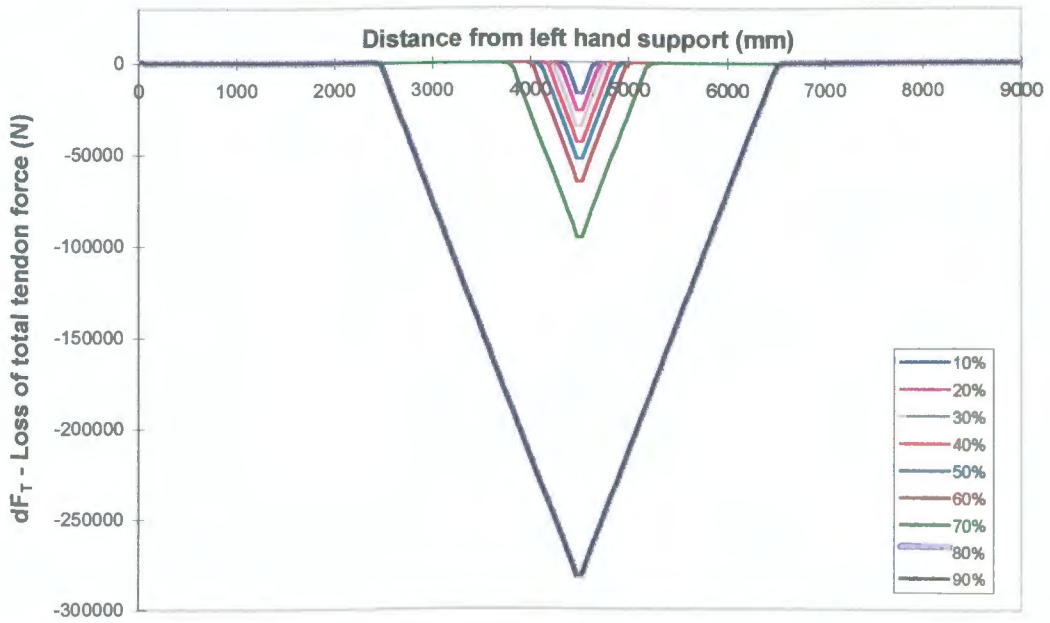

Figure 4.38 Loss of total tendon force due to increasing loss of area in the corroded tendon (Bond strength 2.0 N/mm^2)

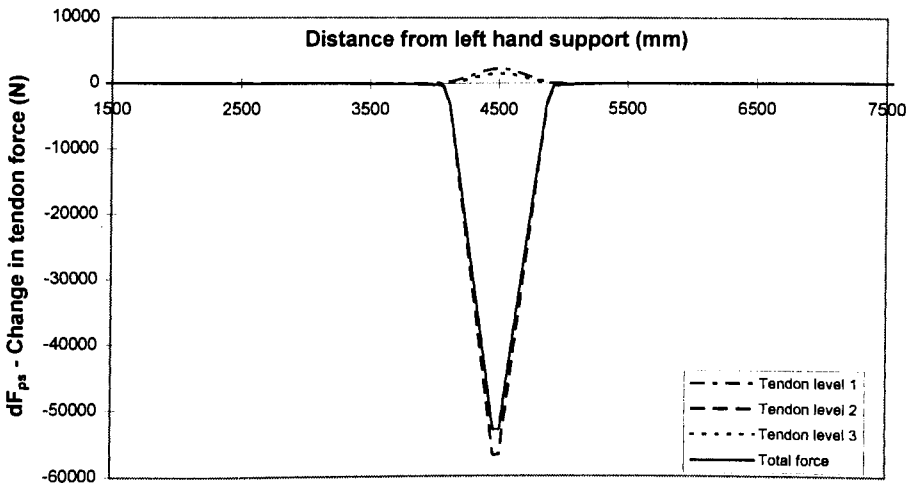

Figure 4.39 Change in tendon force at all tendon levels for 50% loss of area in tendon at level 2 (Bond strength 2.0 N/mm^2)

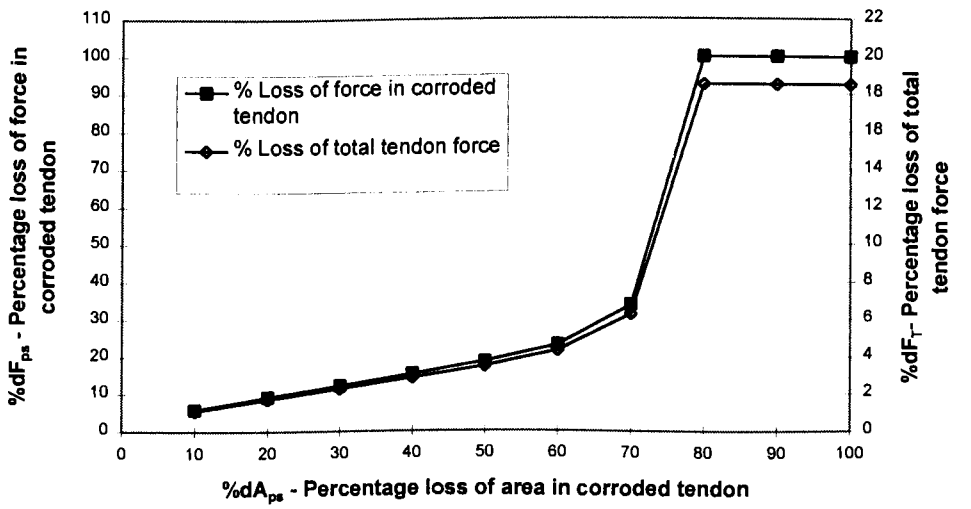

Figure 4.40 Loss of force due to loss of tendon area (Bond strength 2.0 N/mm^2)

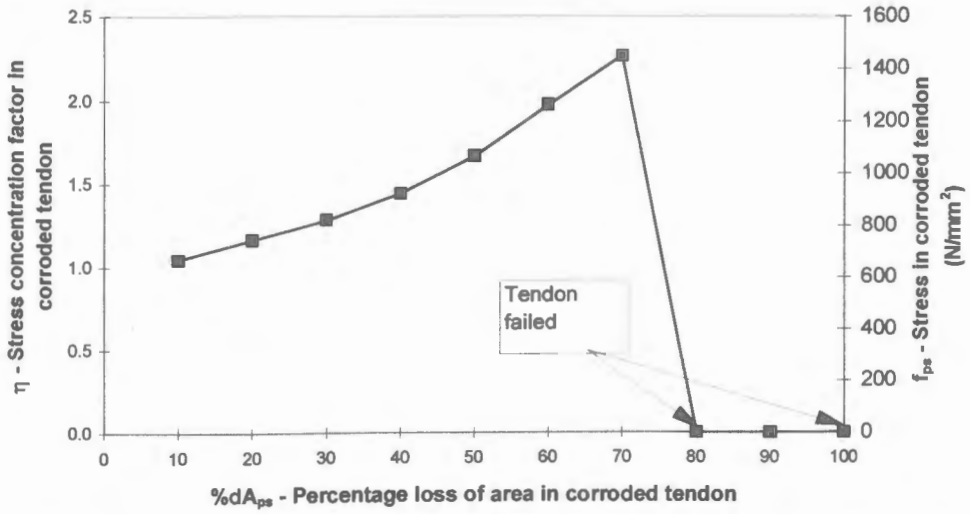

Figure 4.41 Stress enhancement in the corroded tendon for increasing loss of area in the corroded tendon (Bond strength 2.0 N/mm^2)

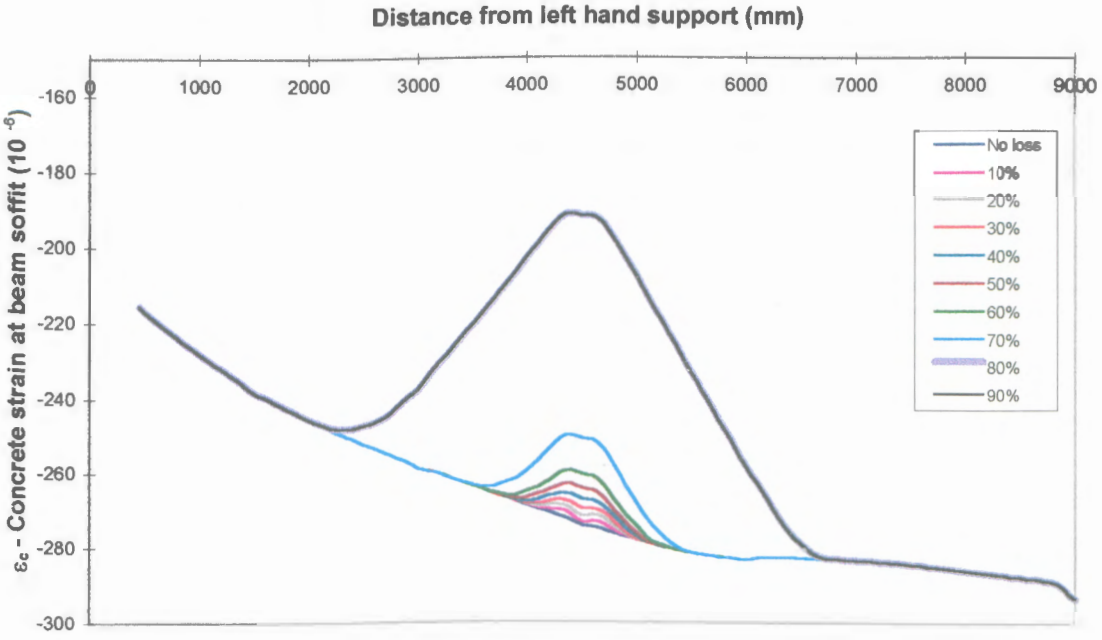

Figure 4.42 Concrete strain increase along beam soffit due to increasing loss of area in the corroded tendon (Bond strength 2.0 N/mm^2)

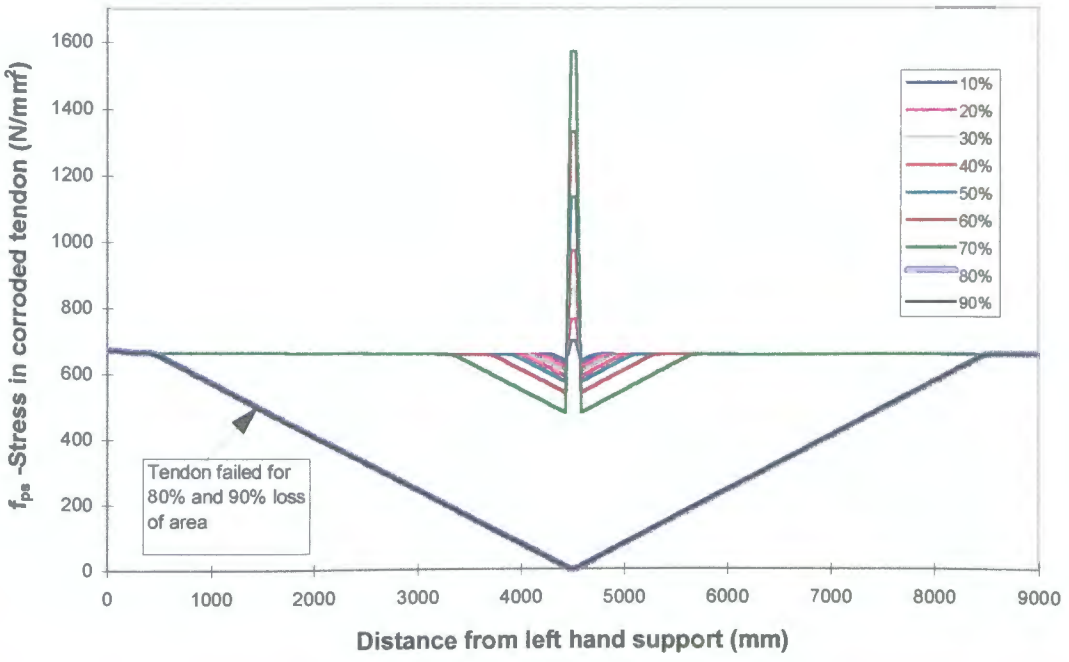

Figure 4.43 Stress in the corroded tendon due to increasing loss of tendon area (Bond strength 1.0 N/mm^2)

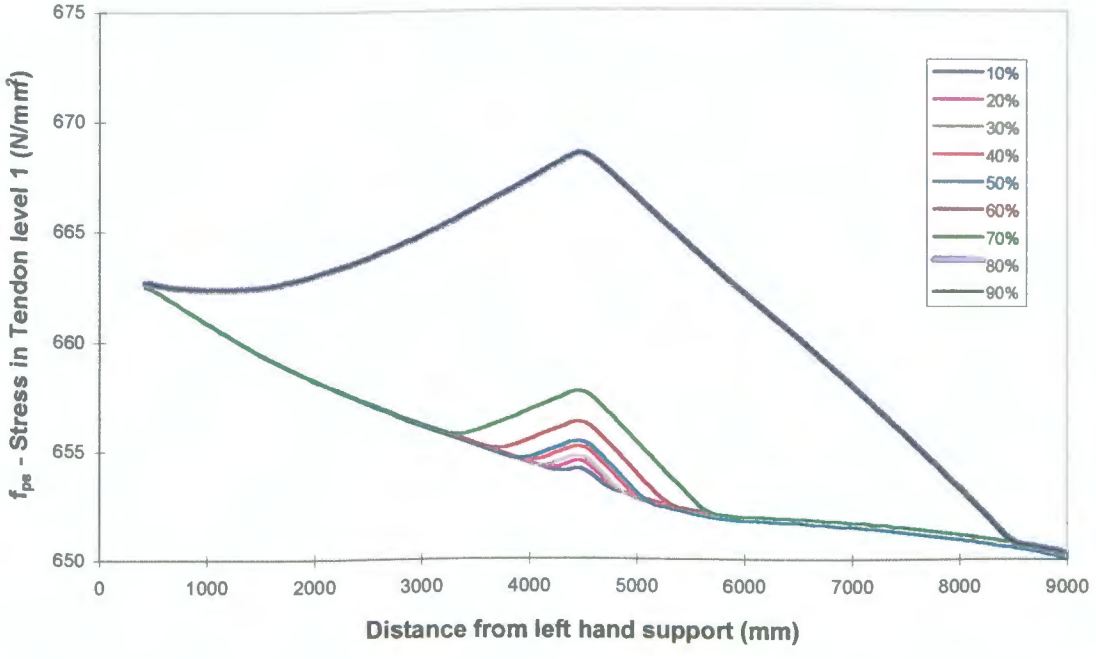

Figure 4.44 Stress in tendon level 1 due to increasing loss of area in the corroded tendon (Bond strength 1.0 N/mm^2)

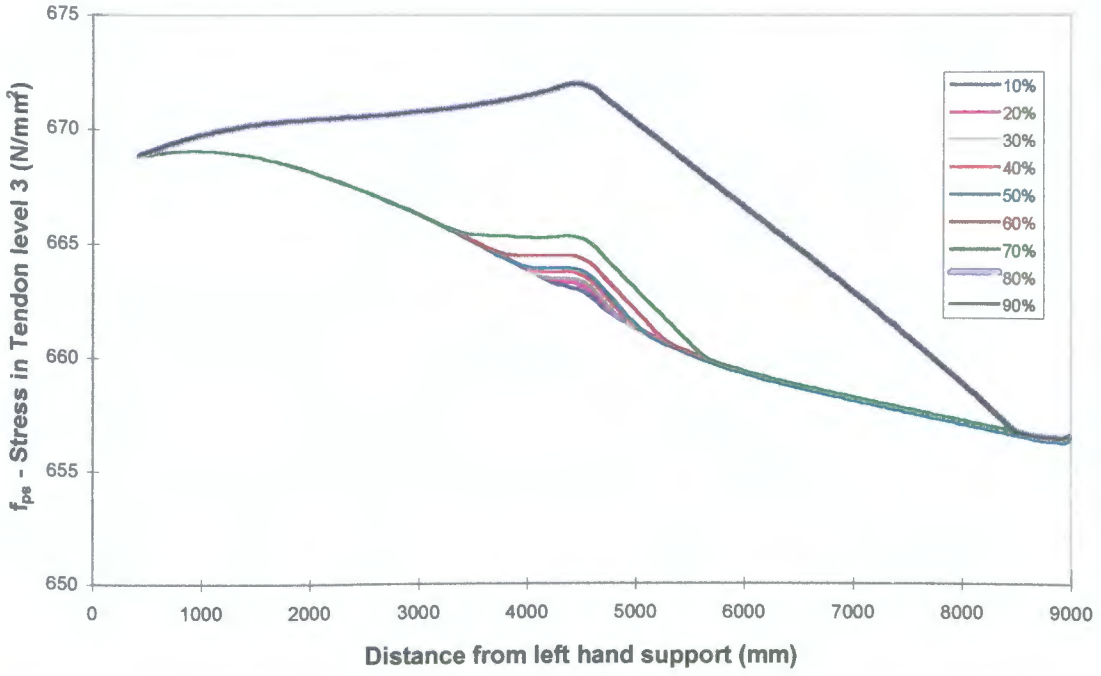

Figure 4.45 Stress in tendon level 3 due to increasing loss of area in the corroded tendon (Bond strength 1.0 N/mm^2)

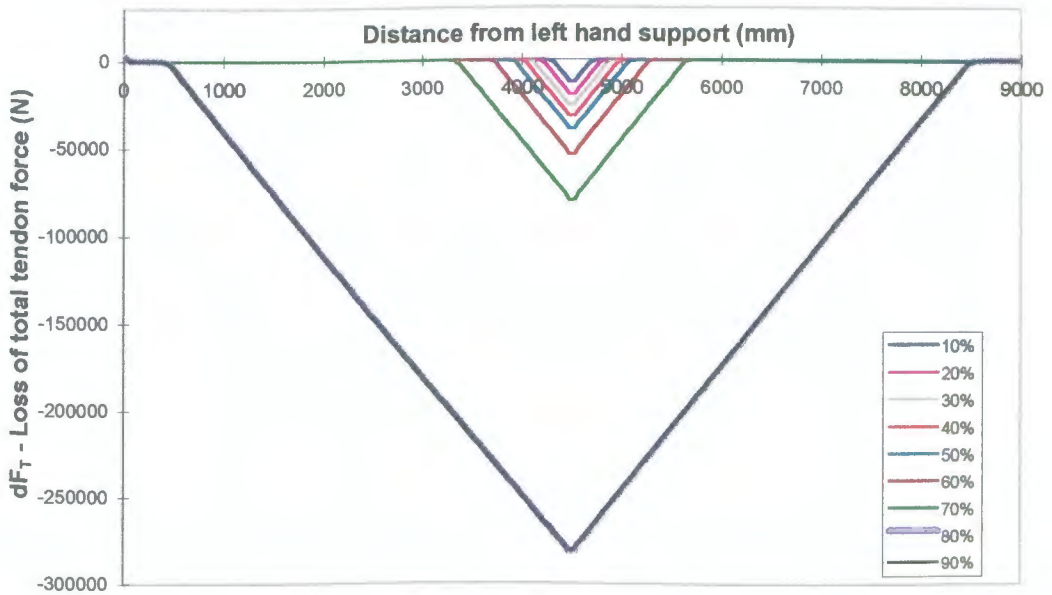

Figure 4.46 Loss of total tendon force due to increasing loss of area in the corroded tendon (Bond strength 1.0 N/mm^2)

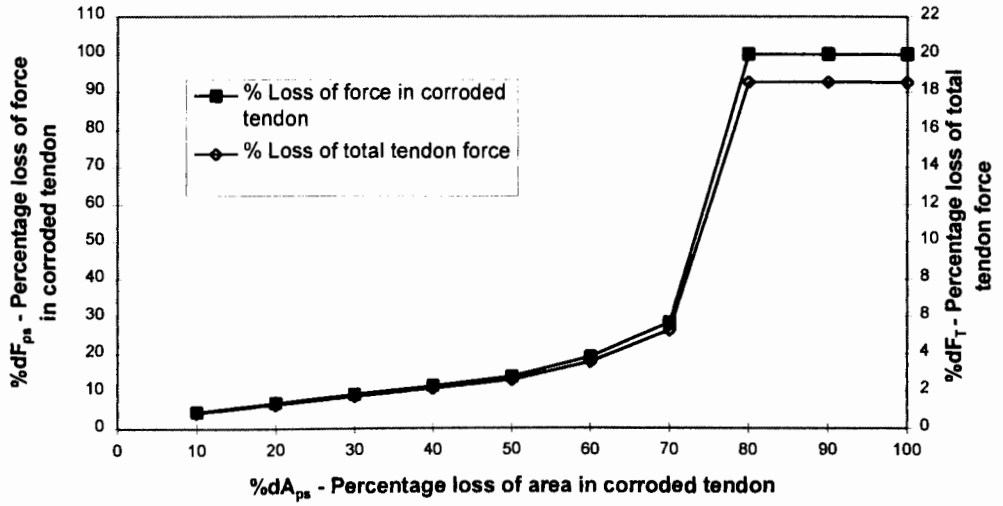

Figure 4.47 Loss of force due to loss of tendon area (Bond strength 1.0 N/mm^2)

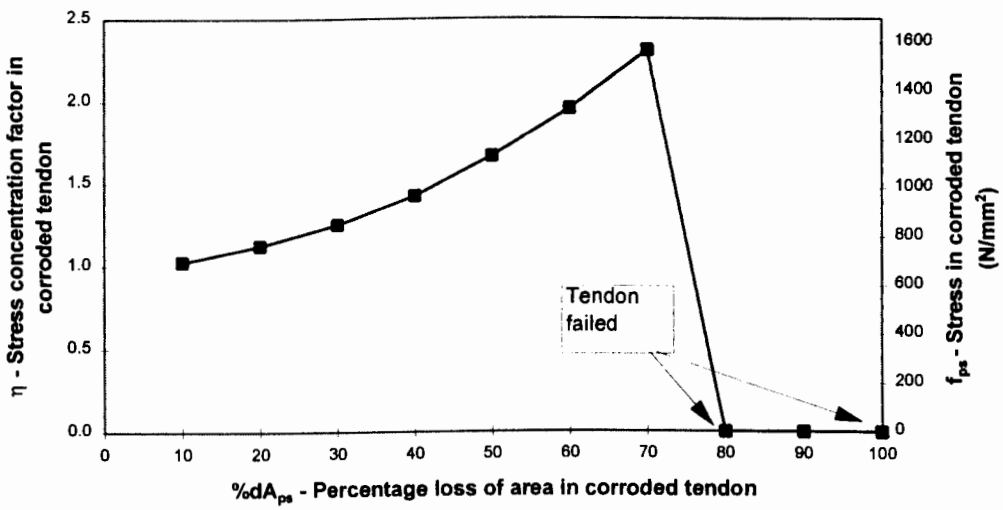

Figure 4.48 Stress enhancement in the corroded tendon for increasing loss of area in the corroded tendon (Bond strength 1.0 N/mm^2)

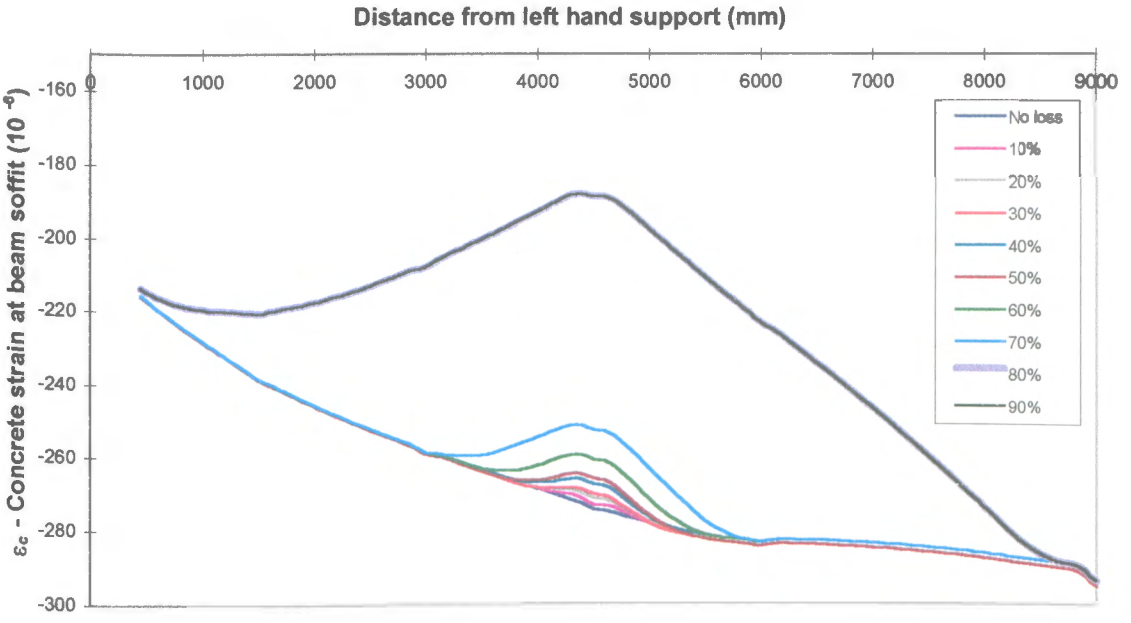

Figure 4.49 Concrete strain increase along beam soffit due to increasing loss of area in the corroded tendon (Bond strength 1.0 N/mm^2)

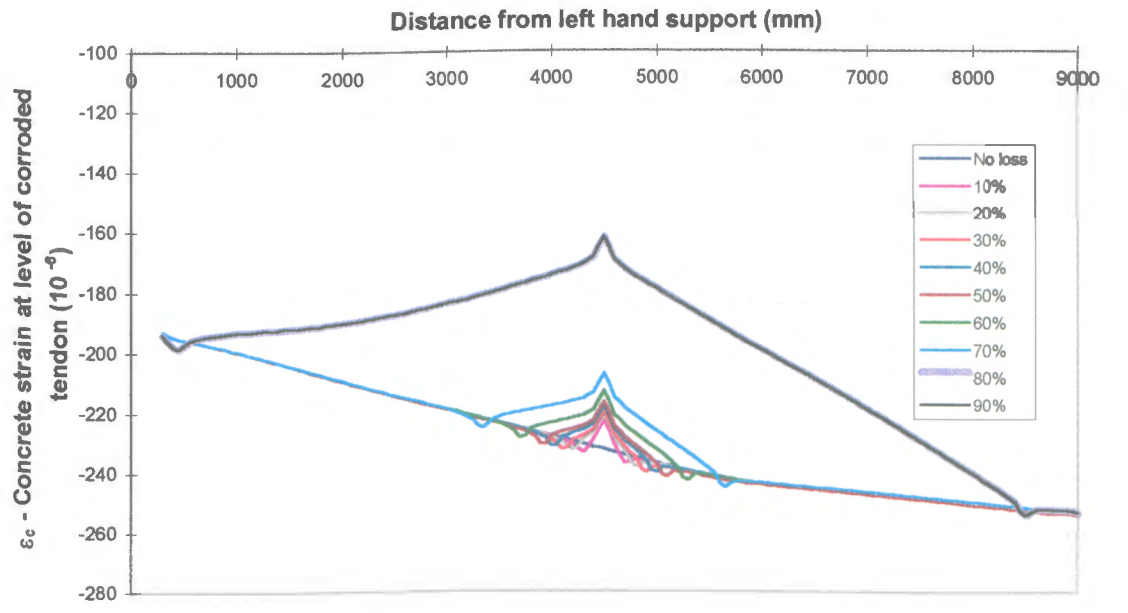

Figure 4.50 Concrete strain increase along level of corroded tendon due to increasing loss of area in the corroded tendon (Bond strength 1.0 N/mm^2)

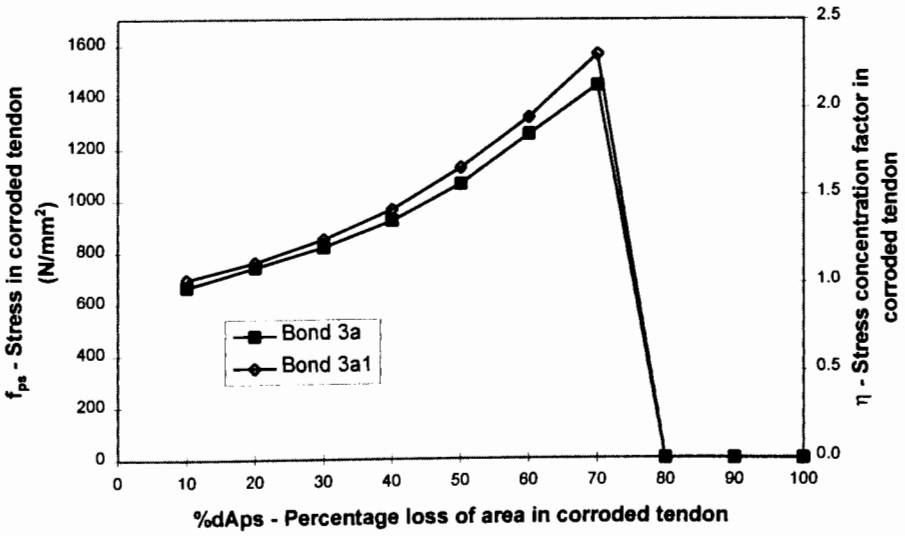

Figure 4.51 Comparison of stress enhancement in the corroded tendon for the two bond models considered

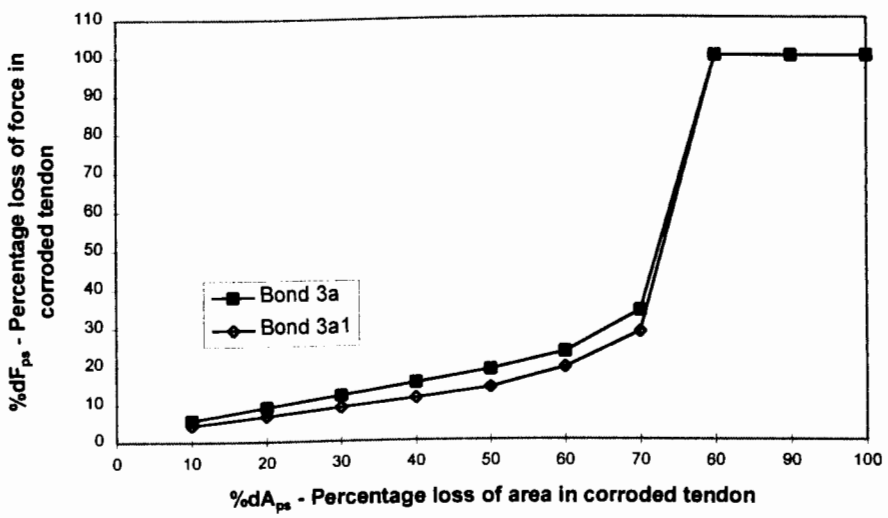

Figure 4.52 Comparison of the amount of force lost in the corroded tendon for the two bond models considered

CHAPTER 5

Development of Analytical Model

5.1 INTRODUCTION

In order to investigate the effect of tendon corrosion and the presence of incomplete grouting on the residual structural capacity of deteriorating post-tensioned concrete bridges, the consequence of tendon failures on the performance of the structure both at service and at ultimate needs to be studied. This will involve consideration of the redistribution of stresses within a tendon group as a result of tendon failure.

In this chapter, the development of an analytical model to assess the residual strength of deteriorating post-tensioned concrete bridges is described. The mechanisms of deterioration addressed are those due to failure of the prestressing tendon as a result of corrosion, and the presence of grout voids within the ducts. The non-linear analysis model proposed is based principally on the method of strain compatibility, but suitably modified to accommodate unbonded tendons in regions of incomplete grouting in the ducts. The computer program, which is written in FORTRAN code, predicts the moment-curvature response of the damaged beam up to the failure condition.

The model also incorporates the phenomenon of tendon re-anchoring of failed tendons to estimate the distribution of residual prestress after tendon failure. The method of analysis for internal unbonded post-tensioned beams, and how it is implemented in the program, is also described in this chapter.

5.2 THE BASIC MODEL

The analytical model described in this chapter is developed to study the effect of tendon failure due to corrosion and the presence of grout voids on the residual strength of deteriorating post-tensioned concrete bridge beams. The program is limited to simply-supported beams of constant cross-section throughout its span. Although it is intended for general application to handle post-tensioned beams of various cross-sectional shapes, it is assumed that the cross-section of the member is symmetrical about the vertical axis. Both the prestressing steel and non-prestressed reinforcement are also assumed to be located at the vertical axis of symmetry, so that any biaxial stresses which may arise in practice (due to eccentricity of force as the prestressing tendons fracture), are reduced to a uniaxial state of stress.

The program requires that the beam to be analysed is divided into a number of segments, thus resulting in a number of nodal sections where the sectional analysis will be carried out.

5.2.1 Assumptions of the Model

In deriving a general theory for the flexural strength of reinforced concrete or prestressed concrete sections, some basic assumptions are normally made. This theory is well-established and documented in the literature (Park and Paulay, 1975; Naaman, 1977). Generally, the assumptions are:

i. Plane sections remain plane after bending
ii. The stress-strain curve for the steel is known
iii. The stress-strain curve for concrete, defining the magnitude and distribution of compressive stress, is known
iv. The tensile strength of the concrete is ignored in the calculation of the moment of resistance (but is considered for the estimation of tension stiffening effects).

All the above assumptions were explicitly adopted in the analytical model developed here. The first assumption implies that the longitudinal strains in the concrete and the steel at the various points over the depth of a section is proportional to the distance from the neutral axis, at which the strain is zero. This also means that the strain in the steel is assumed to be the same as that in the adjacent concrete. This assumption of linear strain distribution is

sufficiently true at all stages of loading up to flexural failure provided good bond exists between the concrete and steel.

The second assumption implies that the stress-strain properties of the steel are well-defined. Normally in design, a bilinear stress-strain curve is assumed for the normal unprestressed reinforcement, and a trilinear stress-strain curve is assumed for the prestressing steel. The third assumption is necessary to assess the true behaviour of the section. The shape of the stress-strain curve of the concrete indicates the shape of the compressive stress block at various stages of loading. Figure 5.1 shows the changing shape of the concrete stress block as the bending moment at a beam cross-section is increased. The section reaches its flexural strength (maximum moment of resistance) when the total compressive force in the concrete multiplied by the lever arm a is a maximum. A number of investigators have recommended the use of an equivalent rectangular stress block to replace the actual shape of the concrete compressive stress block. However, this is only strictly applicable to rectangular concrete sections and is more suitable for design purposes. Moreover, it is only applicable at the ultimate condition. As the model developed here was intended for general application to consider non-rectangular sections as well, a layer-by-layer evaluation of concrete compressive forces was adopted, as will be discussed later.

In the case of the fourth assumption, any tensile stress that exists in the concrete just below the neutral axis is small, and has a small lever arm. This is usually neglected in most analytical work.

The ACI 318 (1989) code recommends a maximum strain of 0.003 at the extreme compression fibre of the concrete at the flexural strength of the section. This figure has been regarded as a reasonably conservative value (Park and Paulay, 1975). At this strain, the compressed concrete in a flexural member will not normally show any visible cracking or spalling. The computed flexural strength is usually relatively insensitive to the value of the assumed maximum concrete strain. However, since the calculation of ultimate curvature at a section depends on the value adopted for the extreme fibre strain, a higher value of 0.004 was recommended. The CEB-FIP (1993) code recommends a maximum concrete strain of 0.0035 at the extreme compression fibre of the concrete at the ultimate

condition. This value has been adopted in the BS 8110 (1985) code for concrete and was adopted in the analytical model developed here.

5.2.2 Estimation of Prestress Losses to the System

The force in the prestressing tendons of a prestressed concrete member continuously decreases with time. The total stress reduction (total loss of prestress) during the life-span of the member is generally attributed to the cumulative contribution of individual sources of prestress loss. These sources of loss of prestress, and how they are numerically determined, are described extensively in the literature (Lin and Burns, 1981; Naaman, 1982; Collins and Mitchell, 1991). Table 5.1 summarizes the main sources of prestress loss in post-tensioned concrete. These are either instantaneous losses due to elastic shortening of concrete, frictional losses and anchorage set, or time-dependent losses due to relaxation of the steel, and the effects of creep and shrinkage in the concrete.

It is essential to estimate the magnitude of the total loss of prestress since it determines the value of the effective prestressing force. Many methods and design recommendations have been proposed to predict the prestress losses, some with different levels of difficulty and accuracy to account for the fact that time-dependent losses are inter-dependent. In the analytical model, the prestress losses to the post-tensioning system was estimated according to Part 4 of BS 5400 (1990), the code of practice for concrete bridges. Reference was also made to BS 8110 (1985) and to the literature.

Elastic shortening:

If all the tendons are tensioned simultaneously, then no elastic shortening loss occurs as jacking proceeds until the required prestress force is achieved. If the tendons are not stressed simultaneously (usually the case), the loss of prestress is different in each tendon as the tensioning of any subsequent tendons will reduce the prestress in those already anchored, except the last tendon which suffers no loss. The computation of such losses is quite complicated (Naaman, 1982), and for practical reasons, it is normally assumed that the loss in each tendon is equal to the average loss in all the tendons. This is equal to half the sum of the loss in the first tendon, and that in the last tendon (which is zero). This assumes that each tendon is stressed to the same value. The loss due to elastic shortening is then given by (Naaman, 1982):

$$\Delta f_{ES} = 0.5\left[\frac{E_{ps}}{E_{ci}}(f_{cgs})_{Fi+G}\right]_{1^{st}\,tendon} \qquad \text{.....(5.1)}$$

where E_{ps} is the elastic modulus of prestressing steel, E_{ci} is the elastic modulus of concrete at time of transfer, and $(f_{cgs})_{Fi+G}$ is the stress in the concrete at the centroid of the steel due to the prestressing force and the dead load of the member immediately after transfer.

At this stage, the initial tendon stress has been reduced by friction as well. By expressing equation (5.1) in terms of the initial jacking stress f_{PJ} and the jacking force P_J,

$$\Delta f_{ES} = 0.5\frac{(f_{cgs})_{FJ}\left[f_{PJ} - \Delta f_{pf}\right] + f_{PJ}(f_{cgs})_G}{f_{PJ} / npi + (f_{cgs})_{FJ}} \qquad \text{.....(5.2)}$$

where $(f_{cgs})_{FJ} = \frac{P_J}{A_c} + \frac{P_J e_0^2}{I}$

$(f_{cgs})_G = -\frac{M_g e_0}{I}$

Δf_{pf} = loss due to friction

$npi = E_{ps}/E_{ci}$.

A_c, I, e_0 and M_g are respectively the concrete cross-sectional area, the second moment of area, the eccentricity of the centroid of the tendons, and the bending moment due to dead load.

Friction:

Friction is generated between the tendons and the inside surface of the duct during the stressing operation. The mechanisms producing friction are due to:

i) Curvature of tendon profile, which is the *intended* change of angle of the tendon profile. The loss of tension due to friction between the curved tendons and their ducts depends on the angle turned through, and the coefficient of friction μ between the tendon and the duct. The prestressing force $P(x)$ at a distance x from the jacking end is given by

$$P(x) = P_J e^{-\mu x / r_{ps}} \qquad \text{.....(5.3)}$$

where P_J is the prestressing force in the tendon at the jacking end, and r_{ps} is the radius of curvature. The coefficient of friction depends on the surface characteristics of the tendon and duct, and for steel moving on steel, $\mu=0.30$ is recommended.

ii) Wobble, which is the *unintended* deviation from the specified profile.

The prestressing force *P(x)* at a distance *x* from the jacking end due to wobble is given by

$$P(x) = P_J e^{-Kx} \qquad \text{.....(5.4)}$$

where *K* is the wobble coefficient per unit length. Its value depends on the type of duct and is typically $33\text{x}10^{-4}$/m.

The prestress losses due to friction increases with distance from the jacking end. The total losses due to both wobble and curvature is then given by

$$P(x) = P_J e^{-(\mu x/r_{ps}+Kx)} \qquad \text{.....(5.5)}$$

In the analytical model, the friction losses were calculated at the nodal sections along the beam, depending on the number of segments the beam was divided into. The reduced tendon stress at the end of a segment was used to compute the frictional loss for the next segment, thus accounting for the gradual reduction in prestress along the beam length.

Anchorage draw-in:

This loss occurs as a result of slip which occurs between the tendons and the wedges at the anchorage during the process of transferring the prestress force from the jack to the anchorage. The amount of pull-in Δl, depends on the anchorage type. This value is usually specified by the manufacturer, and is typically about 5mm. This effect is normally more serious in short members, where the amount of tendon draw-in represents a relatively larger proportion of its total length than those in longer spans (*L*). The prestress loss due to anchorage draw-in was taken as $\frac{\Delta l}{L} E_{ps}$.

Shrinkage:

Since the steel is bonded to the concrete, any shrinkage of the concrete due to the hydration process and the evaporation of surplus water in the concrete, will result in

contraction in the tendon and hence loss of prestress. Shrinkage is dependent on many factors including environmental conditions and the concrete aggregate type and water-cement ratio.

Loss of prestress due to shrinkage $= \varepsilon_{sh} . E_{ps}$ .....(5.6)

BS 5400 (1990) recommends a shrinkage strain $\varepsilon_{sh} = 200x10^{-6}$ for normal exposure.

Creep:

This is defined as additional strain under sustained load. This creep phenomena causes a shortening of the concrete member with time, hence a reduction in prestress force. Creep varies with the level of stress in the concrete.

The loss of prestress due to creep $= \varepsilon_{cc} . E_{ps}$ .....(5.7)

The creep strain is given by $\varepsilon_{cc} = f_c \phi_s$, where f_c is the concrete stress at the centroid of the tendons immediately after transfer. In BS 5400, the specific creep strain of concrete ϕ_s (creep per unit length per unit applied stress) is typically $36x10^{-6}$ per N/mm^2 if the cube strength at transfer f_{ci} is greater than 40 N/mm^2. For lower values of cube strength at transfer and for cases where the maximum concrete stress anywhere in the section at transfer exceeds $1/3f_{ci}$, the specific creep strain should be adjusted accordingly.

Relaxation:

This occurs when the tendon is stressed to a high proportion of its ultimate tensile strength, and gradually loses its prestressing force with time. The amount of relaxation depends on (i) the type of steel, (ii) the initial stress level, and (iii) temperature. BS 8110 (1985) specifies long-term relaxation loss as 1000-hour relaxation test value given by the manufacturer. In the absence of this data, typical maximum values dependent on initial prestress can be obtained from BS 5896 (1980) for wires and strands, and from BS 4486 (1980) for bars. For an initial force less than 60% of the breaking force, the relaxation value can be taken to decrease linearly from the 60% value, to zero at initial force of 30% of the breaking force.

These relaxation values are multiplied by a factor to reflect the reduction in tendon stress (hence less relaxation loss) with elastic shortening and time dependent (creep, shrinkage)

losses. For post-tensioned wires or strands, this factor is given in BS 8110 as 2.0 for Class 1 (normal relaxation), and as 1.5 for Class 2 (low relaxation) wires or strands. For post-tensioned bars, the factor is 2.0.

5.2.3 Non-linear Constitutive Material Relationships

Stress-strain relationship for concrete:

The distribution of compressive stress in the concrete may adopt any shape that results in a reliable prediction of the flexural strength of the member. Some alternative relationships between concrete compressive stress and strain which have been previously employed are bilinear, parabolic, and combined parabolic-linear curves.

The analytical model adopted here is the parabolic-rectangular stress-strain response of concrete as recommended by BS 8110 (1985), but with the partial safety factor $\gamma_m = 1$. This is based on the idealized stress-strain curve for concrete in uniaxial compression proposed by Hognestad (Figure 5.2). This is a widely used approximation for the shape of the stress-strain curve before maximum stress, which is a second degree parabola defined by

$$f_c = f_c'' \left[\frac{2\varepsilon_c}{\varepsilon_0} - \left(\frac{\varepsilon_c}{\varepsilon_0} \right)^2 \right] \qquad \text{.....(5.8)}$$

where f_c'' = maximum stress reached in the concrete

$\varepsilon_0 = 2\, f_c''/E_c$

E_c = modulus of elasticity for concrete.

The extent of the falling branch behaviour depends on the limit of useful concrete strain assumed. BS 8110 recommends a curve consisting of the second degree parabola up to a strain of $2.4 \times 10^{-4}\sqrt{f_{cu}}$ (f_{cu} is the characteristic strength of concrete) followed by a straight horizontal branch to a strain of 0.0035 (Figure 5.3). The coefficient of 0.67 accounts for the relation between cube strength and bending strength in a flexural member.

To find the strain ε_c caused by a stress f_c defined by the parabolic portion of the curve,

$$\varepsilon_c = \varepsilon_o \left(1 - \sqrt{1 - \frac{f_c}{f_c''}}\right) \qquad \text{.....(5.9)}$$

For concrete in uniaxial tension, the stress-strain response of concrete in tension was assumed to be linear prior to cracking:

$$f_c = E_c \varepsilon_c \qquad \text{.....(5.10)}$$

Stress-strain relationship for prestressing steel:

The stress-strain response of prestressed steel can be approximated by the bilinear relationship:

$$f_{ps} = E_{ps}\varepsilon_{ps} \le f_{py} \qquad \text{.....(5.11)}$$

where E_{ps} is the elastic modulus of prestressing steel, ε_{ps} is the strain in the prestressing steel, and f_{py} is the yield stress. However, most strands and wire for prestressing do not exhibit a yield plateau (as in normal reinforcement for reinforced concrete). An equivalent 'yield stress' is normally defined as the stress at a strain of 1%.

In order to obtain a more accurate representation of the stress-strain response of the prestressing strand, Collins and Mitchell (1991) used the modified Ramberg-Osgood function:

$$f_{ps} = E_{ps}\varepsilon_{ps}\left\{A + \frac{1-A}{\left[1+\left(B\varepsilon_{ps}\right)^{C}\right]^{1/C}}\right\} \le f_{pu} \qquad \text{.....(5.12)}$$

where f_{ps} is the stress in the prestressing steel and f_{pu} is the ultimate strength of the prestressing steel. The four coefficients $A,B,C,$ and E_{ps} can be found by representing the actual stress-strain curve for the strand as two straight lines connected by a curve, and solving for these constants (Figure 5.4). As the actual stress-strain curve for the tendons in the existing beams to be modelled is probably not known in practice, a simpler stress-strain curve has to be adopted. The stress-strain relationship for prestressing tendons was therefore defined by the trilinear stress-strain curve recommended by BS 8110 (Figure 5.5). In this case, the limit on the strains ε_2 and ε_3 were defined as

$$\varepsilon_2 = \frac{0.8 f_{pu}}{E_{ps}\gamma_m} \qquad \text{.....(5.13a)}$$

$$\varepsilon_3 = 0.005 + \frac{f_{pu}}{E_{ps}\gamma_m} \qquad \text{.....(5.13b)}$$

where γ_m is the partial safety factor (taken here as 1.0).

For a calculated strain of ε_{ps}, the stress in the prestressing steel f_{ps},

$$f_{ps} = E_{ps}\varepsilon_{ps} \qquad \text{for } \varepsilon_{ps} < \varepsilon_2 \qquad \text{.....(5.14a)}$$

$$f_{ps} = \left(\frac{f_{pu}}{\gamma_m} - \frac{0.8f_{pu}}{\gamma_m}\right)\left(\frac{\varepsilon_{ps} - \varepsilon_2}{\varepsilon_3 - \varepsilon_2}\right) + \frac{0.8f_{pu}}{\gamma_m} \qquad \text{for } \varepsilon_2 < \varepsilon_{ps} < \varepsilon_3 \qquad \text{.....(5.14b)}$$

$$f_{ps} = \frac{f_{pu}}{\gamma_m} \qquad \text{for } \varepsilon_{ps} \geq \varepsilon_3 \qquad \text{.....(5.14c)}$$

Stress-strain relationship for non-prestressed reinforcement:

For non-prestressed reinforcement, the relationship between the stress in the steel f_s and the corresponding strain ε_s is usually assumed to be bilinear, as shown in Figure 5.6. The same relationship is assumed valid for both tension and compression. For a strain of ε_s, the stress in the non-prestressed reinforcement f_s is

$$f_s = E_s\varepsilon_s \qquad \text{for } \varepsilon_s < \varepsilon_1 \qquad \text{.....(5.15a)}$$

$$f_s = \frac{f_y}{\gamma_m} \qquad \text{for } \varepsilon_s \geq \varepsilon_1 \qquad \text{.....(5.15b)}$$

where $\varepsilon_1 = \dfrac{f_y}{E_s\gamma_m}$ (γ_m taken here as 1.0), E_s is the elastic modulus of the reinforcement and f_y is the yield strength of the reinforcement.

5.2.4 Tension Stiffening Effect

Figure 5.7 illustrates the tensile stresses in a cracked concrete element. Before cracking, the concrete is fully effective in resisting tensile stresses. After cracking has occurred, there are no tensile stresses in the concrete at a crack location, and the stresses in the reinforcement will be highest here as well. However, due to bond with the reinforcement, tensile stresses still exist in the concrete between the cracks, and this stiffens the member.

To account for this 'tension stiffening' effect, the analytical model used the average tensile stress-average tensile strain relationship to estimate the average tensile stresses in the concrete f_c after cracking which was proposed by Collins and Mitchell (1991). If the average strain ε_{cf} exceeds the cracking strain ε_{cr}, then

$$f_c = \frac{\alpha_1\alpha_2 f_{cr}}{1 + \sqrt{500\varepsilon_{cf}}} \qquad \text{.....(5.16)}$$

where f_{cr} is the tensile strength of concrete, α_1 is the factor accounting for bond characteristics of reinforcement ($\alpha_1=1.0$ for deformed reinforcing bars, $\alpha_1=0.7$ for plain bars, wires or bonded strands, $\alpha_1=0$ for unbonded reinforcement), and α_2 is the factor accounting for sustained or repeated loading ($\alpha_2=1.0$ for short-term monotonic loading, $\alpha_2=0.7$ for sustained and/or repeated loads)

5.2.5 Shear Resistance

Although the flexural resistance in beams can be analysed by readily available flexural beam theory, the determination of the shear resistance of a section is more difficult. Shear failure is sudden and difficult to predict with accuracy. The current design procedures for prestressed beams are still based essentially on empirical data rather than on any established theory. In BS 5400, the shear resistance of prestressed concrete members is considered at the ultimate limit state. The action of a prestressed concrete member in resisting shear is similar to that for reinforced concrete, but with additional effects of the compression due to the prestress force which increases the shear resistance considerably. Most of the equations proposed are empirical and based on tests on prestressed concrete beams with conventional bonded reinforcement. This may invalidate the relevance of these equations where the shear resistance of a section with unbonded tendons is to be determined.

The shear resistance of a section is said to depend on (i) the resistance of the concrete compression zone, (ii) the aggregate interlock resistance along the diagonal crack and (iii) dowel resistance of the tendon and of any non-prestressed reinforcement. These assumptions hold true for prestressed concrete members with bonded tendons, but may no longer be true for beams containing unbonded tendons.

The shear strength of prestressed concrete beams with unbonded tendons was investigated by Kordina et al (1989). The experimental results showed that as far as the shear cracking behaviour for prestressed beams with and without bond is concerned, no significant differences between the inclination and crack widths have been observed. The stirrup stresses indicated that beams with unbonded tendons do not differ in principle from those with bonded prestressing reinforcement. Evaluation of the shear test results and comparison with various shear design models concluded that the shear strength of

prestressed beams with unbonded tendons can be determined correctly with a truss analogy model.

According to the truss analogy, after the first shear cracks (web shear or flexural shear cracks) have occurred, the shear reinforcement carries tension across the cracks and resists widening of the cracks. The web members of the truss (Figure 5.8) resist applied shear and consist of vertical tension members (vertical legs of stirrups) and diagonal compression struts which represent the diagonal compression in the concrete between the diagonal cracks. The top compressive chord of the truss represents the concrete compressive zone plus any longitudinal compressive reinforcement. The bottom chord models the longitudinal prestressed and non-prestressed reinforcement in the tensile zone. At each panel point along the bottom chord of the truss, the vertical component of the compressive force in the inclined concrete strut must equal the tension in the vertical steel member. Also, the horizontal component must equal the change in the tensile force (prestressing tendon and non-prestressed reinforcement) in the bottom chord. The derivation of the relevant equations on the basis of a truss model is given by Park and Paulay (1975).

The design concepts of the CEB-FIP (1978) model code, based on the truss analogy, was found to be the most appropriate for use on members with unbonded tendons. This was incorporated into the analytical model, with an assumed 45° truss angle. In the case of flexural-shear failure, the shear strength V_u is obtained by

$$V_u = V_c + V_w + V_p \qquad \text{.....(5.17)}$$

where V_c is the shear force carried by the concrete, V_w is the shear force carried by the truss action in the web and V_p is the shear force carried by the vertical component of inclined prestressing tendons if curved cables are used. Near the ends of beams where shear forces are highest and cable slopes generally greatest, a moderate increase in shear resistance V_p can be obtained. This value decreases away from the end of the beam as the angle of inclination of the tendons reduces.

According to the CEB-FIP model, the part of the shear force carried by the concrete is

estimated by

$$V_c = 2.5\tau_{RD} b_w d\left(1 + \frac{M_o}{M_u}\right) \quad \text{.....(5.18)}$$

where τ_{RD} = resistant shear stress provided by the concrete

b_w = width of the web

d = depth of the centroid of the total steel area in the tension zone

M_0 = decompression moment related to the extreme tensile fibre of the section

M_u = the bending moment at the section considered, due to ultimate load.

The contribution of any web reinforcement (in the form of stirrups) V_w, to the shear strength of the beam depends on the area of the two legs of a link A_{sw}, the characteristic strength of the link reinforcement f_{yv}, and the number of stirrups which cross the inclined crack. Based on a 45° truss model (i.e. shear cracks are assumed to occur at 45° to the horizontal),

$$V_w = 0.9d\frac{A_{sw} f_{yv}(1 + \cot\alpha)\sin\alpha}{s} \quad \text{.....(5.19)}$$

where α is the inclination of the shear reinforcement (usually between 45° and 90°) to the horizontal axis and s is the link spacing.

The shear force carried by the inclined prestressing tendons is

$$V_p = N_p \sin\beta \quad \text{.....(5.20)}$$

where N_p is the effective prestressing force (or the residual force if within the re-anchoring zone of a failed tendon) at the section and β is the inclination of the tendon to the horizontal axis of the beam.

Upper limit of resistant shear force:

To avoid web crushing due to the compression diagonals induced by the shear forces, CEB-FIP imposes an upper limit to the shear force, so that

$$V_u \le V_{Rd2} + V_p \quad \text{.....(5.21)}$$

where $V_{Rd2} = 0.3 b_w d f_{cu}(1 + \cot\alpha)$ which should not exceed $0.45 b_w d f_{cu}$.

Since a 45° truss model was adopted (usually the case), it is assumed that the compressive struts are inclined at 45° to the horizontal axis of the beam although, in practice, this could vary depending on the relative quantities of main and shear reinforcement.

5.3 RESIDUAL PRESTRESS LEVELS AFTER TENDON FAILURE

5.3.1 Re-anchoring Length of Failed Tendon

Monitoring of strains released during controlled demolition of post-tensioned concrete bridges by Buchner and Lindsell (1987) and Darby (1996); and the cutting of bonded post-tensioned tendons by Belhadj and Waldron (1993), have indicated that some of the tendons within grouted ducts demonstrated re-anchoring behaviour back into the grout. This re-anchoring phenomenon is the ability of failed wires or tendons to re-anchor back into the available grout and retain the original prestress level (i.e. before loss of prestress due to tendon failure occurred). Clearly, the debonding behaviour and the ability of tendons to re-anchor will depend on whether the tendon is either in a fully grouted duct, a totally ungrouted duct (complete void), or a partially grouted duct. The quality of the grout and the characteristics of the tendon surface are also important factors. The length over which the failed tendon takes to fully re-anchor and regain its original prestress level (known as the re-anchoring length) may be seen to be analogous to the transfer length for pre-tensioned concrete.

When a post-tensioned tendon fractures, a state of anchorage bond stress develops similar to that in the anchorage zone of pre-tensioned concrete beams. Within this re-anchoring zone, the prestressing force is transferred to the concrete by friction and the wedging action as the tendon attempts to return to its original unstressed diameter. Chapter 2 has presented some of the established equations to estimate the transfer length in pre-tensioned concrete. From these equations, an appropriate equation was chosen to estimate the re-anchoring length of post-tensioned tendons which have failed due to corrosion. This then enabled the distribution of residual prestress after tendon failure to be estimated.

Although an analogy has been drawn between the re-anchoring length of failed post-tensioned tendons and the transfer length of pre-tensioned wires, it can only be considered

approximate as the nature of the prestress transfer is somewhat different. In pre-tensioned concrete, the end of the wires are usually flame or saw-cut, resulting in sudden failure of the wires. In post-tensioned concrete, the fracture of wires due to loss of cross-sectional area occurs gradually over time, although the final failure itself may be instantaneous. Generally, the transfer length at flame-cut ends tends to be longer than that with gradual release.

To enable an appropriate equation to be chosen to estimate the re-anchoring length of failed tendons, the equations given in Section 2.5.2 (that by Hoyer, BS 8110, ACI 318-89, and Zia and Mostafa) were compared in estimating the transfer length of a typical 7-wire strand in pre-tensioned concrete. The following data was assumed, where the symbols have been described in Section 2.5.2:

$d_b=12.5\ mm,\ \mu_s=0.3,\ \mu_c=0.2,\ \phi=0.3,\ n=6.3,\ E_c=31.6\ kN/mm^2,\ f_{si}=930\ N/mm^2,$
$f_{se}=790\ N/mm^2,\ f_{ci}=31\ N/mm^2.$

These values were substituted into the respective equations to give the transfer lengths, as shown in Table 5.2. The table shows that the codes tend to give more conservative results as is to be expected. The estimation by Zia and Mostafa (1977) depends on f_{ci}, the compressive strength of concrete at transfer, and has been reported to be more conservative than the ACI Code for low values of f_{ci}. Moreover, in the context of this study for existing post-tensioned beams, f_{ci} should be taken as the grout strength at the time of tendon failure. This value may be difficult to determine in practice considering that the duct may be incompletely grouted. This may limit the use of the equation proposed by BS 8110 which also relies on f_{ci}. Hoyer's equation, and that by the ACI code were therefore considered more suitable to represent the re-anchoring length of a failed post-tensioned tendon.

5.3.2 Distribution of Residual Prestress

Linear Approach:

By assuming that the 7-wire strand considered previously is now a post-tensioned tendon which had failed due to corrosion, the residual prestress distribution was respectively estimated by the equations proposed by BS 8110, ACI 318-89, Hoyer, and Zia and Mostafa. This was done by first estimating the re-anchoring length l_r required to restore the prestress of the tendon to its original value (before failure due to corrosion). A bi-linear

distribution of residual prestress f_s for distance l from the free end of the tendon then resulted:

$$f_s = \frac{f_{se}}{l_r} l \qquad \text{for } l<l_r \qquad \text{.....(5.22a)}$$

$$f_s = f_{se} \qquad \text{for } l \geq l_r \qquad \text{.....(5.22b)}$$

Figure 5.9 shows the distribution of residual prestress estimated by the linear equations considered above. This is compared with that estimated by an exponential equation, as is discussed next.

Exponential Approach:

It is also aimed to estimate the distribution of residual prestress of a failed tendon within a partially grouted duct. Since the re-anchoring of failed tendons is due mainly to friction between the tendon and the grout/concrete, and the wedging action of the tendon due to Poisson's effect, an equation which accounts for these two parameters is required. The formula proposed by Janney (1954) for the distribution of prestress transfer in pre-tensioned concrete (which was based on the frictional bonding phenomena), was considered suitable to study the distribution of residual prestress of a failed post-tensioned tendon in a partially grouted duct. The formula is given by

$$\log_e\left[\frac{f_{se}-f_s}{f_{se}}\right] = \frac{-2\phi\mu_s l}{r\left[1+(1+\mu_c)n\right]} \qquad \text{.....(5.23)}$$

where the symbols have been defined in section 2.5.2. Re-arranging the equation,

$$f_s = f_{se} - f_{se}.e^{\left[\frac{-2\phi\mu_s l}{r(1+(1+\mu_c)n)}\right]} \qquad \text{.....(5.24)}$$

The distribution of stress defined by this equation was taken to be analogous to the distribution of residual prestress of a failed post-tensioned tendon, where f_s represents the residual prestress after corrosion, f_{se} is the effective prestress before corrosion (after all losses to the system). It can be seen that the residual prestress varies inversely with the coefficient of friction between the tendon and the grout/concrete. A smaller coefficient of friction can thus be used to represent poorer grout condition (i.e. less friction), which leads to more gradual gain of prestress and hence a longer re-anchoring length. Figure 5.9

illustrates the exponential distribution of residual prestress which resulted when equation (5.24) was used to estimate the residual prestress distribution of the failed 7-wire strand.

It can be seen that Janney's equation resulted in a relatively long re-anchoring length due to the slow decay of the exponential relation. It should be noted that Janney's equation was based on tests on wires, but that given by ACI 318-89 was based on 7-wire strands. The BS 8110 code however, gave an equation which treated both wires and strands. Hoyer's equation gave the shortest re-anchoring length over which full prestress was restored after tendon failure. This can be seen to represent the most optimistic relationship for residual prestress (i.e. assuming very good quality grout to enable efficient tendon re-anchoring).

Re-anchoring model adopted:

Of the linear models, the ACI 318 (1989) equation was seen as a compromise between all the linear equations considered and was thus adopted to estimate the re-anchoring length of a failed tendon in a well-grouted duct:

$$l_r = \frac{f_{se}}{3} d_b \qquad \text{.....(5.25a)}$$

where f_{se} is the effective prestress in the tendon after losses to the system (*ksi*), and d_b is the nominal strand diameter (*inches*). In SI units (f_{se} *in MPa;* d_b *and* l_r *in mm*), the re-anchoring length is expressed as

$$l_r = \frac{1}{7}\frac{f_{se}}{3} d_b \qquad \text{.....(5.25b)}$$

In order to account for the quality of the grout and the characteristics of the tendon surface in providing frictional restraint to tendon movement, Janney's exponential equation (5.24) was adopted to represent re-anchoring of a failed tendon within poorer grout conditions. Thus the user has a choice of adopting a linear model for tendon re-anchoring in a well-grouted duct, or an exponential model for tendon re-anchoring within a partially grouted duct.

5.3.3 Stress Re-distribution as a Result of Tendon Failure

5.3.3.1 Re-distribution Within a Tendon Group At a Section

Consider a concrete section containing a number of tendons on the vertical axis of symmetry (Figure 5.10). The centre of action of the tendon group is computed by

$$ybs = \frac{\sum_{i=1}^{n} P_e^i . y_{ps}^i}{\sum_{i=1}^{n} P_e^i} = \frac{\sum_{i=1}^{n} f_{ps}^i . A_{ps}^i . y_{ps}^i}{\sum_{i=1}^{n} f_{ps}^i . A_{ps}^i} \quad \text{.....(5.26)}$$

where i designates a tendon, n is the number of tendons; P_e, f_{ps} and A_{ps} are respectively the effective force, effective stress and cross-sectional area in the tendon. The eccentricity of the tendon group is then $e_{yt}=ybg-ybs$, where ybg is the height to the centroid of the section.

Figure 5.10 also shows the strain and corresponding stress diagram of a typical cross-section under minimal service loading, and with no corroded tendons. For a section which has not yet decompressed, the following equations define the extreme top and bottom fibre stresses in the concrete:

$$\sigma_{ct,o} = \frac{T}{A_c} - \frac{T.e_{yt}}{z} + \frac{M}{z} \quad \text{.....(5.27a)}$$

$$\sigma_{cb,o} = \frac{T}{A_c} + \frac{T.e_{yt}}{z} - \frac{M}{z} \quad \text{.....(5.27b)}$$

where A_c, z and M are respectively the cross-sectional area of the concrete, the section modulus, and the applied bending moment; and T is the total effective tendon force after losses to the system. $\sigma_{ct,o}$ and $\sigma_{cb,o}$ represent the original stress in the concrete at the extreme top and bottom fibres respectively.

If tendon failure due to corrosion occurs, it is expected that prestress is lost over a certain distance as the tendon debonds from the position of fracture. In the first instance, it is assumed that the loss of prestressing force is directly proportional to the loss of area of the failed tendons (i.e. $x\%$ loss of total tendon area results in $x\%$ loss of total force). The new extreme fibre stresses are then:

$$\sigma_{ct} = \frac{\beta T}{A_c} - \frac{\beta T.e_{yt}}{z} + \frac{M}{z} \qquad \text{.....(5.28a)}$$

$$\sigma_{cb} = \frac{\beta T}{A_c} + \frac{\beta T.e_{yt}}{z} - \frac{M}{z} \qquad \text{.....(5.28b)}$$

where β is a factor due to loss of prestressing force as a result of tendon failure. The new distributions of strain and stress are shown in Figure 5.11, indicating an expansion in the concrete (less compressive stress in the concrete at the tendon level). The original lever arm a_o has increased, in order to provide the same moment of resistance of the section as that before corrosion. In addition, the curvature of the section has increased as a result of tendon failure. From equation 5.26, it can also be deduced that the centre of action of the tendon group and hence tendon eccentricity, will change slightly due to the tendon stress re-distribution within the section.

From Figure 5.11, the concrete strain adjacent to tendon level *i* is given by

$$\varepsilon_c^i = \varepsilon_{cen} - \phi \,.\, y^i \qquad \text{.....(5.29)}$$

where ε_{cen} is the strain in the concrete at the centroid of the section, ϕ is the curvature and y^i is the distance of tendon level *i* from the centroid of the section. The *change in strains* in the concrete adjacent to the tendon as a result of loss of tendon area can be obtained by

$$\Delta\varepsilon_c^i = \varepsilon_{c,o}^i - \varepsilon_c^i \qquad \text{.....(5.30)}$$

where $\varepsilon_{c,o}^i$ and ε_c^i respectively refer to the concrete strains at tendon level *i*, before and after corrosion. To maintain compatibility of strain, the change in the concrete strain is equal to the change in the tendon strain at their respective levels:

$$\Delta\varepsilon_{ps}^i = \Delta\varepsilon_c^i \qquad \text{.....(5.31)}$$

The respective tendon strain is then computed from

$$\varepsilon_{ps}^i = \varepsilon_{pe}^i + \Delta\varepsilon_{ps}^i \qquad \text{.....(5.32)}$$

where ε_{pe}^i is the effective prestrain in the tendon. By referring to the stress-strain curve for the prestressing steel, the stress f_{ps}^i corresponding to the strain ε_{ps}^i is then obtained.

The total tensile force T can then be computed from

$$T = \sum_{i=1}^{n} f_{ps}^i . A_{ps}^i \qquad \text{.....(5.33)}$$

The total compressive force C is given by

$$C = \int_{A_c} f_c dA_c \qquad \text{.....(5.34)}$$

where f_c is the stress in the concrete. The value of the integral for the total compressive force is approximated by a layer-by-layer evaluation, as will be described later.

Although the failed tendon cannot contribute to the total force in the section, the other tendon layers may carry more load to compensate for some of the prestress force which was lost in the failed tendon. In other words, the stresses in the other tendons are enhanced when compared to the no-corrosion situation. The force equilibrium condition is checked *(C=T)* and if this is not satisfied, the above procedure is repeated for another estimate of the factor β to obtain the stress (and strain) diagrams. The iteration procedure is terminated when $C=T$ within an acceptable error, and the $\Delta\varepsilon_{ps}^{i} = \Delta\varepsilon_{c}^{i}$ condition is also satisfied for every tendon layer.

Therefore, when a tendon fails due to corrosion, it is expected that the other remaining tendons will be slightly higher stressed as they try to recover the prestress lost in the failed tendon. This re-distribution of stresses actually occur between the wires or strands within a tendon, and also among the tendons within a tendon group. In the model, the wires or strands that constitute a tendon are represented by a single large tendon, so that the only redistribution is among the tendons within a tendon group.

The above discussion on the re-distribution of tendon stresses at a section caused by failure of a tendon assumes that the section has not yet cracked. If a section is found to have cracked as a result of failure of tendon(s), then post-cracking analysis is necessary, as will be discussed later.

5.3.3.2 Re-distribution Along the Length of the Beam

From the input of the position of tendon failure, the distribution of residual prestress is first estimated based on an assumed re-anchoring model. However, when there are a number of positions along the tendon where failure has occurred, the residual prestress distribution along it may be modified by the re-anchoring of the same tendon at a neighbouring position, as shown in Figure 5.12. An idealized resultant distribution of

residual prestress after tendon failure at a number of locations in one tendon is as shown shaded in the figure. For ease of illustration, Figure 5.12 shows a linear re-anchoring model adopted for all three tendon failure locations, although the discussion here applies to an exponential re-anchoring model as well.

Clearly, when there are other tendon layers which have failed due to corrosion, a similar approach is taken to estimate the resultant prestress distribution in the other layers, depending on the number of corrosion locations. This then becomes the starting point for the analysis at the respective nodal sections, during which the tendon stress re-distribution at a section is determined. As long as the tendons have not fully re-bonded to restore their original prestress, the nodal sections affected by the corrosion (which are determined by the tendon re-anchoring lengths), will be flagged to indicate the sections requiring an iterative sectional analysis to determine the stress re-distribution within a tendon group as described in section 5.3.3.1. The nodal sections affected by corrosion will also be influenced by regions of grout voids within the ducts, if they affect the re-anchoring of the failed tendon. This is discussed next.

5.4 REGIONS OF UNBONDED TENDON BEHAVIOUR

In the literature, the extent of grout voids within the duct of post-tensioned tendons has been reported to vary considerably, from being continuous over the length of the duct, to the duct being solidly grouted. The distribution of grout voids throughout the beam will determine whether the tendons act as totally ungrouted or partially grouted. If a void is continuous along the length of a tendon, the tendon can be considered to be 'unbonded' and the behaviour of unbonded post-tensioned tendons may dominate. The effect of incomplete grouting on the stress in the tendons can thus be investigated using the theory for internal unbonded beams.

The preceding section has discussed the transfer of residual prestress when tendons re-anchor back into the grout after failure due to corrosion. If grout voids are present within this re-anchoring length, this will affect the ability of the failed tendon to re-anchor and the required length may need to be extended until a sufficient region of grout is available. On

the other hand, if the duct is totally ungrouted, then failure of a tendon at any point along its length will result in its loss of prestress force over the entire unbonded length as the tendon does not re-anchor.

5.4.1 Method of Analysis for Internal Unbonded Post-tensioned Beams

The modelling of regions of unbonded tendon behaviour due to the presence of voids or ungrouted tendons within the duct is based on the method of analysis for internal unbonded post-tensioned beams proposed by Harajli (1990). The method of nonlinear analysis proposed is similar in principle to that normally adopted to evaluate the nonlinear response of fully bonded prestressed concrete members. However, unlike bonded members, and because of the slip of the prestressing tendon relative to the surrounding concrete, the stress in the unbonded tendon cannot be evaluated based solely on moment equilibrium and strain compatibility. Therefore, the assumption of perfect bond is no longer valid within these unbonded regions. Instead, the change in stress in the prestressing steel for any given loading depends on the *total* change in length of the adjacent concrete over the unbonded length. This means that the stress in the prestressing steel is member dependent rather than section dependent.

In the analytical model, the proposed unbonded theory was only used where appropriate (i.e. where voids are present). This is because the post-tensioned tendons within the ducts were not all likely to be unbonded (as in unbonded post-tensioned beams) but instead, consisted of a combination of fully grouted, partially grouted and totally ungrouted tendons. This can make the analysis rather complicated as the problem is now two-fold: (i) to analyse the effect of tendon loss of area on the behaviour of the beam using bonded beam theory, and (ii) where voids are present, to study the additional effect of these voids using unbonded beam theory. It is known from the literature that the behaviour of unbonded post-tensioned beams is affected by factors like the span-depth ratio, the amount of ordinary tension reinforcement, and the geometry of loading. Consideration of these effects itself on the behaviour of the beam to be analysed can involve highly nonlinear and iterative procedures. Therefore, some simplifying assumptions had to be made.

Perfect bond was assumed in fully grouted conditions and where voids were present, the tendons were assumed to be totally unbonded. This then covered the two extreme conditions likely to be present. The effect of span-depth ratio (which is known to be an important parameter in unbonded post-tensioned beams) was not considered in the analysis here as it is not expected that the bonded beams with pockets of voids within the ducts, will behave purely as an unbonded beam.

Consider a length of a bonded post-tensioned beam which contains three layers of tendons (Figure 5.13). Due to the presence of a void, tendon level 2 is unbonded over a length l_{d2}. The behaviour of the tendon over this length is seen to be similar to that of a single internal unbonded tendon. However, tendons at levels 1 and 3 behave as perfectly bonded tendons. Strain compatibility is thus maintained at tendon levels 1 and 3, but the strain at tendon level 2 is not compatible with the adjacent concrete over the length l_{d2}. In this case, the *average* strain increase in the prestressing steel over this unbonded length is obtained by integrating the 'fictitious' concrete strain increase at the respective sections, as explained below.

5.4.1.1 Analysis of Unbonded Tendons At Ultimate

If tendon level 2 is 'unbonded' over N number of segments of the beam, then at each section (Figure 5.14), the 'fictitious' increase in concrete strain above decompression at the level of the unbonded tendon is given by

$$\Delta\varepsilon_2 = \phi e_2 \qquad \text{.....(5.35)}$$

where ϕ is the curvature and e_2 is the eccentricity of tendon 2. At failure, $\phi = \frac{\varepsilon_{cu}}{x}$ where ε_{cu} is the ultimate concrete strain at the top compression fibre and x is the corresponding neutral axis depth at ultimate. In the figure, ε_{pa} is the actual increase in strain in the prestressing steel above the initial prestress level at decompression of the concrete.

The total tendon elongation Δl_{ps} between the ends of the void is thus

$$\Delta l_{ps} = \sum_{i=1}^{N} (\Delta\varepsilon_2 + \varepsilon_{co,2}) l_n \qquad \text{.....(5.36)}$$

where $\varepsilon_{co,2}$ is the precompressive strain in the concrete at the level of the unbonded tendon and l_n is the length of each beam segment.

It is assumed that the stress in the tendon at any given loading is constant along the unbonded length. This means that the frictional forces that could develop between the prestressing steel and surrounding duct are neglected. The average increase in strain in this tendon (above effective value), over its 'unbonded' length, is then

$$\Delta\varepsilon_{ps,2} = \frac{\Delta l_{ps}}{l_{d2}} \qquad \text{.....(5.37)}$$

The above procedure is also used for conditions not at ultimate, but where post-cracking analysis is to be carried out.

5.4.1.2 Analysis of Unbonded Tendons Before Decompression

If the concrete has not yet decompressed, the analysis procedure is the same as for the ultimate condition except that the 'fictitious' increase in concrete strain $\Delta\varepsilon_2$ at the level of the unbonded tendon is obtained by referring to the original strain profile assuming no corrosion or the presence of regions of unbonded tendons (Figure 5.15). At a particular section, the original strain in the concrete adjacent to tendon level 2,

$$\varepsilon_{co,2} = \varepsilon_{cen,o} - \phi_o . e_2 \qquad \text{.....(5.38)}$$

where the subscript 'o' refer to the original strain profile, and $\varepsilon_{cen,0}$ is the concrete strain at the centroid of the section. The curvature is obtained by:

$$\phi_o = \frac{\varepsilon_{ct,o} - \varepsilon_{cb,o}}{h} \qquad \text{.....(5.39)}$$

where $\varepsilon_{ct,o}$ and $\varepsilon_{cb,o}$ are the concrete extreme top and bottom fibre strains respectively, and h is the depth of the section.

Consider now the case where a region of unbonded tendon has modified the original strain profile (shown exaggerated in Figure 5.15). The exact value of the respective extreme top and bottom fibre strains is not known at this stage, but a first estimate can be made. Due to the new strain profile, the strain in the concrete adjacent to tendon level 2:

$$\varepsilon_{c,2} = \varepsilon_{cen} - \phi . e_2 \qquad \text{.....(5.40)}$$

where

$$\phi = \frac{\varepsilon_{ct} - \varepsilon_{cb}}{h} \qquad \text{.....(5.41)}$$

Therefore, the 'fictitious' increase in concrete strain at the level of the unbonded tendon,

$$\Delta\varepsilon_2 = \varepsilon_{co,2} - \varepsilon_{c,2} \qquad \text{.....(5.42)}$$

The total tendon elongation Δl_{ps} between the ends of the void is then obtained by integrating the 'fictitious' concrete strain increases over the unbonded length:

$$\Delta l_{ps} = \sum_{i=1}^{N} (\Delta \varepsilon_2) l_n \qquad \text{.....(5.43)}$$

The average increase in strain in the tendon over its unbonded length is then

$$\Delta \varepsilon_{ps,2} = \frac{\Delta l_{ps}}{l_{d2}} \qquad \text{.....(5.44)}$$

Once the average increase in strain $\Delta\varepsilon_{ps}$ in the unbonded tendon has been established (either by equations (5.36) or (5.43)), the total strain in the unbonded tendon $\varepsilon_{ps,2}$ can now be determined by

$$\varepsilon_{ps,2} = \varepsilon_{pe,2} + \Delta \varepsilon_{ps,2} \qquad \text{.....(5.45)}$$

where $\varepsilon_{pe,2}$ is the effective prestrain in the tendon.

From the strain values, the corresponding stress in the unbonded tendon is determined by reference to the appropriate stress-strain curve. The stresses in the bonded tendons 1 and 3 are found by the conventional strain compatibility methods. As can be seen in Figure 5.15, the strain (and stress) in the bonded tendons have changed as well due to the re-distribution among the tendon layers as the deformation changes as a result of the 'unbonded' tendon. Once all the stresses in both the bonded and unbonded tendons are obtained, the total tensile force is determined from equation (5.33).

For force equilibrium, C=T. If this criteria is not satisfied, then the first estimate of the bottom fibre strain ε_{cb}, for the new concrete strain profile due to regions of voids along the unbonded tendon (Figure 5.15) is adjusted to give a second estimate. The procedure is repeated until the total tensile force at each section is balanced with the respective compressive force within a specified tolerance.

Once force equilibrium is achieved, the section is checked for moment equilibrium. This is achieved when

$$M_r = M_a \qquad \text{.....(5.46)}$$

where M_r is the moment of resistance of the section and M_a is the applied moment. If this moment of resistance is not equal to the applied moment, then the estimate of the top fibre

strain ε_{ct} corresponding to the new concrete strain profile is adjusted and the whole procedure is repeated until the moment of resistance M_r is within some acceptable tolerance of the applied moment M_a.

5.4.2 Detection of Regions of Unbonded Tendons

The discussion so far has considered only one void within the entire length of the beam, which means that only one layer of unbonded tendon need be considered in the analysis. However, when there are a number of voids at various positions along a tendon, and at a number of tendon layers as well, the situation can be quite complicated. At a section, there may be more than one layer of 'unbonded' tendons, and since the discussion has demonstrated that the analysis of unbonded tendons is member dependent (i.e. depend on the length of the tendon being unbonded), the lengths of the voids have to be considered as well. For a particular tendon with a certain void length, there may be 'overlapping' voids from other tendon layers which extends the region of unbonded tendon behaviour (Figure 5.16a). It should be noted that the analysis is carried out from the left hand end of the beam to the right hand end of the beam, so voids present at the furthest left hand end are located first. Referring to Figure 5.16a, a void is picked up at tendon level 3 at section j. The void at this tendon layer does not overlap with that at tendon level 2 but it overlaps with the void at tendon level 1, which in turn detects that at tendon level 2. Therefore, the sections along j_s to j_e have to be analysed by the procedure for unbonded tendon behaviour.

In another possible situation (Figure 5.16b), the voids at tendon levels 1 and 3 start at the same positions but have different lengths. The void at tendon level 1 will not pick up the second void at tendon level 2 because of its shorter void length. However, the second void at tendon level 2 is picked up by the void at tendon level 3 which overlaps with it, and thus extends the region of unbonded tendons. The sections j_s to j_e should be treated as sections with unbonded tendon behaviour. Therefore, for voids starting from the same position but of different lengths, it is important for the program to determine the maximum end position of the voids.

The analysis procedure for unbonded tendons thus requires a highly iterative procedure to obtain the stress in the unbonded tendon, as the curvatures at all nodal positions along the

whole length of the void must be calculated at every iteration until a state of force and moment equilibrium is achieved. At the same time, numerical convergence must be ensured for each stage of loading.

5.4.3 Re-anchoring Length Being Affected by Regions of Unbonded Tendons

In estimating the re-anchoring length of tendons which have failed due to corrosion, the earlier discussion has assumed a linear re-anchoring model if the condition of the grout within the duct is good (i.e. good bond and hence efficient tendon re-anchorage) or an exponential re-anchoring model to represent less efficient tendon re-anchoring within poorer grout quality. However, if there are limited voids present within this re-anchoring length, then the tendon is unbonded over this ungrouted region, and this will increase the re-anchoring length of the failed tendon, resulting in a longer anchorage length needed to restore the required prestress level.

There are two main situations possible:

i. void present at a position of tendon failure
ii. limited voids present within the range of the re-anchoring length

Figure 5.17a illustrates the first situation, where a void exists at the position of tendon failure. The figure illustrates that a linear re-anchoring model is adopted but the discussion here applies to an exponential re-anchoring model as well. It was assumed that as long as the void existed, the tendon cannot start re-anchoring (as it is not bonded to the concrete) until the position at the end of the void is reached. Once the end of the void is reached, the re-anchoring length is estimated. The total re-anchoring length *rltu* is then the sum of the unbonded length from the position of tendon failure and the required re-anchoring length over the fully bonded region. The same reasoning applies to the re-anchoring length of tendons to the left of the point of failure.

The second situation where some tendon re-anchorage has already occurred before the region of void is encountered is shown in Figure 5.17b. The re-anchoring length assuming a bonded tendon is first estimated. When a region of grout void is encountered within this re-anchoring length, it is assumed that no further tendon re-anchoring is possible until the end of the void. The additional length required to restore the rest of the prestress is then

estimated. A third situation may arise which is a combination of situations (i) and (ii) where a void exists at the tendon failure location, with additional limited voids present within the re-anchoring length as well.

5.5 DATA INPUT AND OPTIONS

The developed analytical model was used to study the effect of tendon failure due to corrosion and the presence of grout voids on the flexural behaviour of typical post-tensioned simply supported beams of constant cross section. The program allows the user to input data of the beam cross-section and tendon location, material, loading, corrosion, and location of voids. A user manual and program listing for this developed model is provided by Cavell (1997).

Input of span and loading data:

The span and cross-section of the beam are required as input parameters into the program. The uniformly-distributed load due to the self-weight of the beam is then calculated by the program. Any additional uniformly distributed loading due to the superimposed dead load must also be provided.

Input of material data:

The material properties of the concrete, prestressing steel, and any non-prestressed reinforcement are also required. These are respectively the elastic modulus of the concrete E_c, the elastic modulus of the prestressing steel E_{ps}, and the elastic modulus of the non-prestressed steel E_{ns}.

The other input values required are the concrete strength at transfer f_{ci}, the characteristic strength of concrete f_{cu}, the tensile strength of concrete f_{tu}, the characteristic strength of the prestressing steel f_{pu}, and the characteristic strength of any non-prestressed steel f_y. The value of f_{ci} is required to estimate the modulus of elasticity of concrete at transfer E_{ci}, which is required for the calculation of prestress losses to the system. This is given in Part 2 of BS 8110 (1985) as:

$$E_{ci}=20+0.2f_{ci} \qquad \text{.....(5.47)}$$

If f_{ci} is unknown, then E_{ci} is taken as the value of E_c.

Additional data for the estimation of the tension stiffening effect of concrete is also required if the user chooses to consider this effect. These refer to the factors for the bond of reinforcement (α_1=*1.0, 0.7 or 0.0*) and the factor for short-term or sustained loading (α_2=*1.0 or 0.7*). Also, if an exponential re-anchoring model (instead of a linear one) is adopted for the failed tendon, then Poisson's ratio for both concrete and steel, and a friction value to represent the quality of bond between the steel and concrete, are also required.

Input of stressing operation data:

Details of the prestressing tendon type and the stressing operation of the tendons are required to estimate the total prestess losses to the system. The data required are the percentage of initial jacking force to the ultimate tensile strength of the tendon, the coefficient of friction between the tendon and the duct, the amount of slip at the anchorage to be assumed in the calculation, and the relaxation class of the wire or strand. The relaxation class refer to either Class 1 for normal relaxation, or Class 2 for low relaxation wires or strands. To estimate the frictional losses in the beam, information is required on if the tendon was stressed from one end only or from both ends of the beam. If the tendons were stressed from both ends, then maximum losses due to friction occur at midspan. If the tendons were stressed from one end only, maximum losses occur at the opposite end.

Input of beam cross-sectional details:

The number of segments that the beam is to be divided into is also required for input. The choice of the number of segments is left to the user, but a higher number will allow a more accurate location of position of tendon failure and regions of grout voids, although the computational time may be increased.

The program assumes that the beam cross-section is constant along the span. The beam cross-section is defined by a number of rectangles. For each rectangle, the y and z dimensions, and distances *yrcg* and *zrcg*, of the centroids of the rectangles from the origins of the axes, are defined (Figure 5.18).

Input of prestressing steel and non-prestressed reinforcement data:

Since the program does not consider biaxial bending effects which may arise from the horizontal eccentricity of force as the prestressing tendons fracture due to corrosion, all prestressing tendons at the same level were grouped together and located on the vertical line of symmetry of the cross-section. The same reasoning applied to the non-prestressed reinforcement as well.

The number of tendons (or tendon layers) is defined. For each tendon, the height of the tendon at midspan *(ysm)* and at the end of the span *(yse)* are input, together with the tendon cross-sectional area and the tendon jacking force. From these input data of *ysm* and *yse*, a subroutine estimates the tendon profile of each tendon layer. A parabolic profile is assumed but if *ysm* is input equal to *yse*, then a straight profile is assumed and the height of the tendon remains the same throughout its length. At each nodal section, the eccentricity of the tendon group and the eccentricity of the individual layers are calculated by the program. If there is non-prestressed reinforcement as well, then the number of non-prestressed steel layers is also input. Similarly, the height of the reinforcement and the cross-sectional area is defined for each reinforcement layer.

Input of corrosion details:

If there is corrosion, the number of tendon failure locations is input into the program. For each failed tendon, the distance of the tendon fracture from the left hand end of the beam *xcorros*, is defined. The model also requires the tendon level at which the failure occurred. The re-anchoring model to be assumed (whether linear or exponential) also needs to be input for each tendon failure occurrence. The respective data for the corrosion cases is read from an input file. For each corrosion location, the length *xcorros* is rounded off to the nearest nodal section where calculations will be performed.

Input of details of voids:

If there are regions of ungrouted tendons due to the presence of grout voids within the tendon duct, the number of voids is first input into a data file. For each void location, the distance of the left end of the void from the left hand end of the beam is defined as are the tendon level at which the void exists and the length of the void. For each void, both the length of the void and the location of the void are rounded off to the nearest nodal section.

Option with/without tension stiffening effect:

By default the model includes for the effect of tension stiffening to account for the tensile stresses in the concrete between cracks in the beam. This gives an estimate of average curvature for any given moment. If the user does not want to include the effects of tension stiffening, then zero values can be input for the parameters α_1 and α_2 necessary for calculation of the tension stiffening effect.

5.6 COMPUTATION OF RESULTS

The overall operation of the analytical model can basically be divided into three stages:

5.6.1 The Basic Calculations

When the program is executed, the required data are read from a number of data files. The program first calculates the section properties of the beam which then allows the uniformly distributed load due to the beam self weight, and the permanent load bending moment (due to self weight and superimposed dead load), to be calculated. From given values of the tendon positions at midspan and the endspan, the eccentricity of the tendons at each nodal section is found by assuming either a parabolic or a straight tendon profile and, subsequently, the prestress losses to the system are estimated. The effective prestress of the tendons at each nodal section is then known.

Calculation of section properties

The section properties of the beam are calculated using the input data of the beam cross-section geometry which had been defined as consisting of a number, *nrect,* of individual rectangles. For each rectangle, the *y(i)* and *z(i)* dimensions parallel to the y- and z-axis respectively (Figure 5.18) were also defined, together with their respective distances *zrcg(i)* and *yrcg(i)* of the centroid of each rectangle from the origins of the axes.

Calculation of total area:

The area of each rectangle, $A(i) = y(i).z(i)$

The gross cross-sectional area of the beam,

$$A_g = \sum_{i=1}^{nrecf} A(i) = \sum_{i=1}^{nrecf} y(i).z(i) \qquad \text{.....(5.48)}$$

Calculation of the centroid of the section:

Distance of centroid from z-reference axis, $\bar{y} = \dfrac{\sum_{i=1}^{nrecf} A(i).yrcg(i)}{A_g}$ .....(5.49a)

Distance of centroid from y-reference axis, $\bar{z} = \dfrac{\sum_{i=1}^{nrecf} A(i).zrcg(i)}{A_g}$ .....(5.49b)

Calculation of second moment of area about the centroidal axis:

Referring to Figure 5.18, $hy(i) = yrcg(i) - \bar{y}$

and $hz(i) = zrcg(i) - \bar{z}$

By the parallel axis theorem,

$$I_{zz} = \sum_{i=1}^{nrecf} z(i).y(i)^3/12 + \sum_{i=1}^{nrecf} A(i).hy(i)^2$$

$$I_{zz} = \sum_{i=1}^{nrecf} A(i).y(i)^2/12 + \sum_{i=1}^{nrecf} A(i).hy(i)^2 \qquad \text{.....(5.50a)}$$

$$I_{yy} = \sum_{i=1}^{nrecf} y(i).z(i)^3/12 + \sum_{i=1}^{nrecf} A(i).hz(i)^2$$

$$I_{yy} = \sum_{i=1}^{nrecf} A(i).z(i)^2/12 + \sum_{i=1}^{nrecf} A(i).hz(i)^2 \qquad \text{.....(5.50b)}$$

Since $I_{yz}=0$ about the centroidal axis of a rectangle, $I_{yz} = \sum_{i=1}^{nrecf} A(i).hy(i).hz(i)$

The values of $\bar{z}$, I_{yy} and I_{yz} are actually not required since the program only performs analysis in the uniaxial direction. However, these were included in the program for completeness and to enable it to be developed in the future to calculate unsymmetrical bending stresses.

5.6.2 Pre-cracking Analysis

The analysis commences with the permanent load, and the program first calculates the case where there is no loss of tendon area, nor regions of unbonded tendons in the beam for which it is assumed that all tendons are perfectly bonded to the concrete. This is the control situation which forms the reference base against which other analyses are compared.

The program then reads the additional data referring to tendon failure due to corrosion. Along the segments affected by tendon failures (i.e. segments where the failed tendon is still re-anchoring), the affected nodal sections will be flagged. This flag indicates the nodal sections containing corroded tendons, and where the appropriate subroutines are required to perform a sectional analysis to calculate the tendon stress re-distribution as a result of tendon failure. At all other locations where there is no corrosion, the normal sectional analysis of a bonded post-tensioned beam is performed. If there are regions of ungrouted tendons, the program also reads the location and length of the voids within the ducts. As with the segments affected by tendon failure, the program sets a flag (but with a different value to that used for corrosion flag) on the nodal sections containing regions of unbonded tendons (voids). The appropriate subroutine is then called to handle the analysis of unbonded tendons.

Where a tendon has failed due to corrosion, the re-anchoring length and distribution of residual prestress is first estimated based on a bonded tendon. Where a void is known to be present within this length, the effect of the void in increasing the re-anchoring length is considered. From this, the residual prestress levels in the tendons are estimated. Determination of the tendon stresses due to the combined effects of tendon failure and regions of ungrouted tendons (voids), require a number of iterations and reference to the respective subroutine to analyse each case separately. Once this is resolved, the load is incrementally increased, and the loads to cause decompression in the concrete and cracking in the concrete are noted. At each stage of loading, the applied bending moment, the stresses and strains in the concrete and in the prestressing steel and the decompression and cracking moments are calculated.

5.6.3 Post-cracking Analysis

In an uncracked section, the whole concrete section is assumed to provide the concrete compressive force. When the section has cracked, a nonlinear analysis is required to determine the amount of useful concrete remaining, and this is carried out by solving for the neutral axis position, whilst ensuring force and moment equilibrium. In bonded sections, this is relatively straight-forward although a number of iterations are required to obtain the neutral axis position and the corresponding top fibre strain in the concrete for each stage of loading. For bonded sections containing one or more unbonded tendons due to the presence of grout voids, a further level of iteration is required to obtain a solution. At each iteration, the analysis must be carried out at every nodal section affected by the unbonded tendon(s) behaviour whilst ensuring force and moment equilibrium. This may involve analysis of both uncracked and cracked sections. It is only when all affected nodal sections have been analysed that the stress in the unbonded part of the tendon can be determined (since the stress in unbonded tendons is member dependent). If either the force or moment equilibrium is not achieved, the entire process is repeated again.

The analysis of an uncracked section has already been discussed earlier. It remains to describe the procedure for a cracked section analysis.

Formulation of beam behaviour for post-cracking analysis

Assuming that plane sections remain plane after bending and that perfect bond exists between the steel and concrete, the strains in the concrete ε_c and in the prestressing steel ε_{ps} and non-prestressed steel ε_s can be evaluated. For a given top fibre strain in the concrete ε_{ct} let the neutral axis be a distance x from the top surface of the beam (Figure 5.19).The strain distribution in the section is assumed to remain linear even up to failure.

At a distance y from the top surface of the beam, the strain in the concrete is given by

$$\varepsilon_c = (x - y).\phi \qquad \text{.....(5.51)}$$

where the curvature $\phi = \frac{\varepsilon_{ct}}{x}$.

The strain in the prestressing steel is given by

$$\varepsilon^{i}_{ps} = (d^{i}_{ps} - x).\phi + \varepsilon^{i}_{ps,dec} \qquad \text{.....(5.52)}$$

The strain in the non-prestressed steel is given by

$$\varepsilon_s^i = (d_{ns}^i - x).\phi \qquad \text{.....(5.53)}$$

where d_{ps}^i and d_{ns}^i are respectively the depths of the prestressing steel and non-prestressed steel respectively, and 'i' represents a steel layer designation. A steel layer is defined as a group of bars or tendons with the same stress-strain properties, the same effective prestress, and is assumed to have a combined area with a single centroid. The strain in the prestressing steel layer i at concrete decompression is denoted $\varepsilon_{ps,dec}^i$.

The total compressive force C in the concrete is given by

$$C = \int_{A_c} f_c dA_c \qquad \text{.....(5.54)}$$

where f_c is the stress in the concrete corresponding to ε_c, and A_c is the area of the concrete.

As the reinforcing bars and prestressing tendons consist of a number of discrete elements, the total tensile force in the steel T is obtained by summation of the individual forces in the prestressing steel and in the normal reinforcement.

$$T = \sum_{i=1}^{n} T_{ps}^i + \sum_{i=1}^{ns} T_{ns}^i \qquad \text{.....(5.55)}$$

$$T_{ps}^i = f_{ps}^i . A_{ps}^i \quad \text{and} \quad T_{ns}^i = f_s^i . A_{ns}^i$$

where n is the number of prestressing steel tendon groups, ns is the number of non-prestressed steel bars, A_{ps} and A_{ns} are respectively the cross-sectional area of the prestressing steel and the non-prestressed steel, and f_{ps} and f_s respectively refer to the stress in the prestressing tendon and non-prestressed reinforcement.

Layer-by-layer evaluation of section forces and moments

It remains to evaluate the integrals involving the stresses in the concrete. The integration involved is often complicated by the irregularity of the section's geometry and the nonlinearity of the stress-strain relationship of the material. One simple procedure for evaluating the integrals is to idealize the cross-section as a series of rectangular layers, and to assume that the strain in each layer is uniform and equal to the actual strain at the centre of the layer (Figure 5.19). If the strain is uniform over the layer, the concrete stress will also be uniform over the layer. The force in each layer can then be found by multiplying

the stress in the layer by the area of the layer, while the moment contribution can be found by multiplying the layer force by the distance between the middle of the layer and the reference axis.

In the analytical model, the value of the integral for the concrete was approximated by this layer-by-layer evaluation of section forces. The cross-section is first idealized by a number of rectangles initially defined when its geometry was input. The manner in which the layer-by-layer procedure was used to evaluate the sectional forces corresponding to a given strain distribution is illustrated in Figure 5.19. The total compressive force in the concrete is determined by evaluating the forces in each layer of concrete. In performing the numerical integration, the program further subdivides each rectangular layer into thinner layers. At each iteration, the thickness of the layer is halved (i.e. number of rectangular layers is doubled) and the total compressive force is evaluated. The number of rectangular layers required depends on the level of accuracy to be achieved. Obviously, the discretization will become more accurate but will require more computational effort for greater numbers of layers. In the program, the iteration is repeated until the calculated value is within 0.01% of that calculated by the previous iteration.

The strain ε_c^i in the concrete at the middle of each concrete layer is given by

$$\varepsilon_c^i = (x - y^i).\phi \qquad \text{.....(5.56)}$$

The strains, stresses and forces are then evaluated at the middle of each rectangular layer. The contribution of useful concrete which provides the total compressive force C is obtained by summing the forces in each rectangular layer. For *i=1,nrect'* where *nrect'* is the number of uncracked concrete rectangular layers,

$$C = \sum_{i=1}^{nrect'} C^i = \sum_{i=1}^{nrect'} f_c^i . A^i \qquad \text{.....(5.57)}$$

where the force acting on each layer C^i is obtained from the stress f_c^i and the cross-sectional area A^i for each rectangular layer.

For a given value of top fibre strain in the concrete ε_{ct}, the location of the neutral axis x is solved by the bisection method (Press et al, 1992). In this numerical solution technique, the limits for x are first set, where the lower limit at the top surface of the beam $x_l=0$, and the upper limit at the bottom surface $x_u=h$. The value of x is estimated from the current round of iteration by $x=(x_l+x_u)/2$. The forces C and T are evaluated from equations 5.54 and 5.55 respectively. If $|C-T| \leq \delta$ where δ is an acceptable error, then the current value of x is accepted. If C<T, then set $x_l=x$, which leads to larger values of x and C in the next round of iteration. If C>T, then set $x_u=x$, which leads to smaller values of x and C in the next round of iteration. In either case, the interval between the upper and lower limits is reduced by half after each iteration. This is a characteristic of the bisection method.

For a calculated value of x, the corresponding moment of resistance M_r is determined by

$$M_r = \int_{A_c} f_c.(x-y)dA_c + \sum_{i=1}^{n} T_{ps}^i.(d_{ps}^i - x) + \sum_{i=1}^{ns} T_{ns}^i(d_{ns}^i - x) \quad \text{.....(5.58)}$$

Iterative procedure:

The nonlinear analysis method adopted requires an iterative numerical solution because of the interrelation of the unknown parameters. The objective is to determine the moment of resistance M_r and neutral axis location x corresponding to a given curvature ϕ. The developed iterative procedure for a cracked section analysis can generally be summarised as:

1. Assume a top fibre strain in the concrete, ε_{ct}
2. Assume a neutral axis depth, x
3. Substitute x into the compatibility equation to obtain the strain in the concrete and the strain in each steel layer in the section
4. Determine the concrete and steel stresses from the relevant stress-strain curves
5. Calculate the net compressive *(C)* and tensile *(T)* forces at the section and check for force equilibrium *(C=T)*. If these are not equal to within reasonable accuracy, repeat steps 2-5.
6. Determine the moment of resistance M_r. If the moment of resistance is not equal to the applied bending moment (within a specified tolerance), then repeat steps 1-6.

Determination of the full M-ϕ relationship thus requires a large number of calculations. In addition, there is a need to determine some special points on the M-ϕ curve at which, for example, decompression of the concrete or cracking of the concrete occurs. The ultimate condition is reached when either the concrete crushes in compression, or the steel yields or fails before failure of the concrete.

5.7 COMPARISON OF ANALYTICAL MODEL WITH FIELD TESTS RESULTS

The results from two of the field tests on the Botley beams (discussed in Chapter 3) were used to validate the developed analytical model. The two particular tests referred to are:

Beam 31 - Coring of the middle Tendon C at north quarter point

Beam 1 - Coring of the lower Tendon D at north quarter point

The analysis was carried out under the action of dead load alone, in order to be consistent with the field conditions of the beams. The tendons were simulated on the vertical axis of symmetry as shown in Figure 4.11.

In Beam 31, Tendon C was severed at the north quarter point. If the surrounding grout is sound, immediate tendon re-anchoring on either side of the cut point is expected. The re-anchoring length of the failed tendon was estimated to be 728mm by the linear re-anchoring model adopted (equation 5.25b).

The field test had revealed that the duct containing this Tendon C in Beam 31 was moderately well grouted. The volume of void varied from 4.18 litres at the north end, to 2.48 litres at the south end (volume of completely empty duct is 34 litres). Although the Belmec test has indicated that the north end contained more voids, it cannot determine the location and length of the voids, as is required for input into the developed model. Nonetheless, an estimate can be made from knowledge of the likelihood of void locations.

In the analysis here, a length of void was modelled around the tendon failure position. As mentioned earlier, where a grout void has been simulated, the tendon is assumed to be unbonded over the void length. Therefore, if the tendon fails in a position where a void

exists, it is assumed that tendon re-anchoring will not occur until the end of the void is reached. As can be seen in Figure 5.20a, the effect of modelling Tendon C as a single tendon which failed where a void existed resulted in the stepped strain distribution when the duct changes from an ungrouted condition, to a grouted one. The tendon only started to re-anchor at the ends of the void.

In practice, the duct will probably be partially grouted, and some partial re-anchoring will occur. An attempt was made to model a partially grouted tendon by representing Tendon C as 4 smaller tendons, all situated at the same level. The length of void surrounding each individual tendon was different, such that a staggered distribution of strain at the soffit of the beam was obtained (Figure 5.20b). At each void level, tendon re-anchoring occur at the ends of the void. It can be seen that the results are improved as compared to using a single tendon. This profile of stepped distribution can be smoothed out by using a greater number of tendons to represent the failed tendon. This approach however is unsatisfactory as it is dependent on the user input of the length of void, which resulted in such a strain distribution.

Results of the Botley beams show that the failed tendon required a relatively longer re-anchoring length than that predicted by the linear re-anchoring model. Since the strain measurements were obtained at specific distances from the tendon failure position, the exact re-anchoring profile cannot be accurately determined. However, they seem to exhibit an exponential relationship, with a relatively quick gain of prestress followed by a decaying pattern. It was considered that this slow decay of strain increase was due to partial re-anchoring of the tendon within a partially grouted duct. A totally ungrouted length of duct would not have allowed tendon re-anchoring within the unbonded length. Some tendon re-anchoring is however possible in a partially grouted duct although a longer length is required to achieve the full prestress. The void which occupy a greater length of partially grouted duct (compared to the same volume of void within an ungrouted duct) can be modelled as a smeared void.

The exponential re-anchoring model (Section 5.3.2) which had been incorporated into the analytical model to estimate the distribution of residual prestress of a failed tendon in a partially grouted duct was adopted to investigate the failure of Tendon C in Beam 31. The

coefficients of friction considered for this exponential re-anchoring model were ϕ=0.1, ϕ=0.2 and ϕ=0.35. It was found that ϕ=0.1 approximated the re-anchoring profile of Tendon C best, as shown in Figure 5.21.

The analysis was carried out with the beam divided into 20, 40, 80 and 160 segments in order to determine the accuracy of solution provided in each case. The time taken to complete the analysis (up to ultimate condition) was also monitored. It was aimed to choose an appropriate number of segments which will enable a time-efficient analysis to be undertaken without compromising the accuracy of results. The analysis time taken and results obtained for each case is as shown below:

Number of segments	Time (minutes)	Ultimate moment (kNm)	Midspan curvature (10^{-6} rad/mm)	Midspan deflection (mm)
20	2	1247.1	10.38	310.0
40	4	1247.1	10.37	305.8
80	7	1247.8	10.09	302.2
160	14	1247.8	10.09	302.2

It was found that sufficient accuracy was obtained with 80 segments and this number of segments was adopted in the parametric study described in the next chapter.

Figure 5.22 illustrates the strain profile on cutting Tendon D in Beam 1. In this case, a coefficient of friction of 0.2 was found to estimate the residual prestress distribution better.

5.8 CONCLUSIONS

- In this chapter, the development of an analytical model to assess the residual strength of deteriorating post-tensioned concrete bridges has been described. The damage mechanisms considered are those due to failure of prestressing tendons due to corrosion, and the presence of voids within the grouted ducts.

- The non-linear model was based on the strain compatibility method, but modified to incorporate unbonded tendon behaviour due to regions of incomplete grouting in the ducts.

- The phenomenon of tendon re-anchoring of failed tendons was also incorporated into the model to estimate the distribution of residual prestress after tendon failure. Both linear and exponential expressions to describe the re-anchoring behaviour have been considered. This then enabled the re-distribution of tendon stresses within a tendon group as a result of tendon failure at a section to be evaluated.

- The influence of the presence of limited voids within the grouted ducts, on the re-anchoring ability of failed tendons was considered. This include the presence of a complete void at the position of tendon failure, and of secondary importance, the presence of limited grout voids within the re-anchoring length of the failed tendon.

- The exponential re-anchoring model was found suitable to estimate the re-anchoring profile of a failed tendon within a partially grouted duct, as exhibited by the field tests.

Source of prestress loss	Stage of occurrence
Elastic shortening	At jacking
Friction	At jacking
Anchorage draw-in	At transfer
Concrete shrinkage	After transfer
Concrete creep	After transfer
Relaxation of tendons	After transfer

Table 5.1 Main sources of prestress loss in post-tensioned concrete, and stage at which they occur

Code/equation by	Transfer length L_t
BS 8110	539 mm
ACI 318-89	478 mm
Zia & Mostafa	446 mm
Hoyer	388 mm

Table 5.2 Transfer lengths estimated for a typical 7-wire strand

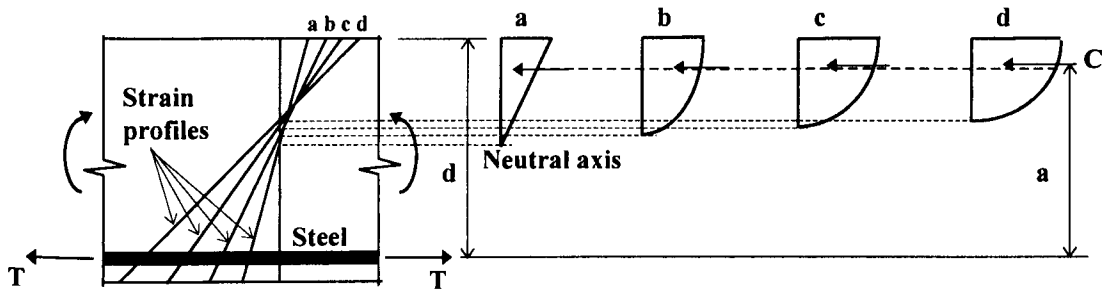

(a) strain profiles

(b) compression stress distributions in concrete corresponding to strain profiles a, b, c, and d

Figure 5.1 Strain and stress distributions in the concrete for increasing levels of bending moment up to failure (Park and Paulay, 1975)

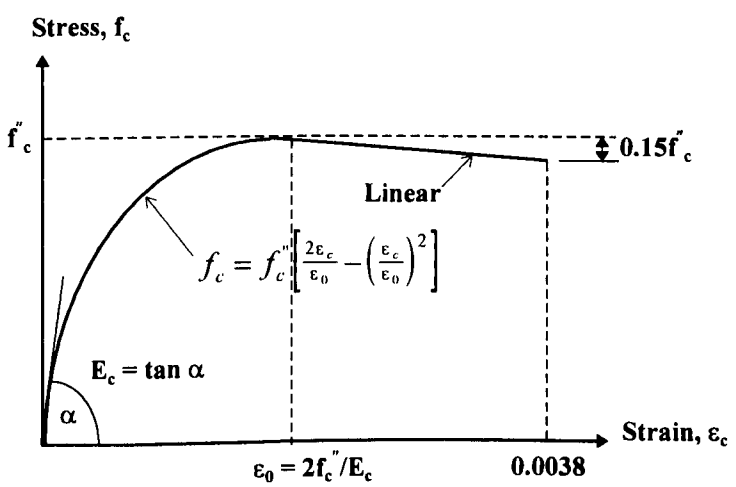

Figure 5.2 Hognestad's idealized stress-strain curve for concrete in uniaxial compression (Park and Paulay, 1975)

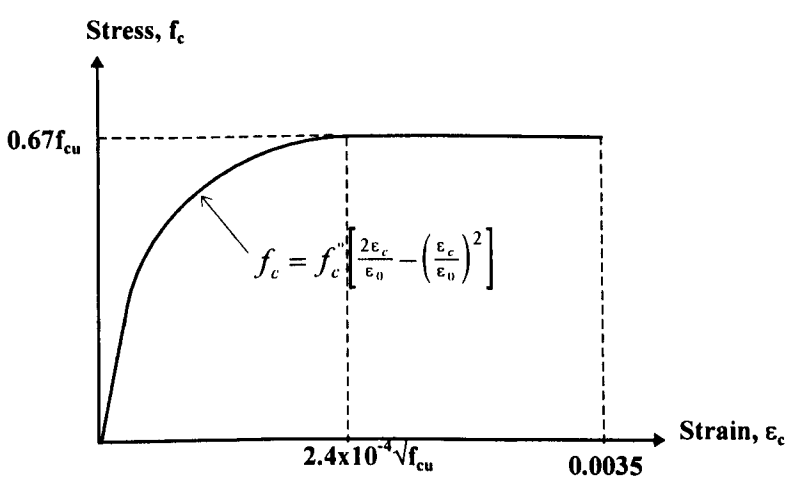

Figure 5.3 Stress-strain curve for concrete which was adopted in the model

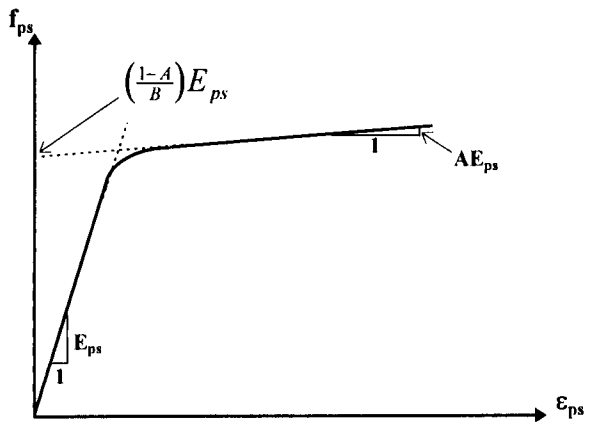

Figure 5.4 Modified Ramberg-Osgood function for prestressing steel (Collins and Mitchell, 1991)

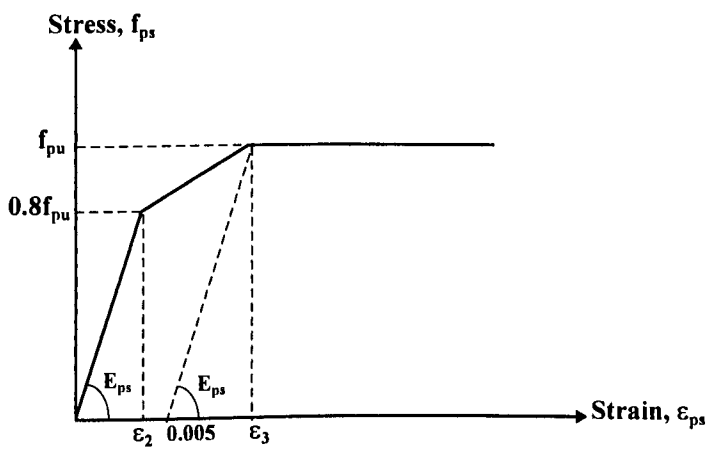

Figure 5.5 Stress-strain curve for prestressing steel (BS 8110, 1985)

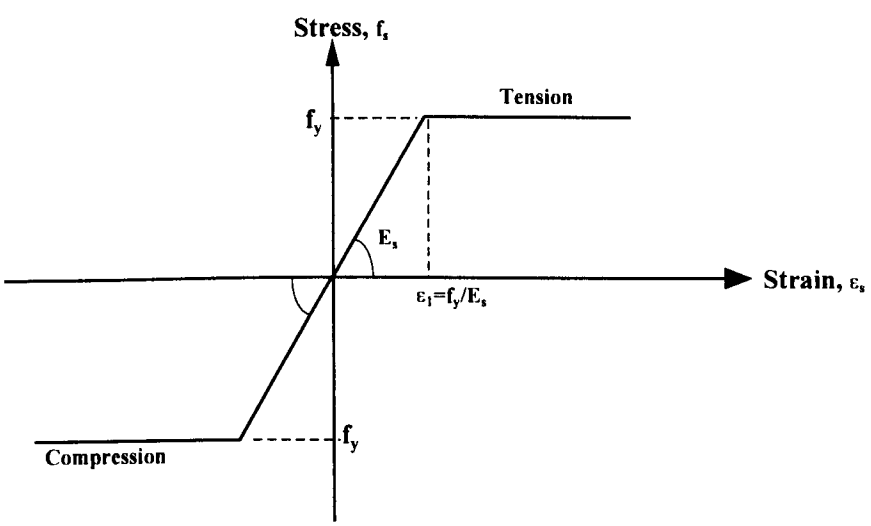

Figure 5.6 Stress-strain curve for nonprestressed reinforcement (BS 8110, 1985)

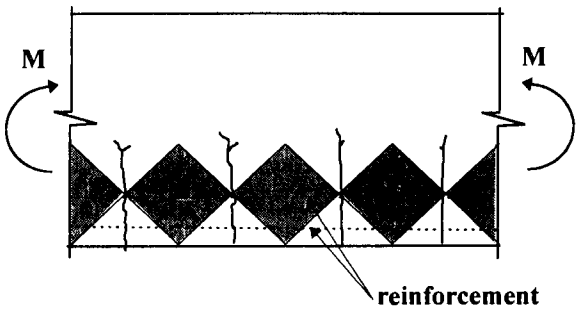

Figure 5.7 Tensile stress in cracked concrete

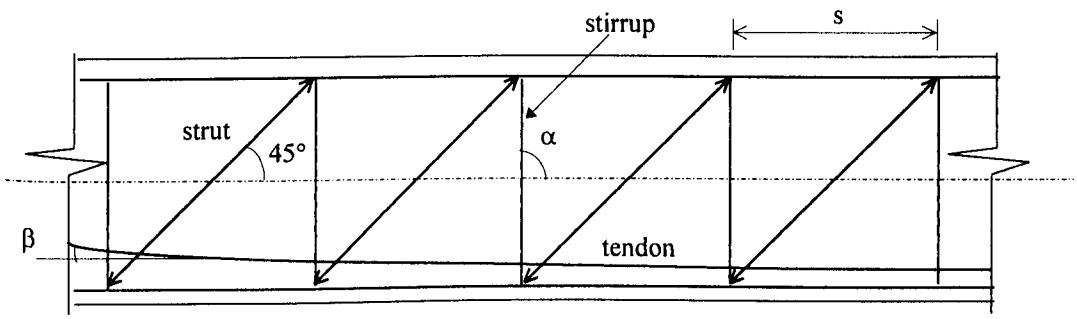

Figure 5.8 The truss analogy

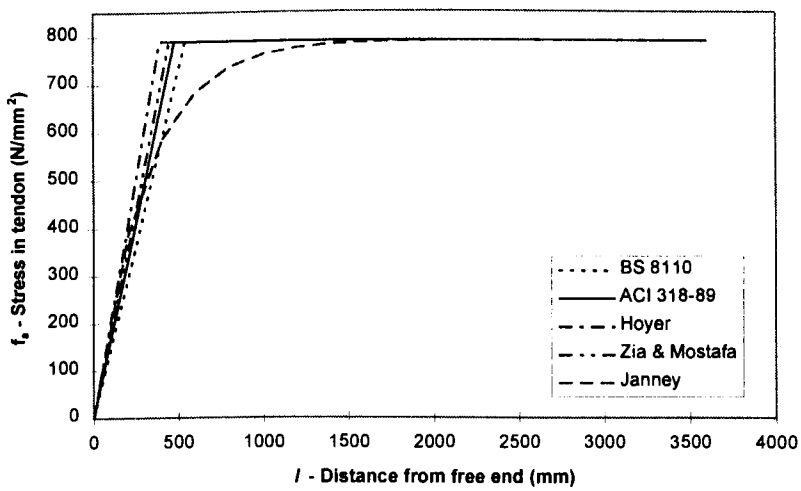

Figure 5.9 Estimation of distribution of residual prestress

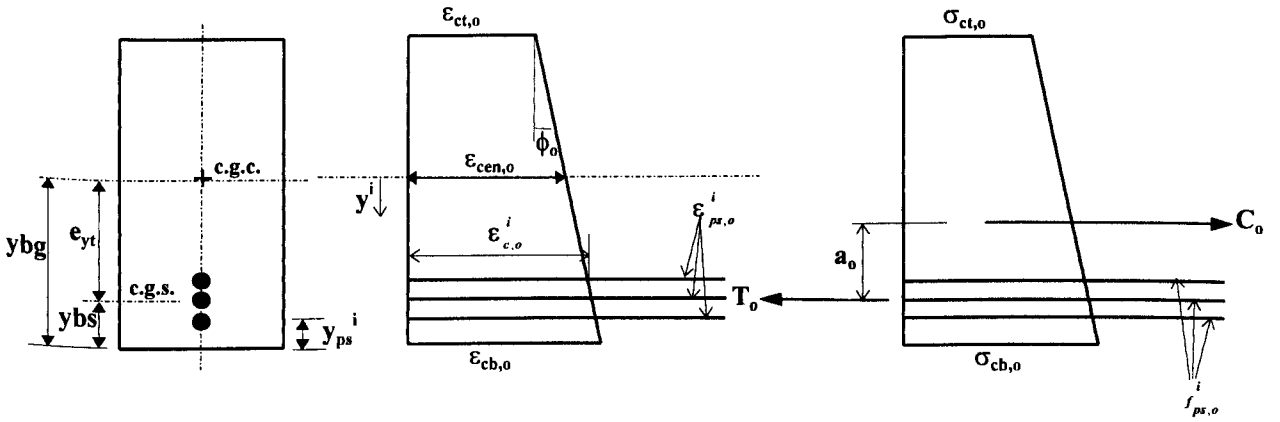

(a) Cross-section (b) Strain (c) Stress

Figure 5.10 Strain and stress distribution in a typical section before loss of tendon area

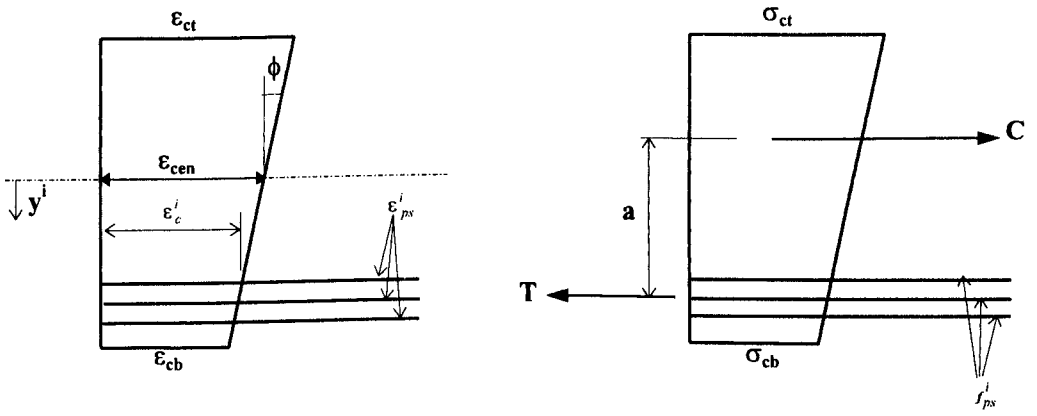

(a) Strain (b) Stress

Figure 5.11 Strain and stress distribution in a typical section after the loss of tendon area

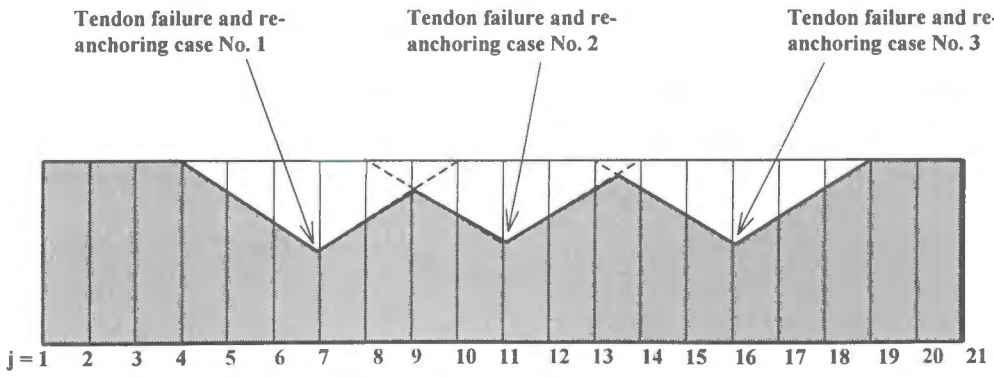

Figure 5.12 Distribution of residual prestress along beam after corrosion at a number of locations

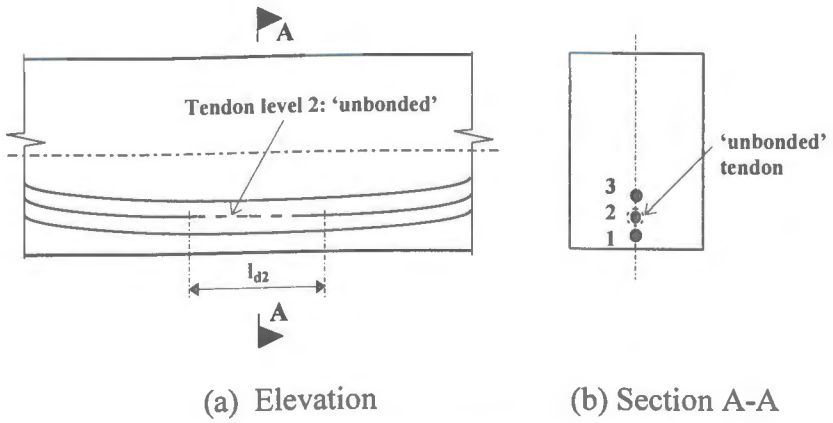

Figure 5.13 Length of beam showing tendon level 2 unbonded over length l_{d2}

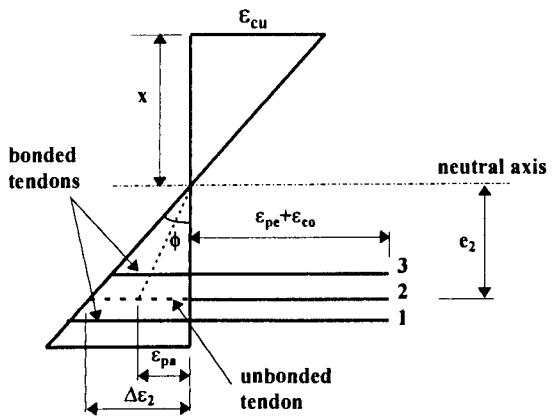

Figure 5.14 Typical strain distribution at ultimate due to middle tendon being unbonded

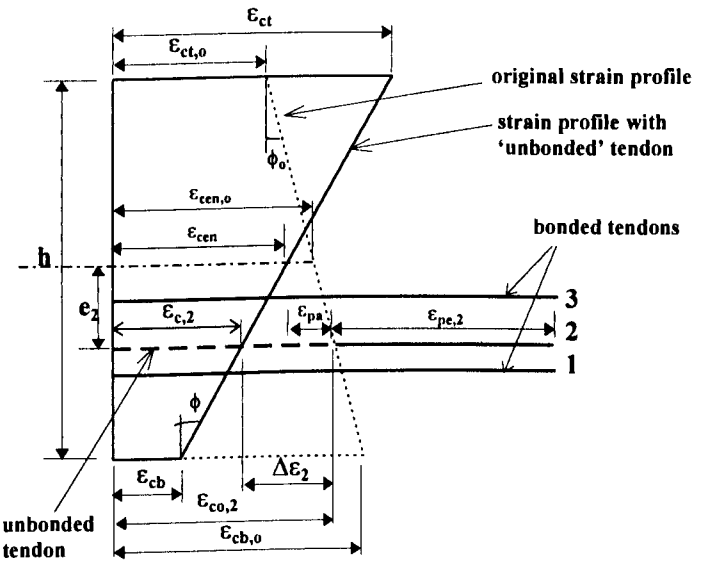

Figure 5.15 Typical change of strain distribution (before decompression of concrete) due to the middle tendon being unbonded

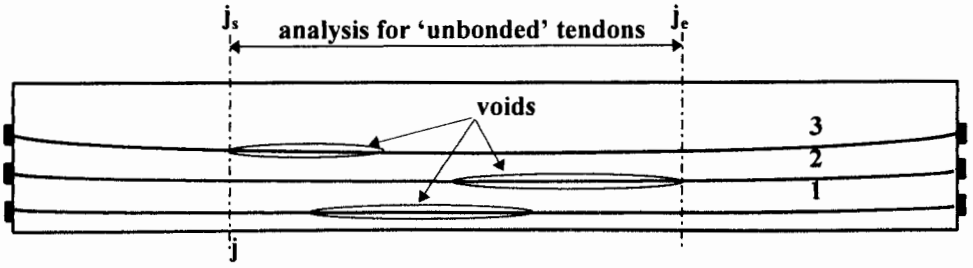

(a) 'Overlapping' voids extending the region of unbonded tendon behaviour

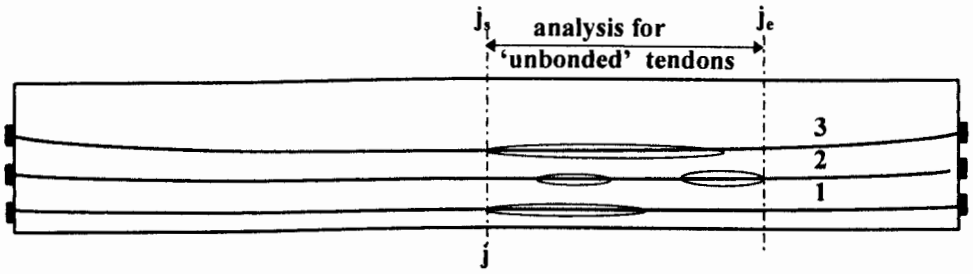

(b) Detecting a second void in the same tendon layer

Figure 5.16 Idealization of regions of unbonded tendons (voids)

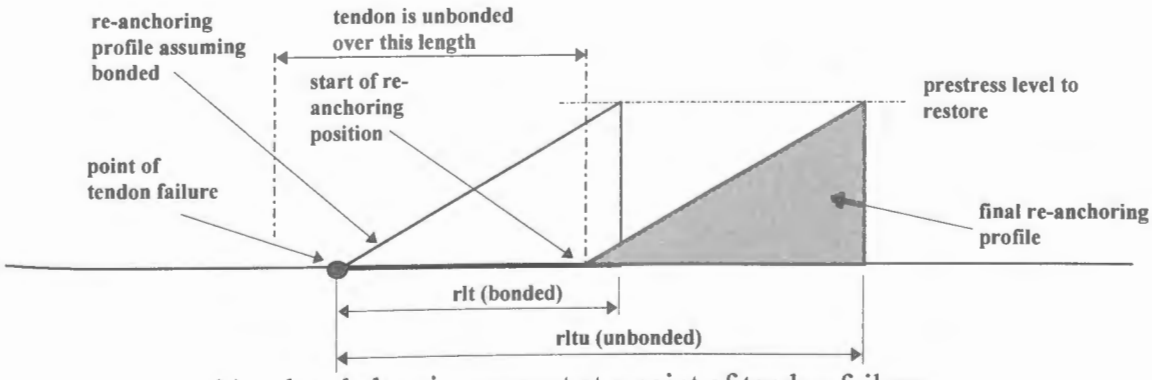

(a) unbonded region present at a point of tendon failure

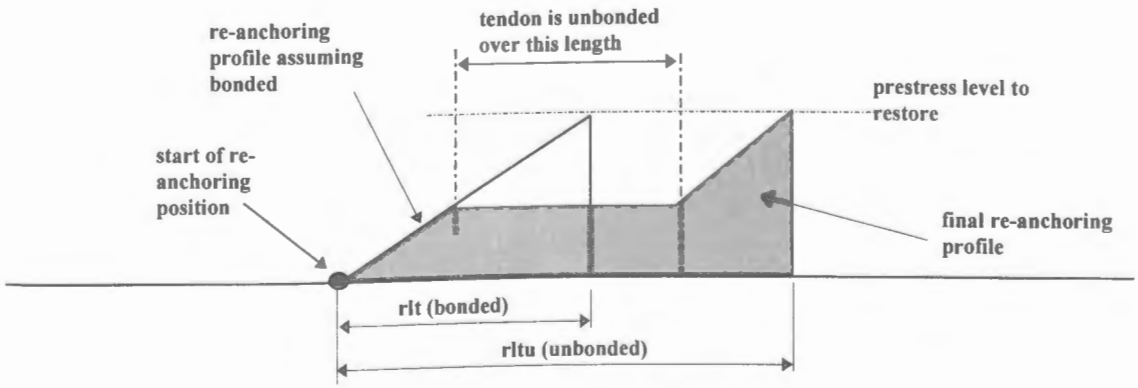

(b) unbonded region within range of re-anchoring length

Figure 5.17 Re-anchoring length being affected by regions of 'unbonded' tendons

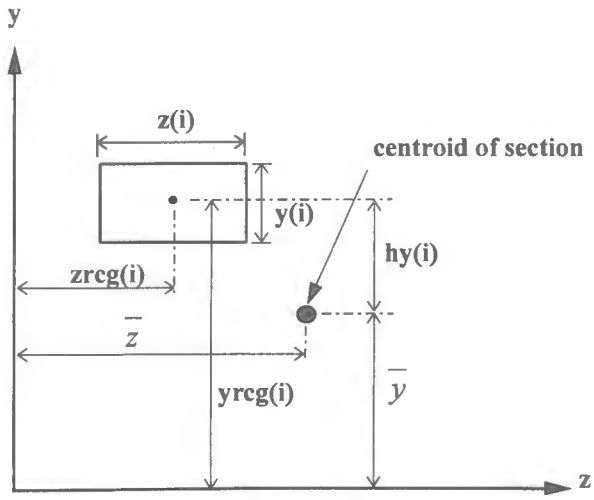

Figure 5.18 Input of rectangles defining beam cross-section

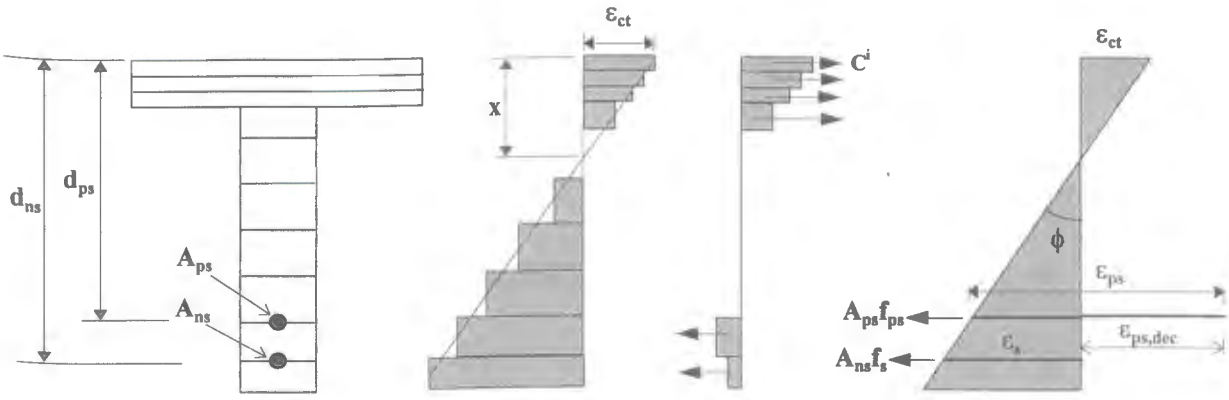

Figure 5.19 Determining sectional forces using layer-by-layer evaluation

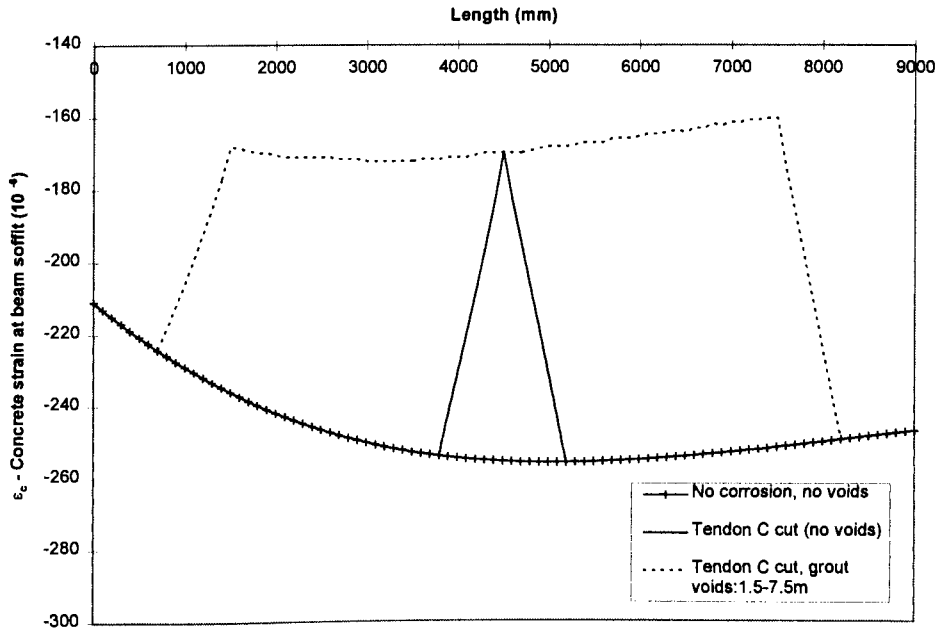

(a) Tendon C modelled as 1 single tendon

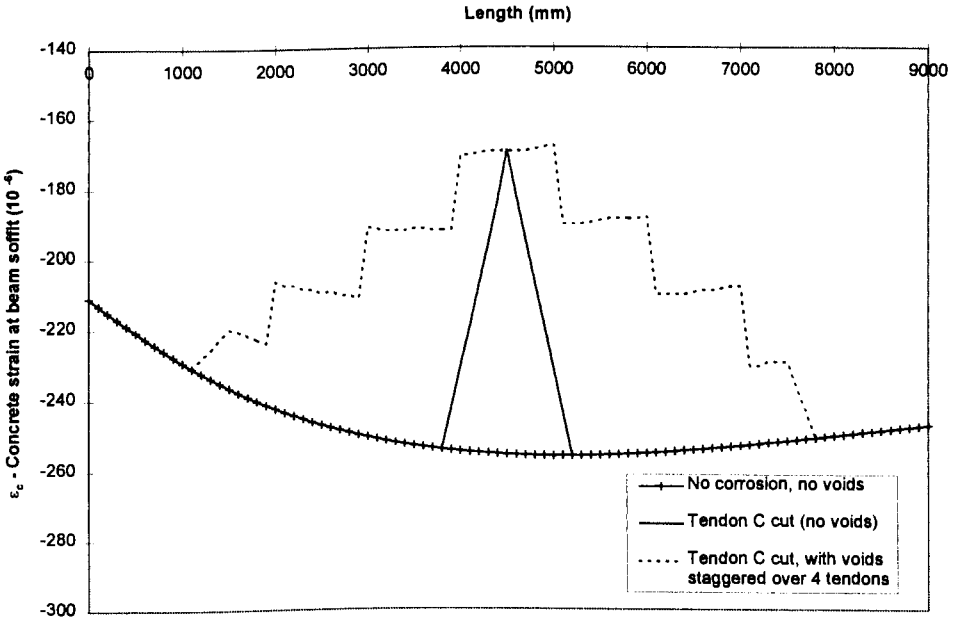

(b) Tendon C modelled as 4 tendons

Figure 5.20 Concrete strain increase along Beam 31 as a result of Tendon C cored at north quarter point (linear re-anchoring model)

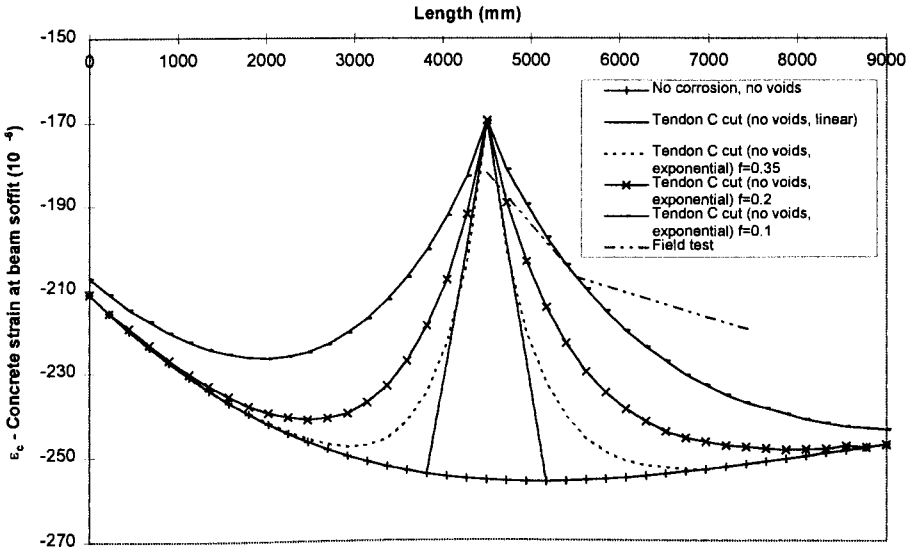

Figure 5.21 Beam 31, Tendon C cut: Strain increase obtained by assumed exponential distribution over the re-anchoring length

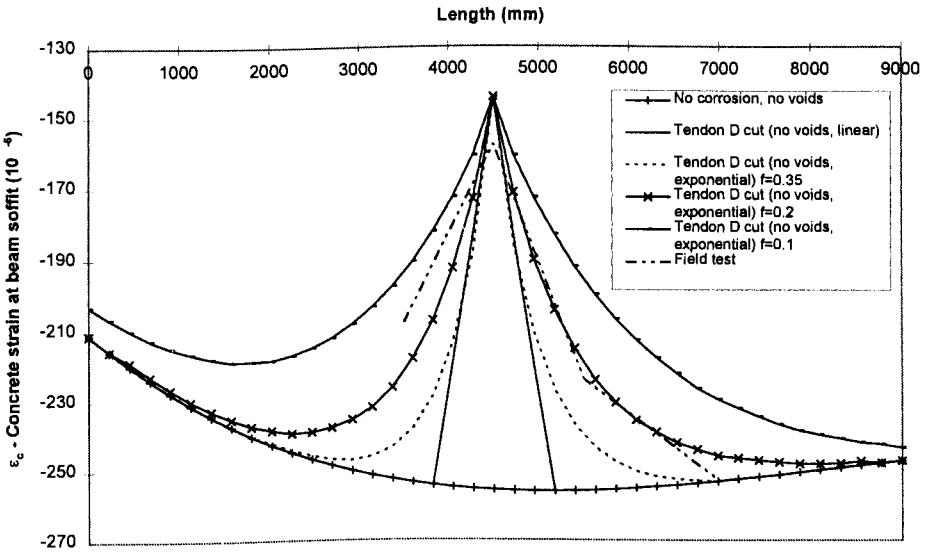

Figure 5.22 Beam 1, Tendon D cut: Strain increase obtained by assumed exponential distribution over the re-anchoring length

CHAPTER 6

Parametric Study of Factors affecting the Residual Strength of Deteriorating Post-tensioned Beams

6.1 INTRODUCTION

The development of an analytical model to assess the residual strength of deteriorating post-tensioned concrete bridge beams was described in Chapter 5. In this chapter, the results of a parametric study utilising the developed non-linear analytical model are presented and discussed. The mechanisms of deterioration addressed are those due to failure of the prestressing tendons as a result of corrosion, and the presence of grout voids within the ducts. The aim is to identify the factors affecting the residual strength of such deteriorating beams, and to provide a quantitative assessment of the residual structural capacity of such beams whilst accounting for the level of damage that has been discovered.

The model which had been validated against available field test results of the Botley beams (described in Chapter 3) is used here to study the effect of tendon failure and regions of ungrouted tendons on the residual structural capacity of typical bridge beams incorporating a variety of typical defects.

6.2 DESCRIPTION OF THE CONTROL BEAM

A single simply-supported beam representing a typical beam from the Botley Flyover was modelled. Although a rectangular cross-section was adopted for this analysis, the program had been written for general application. Figure 6.1 shows the idealised cross-sectional details at midspan of the modelled beam. The twelve 7 mm wires within each of the five ducts in each beam were modelled as a single tendon of equivalent cross-sectional area,

and tendons at the same level were grouped together and located on the vertical axis of symmetry. This eliminates any biaxial bending effects resulting from horizontal eccentricity of force as the prestressing tendons fracture.

Tendon fracture due to corrosion, and regions of grout voids, were modelled in the beam (Figure 6.2). Some typical deterioration cases considered in this chapter are presented in Table 6.1. This was based on the various defects reported to date following the mandatory inspection of the entire stock of post-tensioned concrete bridges in the UK. The early results of this investigation were reported by the author (Cavell and Waldron, 1996, 1997). The material properties adopted for the beam are given in Table 6.2. The analyses commenced with the beam's permanent load. This load was then incrementally increased until failure. The control beam represents the idealised situation of perfect bond in the absence of corrosion or regions of incomplete grouting. For this beam, the moments required to cause decompression and first cracking in the concrete were calculated to be 492 kNm and 631 kNm respectively. Failure occurred at midspan at an ultimate moment of 1242 kNm; the values of the curvature and deflection at this stage are shown in Table 6.3 and the corresponding tendon stresses are recorded in Table 6.4.

The original design calculations allowed for live loads consisting of HA uniformly distributed load of 10.5kN/m^2 and a knife edge load of 39.4kN/m. Together with the dead load of the beam and the superimposed dead load, this gave a design bending moment at service of 601 kNm and a design ultimate moment of 941 kNm. Therefore, if the beam is to serve as a Class 1 member (no tensile stresses permitted) according to the current bridge design code of BS 5400 (1990), the decompression moment of the beam needs to be at least 601 kNm so that the minimum stress in the extreme bottom fibre of the concrete under service loads is zero. However, even for the control beam with no damage simulated, the predicted decompression moment was only 492kNm. The beam thus did not meet the serviceability criteria as a Class 1 member. This is shown in Table 6.5 for the decompression moment normalised against the design bending moment at service.

In Class 2 members, tensile stresses are allowed provided they do not exceed the design flexural tensile strength of concrete (given by $0.36\sqrt{f_{cu}}$ in BS 5400). In the analytical model, the cracking moment was calculated from the tensile strength of concrete with a

partial safety factor $\gamma_m=1$. Hence, for the control beam, the value of 1.05 for the cracking moment normalised against the design bending moment (Table 6.5) is actually more generous than that limited by the serviceability criteria as a Class 2 member. All further discussion of the beam at serviceability limit state thus refer to the cracking limit rather than the Class 2 limit.

The results of the other investigations are discussed in the proceeding sections. Basically, this analytical study consisted of three parts, principally aimed at investigating:

- the effect of tendon failure within a well-grouted duct (i.e. no voids)
- the effect of tendon failure and presence of limited voids within the grout
- the effect of unbonded tendons alone due to the presence of grout voids (i.e. no corrosion).

6.3 EFFECT OF TENDON FAILURE WITHIN A WELL-GROUTED DUCT

For most deterioration cases in post-tensioned concrete beams containing integral grouted tendons, tendon failure due to corrosion will normally co-exist with regions of incomplete grouting within the duct. It is known that the presence of grout voids in a duct increases the likelihood of tendon corrosion. This is because when chlorides, moisture and oxygen are able to leak into the duct through the anchorages or construction joints, the voids then act as a route for the passage of the contaminants along the 'exposed' ungrouted tendon. However, in some cases (e.g. segmental bridges), tendon corrosion has been known to occur even in a relatively well-grouted duct. In such circumstances, it is expected that the failed tendon will be able to re-anchor quickly in the presence of a sufficient region of surrounding grout.

Figure 6.3 shows the moment-curvature response at midspan of the modelled beam when failure of the central Tendon C was respectively simulated at different locations along the beam. As this analysis represents tendon failure within a well-grouted duct, no grout voids have been modelled along the beam. It can be seen that neither failure of the tendon at the quarter point position (case P2a) or at the anchorage end (case P2c), resulted in any reduction in flexural capacity. In both cases, collapse occurred at midspan at a strength of

1242 kNm, which is comparable to that of the control beam. This is because the failed tendon had re-anchored quickly within a relatively short distance of 675mm, and thus did not compromise the strength of the beam. When the tendon failed at midspan instead (case P2b), collapse occurred at a reduced strength of 1127 kNm. In this case, tendon failure corresponding to an overall 20% loss of tendon area at midspan resulted in a strength reduction of 9.3% over the control beam. The remaining factor of safety provided by the residual structural capacity of this beam compared to the design ultimate moment is 1.20, as shown in Table 6.5. However, the decompression and cracking moments had reduced to 395 kNm and 531 kNm respectively. The normalised cracking moment was thus reduced to 0.88 as a result of failure of Tendon C at midspan (Table 6.5). In all three simulations considered, failure of Tendon C did not result in shear resistance deficiency, even at the anchorage where shear forces are maximum. This is shown in Table 6.5 for the shear capacity normalised against the ultimate shear force at the support position.

Figure 6.4 shows the moment-deflection response due to failure of Tendon C at the various positions investigated. It can be seen that failure of the tendon even at the critical midspan section, did not reveal any significant increase in deflection. This behaviour supports the suggestion by previous investigators (Woodward and Wilson, 1991; Lindsell et al, 1993) that local failure of grouted prestressing tendons is not necessarily accompanied by readily measurable deflections, thus the lack of visible warning signs of distress in such beams.

The above analysis had been carried out assuming a linear distribution of residual prestress when the failed tendon re-anchors. It was found that adopting an exponential re-anchoring model with a relatively high friction coefficient (ϕ=0.35) to represent good bond between the tendon and surrounding grout within the duct, did not result in any significant difference in the residual strength although a relatively longer re-anchoring length of 2475mm was required with this latter model. It must be stressed that although the length taken for the failed tendon to fully re-anchor is much longer than that assuming a linear distribution, the re-anchorage of the failed tendon is relatively quick initially, followed by a decaying tendon re-anchorage for the rest of the length. This was discussed in the previous chapter, and is illustrated in Figure 6.5 where P2b1 represents failure of Tendon C at midspan, assuming an exponential re-anchoring model. It can be seen from Table 6.3 that for the analysis with both linear (P2a, P2b and P2c) and exponential re-anchoring

models (P2a1, P2b1 and P2c1) for failure of Tendon C at the three positions considered, the residual strength does not appear to be sensitive to the re-anchoring model adopted. The rest of the discussion will therefore refer to a linear re-anchoring model unless otherwise stated.

Figure 6.6 shows a similar trend of moment-curvature response if one of the bottom tendons (Tendon D) were to fail. The corresponding moment-deflection diagram is shown in Figure 6.7, which again illustrates the lack of signs of distress even up to the ultimate condition. However, failure of this tendon at midspan (case P3b) resulted in a slightly greater reduction in flexural strength compared to failure of Tendon C at midspan (case P2b) because of the greater lever arm of Tendon D. In this case, failure of tendon D at midspan corresponding to a 20% loss of overall tendon area, resulted in a reduced ultimate capacity of 1093 kNm, which represents a 12% reduction in strength compared to the control beam. When this loss in tendon area occurred away from the critical midspan section, the reduction in ultimate capacity was further reduced. This is demonstrated by the loss of tendon D at the quarter point position (case P3a) where failure occurred at an ultimate moment of 1234 kNm (i.e. 0.7% strength reduction compared to control beam) when the limiting compressive strain of concrete was reached first at the quarter point position. When this tendon failed at the anchorage position instead (case P3c), the flexural strength of the beam was not compromised, neither was the shear capacity at that section found to be deficient compared to the maximum applied shear force (Figure 6.8). Table 6.5 shows that for case P3b, the normalised cracking moment reduced to 0.86 as a result of a reduced cracking moment of 515kNm.

It was also found that neither failure of Tendon C nor Tendon D at midspan resulted in decompression or cracking of the concrete under permanent load alone. This is due to the high level of pre-compression initially present in the beam, and the relatively low permanent load under which the analysis commenced. Decompression without any additional loading was only achieved if both the bottom tendons (Tendons D+E) failed at midspan, as analysed in case P4a. The beam failed at a much lower moment of 893 kNm, representing a 28% reduction in strength over the control beam. Table 6.5 shows that the factor of safety provided by the residual capacity had reduced to 0.95. The flexural strength is significantly reduced in this case, but only after the beam had accommodated a

40% loss of overall tendon area. The cracking moment had reduced to 399 kNm, and this corresponded to a normalised cracking moment of only 0.66 (Table 6.5). The increased curvature at midspan compared to that for the failure of Tendon C or Tendon D alone is shown in Figure 6.9.

Figure 6.10 demonstrates that the deformation of the beam is not significantly affected by tendon loss of area until collapse is imminent. Even when both the bottom tendons failed (case P4a), corresponding to an overall 40% loss of tendon area, the deflection profile hardly departs from the control situation. The only significant change in behaviour is that the beam failed at a much lower ultimate moment. At this stage, the stress in the remaining tendons had already reached values of 1349 N/mm^2 and 1313 N/mm^2. This respectively represents 86% and 84% of the ultimate tensile strength (UTS) of the tendon.

The literature has indicated that the anchorage area is very vulnerable to corrosion especially if it has not been properly sealed against the ingress of surface water which may contain chlorides and other contaminants. Very localised corrosion resulting in a high proportion of loss of tendon area and consequently tendon failure is possible in this region. This is investigated in case P4b where the two bottom tendons failed at 1.0m from the anchorage end. In addition, the nominal shear reinforcement present in the Botley beam was ignored. It can be seen that although the flexural strength of the beam was not compromised (Figures 6.11, 6.12), the combined shear resistance provided by the residual prestressing force and the concrete alone is marginally insufficient to resist the high shear force near the anchorage end (Figure 6.13). In this case, premature shear failure would occur without the addition of a moderate amount of traditional shear reinforcement.

The record drawings of the Botley beams indicate that nominal mild steel reinforcement in the form of 3/8" stirrups at 18" (450mm) centres had been provided throughout the beam. This amount of shear reinforcement is actually less than the current minimum shear reinforcement requirement of BS 5400 (1990). Nonetheless, when the resistance provided by this nominal shear reinforcement was considered together with that provided by the residual prestressing force and the concrete (case P4c), the total shear resistance was found to be sufficient to resist the shear force existing near the anchorage end. This is illustrated in Figure 6.13.

6.4 EFFECT OF TENDON FAILURE AND PRESENCE OF LIMITED VOIDS WITHIN THE GROUT

Currently, it still remains difficult to locate the presence and extent of voids precisely using currently available inspection techniques. In the field tests on the Botley beams, voids were identified by drilling into the ends of the ducts, and pressure testing by the Belmec method to obtain the void volume. By drilling additional holes at intermediate locations, the continuity of voids can also be determined. This technique does not actually locate the voids as is required for input in this analysis, but, from knowledge gained of the likelihood of void locations, a good estimate can be made. The conditions most likely to occur in practice were then used to carry out a sensitivity analysis. Moreover, in the near future, it is expected that the more promising NDT methods like the CANDI ultrasonic scanning system (Duncan et al, 1995) and the impact-echo method (Jaeger et al, 1997) will be sufficiently developed to detect grout voids within a duct with greater reliability and accuracy.

6.4.1 Effect of Void Length

Results emerging from bridge inspections indicate that widespread voids tend to exist at positions near the anchorages (Darby, 1996; Keiller and Nandlal, 1996). It is also in this vicinity that corrosion of a tendon is most likely to occur. Case P5a considers the failure of Tendon C at the anchorage position, with the presence of a long concentrated void extending from the anchorage to midspan. It was found that the shear resistance had not been reduced to levels such that it was insufficient to resist the shear force at the anchorage ends (Table 6.5). When failure of the two bottom tendons at the anchorage was simulated instead in case P5b, it was expected that the shear resistance would be deficient at the anchorage. However, this was found not to be so, due to the fact that failure occurred at midspan at a much reduced ultimate moment of 892 kNm (28% reduction in strength compared to the control beam). At this lower load, the shear force at the anchorage was not sufficiently large as to exceed the shear resistance provided. This is illustrated in Figure 6.14.

Figure 6.15 illustrates the increased curvature and significantly lower flexural capacity associated with case P5b. Although tendon failure did not occur at the critical midspan

section in both cases P5a and P5b, the presence of the long length of void did not allow the failed tendon to re-anchor, thereby the capacity at midspan was compromised, as if tendon failure occurred at midspan itself. As a result of reduced cracking moment of 531 kNm and 399 kNm for case P5a and P5b respectively, the normalised cracking moment was also reduced in both cases (Table 6.5). Case P5b also failed to provide sufficient factor of safety against collapse as a result of the reduced flexural capacity.

Figure 6.16 shows rather interesting moment-deflection results for both cases P5a and P5b. As a result of increased debonding (i.e. loss of prestress force) of the failed tendon(s) over the length of void, the deflection was found to increase appreciably. The void can be seen to distribute the effect of tendon failure over a longer distance, thus resulting in larger deflection than those produced due to tendon failure within a well-grouted duct (Figures 6.4, 6.10, 6.12). It can hence be deduced that tendon failure will not result in significant increase in deflection unless it loses its prestress force over an appreciable distance.

The stress in the remaining tendons was found to increase significantly along regions containing the failed tendon (Figures 6.17 and 6.18), compared to regions where the tendon had re-anchored. This is more significant in case P5b where the concrete had already decompressed as a result of failure of the two bottom tendons. Although the beam failed at midspan at a much lower ultimate moment when the limiting compressive strain of concrete was reached, the stress levels in the remaining tendons in regions containing the failed tendons were critically high, reaching a maximum of 1347 N/mm^2 (86% UTS) and 1311 N/mm^2 (84% UTS) for tendons at levels 2 and 3 respectively (Figure 6.18). As a comparison, Figure 6.19 illustrates the tendon stress distribution due to failure of Tendon C at midspan within a well-grouted duct (case P2b). It can be seen that, as a result of the efficient bond provided by the sound grout, the failed tendon re-anchored quickly and the maximum stress in the remaining tendons was localised instead of being spread over almost a quarter span of the beam as in case P5a. Nevertheless, the magnitude of maximum tendon stress in the critical tendon, is similar in both cases (1296 N/mm^2 for case P2b and 1295 N/mm^2 for case P5a).

Cases P6a, P6b and P6c represent the failure of Tendon C at the quarter point position, with the presence of limited voids in the grout. The length of the void around the tendon

failure position was varied in each case, as illustrated in Table 6.1. This sensitivity analysis revealed that for case P6a with the shortest void, the strength of the beam was not compromised. Failure occurred at midspan at an ultimate moment of 1242 kNm, similar to that of the control beam (Figure 6.20). The longer void in case P6b resulted in a reduction in strength of 7% as failure occurred at the section at the right hand end of the void (but not at midspan). For a void which extends past the midspan of the beam, as analysed in P6c, failure occurred at midspan instead at a lower ultimate moment of 1127 kNm, representing a 9.3% reduction in strength. In this case, the longer re-anchoring length which was required by the failed tendon, resulted in the flexural strength being compromised. As a result of the presence of voids at the tendon failure position, thereby loss of prestress force over the void length, the moment-deflection diagram (Figure 6.21) shows that even for case P6a (where flexural strength was not compromised), the deflection profile departed from the control situation. In the cases considered here, the deterioration was more easily detected by referring to the moment-deflection diagram rather than the moment-curvature diagram. Table 6.5 shows the reduced normalised cracking moment for both cases P6b and P6c.

Figure 6.22 illustrates the tendon stress variation along the beam as a result of failure of Tendon C within the short length of void (case P6a). It can be seen in Figure 6.22b that, where a void has been modelled, the tendon is assumed to be totally unbonded within that void length and does not re-anchor until sound grouting conditions are re-established. The slight increase in tendon stress in the remaining tendons at levels 1 and 3 is a result of the redistribution of stress within the tendon group over the length of the void. This relatively small increase in stress in the remaining tendons does not really compensate for the prestressing force which was lost in the failed tendon, hence the overall loss of tendon force as a result of tendon failure is almost proportionate to the amount of loss of tendon area. This was also shown to be the case in the finite element work discussed in Chapter 4.

A similar distribution of tendon stress was also obtained for the other two cases P6b and P6c having longer void lengths. Figure 6.23 shows the tendon stress distribution for all three cases at the first post-cracking load step. At this stage, the stresses in the remaining tendons at the sections containing the failed tendon are not much higher than at those where the tendon has re-anchored on the right hand side. However, at the ultimate

condition (Figure 6.24), the stress in the remaining tendons has increased significantly along the regions containing the failed tendon, and the maximum tendon stress is not necessarily at the critical midspan section. The shift in the section containing the maximum tendon stress, with the length of the void, is also demonstrated in Figure 6.24. The values of the maximum stresses in the tendons are given in Table 6.4.

From this study, it can be inferred that the distribution of voids along the beam is an important factor when considering the re-anchoring of failed tendons. This will also affect the distribution of residual prestress which can be assumed after failure of a tendon.

6.4.2 Effect of Partially Ungrouted Ducts

In the investigation of 34 post-tensioned concrete bridges which had been in service for about 25-30 years, voids of up to 5 litres were reported near the anchorages (Keiller and Nandlal, 1996). For a typical post-tensioning system, this volume of void normally occupies a length of 2.5m to 3.5m of completely ungrouted duct. For example, for the Botley beams, the cross sectional area of each duct (diameter 50mm) is $\pi(50)^2/4=1964mm^2$. For an incompletely grouted duct along the 18m span of the beam and allowing for the tendon cross-sectional area ($462mm^2$), the void volume is (1964-462)x18000=27litres. Therefore for a 5 litre void, this occupies a length of 3.3m of completely ungrouted duct. However, visual evidence suggest that the voids occupy a much greater length of partially grouted duct with the tendons partially exposed above the level of the grout. Thus, when a tendon fails, there would be some loss of effectiveness of the tendon due to incomplete re-anchorage of the tendon in the grout. Some tendon re-anchoring is however possible in a partially grouted duct although a longer length is required to achieve the full prestress.

The voids considered so far in the analysis have been concerned with a totally ungrouted length of duct which would not have enabled tendon re-anchoring within the unbonded length. It is now aimed to compare this with the re-anchoring of failed tendons within a partially grouted duct. This is first demonstrated by failure of Tendon C at the anchorage within a 3.5m length of void. Cases P5c, P5c2, P5c3 simulate the re-anchoring of this tendon with different re-anchoring models adopted: linear for case P5c to signify efficient re-anchoring, and exponential re-anchoring for cases P5c2 and P5c3 with friction

coefficients ϕ=0.2 and ϕ=0.1 respectively to represent less efficient re-anchoring. This is compared with case P5d and P5d2 where no voids have been modelled but friction coefficients of 0.1 and 0.2 were used respectively in the exponential re-anchoring model to simulate generally poorer bond in a partially grouted duct. In these latter two cases, immediate (but partial) re-anchoring of the failed tendon is expected since there is no 'total' void present but rather a smeared region of partially ungrouted tendon.

Figure 6.25 illustrates the tendon stress distribution along the beam at the ultimate condition for cases P5c, P5c2 and P5c3. No significant difference in the stress distributions was apparent, except that the failed tendon in the beam with poorer grout (P5c2 and P5c3) showed a more gradual gain of prestress compared to that with the linear re-anchoring model. In all cases, failure occurred at an ultimate moment comparable to that of the control beam. A similar pattern was obtained in cases P5d and P5d2 when no void was modelled at the anchorage, but only poorer grout was simulated. Comparing Figures 6.25 and 6.26, the presence of the void at the anchorage has merely disallowed tendon re-anchoring to occur until sound grout is encountered. However, similar re-anchoring behaviour is exhibited in both figures. Although the stress distribution at the ultimate condition was slightly different, this did not affect the flexural strength of the beam for the simulations considered here. This study has demonstrated that failure of a tendon even within a short length of void, followed by more gradual re-anchoring of the tendon due to poorer quality grout may still not be detrimental to the flexural strength of the beam. As discussed in Chapter 5, the CEB-FIP (1978) model based on the truss analogy was found suitable to determine the shear strength of beams containing unbonded tendons, and was also used for beams with partially filled ducts. Table 6.5 shows that for the deterioration cases considered here, the shear capacity at the support was still sufficient. Table 6.5 also shows that the cracking limit was not exceeded in all the cases considered here.

Case P10a and P10b investigated the effect of failure of the two bottom tendons at the anchorage with no voids modelled (as opposed to P5b) but instead, lower friction values ϕ=0.2 and ϕ=0.1 were used to represent partial re-anchoring of the failed tendon. As shown in Figure 6.27, the strength of the beam was not compromised although much longer re-anchoring lengths of 4050mm and 8100mm were required in cases P10a and

P10b respectively before the full prestress was restored. Figure 6.28 shows only marginal increase in deflection since some re-anchoring occurred immediately after tendon failure (ie. no extensive debonding as in case P5b). However, this study has revealed rather interesting results. Compared to case P5b which had a concentrated void modelled over half the length of the duct, the failed tendon could not re-anchor until past the midspan position. As a result, the flexural strength was compromised and collapse occurred at a much reduced moment of 892 kNm, whereas when partial grout was considered here, the flexural strength of the beam was not reduced (1242 kNm). However, as a result of the higher ultimate load achieved in cases P10a and P10b, hence higher shear force at ultimate, the shear resistance at the anchorage was found to be deficient even when nominal links were included (Figure 6.29). Hence, premature shear failure predominated the failure mode. Figure 6.30 illustrates a fairly uniform stress distribution along the beam, and the gradual restoration of residual prestress in the failed tendon. This is compared with Figure 6.18 where the stress had increased almost close to its breaking strength (86% UTS) whilst the load was still relatively low.

The failure of Tendon C at the quarter point position within a partially grouted duct was investigated in cases P9a and P9b with ϕ=0.2 and ϕ=0.1 respectively. Figures 6.31 and 6.32 show that the strength was not dissimilar to that of case P6a where tendon failure with the presence of limited voids was considered. The tendon stress distribution along the beam for case P9a (Figure 6.33) illustrates the difference in distribution when compared with P6a (Figure 6.22). Figures 6.34 and 6.35 respectively show the tendon stress distribution for cases P9a and P9b at the first post-cracking load step and at the ultimate condition. Compared to P6a (Figures 6.23 and 6.24), the stresses in the remaining tendons in cases P9a and P9b are slightly lower where a void is present in P6a. This is because the failed tendon has started to re-anchor immediately and thereby contributed to the overall stress system, hence resulting in lower stresses in the other tendons. Although a relatively gradual increase in prestress occurred over a length of 4050mm in P9a and 8100mm in P9b, the final result was the same in terms of residual strength. In fact, the presence of a concentrated void is more critical if it extends for a long distance and does not then allow tendon re-anchoring to occur. This was demonstrated in cases P6b and P6c. Table 6.5 shows that in both cases P9a and P9b, the cracking limit was unaffected.

6.4.3 Presence of Limited Voids After a Failed Tendon Has Started to Re-anchor

Figures 6.36 to 6.39 illustrate the secondary effect of the presence of limited grout voids within the re-anchoring length of a failed tendon after the tendon has started to re-anchor. In this case, some increase in prestress had already occurred before the tendon encountered a void. It is assumed that no further increase in prestress is possible until the end of the void length as shown in Figure 6.38 for failure of Tendon C at the quarter point position. Due to a short length of void present within the re-anchoring length, a small increase in deflection is apparent in Figure 6.37 compared to the control beam. The void length was kept the same in all three cases, but the difference is the re-anchoring model adopted to simulate various grout conditions surrounding the failed tendon. Case P6d modelled linear re-anchoring of the tendon within relatively good bond. This is compared with cases P6e and P6f which model exponential tendon re-anchoring with ϕ=0.35 and ϕ=0.2 respectively. Figure 6.36 shows that the re-anchoring model used does not significantly affect the residual strength obtained. The main difference is that, with the poorest bond modelled (case P6f), the restoration of prestress is more gradual hence, when the void is reached, the residual stress in the failed tendon is less than that for cases P6d and P6e (Figure 6.38). However, the final tendon stress distributions (Figure 6.39) are not significantly dissimilar from one another. In case P6f, collapse occurred at an ultimate moment of 1210 kNm, which is only 2.6% lower than for the control beam. However, Table 6.5 shows that the normalised cracking moment was reduced to a value of 0.98 in this case.

This study demonstrates that the presence of limited voids after a failed tendon has started to re-anchor is not as critical as the presence of voids within a region of tendon failure. The main concern is the condition of the grout and whether it is sufficient in quality and integrity as to allow some partial re-anchoring to occur.

6.5 EFFECT OF UNBONDED TENDONS DUE TO PRESENCE OF VOIDS

6.5.1 Totally Ungrouted Tendon

Inspection of the Botley beams revealed that one had a totally ungrouted duct. This situation was simulated in case P7a for the central Tendon C, with the remaining four

tendons assumed to be fully grouted. Failure occurred at an ultimate moment of 1234 kNm. The stress in the tendons at the ultimate condition is shown in Table 6.4. Although the stress in the central unbonded tendon (901 N/mm^2) was appreciably different from that of the fully grouted control beam (1143 N/mm^2), the reduction in overall strength was marginal (0.8%). This is illustrated in Figure 6.40. It also shows that the performance at service is not dissimilar from that of the fully grouted beam. However, as conditions approach ultimate, the small loss in strength is apparent. This is also shown in the moment-deflection diagram (Figure 6.41) which indicates that a totally unbonded tendon alone (no tendon failure) will not reveal significant increase in deflection. This analysis required a relatively long run time (about 4.5 hours on a normal PC) since the stress in the unbonded tendon is member-dependent and the curvatures at all nodal positions along the whole length of the beam had to be calculated at every iteration until a state of force and moment equilibrium was achieved. Table 6.6 shows the time taken for this analysis compared to that taken for the other deterioration cases. It also shows that where a void has been simulated, the run time was increased, depending on the void length. Where no void was simulated, the time taken for analysis of the beam with grouted (or partially grouted) tendons was relatively short.

If the tendon within this totally ungrouted duct were to fail at any point due to corrosion, as was analysed in case P7b, this would result in a strength reduction of 9.3% over the control beam. This is due to the loss of prestress force over the entire unbonded length as the failed tendon is not able to re-anchor. As a result of debonding and loss of prestress force over such an extensive length, an increase in deflection to indicate signs of distress is apparent even from an early stage (Figure 6.41). Figure 6.42 shows the resulting concrete strain increase which can be expected along the soffit of the beam as a result of failure of the central Tendon C within a totally ungrouted duct (compressive strains are negative). This shows a greater strain increase at the critical midspan section, which reduces away from the midspan section. As a result of failure of this tendon, the cracking moment had reduced to 531 kNm.

This analysis has shown that voids alone within a duct may not pose a great risk to the integrity of the beam, and should not be of immediate concern if the conditions within it are dry. The presence of grout voids however, will reduce the capacity of the beam to

accommodate further deterioration, as exemplified in case P7b where the strength of the beam was compromised when prestress was ineffective over the whole length of ungrouted duct. However, it is only when corrosion is allowed to occur (through the ingress of water and chlorides) in this area that the strength of the beam may be significantly affected.

6.5.2 Ungrouted Tendons Alone at Anchorages

It is reported that for simply-supported beams, voids in the grout are most likely to exist near the anchorages (Darby, 1996; Keiller and Nandlal, 1996). This is usually the result of improper grouting practice on site when the air vents are prematurely shut off before ensuring that the duct is completely filled with grout or due to the movement of entrapped air to the high points at the ends of the ducts. The integrity of the anchorages are normally of secondary concern if the ducts are fully grouted, since, in the event of failure of the anchorage or the tendon itself at the anchorage, this would lead to re-anchorage of the tendon in the available grout. The main concern arises when there is incomplete grouting of the ducts at the vulnerable anchorage area, thus not enabling a failed tendon to re-anchor in this region.

Case P8a considers the most undesirable situation where voids exist near the anchorages at both ends of the beam for all the five tendons. The aim was to investigate if the presence of grout voids alone at the anchorages, with no tendon fractures, is detrimental to the capacity of the beam. In this case, since a relatively long length of void (4.5m at each end) was modelled at each tendon level, the compressive strain of concrete was approached first at the ends of the void nearer to the midspan, which precipitated an earlier collapse moment of 1117 kNm (10.1% reduction in strength) as shown in Figures 6.43 and 6.44. However, the shear capacity at the anchorages was found to be sufficient, as shown in Table 6.5.

6.6 CONCLUSIONS

Based on the analytical results presented in this chapter, the following conclusions can be made:

- The consequences of tendon failure on the performance of the structure at service and at ultimate were studied with reference to the re-distribution of tendon stresses within a

tendon group. The study revealed that, when a tendon fails as a result of corrosion, the stress in the remaining tendons is slightly enhanced, which compensates for some of the prestress force which was lost in the failed tendon. Moment equilibrium is restored by a re-distribution of the concrete stress block and an increase in the lever arm and curvature. The total loss of prestressing force in the beam is almost proportional to the loss of tendon area.

- The amount of prestressing force lost due to loss of tendon area, governs the load at which the behaviour of the beam first becomes non-linear. It was found that significant levels of deterioration do not always compromise ultimate strength to the same degree. In the cases presented here, tendon failure corresponding to an overall 20% loss of tendon area in the section, resulted in a loss of flexural strength of 9.3% and 12% depending on the level at which tendon failure occurred, as lower tendons have a greater lever arm. For a 40% overall loss of tendon area, a reduction in strength of 28% resulted. Where this loss occurs away from the critical midspan section, the reduction in ultimate capacity is further reduced.

- In the numerical model developed, the effect of incomplete grouting on the stress in the tendons was investigated using the theory for internal unbonded beams. It was found that although the presence of grout voids alone (no tendon failure) may not significantly affect the strength of the structure, the presence of voids will however, reduce the capacity of the beam to accommodate further deterioration. For instance, failure of a tendon in a grouted duct will result in a local reduction in the prestressing force which may be insignificant if it occurs at non-critical sections, whereas a similar defect in an ungrouted duct will cause a loss of prestress over the whole length of the tendon.

- The presence of voids within the re-anchoring length of failed tendons does not significantly affect the deformation behaviour of the beam, but may influence the section at which failure occurs. However, the presence of voids at or near a position of tendon fracture will affect the ability of a failed tendon to re-anchor fully. This may have a profound effect on the residual strength of the beam, particularly when a duct contains long or continuous voids. The distribution of grout voids along the beam is thus an important factor when considering loss of strength.

- The deflection of a beam is not significantly affected by local failure of grouted prestressing tendons until collapse is imminent. Thus monitoring of deflection may not reveal signs of distress unless the failed tendon has lost its prestress force over an appreciable distance due to the absence of grout.

- The re-anchoring model adopted, irrespective of whether linear or exponential expressions are used, does not significantly affect the residual strength of the beam. Although this is the case, a much longer tendon re-anchoring length results from the exponential re-anchoring models.

- The failure of tendons within a partially grouted duct is not as detrimental as the failure of tendons within an ungrouted region. This is because some tendon re-anchoring is possible within a partially grouted duct but not where a void exists. In practice, most ducts have been found to be at least partially grouted and some immediate tendon re-anchoring is possible.

- The presence of limited voids within the grout where a failed tendon had started to re-anchor was found to be of secondary concern compared to the presence of voids within a region of tendon failure. The condition of the grout and whether it is sufficient in quality and integrity as to permit some partial re-anchoring to occur, will determine the re-anchoring behaviour of the failed tendon in this case.

- The anchorages have been shown to be a potential point of weakness in a bridge beam due to its vulnerability to corrosion, and thus precautions should be taken to strengthen the beam against possible shear failure. However, a relatively high percentage of tendon loss of area may be accommodated before the shear resistance is found to be deficient (40% loss of overall tendon area in the case considered here).

Case No.	Description	Number of failed tendons	xcorros (m)	Re-anchoring model	Tendon failure level	Grout void level	xvoid (m)	Void length, l_u (m)
Control		0	-	-	-	-	-	-
	Tendon C fail:							
P2a	quarter point	1	4.5	linear	2	-	-	-
P2b	midspan	1	9.0	linear	2	-	-	-
P2c	anchorage	1	0.0	linear	2	-	-	-
P2a1		1	4.5	$\phi = 0.35$	2	-	-	-
P2b1		1	9.0	$\phi = 0.35$	2	-	-	-
P2c1		1	0.0	$\phi = 0.35$	2	-	-	-
	Tendon D fail:							
P3a	quarter point	1	4.5	linear	1	-	-	-
P3b	midspan	1	9.0	linear	1	-	-	-
P3c	anchorage	1	0.0	linear	1	-	-	-
	Tendons D+E fail:							
P4a	midspan	2	9.0	linear	1	-	-	-
P4b*	near anchorage	2	1.0	linear	1	-	-	-
P4c	near anchorage	2	1.0	linear	1	-	-	-
	Failure at anchorage, voids present							
P5a	Tendon C	1	0.0	linear	2	2	0.0	9.0
P5b	Tendons D+E	2	0.0	linear	1	1	0.0	9.0
P5c	Failure of Tendon C	1	0.0	linear	2	2	0.0	3.5
P5c2	at anchorage with	1	0.0	$\phi = 0.20$	2	2	0.0	3.5
P5c3	limited voids present	1	0.0	$\phi = 0.10$	2	2	0.0	3.5
P5d	Failure of Tendon C at anchorage, tendon re-anchoring within partial grout	1	0.0	$\phi = 0.10$	2	-	-	-
P5d2		1	0.0	$\phi = 0.20$	2	-	-	-
P6a	Failure of Tendon C at quarter point within presence of limited voids	1	4.5	linear	2	2	1.0	4.0
P6b		1	4.5	linear	2	2	1.0	6.0
P6c		1	4.5	linear	2	2	1.0	9.0
P6d	Failure of Tendon C at quarter point, voids within re-anchoring length	1	4.5	linear	2	2	5.0	3.0
P6e		1	4.5	$\phi = 0.35$	2	2	5.0	3.0
P6f		1	4.5	$\phi = 0.20$	2	2	5.0	3.0
P7a	Tendon C totally	0	-	-	-	2	0.0	18.0
P7b	unbonded	1	0.0	linear	2	2	0.0	18.0
P8a	Voids near anchorage ends	0	-	-	-	1	0.0	4.5
						1	13.5	4.5
						2	0.0	4.5
						2	13.5	4.5
						3	0.0	4.5
						3	13.5	4.5
P9a	Failure of Tendon C at quarter point, tendon re-anchoring within partial grout	1	4.5	$\phi = 0.20$	2	-	-	-
P9b		1	4.5	$\phi = 0.10$	2	-	-	-
P10a	Failure of Tendons (D+E) at anchorage, tendon re-anchoring within partial grout	2	0.0	$\phi = 0.20$	1	-	-	-
P10b		2	0.0	$\phi = 0.10$	1	-	-	-

* *Nominal links not included in calculation of shear resistance*

Table 6.1 List of deterioration cases

Material Property	Value
Characteristic strength of concrete, f_{cu}	42 N/mm^2
Characteristic strength of prestressing steel, f_{pu}	1569 N/mm^2
Tensile strength of concrete, f_{tu}	4.2 N/mm^2
Young's Modulus for concrete, E_c	32 kN/mm^2
Young's Modulus for prestressing steel, E_{ps}	200 kN/mm^2

Table 6.2 Material properties used to model the Botley beam

Case No.	Decompression moment (kNm) M_{dec}	Cracking moment (kNm) M_{cr}	Ultimate moment (kNm) M_u	Shear resistance at support (kN) V_{tot}	Ultimate midspan curvature 10^{-6} (rad/mm) ϕ	Ultimate midspan deflection (mm) δ
Control	492	631	1242	516	10.43	303.5
P2a	349	631	1242	516	10.43	310.5
P2b	395	531	1127	516	11.84	212.8
P2c	492	631	1242	493	10.43	303.6
P2a1	349	631	1242	516	10.43	312.6
P2b1	395	531	1127	516	11.84	214.6
P2c1	492	631	1242	493	10.43	303.6
P3a	323	454	1234	516	9.87	305.6
P3b	380	515	1093	511	11.86	194.6
P3c	492	631	1242	453	10.43	303.6
P4a	decompressed	399	893	503	14.76	106.1
P4b	decompressed	631	1242	233*	10.43	303.9
P4c	decompressed	631	1242	256*	10.43	303.9
P5a	395	531	1127	492	11.47	324.8
P5b	decompressed	399	892	210	14.67	444.1
P5c	492	631	1242	493	10.43	312.9
P5c2	492	631	1242	493	10.43	317.8
P5c3	490	629	1241	493	10.44	324.3
P5d	492	631	1242	493	10.43	307.3
P5d2	492	631	1242	493	10.43	303.9
P6a	359	493	1242	516	10.43	330.3
P6b	389	525	1155	516	7.85	295.5
P6c	395	531	1127	516	11.47	327.8
P6d	349	598	1225	516	9.87	307.6
P6e	453	592	1222	516	9.89	309.0
P6f	435	574	1210	516	9.83	309.8
P7a	496	634	1234	523	10.71	310.5
P7b	395	531	1127	492	11.47	327.8
P8a	492	631	1117	531	6.74	208.7
P9a	349	631	1242	516	10.43	318.6
P9b	349	627	1242	514	10.28	322.3
P10a	decompressed	631	1242	218	10.43	304.4
P10b	decompressed	631	1242 -	218	10.43	313.1

** Values at 1.0m from left hand support*

Note: In all cases, failure occurred by crushing of the concrete at the top compression zone

Table 6.3 Results for deterioration cases considered

Case No.	Tendon stresses at ultimate at the section with maximum tendon stress (N/mm^2)		
	Tendon level 1	**Tendon level 2**	**Tendon level 3**
Control	1248	1143	1038
P2a	1256	tendon failed	924
P2b	1296	tendon failed	1187
P2c	1248	1143	1038
P2a1	1256	tendon failed	924
P2b1	1296	tendon failed	1187
P2c1	1248	1143	1038
P3a	1318 other tendon failed	1269	1042
P3b	1297 other tendon failed	1268	1190
P3c	1248	1143	1038
P4a	both tendons failed	1349	1313
P4b	1248	1143	1038
P4c	1248	1143	1038
P5a	1295	tendon failed	1183
P5b	both tendons failed	1347	1311
P5c	1248	1143	1038
P5c2	1248	1143	1038
P5c3	1250	1133	1039
P5d	1248	1143	1038
P5d2	1248	1143	1038
P6a	1299	tendon failed	1043
P6b	1300	tendon failed	1159
P6c	1295	tendon failed	1183
P6d	1263	866	1058
P6e	1265	829	1068
P6f	1268	724	1078
P7a	1270	901	1089
P7b	1295	tendon failed	1183
P8a	1041	973	906
P9a	1256	tendon failed	924
P9b	1256	1092	1040
P10a	1248	1143	1038
P10b	1248	1143	1038

Note: Failure strength of wire is 1569 N/mm^2

Table 6.4 Tendon stresses at ultimate at the section with the maximum tendon stress

Case No.	$\frac{M_{dec}}{M_s}$ (Class 1 limit)	$\frac{M_{cr}}{M_s}$ (cracking limit)	$\frac{M_u}{M_t}$	$\frac{V_{tot}}{V_u}$
Control	0.82	1.05	1.32	1.87
P2a	0.81	1.05	1.32	1.87
P2b	0.66	0.88	1.20	2.06
P2c	0.82	1.05	1.32	1.78
P2a1	0.81	1.05	1.32	1.87
P2b1	0.66	0.88	1.20	2.06
P2c1	0.82	1.05	1.32	1.78
P3a	0.75	1.05	1.31	1.88
P3b	0.63	0.86	1.16	2.10
P3c	0.82	1.05	1.32	1.64
P4a	-	0.66	0.95	2.53
P4b	-	1.05	1.32	0.94*
P4c	-	1.05	1.32	1.03*
P5a	0.66	0.88	1.20	1.97
P5b	-	0.66	0.95	1.06
P5c	0.82	1.05	1.32	1.78
P5c2	0.82	1.05	1.32	1.78
P5c3	0.82	1.05	1.32	1.78
P5d	0.82	1.05	1.32	1.78
P5d2	0.82	1.05	1.32	1.78
P6a	0.78	1.07	1.32	1.87
P6b	0.70	0.94	1.23	2.01
P6c	0.66	0.88	1.20	2.06
P6d	0.81	1.02	1.30	1.90
P6e	0.78	1.01	1.30	1.90
P6f	0.75	0.98	1.29	1.92
P7a	0.83	1.05	1.31	1.91
P7b	0.66	0.88	1.20	1.97
P8a	0.82	1.05	1.19	2.18
P9a	0.81	1.05	1.32	1.87
P9b	0.81	1.05	1.32	1.86
P10a	-	1.05	1.32	0.79
P10b	-	1.05	1.32	0.79

** Values at 1.0m from left hand support*

M_{dec} *- Decompression moment*

M_{cr} *- Cracking moment*

M_u *- Ultimate moment calculated by program*

M_s *- Design bending moment at service*

M_t *- Design bending moment at ultimate*

V_{tot} *- Total shear resistance at support*

V_u *- Ultimate shear force at support*

Table 6.5 Normalised values for serviceability and ultimate limit states

Case No.	Description	Time taken to run analysis (minutes)
Control		7
	Tendon C fail:	
P2a	quarter point	7
P2b	midspan	5
P2c	anchorage	7
P2a1		7
P2b1		5
P2c1		7
	Tendon D fail:	
P3a	quarter point	7
P3b	midspan	5
P3c	anchorage	7
	Tendons D+E fail:	
P4a	midspan	3
P4b	near anchorage	7
P4c	near anchorage	7
	Failure at anchorage, voids present	
P5a	Tendon C	31
P5b	Tendons D+E	24
P5c	Failure of Tendon C	19
P5c2	at anchorage with	19
P5c3	limited voids present	19
P5d	Failure of Tendon C at anchorage, tendon	7
P5d2	re-anchoring within partial grout	7
P6a	Failure of Tendon C at quarter point within	20
P6b	presence of limited	24
P6c	voids	28
P6d	Failure of Tendon C at quarter point, voids	19
P6e	within re-anchoring	17
P6f	length	17
P7a	Tendon C totally	272
P7b	unbonded	54
P8a	Voids near anchorage ends	95
P9a	Failure of Tendon C at quarter point, tendon re-anchoring	7
P9b	within partial grout	7
P10a	Failure of Tendons (D+E) at anchorage, tendon re-anchoring	7
P10b	within partial grout	7

Note: See Table 6.1 for further details of number of failed tendons and void length

Table 6.6 Time taken to run analysis of the deterioration cases considered

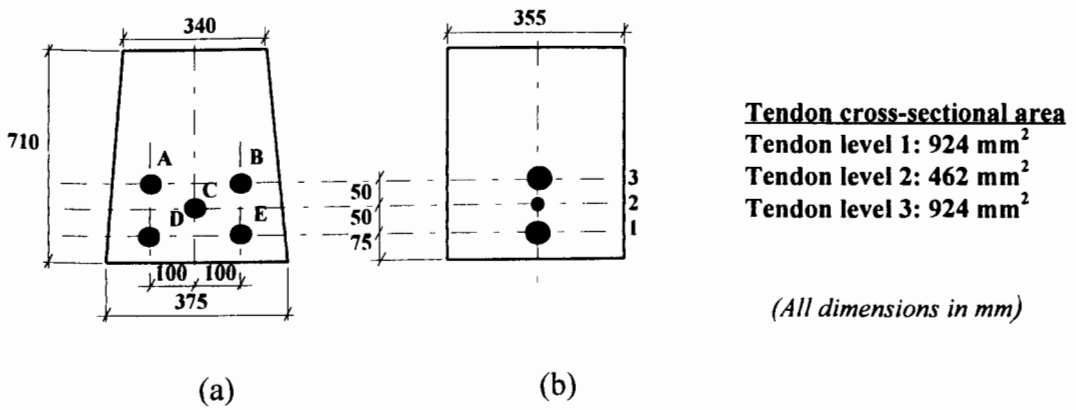

Figure 6.1 Cross-section at midspan of Botley beam - (a) actual cross-section, (b) modelled cross-section

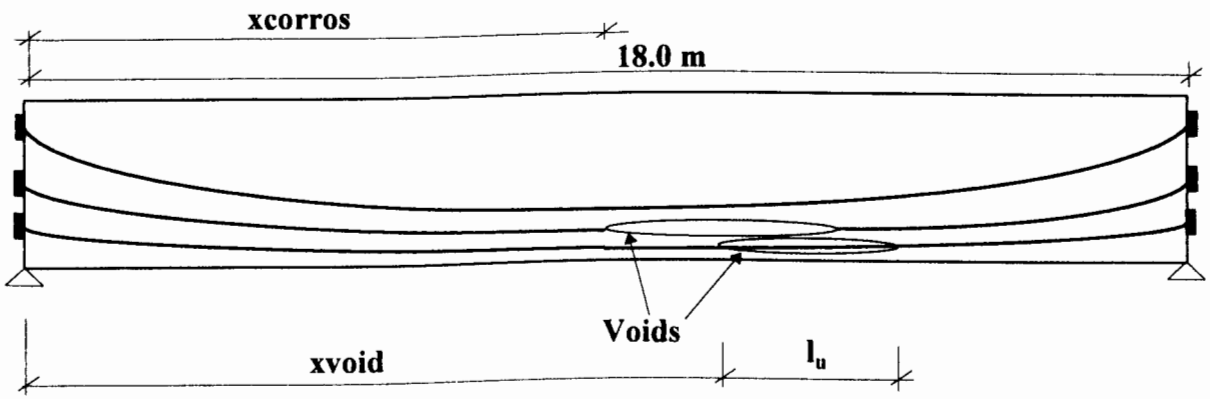

Figure 6.2 Elevation of the Botley beam, illustrating notation used to describe the deterioration

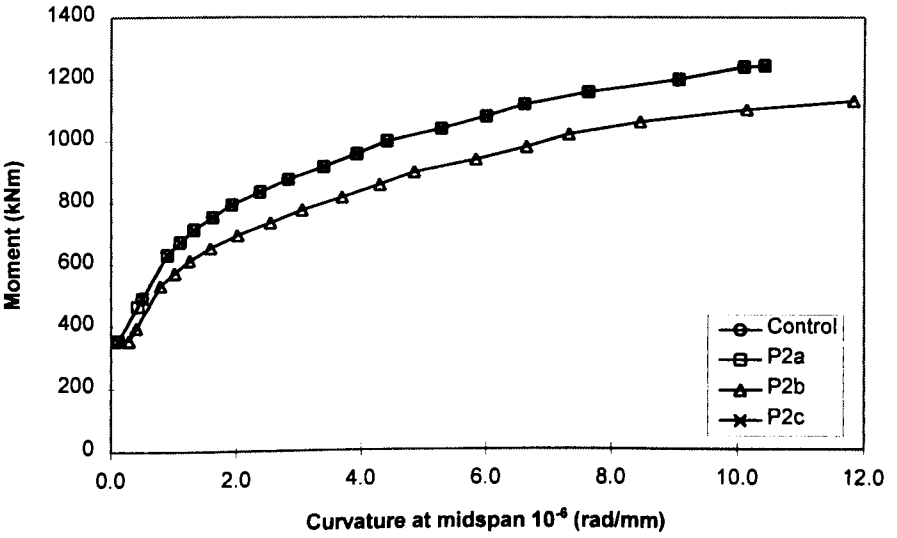

Note: See Table 6.3 for values of ultimate moment and curvature

Figure 6.3 Moment-curvature diagram for failure of Tendon C within a well-grouted duct

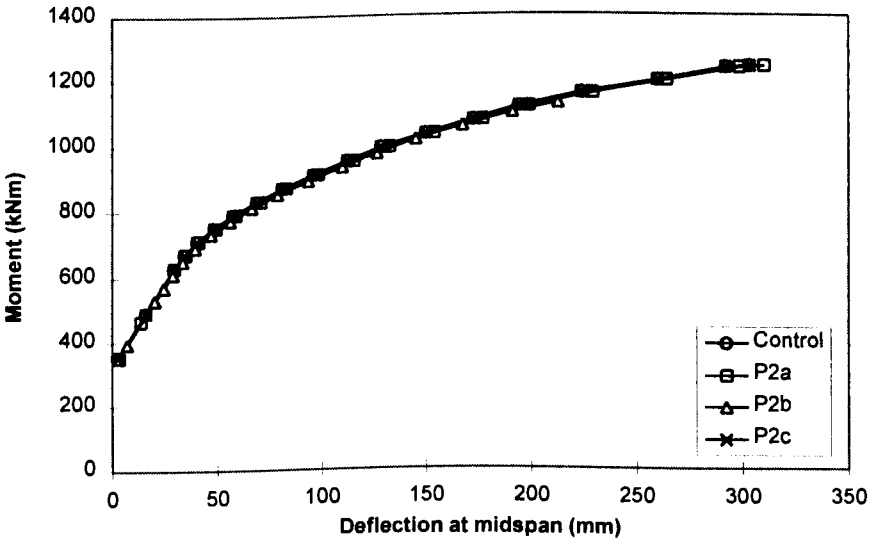

Note: See Table 6.3 for values of ultimate moment and deflection

Figure 6.4 Moment-deflection diagram for failure of Tendon C within a well-grouted duct

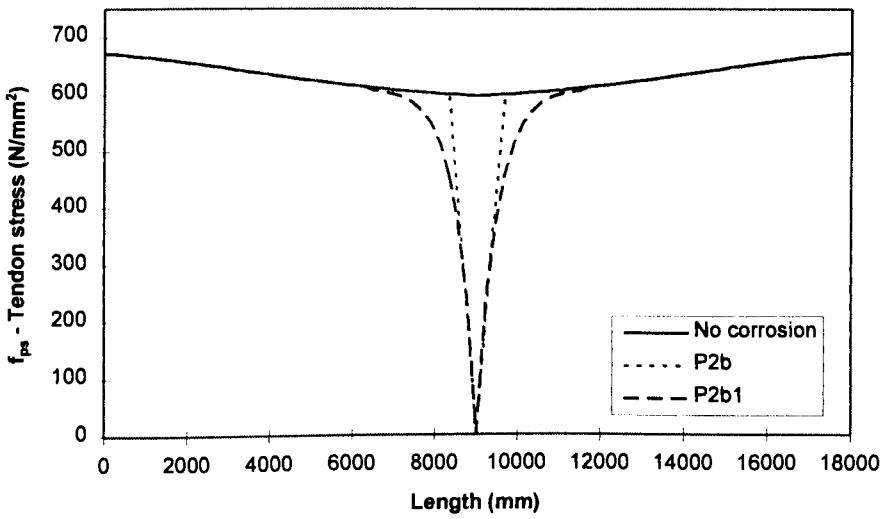

Figure 6.5 Distribution of residual prestress along failed Tendon C for linear and exponential re-anchoring models adopted

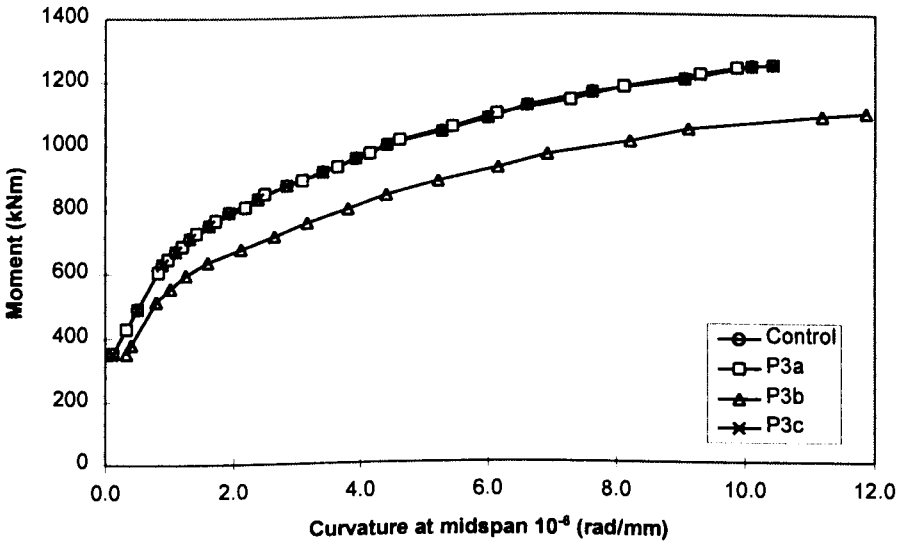

Note: See Table 6.3 for values of ultimate moment and curvature

Figure 6.6 Moment-curvature diagram for failure of Tendon D within a well-grouted duct

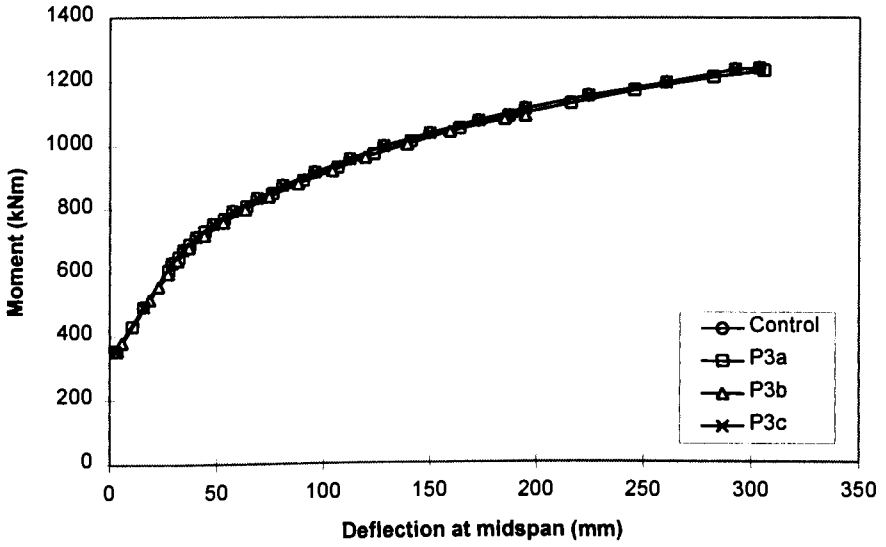

Note: See Table 6.3 for values of ultimate moment and deflection

Figure 6.7 Moment-deflection diagram for failure of Tendon D within a well-grouted duct

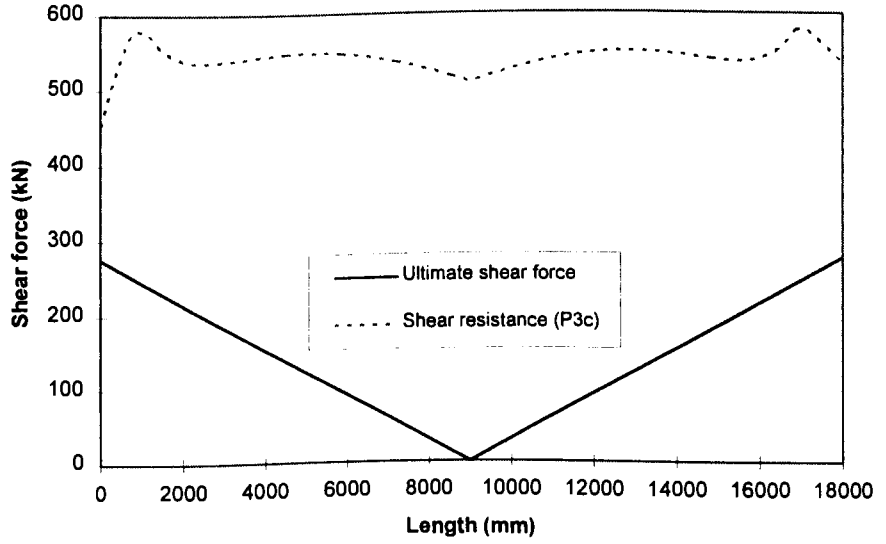

Figure 6.8 Shear resistance provided after failure of Tendon D at the anchorage

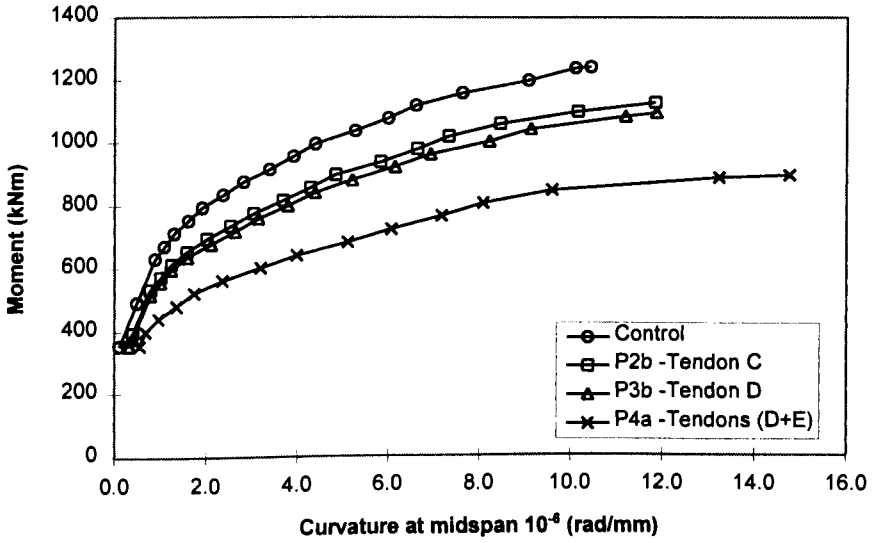

Figure 6.9 Moment-curvature diagram for failure of Tendon C, Tendon D or Tendons (D+E) at midspan

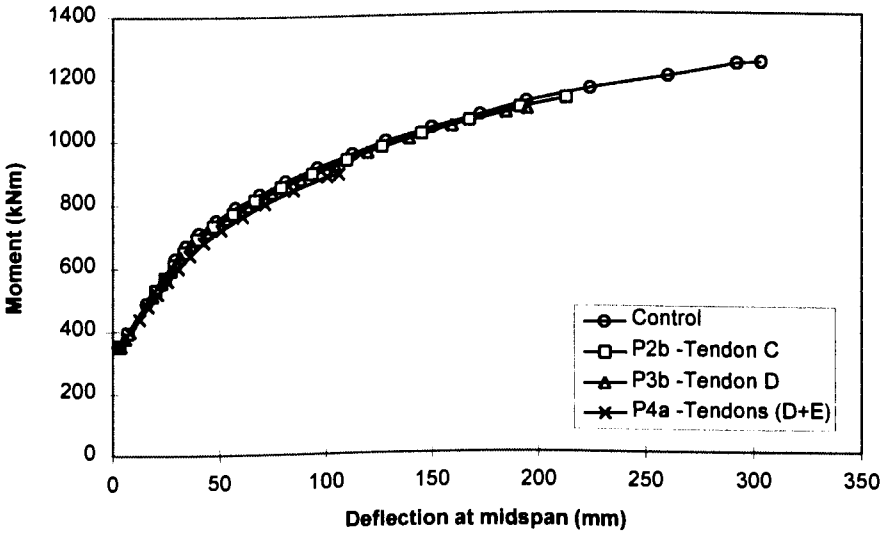

Note: See Table 6.3 for values of ultimate moment and deflection

Figure 6.10 Moment-deflection diagram for failure of Tendon C, Tendon D or Tendons (D+E) at midspan

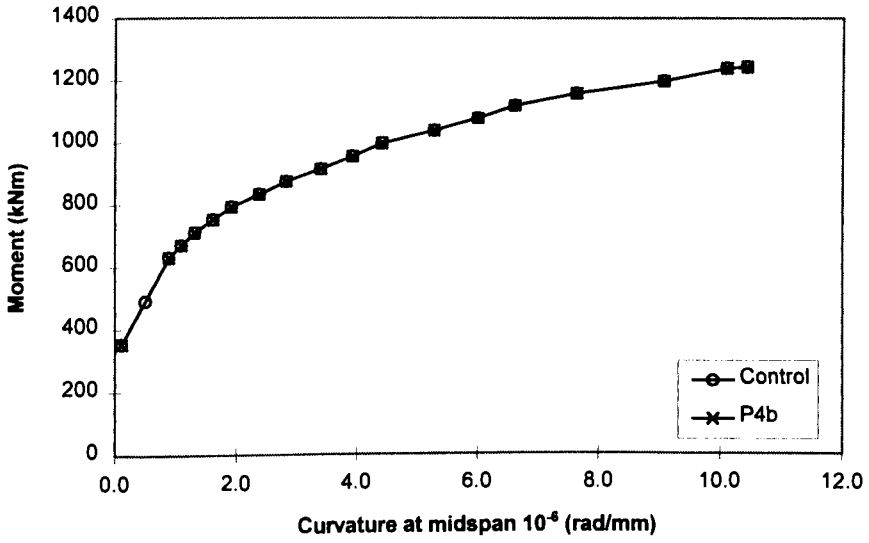

Note: See Table 6.3 for values of ultimate moment and curvature

Figure 6.11 Moment-curvature diagram for failure of Tendons (D+E) near anchorage

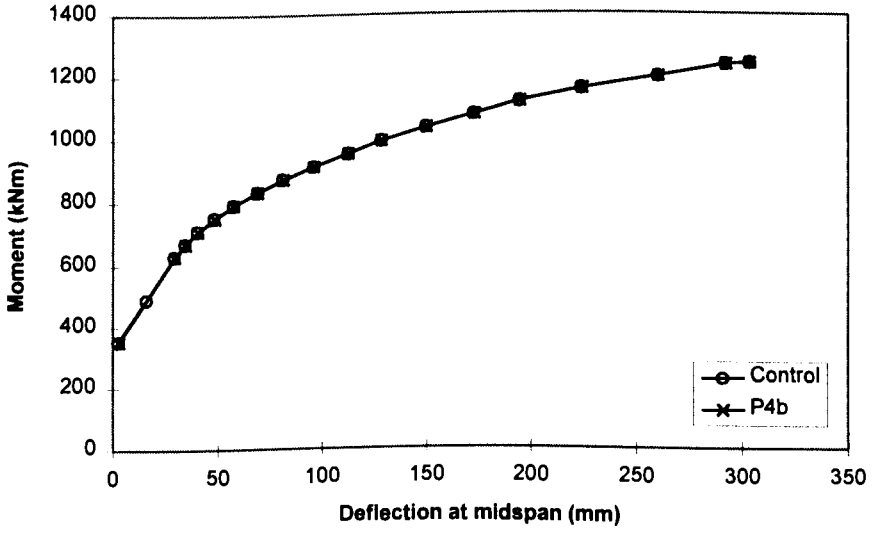

Note: See Table 6.3 for values of ultimate moment and deflection

Figure 6.12 Moment-deflection diagram for failure of Tendons (D+E) near anchorage

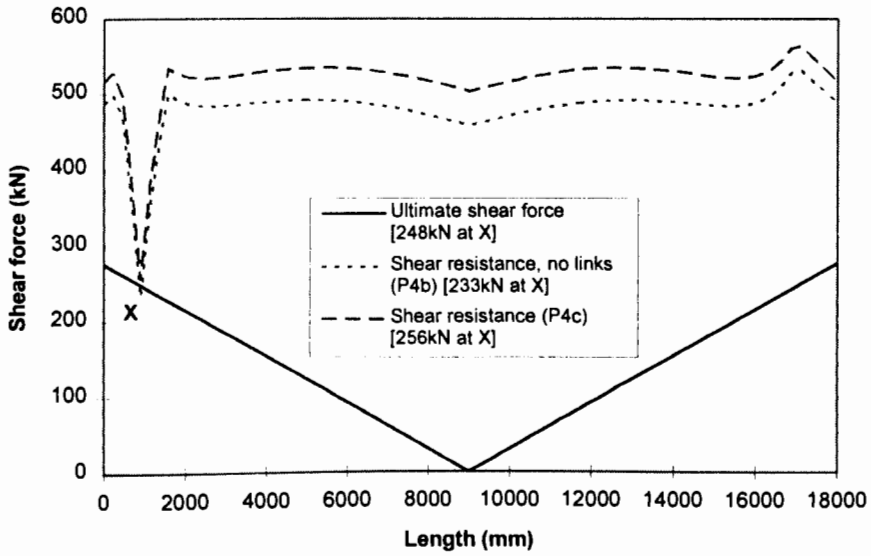

Figure 6.13 Reduced shear resistance provided after failure of Tendons (D+E) near the anchorage

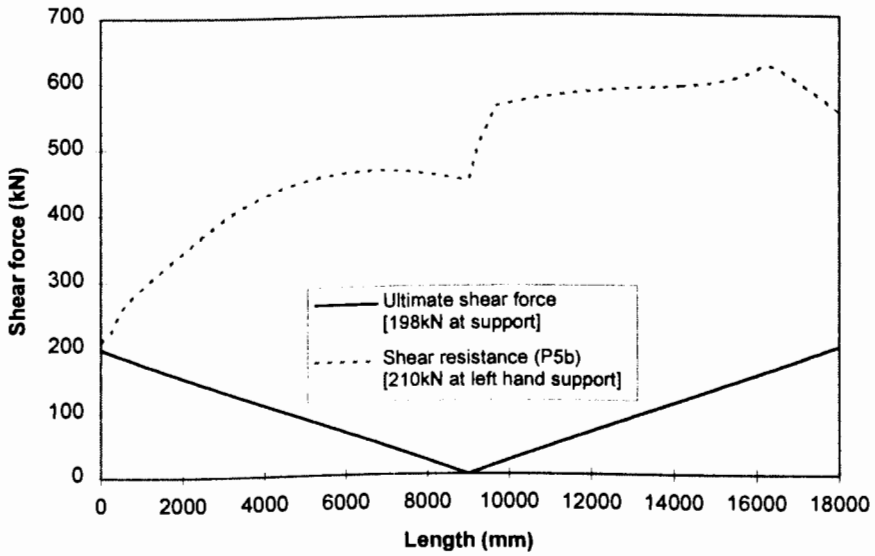

Figure 6.14 Reduced shear resistance provided after failure of Tendons (D+E) at the anchorage, voids present (Case P5b)

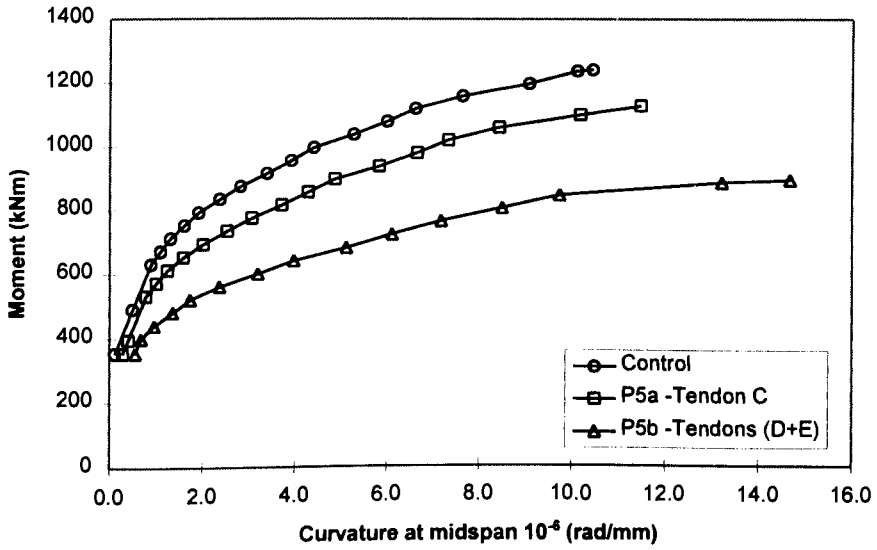

Figure 6.15 Moment-curvature diagram for failure of Tendon C or Tendons (D+E) at the anchorage, with presence of voids in the grout

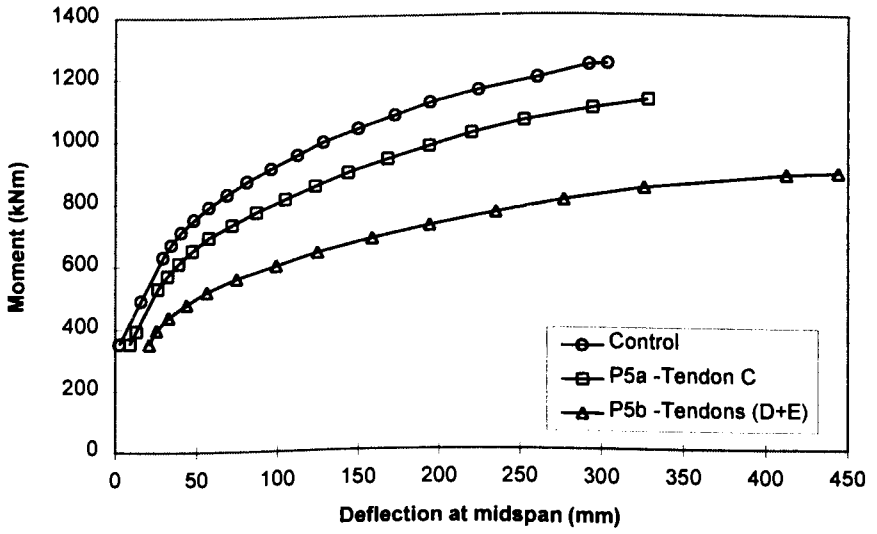

Figure 6.16 Moment-deflection diagram for failure of Tendon C or Tendons (D+E) at the anchorage, with presence of voids in the grout

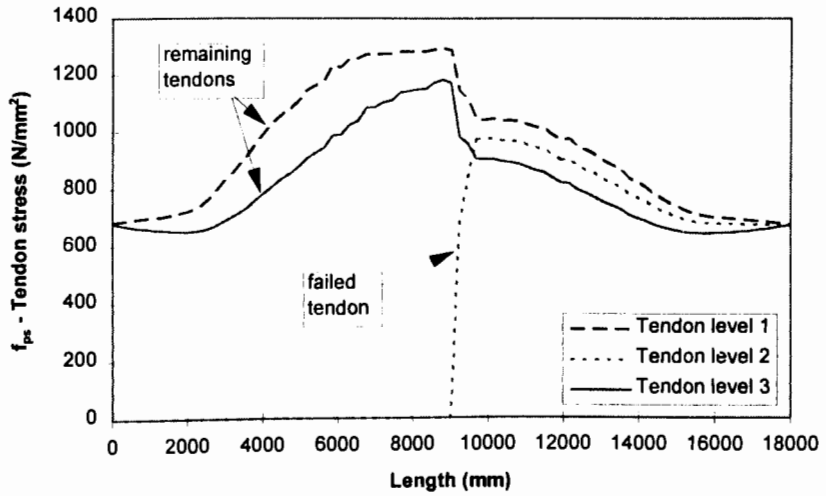

Figure 6.17 Tendon stress distribution at the ultimate condition for Case P5a

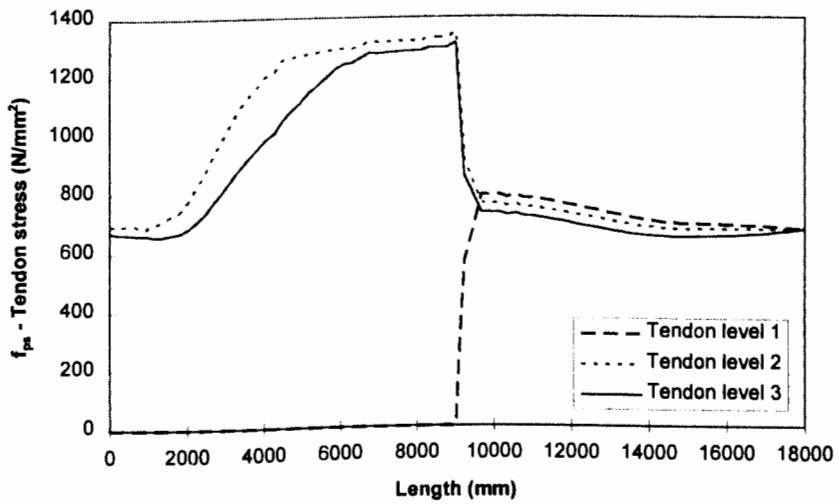

Figure 6.18 Tendon stress distribution at the ultimate condition for Case P5b

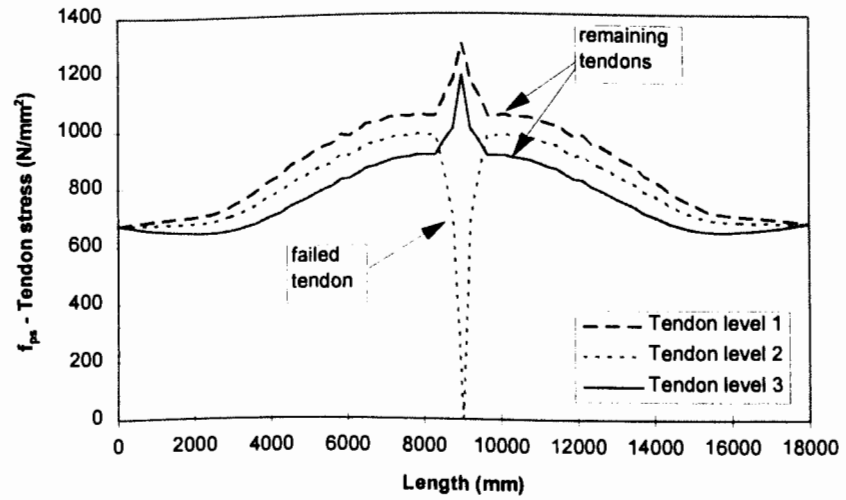

Figure 6.19 Tendon stress distribution at the ultimate condition for Case P2b

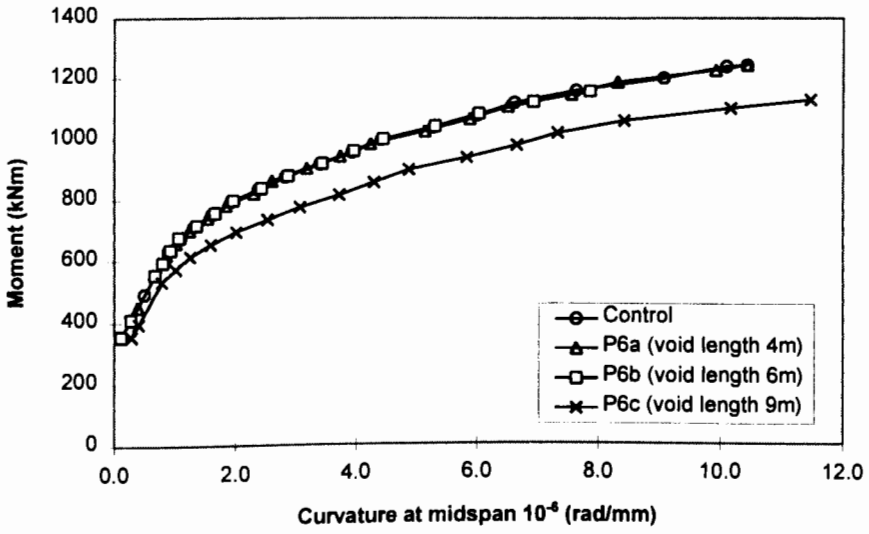

Note: See Table 6.3 for values of ultimate moment and curvature

Figure 6.20 Moment-curvature diagram for failure of Tendon C at the quarter point position within different lengths of grout voids

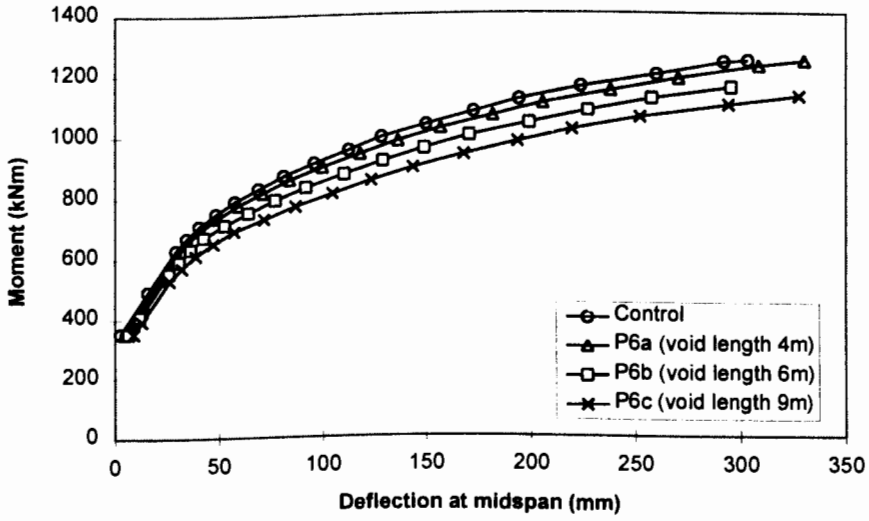

Figure 6.21 Moment-deflection diagram for failure of Tendon C at the quarter point position within different lengths of grout voids

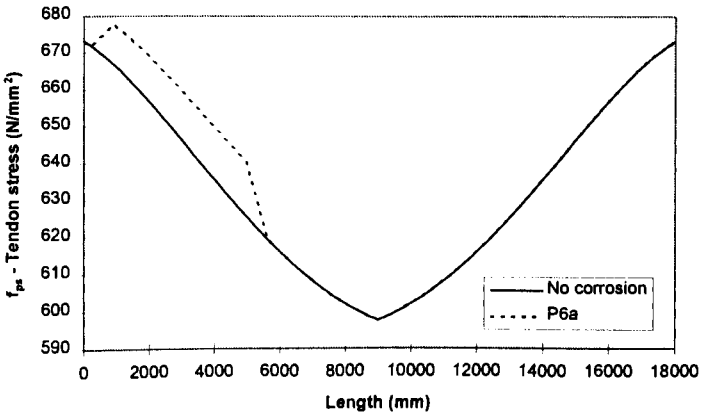

(a) Stress in Tendon level 1

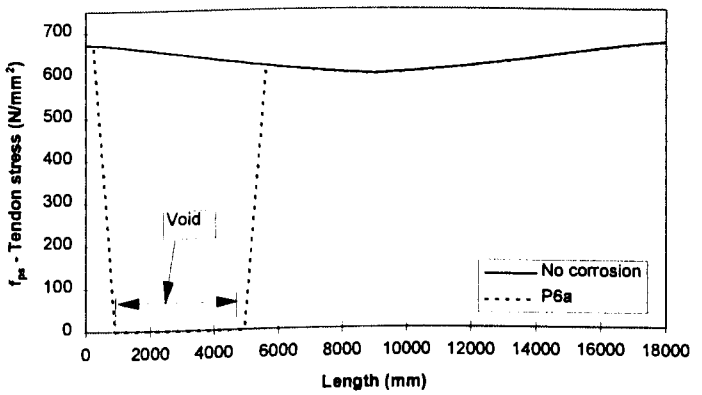

(b) Stress along the fractured Tendon C

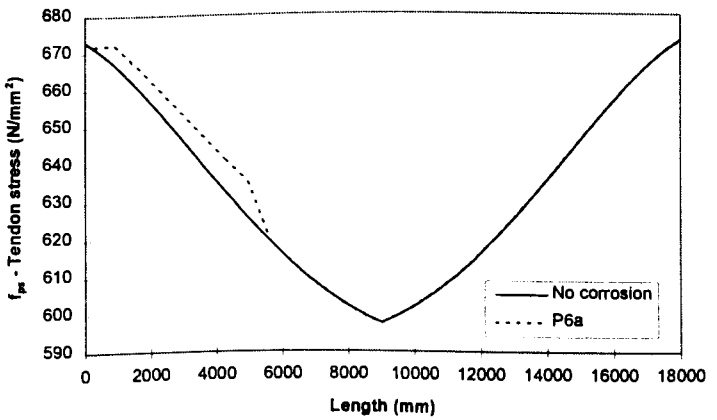

(c) Stress in Tendon level 3

Figure 6.22 Distribution of tendon stress as a result of failure of Tendon C within a region of short void (Case P6a)

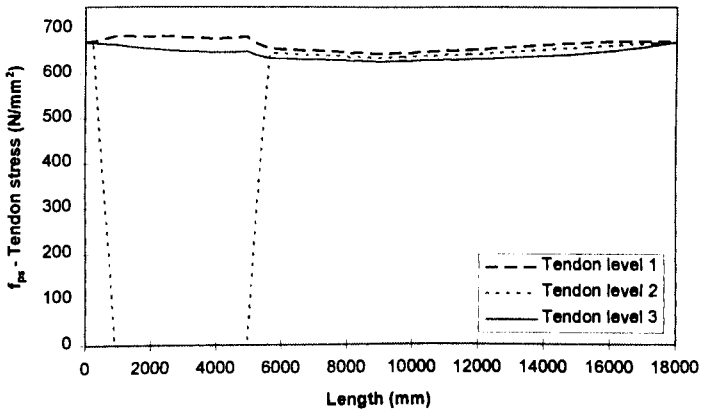

(a) P6a (void length 4m)

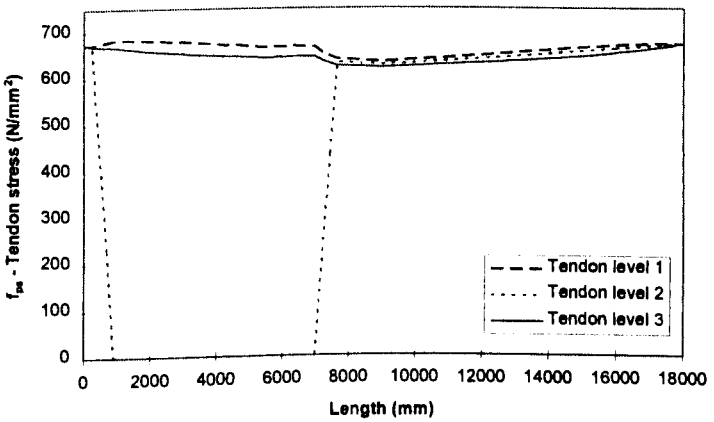

(b) P6b (void length 6m)

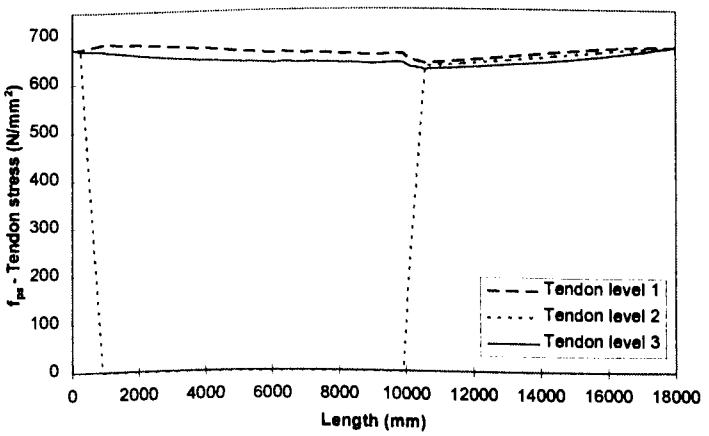

(c) P6c (void length 9m)

Figure 6.23 Tendon stress distribution at the first post-cracking load step for cases P6a, P6b and P6c

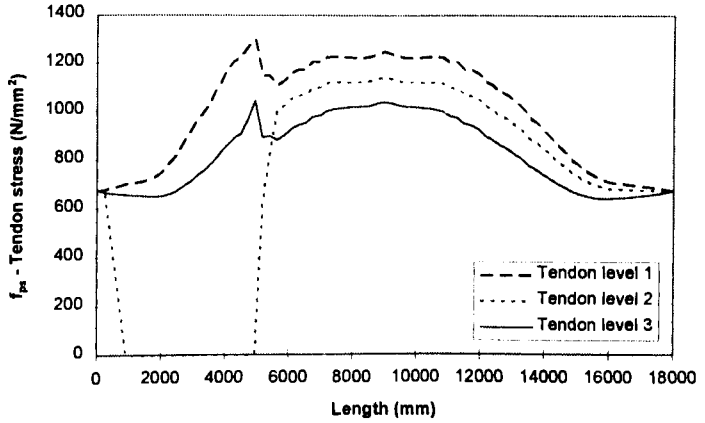

(a) P6a (void length 4m)

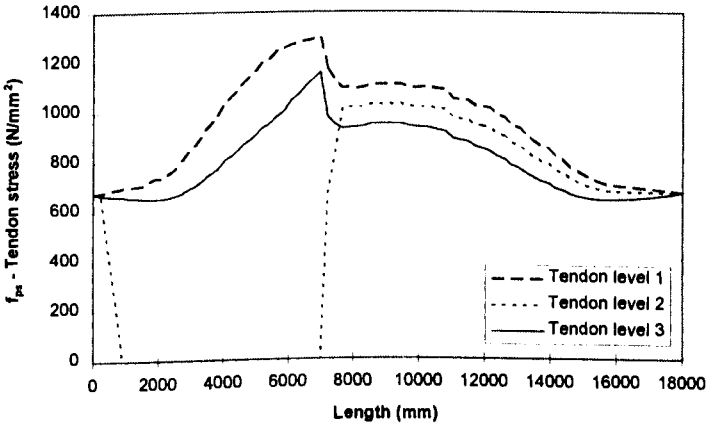

(b) P6b (void length 6m)

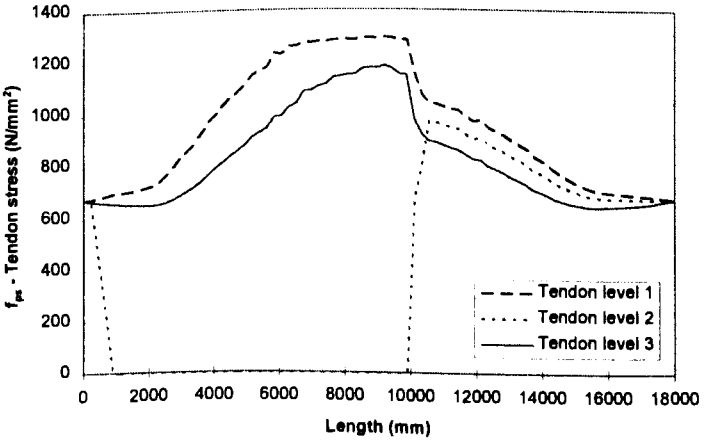

(c) P6c (void length 9m)

Figure 6.24 Tendon stress distribution at the ultimate condition for cases P6a, P6b and P6c

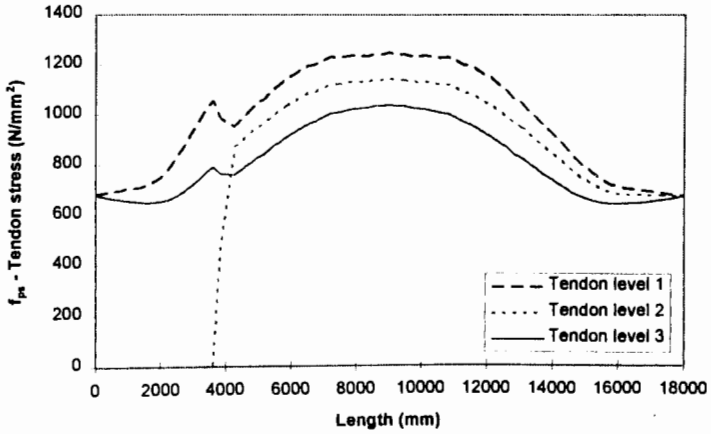

(a) 5c (linear re-anchoring)

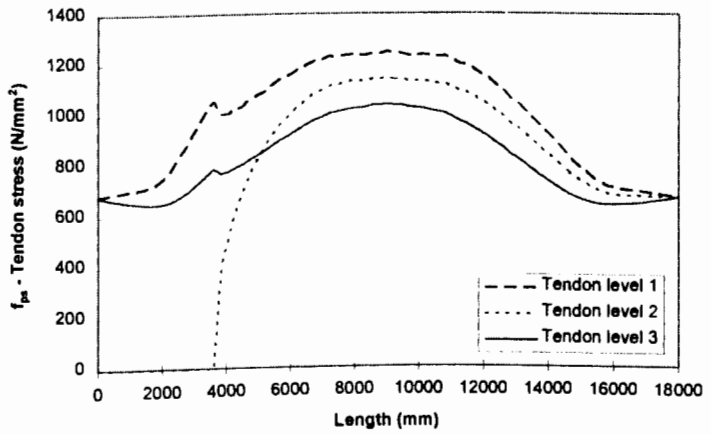

(b) P5c2 (ϕ=0.2)

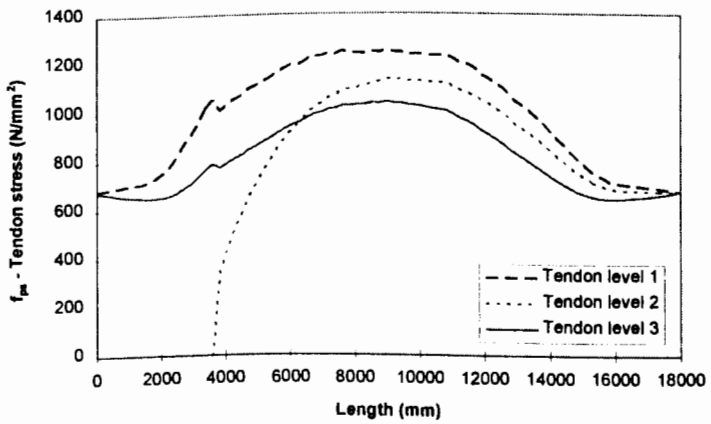

(c) P5c3 (ϕ=0.1)

Figure 6.25 Tendon stress distribution at the ultimate condition for cases P5c, P5c2 and P5c3 (Tendon C fail at anchorage with limited voids present)

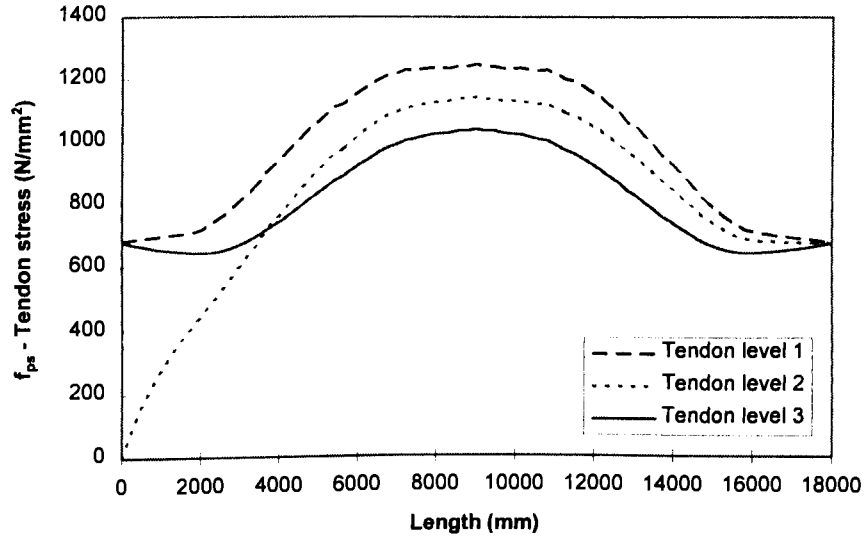

(a) P5d (ϕ=0.1)

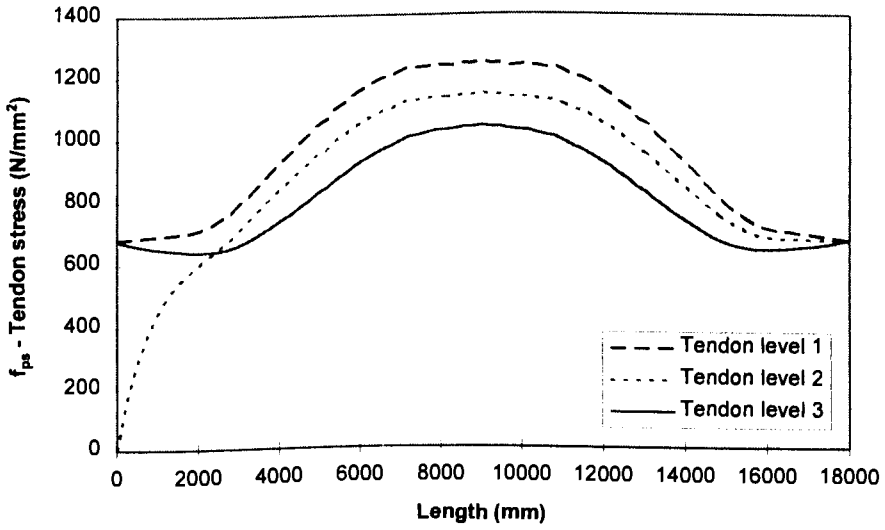

(b) P5d2 (ϕ=0.2)

Figure 6.26 Tendon stress distribution at the ultimate condition for cases P5d and P5d2 (Tendon C fail at anchorage, tendon re-anchoring within partial grout)

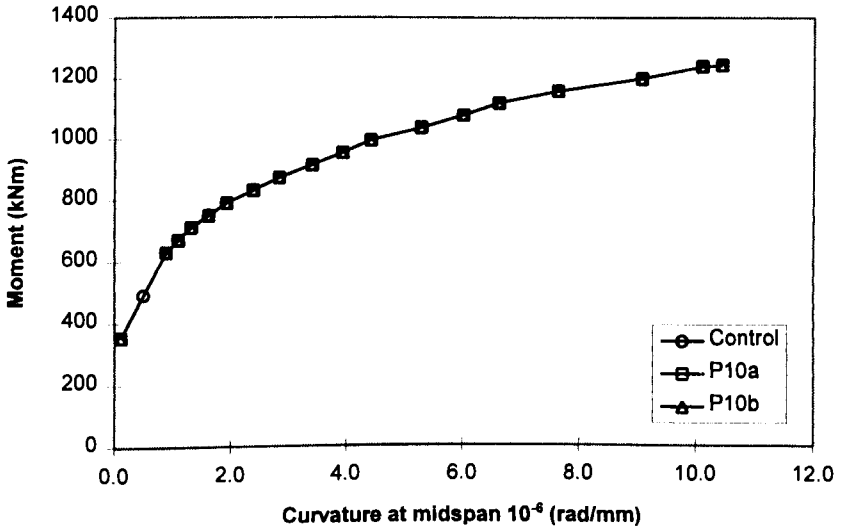

Note: See Table 6.3 for values of ultimate moment and curvature

Figure 6.27 Moment-curvature diagram for failure of Tendons (D+E) at the anchorage, tendon re-anchoring within partial grout

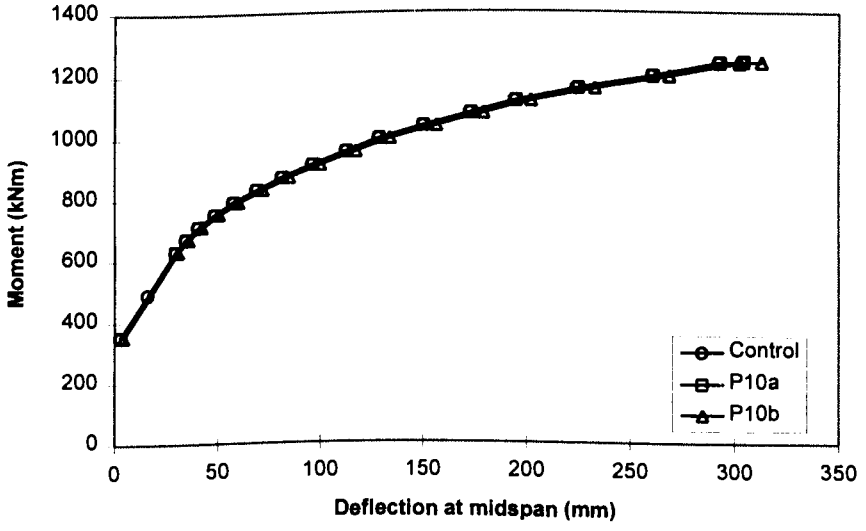

Note: See Table 6.3 for values of ultimate moment and deflection

Figure 6.28 Moment-deflection diagram for failure of Tendons (D+E) at the anchorage, tendon re-anchoring within partial grout

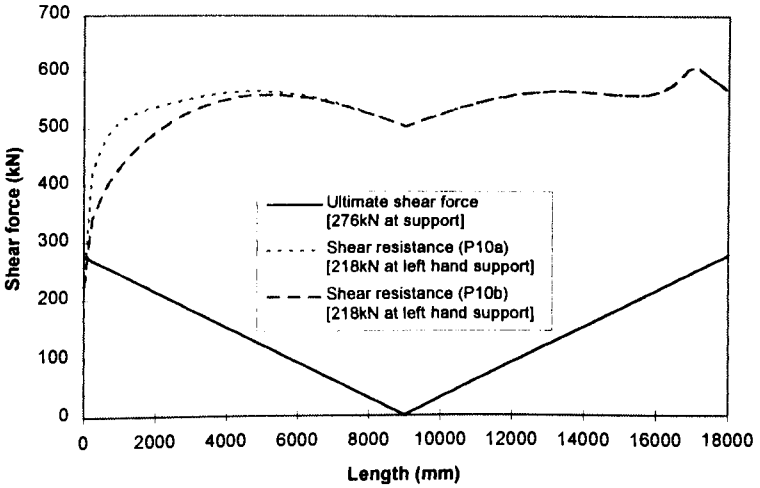

Figure 6.29 Reduced shear resistance provided after failure of Tendons (D+E) at the anchorage

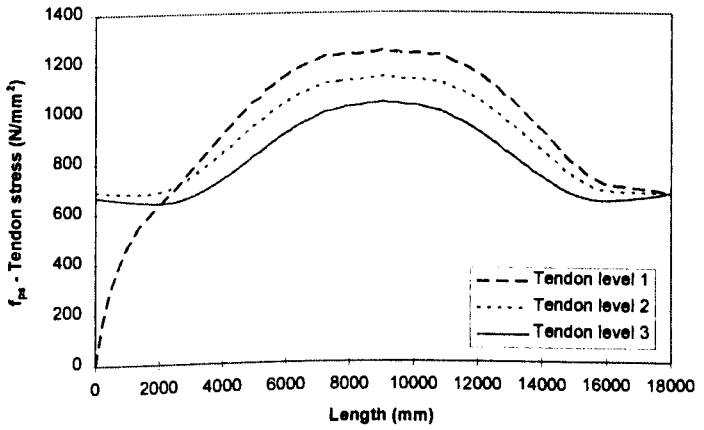

(a) P10a (ϕ=0.2)

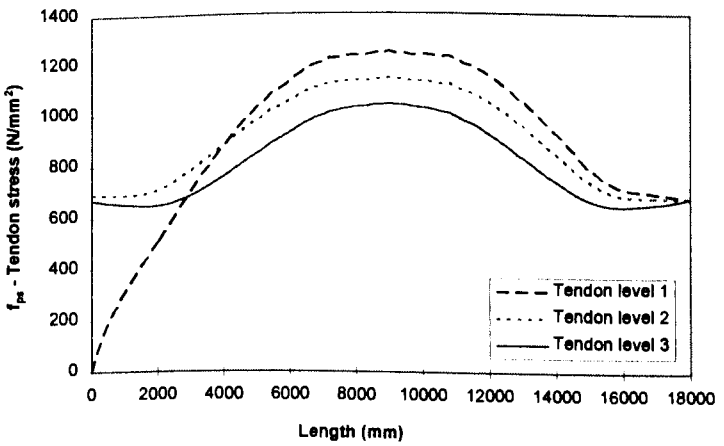

(b) P10b (ϕ=0.1)

Figure 6.30 Tendon stress distribution at the ultimate condition for cases P10a and P10b

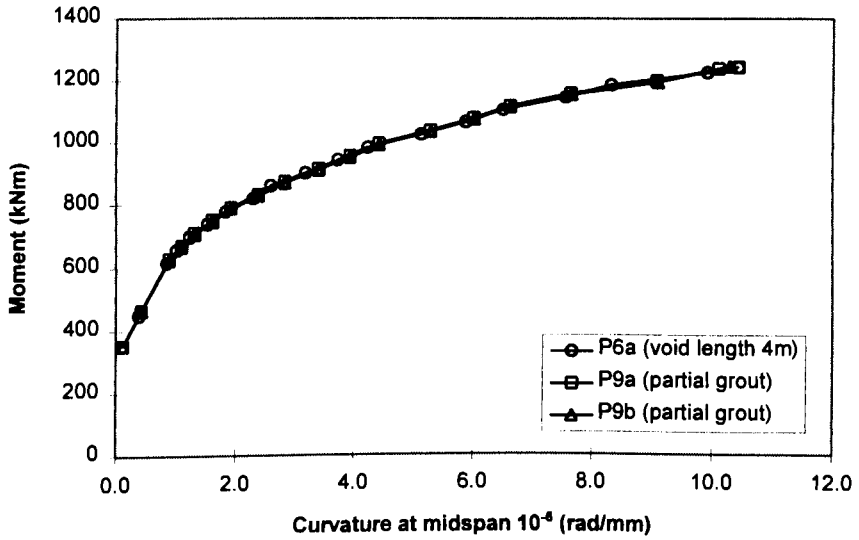

Note: See Table 6.3 for values of ultimate moment and curvature

Figure 6.31 Moment-curvature diagram for failure of Tendon C at the quarter point position, tendon re-anchoring within partial grout

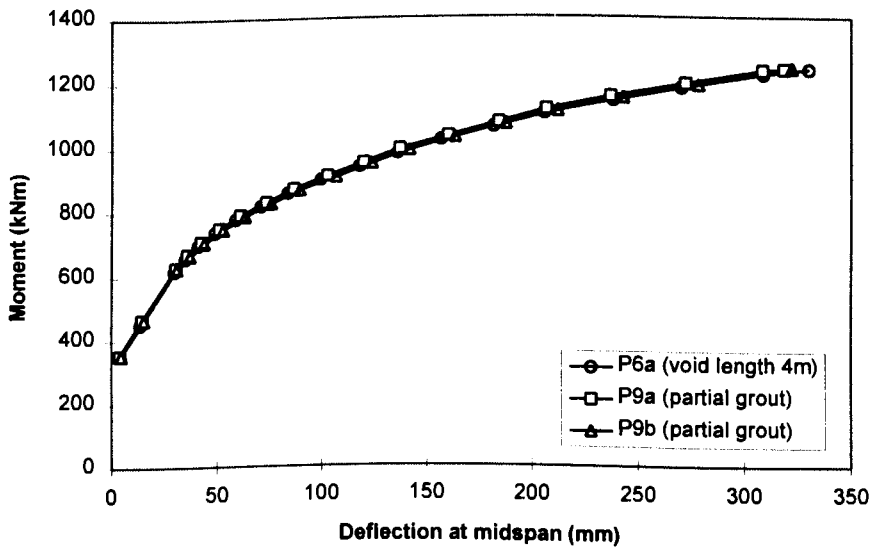

Note: See Table 6.3 for values of ultimate moment and deflection

Figure 6.32 Moment-deflection diagram for failure of Tendon C at the quarter point position, tendon re-anchoring within partial grout

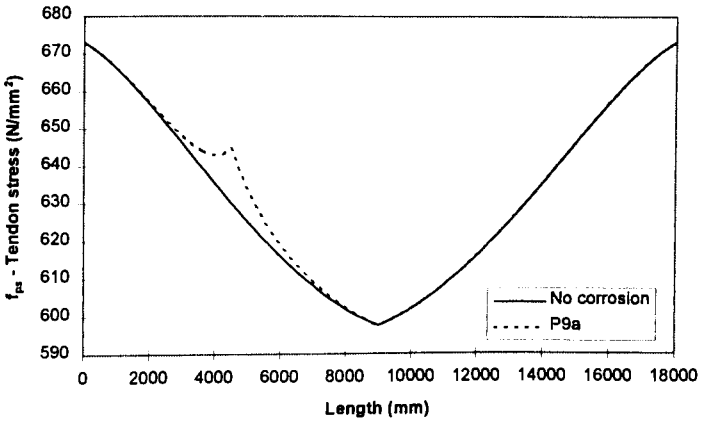

(a) Stress in Tendon level 1

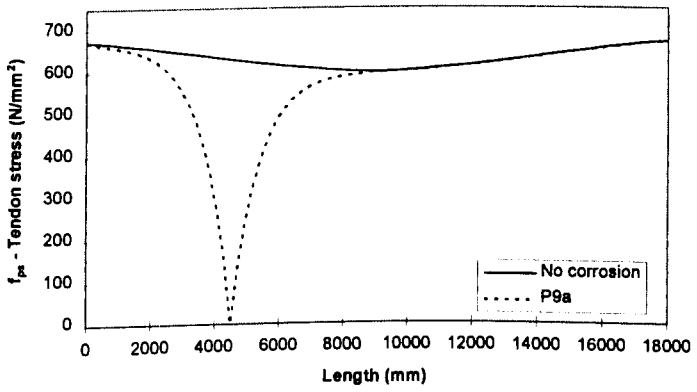

(b) Stress in the fractured Tendon C

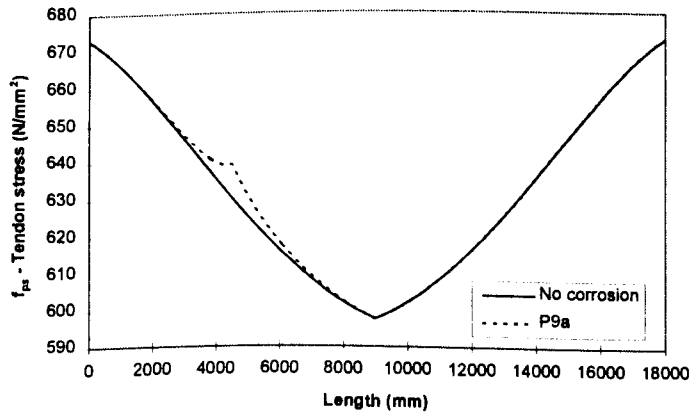

(c) Stress in Tendon level 3

Figure 6.33 Distribution of tendon stress as a result of failure of Tendon C at the quarter point position, tendon re-anchoring within partial grout for Case P9a

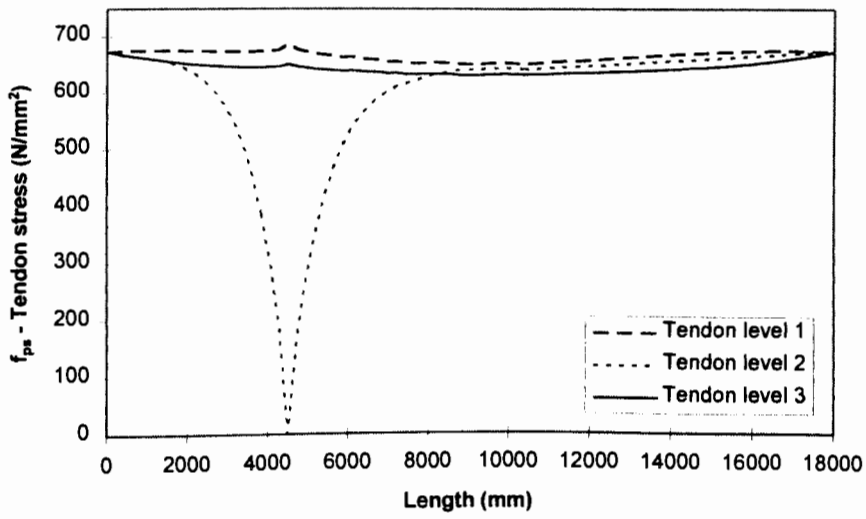

(a) P9a (ϕ=0.2)

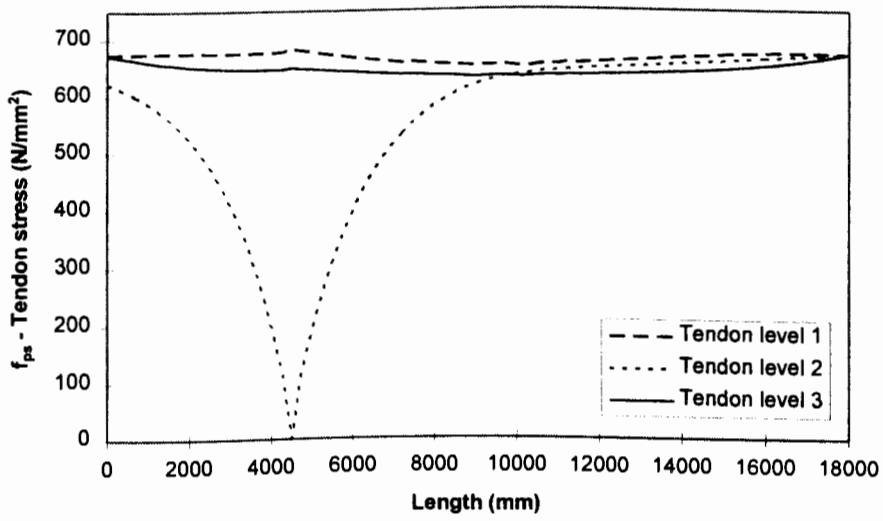

(b) P9b (ϕ=0.1)

Figure 6.34 Tendon stress distribution at the first post-cracking load step for cases P9a and P9b

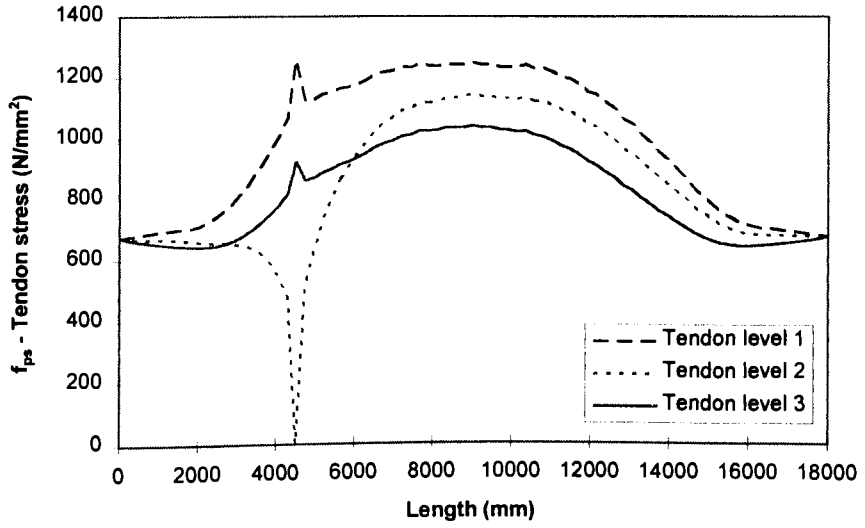

(a) P9a (ϕ=0.2)

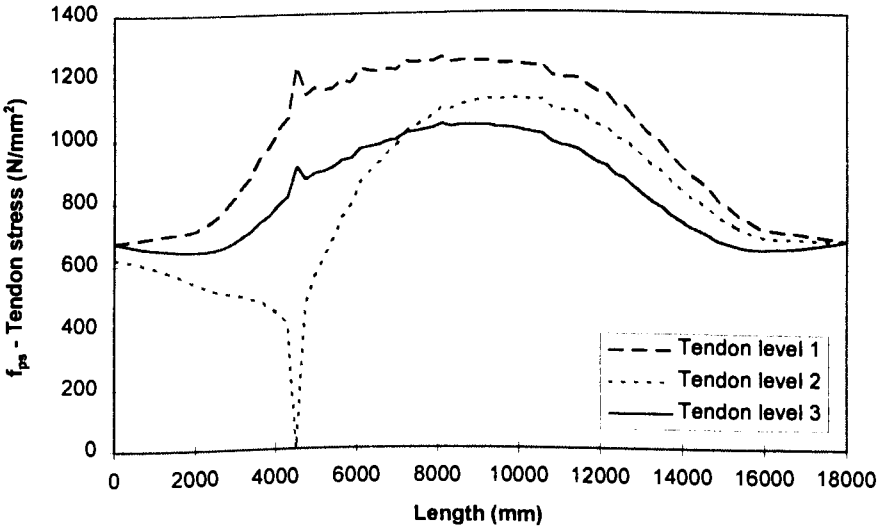

(b) P9b (ϕ=0.1)

Figure 6.35 Tendon stress distribution at the ultimate condition for cases P9a and P9b

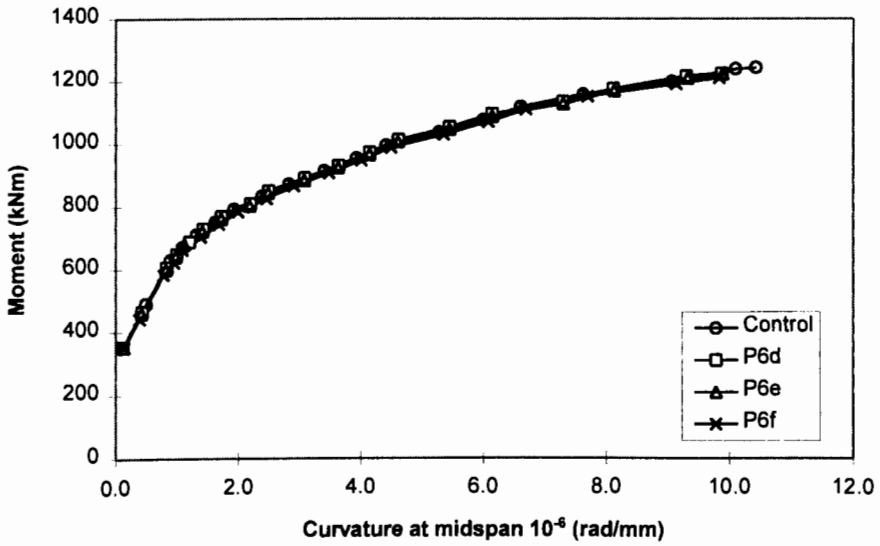

Note: See Table 6.3 for values of ultimate moment and curvature

Figure 6.36 Moment-curvature diagram for failure of Tendon C at the quarter point position, with the presence of voids within re-anchoring length

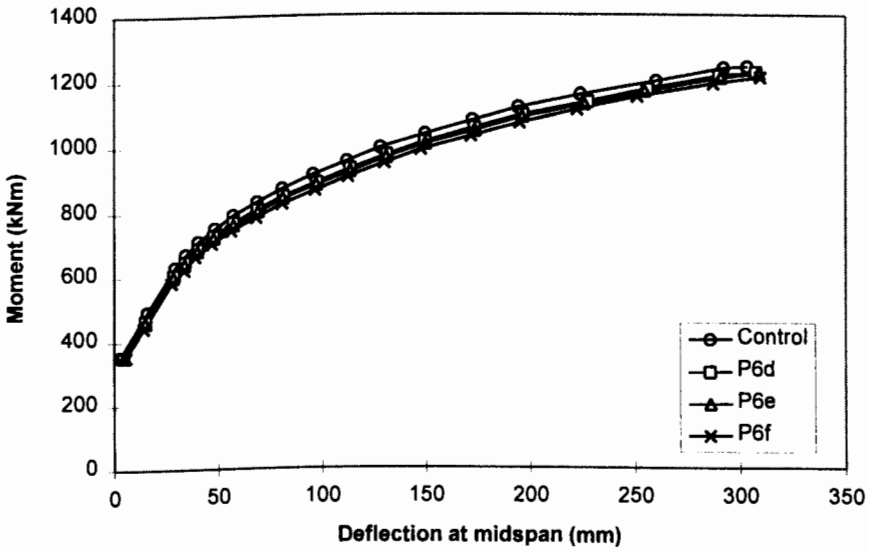

Note: See Table 6.3 for values of ultimate moment and deflection

Figure 6.37 Moment-deflection diagram for failure of Tendon C at the quarter point position, with the presence of voids within re-anchoring length

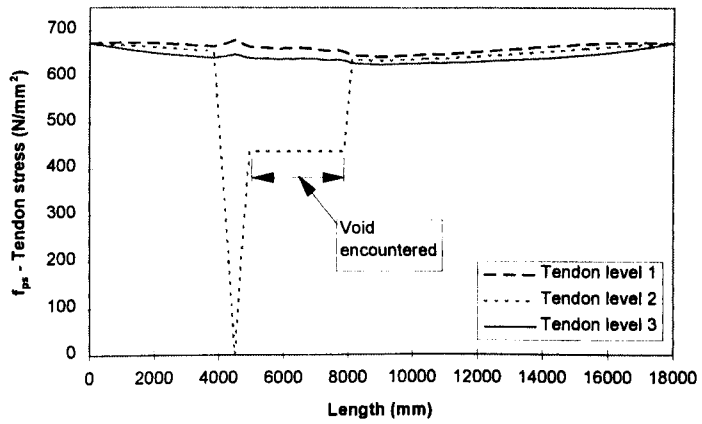

(a) P6d (linear)

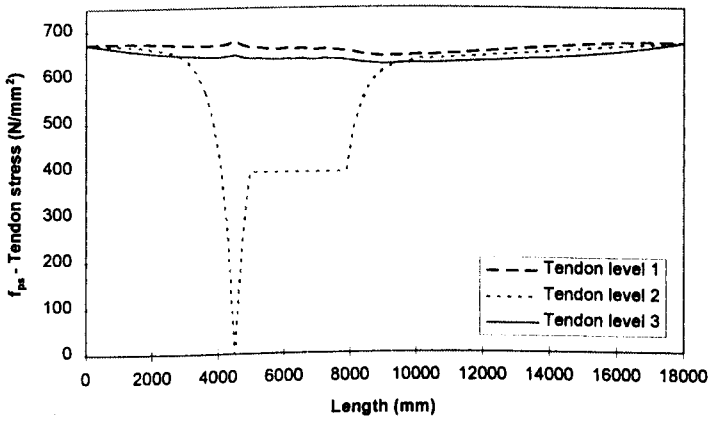

(b) P6e (ϕ=0.35)

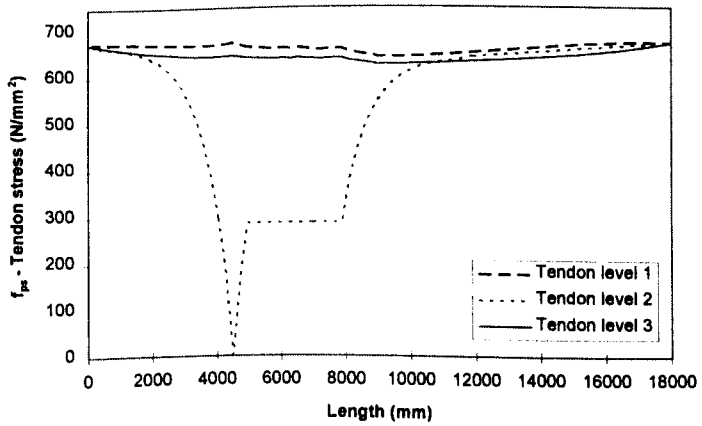

(c) P6f (ϕ=0.2)

Figure 6.38 Tendon stress distribution at the first post-cracking load step for cases P6d, P6e and P6f